THE ROLE OF IRE1 IN METAFLAMMATION AND ATHEROSCLEROSIS

A DISSERTATION SUBMITTED TO

THE GRADUATE SCHOOL OF ENGINEERING AND SCIENCE

OF BILKENT UNIVERSITY

IN PARTIAL FULFILLMENT OF THE REQUIREMENTS FOR

THE DEGREE OF

DOCTOR OF PHILOSOPHY

IN

MOLECULAR BIOLOGY AND GENETICS

By

Özlem TUFANLI

May, 2017

THE ROLE OF IRE1 IN METAFLAMMATION AND ATHEROSCLEROSIS

By Özlem TUFANLI

May, 2017

We certify that we have read this dissertation and that in our opinion it is fully adequate, in scope and in quality, as a thesis for the degree of Doctor of Philosophy.

_____

Ebru Erbay

(Advisor)

_____

Özgür Şahin

_____

Urartu Özgür Şafak Şeker

_____

Çağdaş Devrim Son

_____

Erkan Yılmaz

Approved for the Graduate School of Engineering and Science

_____

Ezhan Karaşan

Director of the Graduate School of Engineering and Science

ABSTRACT

THE ROLE OF IRE1 IN METAFLAMMATION AND ATHEROSCLEROSIS

Özlem TUFANLI
Ph.D. in Molecular Biology and Genetics
Advisor: Ebru ERBAY
May 2017

Chronic metabolic overloading of anabolic and catabolic organelles such as the endoplasmic reticulum (ER) and mitochondria is a major cause of inflammation in obesity. ER serves as a critical metabolic center for protein, lipid and calcium metabolism. ER's vital functions are maintained by a conserved, adaptive stress response known as the Unfolded Protein Response (UPR), which strives to re-establish homeostasis. Irremediable ER stress, however, can push the UPR to initiate pro-inflammatory and pro-apoptotic signaling. UPR activation is seen in all stages of atherosclerotic plaque formation and ER stress is causally associated with atherosclerosis. A profound interest in therapeutically limiting ER stress in a variety of human diseases has driven the discovery of small molecules that can modulate specific UPR signaling arms. These UPR modulators can also become tools to understand the distinct contribution of UPR branches to atherogenesis. In my studies I utilized a specific inhibitor for Inositol-requiring enzyme-1 (IRE1), a dual kinase and endoribonuclease (RNase) in the UPR, to define IRE1's RNA substrates in macrophages. Using RNA sequencing, I discovered that IRE1's RNase activity regulates many pro-atherogenic and pro-inflammatory genes in macrophages. The outcome of my studies provides compelling evidence that IRE1, through its target XBP1, regulates the inflammatory response to lipid excess. The data shows that specific inhibitors of IRE1's RNase activity can uncouple lipid-induced ER stress from immune response in both mouse and human macrophages by blocking mitochondrial reactive oxygen species production and NLRP3 inflammasome activation. Furthermore, administrating two small molecule inhibitors of IRE1's RNase activity to hypercholestrolemic ApoE-

deficient ($ApoE^{-/-}$) mice led to profound suppression of pro-atherogenic cytokine levels in the circulation and blunted T helper-1 type immune response, thus alleviating atherosclerosis. These results demonstrate that therapeutic fine-tuning of IRE1's RNase activity with small molecule inhibitors could be developed further for atherosclerosis.

Keywords: Metaflammation, unfolded protein response, mitochondrial oxidative stress, reactive oxygen species, endoplasmic reticulum stress, inflammasome, atherosclerosis

ÖZET

IRE1'IN METAFLAMASYON VE ATEROSKLEROZDAKİ ROLÜ

Özlem TUFANLI
Moleküler Biyoloji ve Genetik, Doktora
Tez Danışmanı: Ebru ERBAY
Mayıs 2017

Obezitede endoplazmik retikulum (ER) ve mitokondri gibi anabolik ve katabolik organellere kronik olarak ve metabolik olarak yüklenilmesi, inflamasyona neden olan ana etmenlerden biridir. ER, protein, lipit ve kalsiyum metabolizması için kritik bir metabolik merkez olarak hizmet vermektedir. ER, Katlanmamış Protein Yanıt (KPY) olarak bilinen, evrimsel olarak korunmuş, adaptif bir stres tepkisini başlatarak hayati fonksiyonların ve homeostazın yeniden kurulmasını sağlamaktadır. Bununla birlikte, uzun süreli, üstesinden gelinemeyen stres durumlarında, ER KPY'yi, pro-inflamatuar ve pro-apoptotik sinyal yolaklarını başlatması için uyarabilir. KPY aktivasyonu ve aterosklerosis arasında sıkı bir bağ vardır, çünkü aterosklerotik plak oluşumunun her aşamasında KPY aktivasyonu görülmektedir. Belirli KPY enzimlerini modüle edebilen küçük moleküllerin keşfedilmesiyle, metabolik hastalıklarda ER stresin terapötik olarak sınırlanması büyük ilgi uyandırmaktadır. Bu KPY modülatörleri, her bir, KPY yolağının aterosklerosis indüksiyonuna farklı katkısını anlamak için yeni araçlar sağlayabilir. Bu çalışmamda, IRE1'in RNaz substratlarını makrofajlarda tanımlamak için KPY'de bir kinaz ve endoribonükleaz (RNaz) özelliği olan inositol gerektiren enzim-1 (IRE1)'in çok özel bir RNaz inhibitörünü kullandım. RNA dizilimi yöntemini kullanarak, IRE1'in RNA etkinliğinin makrofajlardaki birçok pro-aterojenik ve pro-inflamatuar genini düzenlediğini keşfettim. Çalışmalarım, IRE1'in RNaz hedefi olan XBP1 aracılığıyla lipit fazlalığının neden olduğu inflamatuar cevabı düzenlediğine dair güçlü kanıtlar sağlanmaktadır. Veriler, IRE1'in RNaz aktivitesine özgü inhibitörlerinin, mtROS üretimini ve NLRP3 inflamazom aktivasyonunu bloke ederek hem fare hem de insan makrofajlarında inflamasyon tepkisini lipit kaynaklı ER stres tepkisinden ayırabildiğini göstermektedir.

Ayrıca, IRE1'in RNaz aktivitesinin iki farklı küçük molekül inhibitörünün, hiperkolestrolemik ApoE eksikliği olan ($ApoE^{-/-}$) farelere uygulanması, hem dokularda hem de T yardımcı-1 tipi bağışıklık tepkisinde pro-aterojenik sitokin seviyelerinin bastırılmasına yol açmıştır. Böylece aterosklerozun ilerlemesi engellenmiştir. Bu sonuçlar, küçük molekül inhibitörleri ile IRE1'in RNaz aktivitesinin terapötik ayarlamasının ateroskleroz tedavisi için daha da geliştirilebileceğini ortaya koymaktadır

Anahtar sözcükler: metaflamasyon, katlanmamış protein yanıtı, mitokondriyal oksidatif stres, reaktif oksijen türleri, endoplazmik retikulum stres, inflamazom, ateroskleroz

To my precious family…

Acknowledgement

First of all, I would like to express my gratitude to my supervisor Assist. Prof. Dr. Ebru ERBAY for her guidance and support. As a first PhD. student of her laboratory, I am very happy and honored to contribute the foundation of this lab. I am very grateful to my advisor Assist. Prof. Dr. Ebru ERBAY's mentorship and help in publishing my discoveries and teaching me the scientific approach.

I also want to thank Bilkent University and METU's valuable scientists. All the things that I learned during my education life enlightened my scientific way.

I would like to express my deepest appreciations to the thesis committee members, Assist. Prof. Dr. Özgür Şahin and Assist. Prof. Dr. Urartu Özgür Şafak Şeker for their availability and valuable contributions during meetings. Furthermore, I would like to thank Assoc. Prof. Dr. Erkan Yılmaz and Assoc. Prof. Dr. Çagdaş Devrim Son for guidance during my dissertation and for their contribution as members of my thesis jury.

A special thanks to our collaborators, Prof. Dr. Christian Weber and his team for guidance in atherosclerosis experiments and Prof. Dr. Peter Walter and his postdoctoral fellow, Diego Acosta-Alvear, for their assistance for RNA-Seq data analysis presented in this study. They also helped in the preparing of manuscript and provided many valuable inputs to the design of our experiments.

During my thesis, we were like a family in our laboratory. Firstly, I want to thank to our lab's previous members, Şeyma Demirsory and Büşra Yağabasan. We studied hard during tiring days and nights together. Also, we shared fun memories both in the laboratory and outside of work. We learned lots of things together. Also with new additions to our laboratory, our family enlarged. Thus, I wanted to express my special thanks to İnci Şimşek Onat, Begüm Kocatürk, Pelin Telkoparan, Hamid Sayed Muhammed, İsmail Çimen, Aslı Dilber Yıldırım, Zehra Yıldırım, Aslı Ekin Doğan,

Zehra Veli and Buket Gültekin. There are not enough words to express the extent of my gratitude to them. Whenever I was in trouble, I knew I could consent with them and solve problems together. During our tiring and dense working ours, Buket Gültekin, both our lab manager and a close friend, always supported me. Also, I want to thank to our lab's past members, Seda Koyuncu and Erdem Murat Terzi, for their friendship.

I want to thank to veterinarians Z. Gamze Aykut and Mojtaba Beyramzadeh for their technical support with animal experiments.

Furthermore, I feel very lucky to have some special friends. Ayşegül Örs and Banu Bayyurt, who always were great friends and offered their endless support. I want to thank Verda Bitirim, Gözde Güçlüler, Defne Bayık. We spent many funny moments together during our PhD studies at Bilkent University.

I also want to express my gratitude for the funding agencies that supported my thesis work; Scientific and Technological Research Council of Turkey (TUBITAK)-German Federal Ministry of Education and Research (BMBF) Intensified Cooperation Grant 110S293, TUBITAK Grant 113Z023 and European Research Council (ERC) Starting Grant 336643.

This is the most difficult part for me to write. I know whatever I write here will not be complete. My family and my loved ones are my life. Without them, I would not have reached to this stage.

Contents

List of Figures

List of Tables

Abbreviations

Abbreviation	Explanation
4μ8c	7-Hydroxy-4-methyl-2-oxo-2H-1-benzopyran-8-carboxaldehyde
Ab	Antibody
Ag	Antigen
AIM	absent in melanoma-2 receptors
APC	Allophycocyanin
ASC	apoptosis associated speck-like protein containing a CARD
ATF	Activating transcription factor
ATP	Adenozin triphosphate
BM-DM	Bone marrow-derived macrophages
CARD	Caspase recruitment domains
DAMPs	danger-associated molecular patterns
DAPI	4',6-diamidino-2-phenylindole
DDX58 (RIGI)	DEAD box proteins
DMEM	Dulbecco's Modified Eagle's Medium
DNA	Deoxyribonucleic acid
RNA	Ribonucleic acid
ECL	enhanced chemiluminescence
EDTA	Ethylenediaminetetraacetic acid
eIF2α	Eukaryotic Initiation Factor 2
ELISA	The enzyme-linked immunosorbent assay
ER	Endoplasmic reticulum
ERAD	ER associated degradation
FACS	Fluorescence-activated cell sorting
FBS	fetal bovine serum
FDA	Food and Drug Administration
GADD34	growth arrest and DNA damage 34
GAPDH	glyceraldehyde-3-phosphate dehydrogenase
GSK	Glycogen synthase kinase
HAC1	homolog of mammalian XBP1
HEPES	4-(2-hydroxyethyl)-1-piperazineethanesulfonic acid
i.p.	Intraperitonel
IFN	Interferon
IPA	Ingenuity Pathway Analysis
IRE1	inositol-requiring enzyme-1
ISR	integrated signal response
IκB	inhibitor of NF-κB
JNK	JUN N-terminal kinase

Abbreviation	Explanation
KLF	Kruppel-like factor
LDL	Low density lipoprotein
LP	Lipoprotein
LPS	Lipopolysaccharide
MAM	mitochondria associated membranes
MAPK	mitogen-activated protein kinase
MAVS	mitochondrial antiviral signaling protein
MDP	muramyl dipeptidemitochondrial antiviral signaling protein
MEF	Mouse fibroblast cells
MerTK	MER Proto-Oncogene, Tyrosine Kinase
MHC	major histocompatibility complex
MMP	Matrix metallaproteinase
MOMA	Monocyte/Macrophage Marker Antibody
MSU	uric acid crystals
NBD	
NF-κB	Nuclear factor-kappa B
NK	Naturel killer
NLR	Nucleotide binding and oligomerization domain (NOD) -like receptors
PAMP	Pathogen-associated molecular patterns
PBS	Phosphate buffer saline
PDGF	Platelet-derived growth factor
PERK	protein kinase RNA-like ER kinase
PMSF	phenylmethane sulfonyl fluoride
PRRs	pattern recognition receptors
RHOD-2AM	Rhod-2 Acetoxymethyl ester
ROS	Reactive oxygen species
RPMI	Roswell Park Memorial Institute
RT-PCR	Reverse transcriptase PCR
siRNA	Small interfering RNA
SMC	Smooth muscle cell
STAT	signal transducer and activator of transcription
STF-083010	N-[(2-Hydroxy-1-naphthalenyl)methylene]-2-thiophenesulfonamide
TBS	Tris-buffered saline
Th	Helper T cell
TLR	Toll-like Receptor
TNF	Tumor Necrosis Factor
TRAF	TNF receptor associated factor
Treg	Regulatory T cells
TUDCA	auroursodeoxycholic acid
TUNEL	Terminal deoxynucleotidyl transferase dUTP nick end labeling
TXNIP	Thioredoxin Interacting Protein
UPR	Unfolded protein response

Abbreviation	Explanation
UPRE	unfolded protein response element
XBP1	X-box binding protein 1

Chapter 1.

Introduction

1.1. The Endoplasmic Reticulum

Endoplasmic reticulum (ER) is one of the largest organelles in the cell surrounded with a single, continuous membrane. ER is composed of interconnected branching tubules and flattened sacs. This membranous structure surrounds the nucleus and extends throughout the cytosol with dynamic tubules and sacs (1, 2). It contains multiple domains divided by their location and function. One of the major domains is juxtaposed to the nuclear envelope that separates the genetic material from the cytosol and regulates the transport of important molecules such as RNA and proteins. The other one is the peripheral ER, which extends from the nucleus to the cytosol and is comprised of cisternal sheets and dynamic tubules. Some regions of ER membrane are associated with ribosomes during protein synthesis and have been named the 'rough' ER. Hence, the ER regions free from ribosomes have become known as the smooth ER. There are also some ER regions very closely associated with the mitochondria and named the mitochondria associated membranes (MAMs) that play important roles in metabolic and inflammatory regulations (1, 3). Plasma membrane and secreted proteins are folded in the ER and transported to the Golgi apparatus. During this transportation, an intermediate compartment between Golgi and ER is created mainly as a continuum of the ER and contains vesicles and tubules that partake in intracellular trafficking (3). With the development of high resolution imaging techniques, the biological importance and the

complex architecture of ER is better understood. Also ongoing studies that aim to identify functions of new ER proteins and ER domains will generate a complete understanding of this highly important organelle (1).

1.1.1. Endoplasmic Reticulum Function

ER has four major functions in the cell; proper protein synthesis and folding, degradation of improper or misfolded proteins, biogenesis of important lipids and regulation of Ca^{2+} metabolism.

Protein Synthesis and Folding. ER is one of the major sites of protein synthesis in the cell. Ribosome-mRNA complexes are positioned on ER membranes after initiation of the synthesis of the polypeptide chain and the translation progresses on these ribosomes. Nascent polypeptides enter the ER through an ER membrane-spanning channel. Two types of proteins are synthesized by the ER; transmembrane proteins and soluble proteins. After translocation of proteins into the ER membrane through N-terminal signal sequences, hydrophobic residues called stop-transfer signals allow transmembrane protein folding and finally direct them to the ER membrane. Newly synthesized transmembrane proteins are then targeted into different destinations such as the plasma membrane; membrane bound organelles or ER membranes. On the other hand, proteins destined to be secreted or to remain in the lumen of membrane-bound organelles are directed into the ER lumen right after the cleavage of ER signal peptide sequence. Proper folding and many modifications occur in ER such as N-linked glycosylation, disulfide bond formation and oligomerization take place in the ER. These modifications have a crucial role in defining the intracellular destination of the proteins as well as the functions of the soluble proteins (2, 4). However, many proteins can be misfolded and cannot reach their correct 3 dimensional conformations. Hence, they remain in the ER as insoluble aggregates. These misfolded proteins can be cleared with the help of an ER associated degradation (ERAD) pathway (5).

ER-Associated Degradation ER has an elaborative quality-control system that can detect improperly processed or misfolded proteins within the ER lumen. If for any reason the proteins cannot achieve their functional forms, they are translocated to the cytosol for degradation through ER-associated degradation (ERAD) pathway. These proteins are de-glycosylated, ubiquitinylated and finally, degraded by the proteasome. The ERAD pathway thus provides an efficient, selective waste removal, so it can be viewed as a quality-control process (5).

Lipid Biogenesis In addition to its role in protein secretion, ER plays an important part in membrane lipid biogenesis. ER and Golgi can together form an endomembrane compartment that provides a special site for lipid synthesis. Lipids are transferred to the regions near Golgi on ER and exposed to modifications there (3). Especially the synthesis of phospholipids and cholesterol takes place on the ER and contributes to new cell membrane production. The first step of lipid bilayer enlargement begins with the addition of two fatty acids to glycerol phosphate to obtain phosphatidic acid and occurs on the cytosolic leaflet of the ER membrane. The following steps, that consist of determining the chemical nature and the addition of the head groups to lipids, are performed in endomembrane compartments that are formed together with ER and Golgi (3). Furthermore, ER-mitochondria contact sites are also enriched with some important enzymes that have a role in some lipid biosynthesis pathways. Especially, both ER and mitochondria are required for the synthesis of phosphatidylethanolamine (PE) and phosphatidylcholine (PC), the most abundant phospholipids of the cell. Hence contact sites of these two organelles allow lipid biosynthesis and lipid transfer between these organelles (6, 7).

In addition to its role in lipid bilayer biogenesis and assembly, ER can control transcriptional regulation of lipid metabolism-related genes. Under certain conditions, inactive transcription factors that are found on the ER are translocated first to the Golgi

for processing and maturation and then to the nucleus to initiate the expression of the genes required for lipid biosynthesis and uptake (8-10). For example SREBP-1c and SREBP-2 which are the key transcription factors in hepatic lipogenesis and cholesterol biosynthetic pathways are normally localized to the ER and sense lipid changes on the ER (9).

Ca^{2+} Metabolism ER also plays a central role as an intracellular Ca^{2+} store (11). Calcium concentrations in the cytosol and extracellular compartments are maintained tightly (~100 nM and is ~2 mM respectively). The ER lumen Ca^{2+} concentration changes between ~100-800 μM.(12) This high amount of ER calcium concentration, compared to cytosol calcium concentrations, clearly shows the pivotal role of ER as a major storage for Ca^{2+}. There are several calcium channels, ryanodine receptors and inositol 1, 4, 5-trisphosphate (IP3) receptors (IP3R) on ER and all of them regulate the transfer of Ca^{2+} from ER to cytosol when needed (2, 12). Calcium is a very important molecule that can regulate a wide variety of processes from protein localization, function and association (with other proteins, organelles or nucleic acids) and the reshaping of ER under certain conditions (such as physiological responses to neurotransmitter release and muscle contraction) (2, 13). Furthermore, changes in Ca^{2+} concentrations or Ca^{2+} transfer between cytosol and mitochondria have a crucial role in metabolic regulation. For example Ca^{2+} oscillations can regulate mitochondrial metabolism such as ATP production and mitochondrial permeability so regulate cell death. Also release of Ca^{2+} from ER can regulate redox state of mitochondrial chaperones (14-16). The Ca^{2+} transfer from ER to mitochondria deserves special emphasis and will be mentioned in a later section of this thesis.

1.1.2. Endoplasmic Reticulum Stress and UPR

Most secretory and transmembrane proteins that enter the ER lumen as nascent unfolded chains fold and mature by ER resident chaperones, foldases, and cofactor proteins (4).

Generally, a small portion of proteins cannot be folded properly due to highly complex stochastic processes in the ER (17, 18). In those cases, the unfolded proteins are detected in the ER and initiate a highly efficient response known as ERAD that results in their removal (17). Many environmental and physiological factors such as increased rate of protein synthesis, genetic abnormalities, depletion of ATP, oxidative stress, viral infection, increased temperature, alterations in Ca^{2+} level and exposure to excess cholesterol or fatty acids (such as in obesity and dyslipidemia) and aging can lead to disturbances in ER functions, leading to increases in the accumulation of misfolded proteins that exceed ER folding capacity (18, 19). Hence, in such conditions, ER homeostasis is disturbed, a situation known ER stress. To cope with ER stress, cells provoke a strong adaptive response called as unfolded protein response (UPR) or the ER stress response (20, 21). UPR is a collection of signaling networks that include a wide variety of transcriptional and translational events mediated by three transmembrane ER stress sensors; inositol-requiring enzyme-1 (IRE1), the protein kinase RNA (PKR)-like ER kinase (PERK), and the activating transcription factor 6 (ATF6) (Figure 1.1). Under ER stress conditions, chaperones that normally associate with UPR sensors dissociate to engage with unfolded proteins, leading to the activation of UPR sensors and downstream signaling. Depending on the duration or the dose of the stressors, ER activates transcriptional or translational processes either to reestablish homeostasis in the cell or to initiate apoptotic pathways (20, 22, 23).

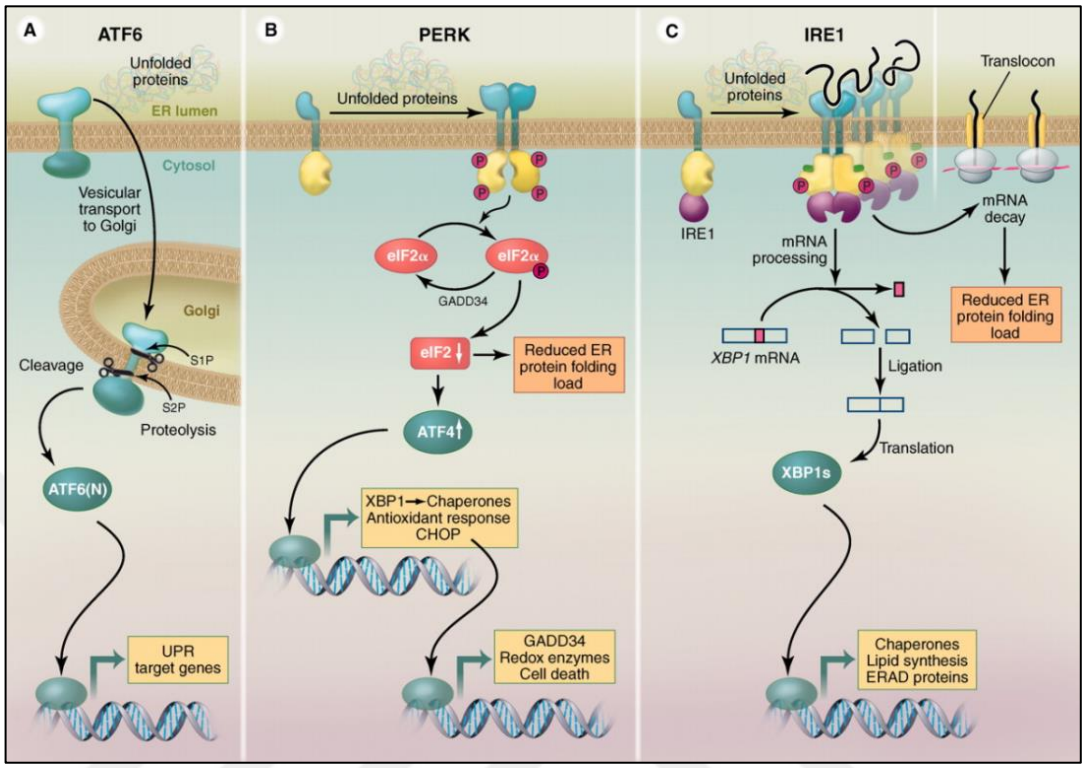

Figure 1.1. Three main branches of unfolded protein response

1.2. Unfolded Protein Response Signaling

Unfolded protein response is mediated by three major stress sensors located on the ER membranes; IRE1, PERK and ATF6 in response to certain environmental or cellular stress conditions.

1.2.1. IRE1

IRE1 is the first identified and major ER stress sensor located on ER membranes. It is highly conserved from yeast to mammalian cells. The metazoan IRE1 has two homologues, IRE1α and IRE1β. IRE1α is expressed in all cells and tissues, whereas IRE1β is expressed only in the gastrointestinal and respiratory tracts. The function of

IRE1β is still unknown and UPR signaling is mainly mediated through IRE1α (24, 25) IRE1 molecules include 3 important domains; a luminal domain, a transmembrane domain and a cytosolic domain that contains two enzymatic activities, namely endoribonuclease (RNase) and kinase. When IRE1's luminal domain senses the unfolded proteins, this leads to autophosphorylation by IRE1's kinase domain and oligomerization. Activation of its kinase domain further activates its RNase domain. (Figure 1.2). Through its RNase and kinase domains, IRE1 contributes to re-establishing ER homeostasis. IRE1 and its targets, mainly XBP1 transcription factor, can perform a wide variety of functions in the cell (26). Next, I will present a review of the functions of IRE1 protein in two categorizes; RNase domain functions and kinase domain functions.

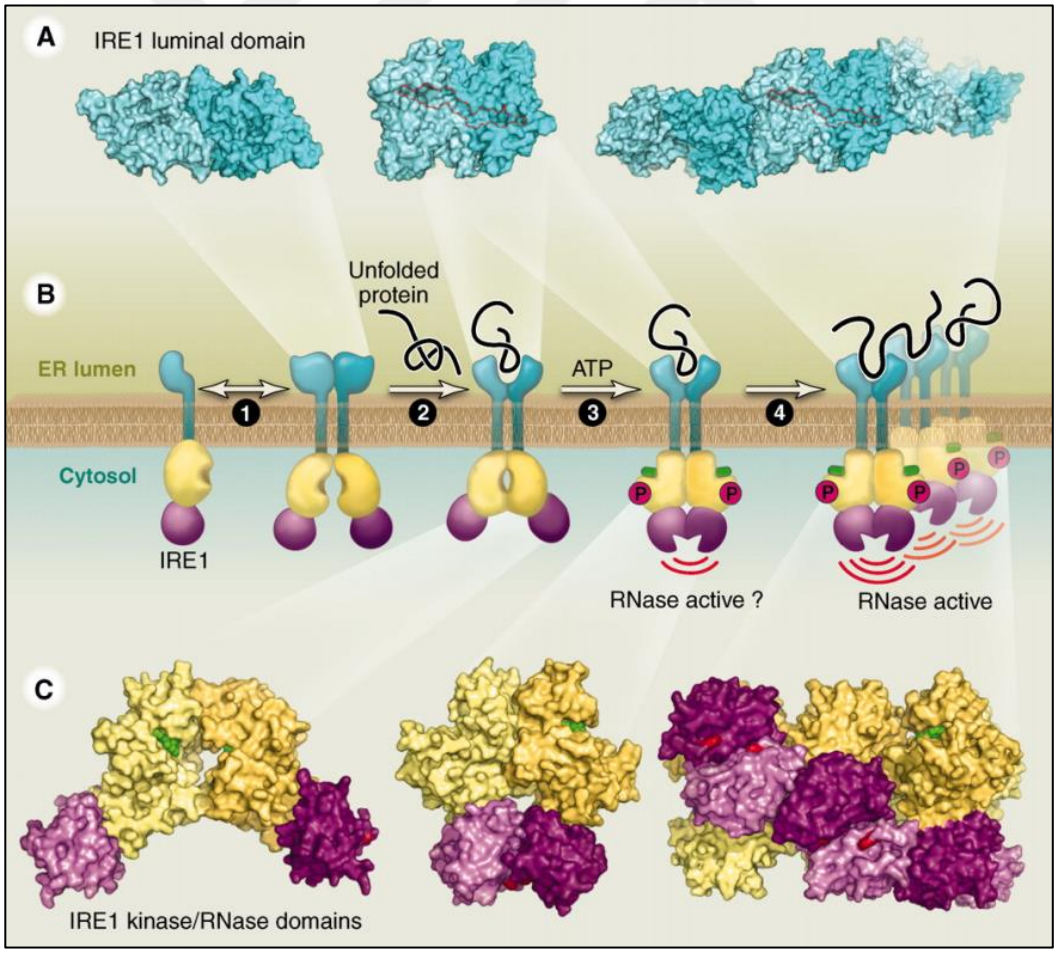

Figure 1.2. IRE1 assembly and activation mechanism with ER stress

RNase Domain Function After activation, IRE1α can initiate a wide variety of signaling pathways ranging from pro-survival to apoptotic and depending on the nature of the stimuli (27). The best known RNase substrate of IRE1α is the mRNA encoding X-box binding protein 1 (XBP1). Pre-mature XBP1 (U) mRNA exists in a specific stem loop structure in the cytosol. Active IRE1 can recognize this stem loop structure and through an unconventional splicing event, remove 26 nucleotides in the intron of XBP1 (U). This spliced XBP1(S) produces a larger and active protein due to a frame-shift (28). XBP1 protein contains both a DNA binding domain and a transcriptional activation domain. This mature form of XBP1(S), by binding to the unfolded protein response element (UPRE) regions, regulates the transcription of UPR target genes such as chaperones, protein disulfide isomerases (PDIs) and the components of ERAD pathway (29, 30). In addition, XBP1 can regulate ER's membrane expansion by increasing the transcription of genes involved in phospholipid biosynthesis (31). All of these XBP1 functions show that XBP1 is an important molecule in relieving stress in the ER stress.

Furthermore, there are factors and ways that affect XBP1 activity. For example, the stability of XBP1(S) is increased by binding of small ubiquitin-like modifier (SUMO) ubiquitin-conjugating enzyme 9 (UBC9) in the cytosol (32). On the other hand XBP (U) translation can be paused due to a peptide motif on its carboxyl terminus, and this makes it more susceptible to splicing by IRE1 (33). Under unstressed conditions, XBP1(S) forms a complex with XBP1 (U) protein, and then undergoes proteasomal degradation (34).

IRE1 also has another function to degrade specific mRNAs that are associated with ribosome on ER membrane for translation. By degrading these mRNAs, IRE1 tries to reduce protein load under stress conditions (35, 36). IRE1 can specifically target 5'-UGCU-3' sequence in the stem loop structures of mRNAs. However, there are some mammalian regulated IRE1-dependent decay (RIDD) target genes that do not contain this consensus sequence. Basal RIDD activity is needed for cellular homeostasis and cell recovery; however, sustained activation of RIDD is associated with the induction of

apoptotic pathways (20, 37). RIDD activity has been shown to selectively degrade some microRNAs that can repress apoptotic pathways. Increasing RIDD activity leads to apoptosis through degradation of premature mir-17, specifically targeting caspase-2 mRNA. Caspase 2 cleaves the pro-apoptotic BH3 only protein BH3 interacting domain death agonist (BID) that activates BCL2 associated X, apoptosis regulator (BAX) and BCL2 antagonist/killer 1 (BAK) (38).

Kinase Domain Function To date, IRE1 is only known to phosphorylate itself (39). Through its kinase domain IRE1 can associate with some adaptor proteins to regulate different pathways. For example, TNF receptor associated factor 2 (TRAF2) binds to phosphorylated IRE1 and initiates the mitogen-activated protein kinase (MAPK) pathway to regulate inflammatory and apoptotic pathways (40). Also phosphorylated IRE1 can activate NF-κB via binding with inhibitor of NF-κB (IκB) kinase (41).

1.2.2. PERK

PERK is another major ER stress sensor located on the ER membranes. It is composed of luminal (stress sensing), transmembrane and cytoplasmic (kinase) domains. PERK can autophosphorylate and dimerize under ER stress conditions (42). The best known substrate of PERK is eukaryotic translation initiation factor 2α (eIF2α). Phosphorylated eIF2α leads to general inhibition of translation of capped mRNAs in the cell and blocks further accumulation of unfolded proteins in the ER (42, 43). However, during ER stress there is a small subset of mRNAs that are preferentially translated. For example, activating transcription factor 4 (ATF4), preferentially translated during ER stress, is an important transcriptional factor, which can regulate the expression of genes required for amino acid import, metabolism and resistance to oxidative stress. PERK-ATF4 signaling is thought to play an important role in cytoprotection at the early stage of ER stress. However, if ER stress is irremediable or severe, ATF4 can also induce the transcription of C/EBP-homologous protein (CHOP), a transcription factor, which drives the stressed

cells to apoptosis (42, 44). CHOP leads to the activation of apoptotic pathways by inhibiting B cell leukemia 2 (BCL2) family members. On the other hand CHOP has a role in the dephosphorylation of eIF2α by upregulating the expression of protein phosphatase 1 regulatory subunit 15A (PP1R15A (also known as growth arrest and DNA damage 34 (GADD34). PP1R15A removes the blockage on protein translation and stimulates the translation of proteins necessary to reinstate homeostasis in the ER (45). Also, another PERK substrate is NF-κB repressing factor B (NRF2), which regulates transcription of antioxidant proteins and helps establish ER homeostasis (46). Finally, PERK can activate NF-κB and regulate inflammatory pathways (41). Thus, PERK performs opposing functions of cytoprotection, apoptosis and inflammation under specific cellular conditions.

1.2.3. ATF6

ATF6, an ER transmembrane protein with a transcription factor function, controls the third arm of the UPR. ATF6α and ATF6β are two homologous proteins. They are transmembrane protein containing multiple domains with different functions; luminal BIP-associated domain, cytosolic domain with bZIP motif, and transmembrane domain with a Golgi target sequence (47, 48). Under stress conditions, ATF6 dissociates from the ER membrane and is transported to the Golgi via coat protein complex II (COPII)-containing vesicles. The cytoplasmic domain of ATF6 is phosphorylated and cleaved by membrane-bound transcription factor site 1 and site 2 proteases (S1P and S2P, respectively). This process is called regulated intramembrane proteolysis. After cleavage of its luminal domain by SP1 and transmembrane domain by SP2, the phosphorylated N-terminal domain of ATF6 (N) is released from Golgi and activates the expression of UPR target genes like ATF4 and XBP1(S) (28, 49, 50). These target genes contribute to ER quality control, protein folding, secretion, ER expansion, chaperone synthesis and ERAD (51-54). ATF6 together with ATF4 and XBP1(S) can transcriptionally regulate overlapping genes and modulate ER stress response or initiation of cell death pathways under different ER stress conditions (55). Some studies showed that ATF6 could play a

role in cell protection. For example, mice lacking *Atf6α* displayed increased susceptibility to ER stress induced cell death and also embryonic lethality was observed when both Atf6α Atf6β are deleted (51, 52, 56).

On the other hand, ATF6 also plays a role in the regulation of NF-κB under special toxin induced ER stress conditions that depend on mTOR related dephosphorylation of Protein Kinase B (AKT) protein (57). However, the relationship between ATF6 and inflammatory response needs further investigation.

1.3. Endoplasmic Reticulum Stress and Immune Response

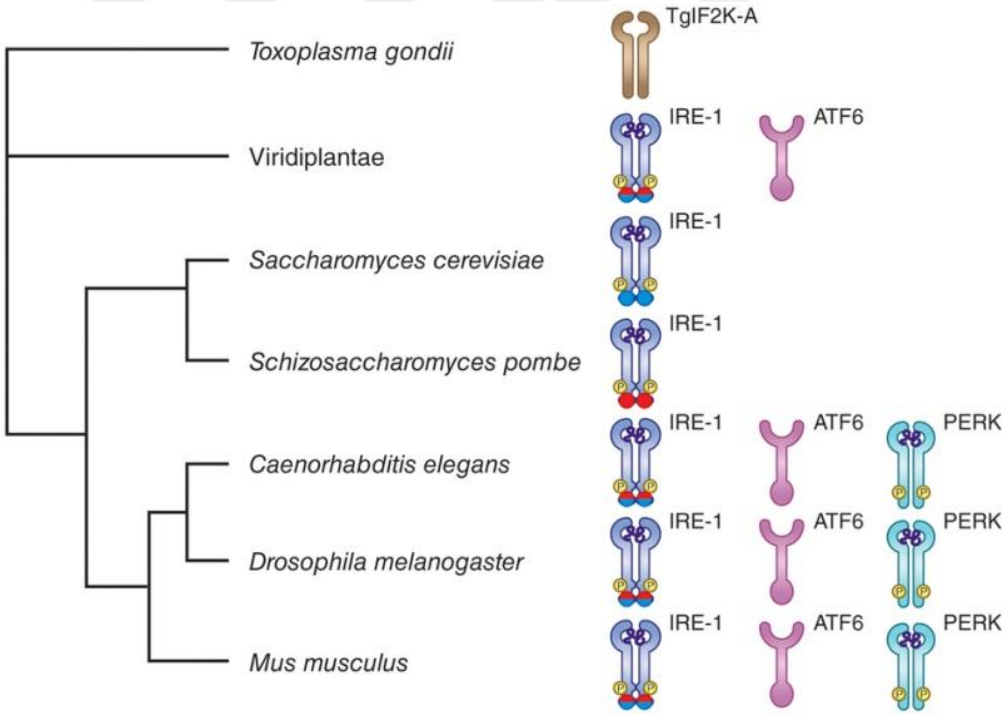

Figure 1.3. Evolution of unfolded protein response proteins

The IRE1 branch of the UPR is the only arm that is conserved from yeast to mammals. (Figure1.3). *Saccharomyces cerevisiae* IRE1 also has the conserved endoribonuclease

activity that splices HAC1 (homolog of mammalian XBP1) mRNA. This signaling controls the transcriptional response to regulate the folding capacity of ER in yeast. On the other hand *Schizosaccharomyces pombe* IRE1's endoribonuclease activity only performs the RIDD function, because there is no HAC1 coding gene in this organism (58-60). In pathogenic fungi, UPR has a role in adapting the fungi to its host's microenvironment by regulating pathogen virulence through the secreted toxic compounds (61).

In plants, on the other hand, ATF6 and IRE1 dominate the UPR, because there is no PERK protein. Here, a more prominent RIDD activity of IRE1 tries to compensate for the missing PERK-regulated translational control. UPR activation controls protein load during seed development and under abiotic stress conditions such as salt or heat shock stress (58, 62, 63). Furthermore, IRE1 mounts an antibacterial defense by inducing the secreted foldases that function in protein folding as well as secreted hydrolases (64).

Caenorhabditis elegans has all three sensors of the UPR (65). The IRE1-XBP1 axis serves to sustain larval survival under pathogen threat. IRE1 arm does not directly control infection; instead it reinforces ER's functions involved in adaptive immunity against the detrimental pathogen. Also XBP1 resolves ER toxicity that is caused by severe inflammatory conditions (66).

In metazoans, there is a more complex UPR pathway with three sensors. It has close-relationship with other stress-controlled translational regulatory pathways known as the integrated signal response (ISR). Bacterial or viral infections can activate UPR or ISR pathways as a host defense (59, 67).

Initially, UPR activation aims to resolve ER stress, but under prolonged ER stress conditions UPR can activate many pro-apoptotic and inflammatory pathways. Chronic exposure to metabolic stress factors such as excess of lipids, glucose or inflammatory

agents such as cytokines can trigger or sustain UPR activity in many cell types, but especially in cells specialized for the secretion of large amounts of proteins (such as pancreatic beta cells, adipocytes, oligodendrocytes) and immune factors (such as B cells and macrophages) (68-73). Many metabolic stress factors affect not only the ER but also a closely associated organelle, the mitochondria, inducing UPR, oxidative stress and inflammation (74, 75). How ER and mitochondria are coupled in stress is an area of intense research. For example, ER stress-induced calcium transfer from the ER to the mitochondria can induce reactive oxygen species (ROS) production from the latter organelle (76). These organelles also exchange ROS, lipids and other molecules that may synchronize their response to the stressor (76, 77). Activation of ER stress by metabolic stress as in the case of obesity and dyslipidemia, and consequent induction of inflammation can also contribute to impairment of cellular and systemic lipid and glucose metabolism, resulting in cell death or dysfunction, insulin resistance and diabetes (73, 78) (Figure 1.4). This vicious loop between ER stress and inflammation can accelerate the progression of many metabolic diseases, such as atherosclerosis, obesity, type 2 diabetes and neurodegenerative diseases (79-82).

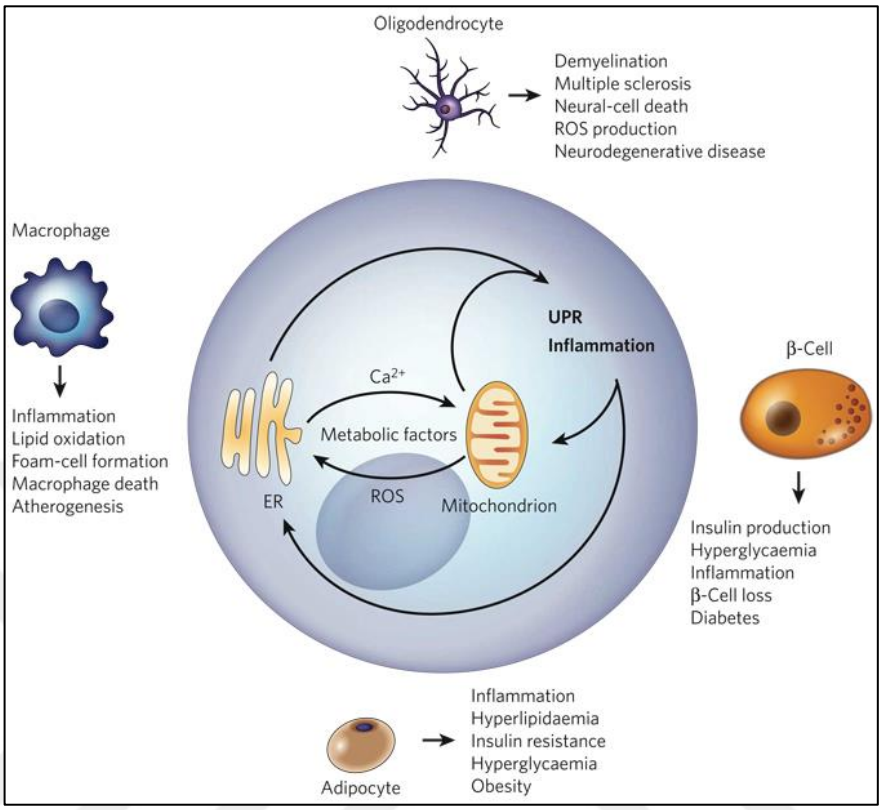

Figure 1.4. Connection between ER stress, metabolic diseases and inflammation

1.3.1. UPR Connection with Inflammatory Pathways

The connection between UPR and inflammation underlies many complex diseases. Environmentally-induced or genetic defects in the UPR branches have been associated with inflammatory phenotypes such as inflammatory bovine disease, lung respiratory disease, type 1 diabetes or other metabolic diseases (58, 83). Inflammatory pathways such as the downstream of the Toll-like receptor (TLR) and stress kinase signaling pathways share similar consequences with the UPR such as the induction of reactive oxygen species (ROS) and activation of the nuclear factor-κB (NF-κB) (84-86). NF-κB is an important transcription factor in inflammation (87). It is normally found in an inactive state and associated with its inhibitor (IκB) in the cytosol. With stimulation, the phosphorylation of IκB by a kinase IKK triggers its release from the inhibitory protein and translocation into the nuclei, where it initiates the transcription of pro-inflammatory

genes (88). ER stress can also lead to NF-κB activation (89). All branches of UPR have been implicated in the regulation of NF-κB. The PERK activation leads to translation inhibition of IκB, which is constitutively expressed in cells under normal conditions and is rapidly degraded under inflammatory stimuli (90). IRE1 activation indirectly leads to IκB phosphorylation. The TNF receptor-associated factor 2 (TRAF2) is recruited to the phosphorylated domain of IRE1, followed by the recruitment of IκB kinase (IKK). Here, IKK phosphorylates inhibitory IκB leading to its degradation. Thus NF-κB dissociates from its inhibitory partner and becomes active. On the other hand, ATF6 plays a role in NF-κB activation through its impact on the mTOR-AKT pathway. Silencing of ATF6 in liver immune cells reduced immune response that was caused by ER stress through the alleviation of NF-κB activation and restoration of AKT pathway. Nonetheless more detailed studies on this subject are needed (57, 91) .

In addition to their roles in NF-κB activation, IRE1 and PERK can coordinate inflammatory responses by many other ways. For example, IRE1-TRAF2 association can regulate production of interleukin-6 (IL-6). IL6 is an important cytokine dependent on the binding of TRAF2 protein to oligomerization domain (NOD)-containing proteins 1 and 2 (NOD1 and NOD2). That association can activate NF-κB dependent IL6 expression (92). Also IRE1-TRAF2 association activates mitogen-activated protein kinase (MAPK) kinase 5 (MAP3K5). MAP3K5 then phosphorylates and activates MAPK8 (or JUN N-terminal kinase (JNK1) and MAPK14 (93, 94). Subsequently, JNK1 phosphorylates and activates Activator protein 1 (AP-1) that is an important transcription factor. Additionally, IRE1 through XBP1, can regulate the expression of several pro-inflammatory cytokines such as interleukin 6 (IL-6), tumor-necrosis factor-α (TNFα) and interferon β (IFNβ) (95, 96). Furthermore, an XBP1-induced miRNA (miR)-346 can regulate major histocompatibility complex (MHC) class I Ag presentation. This microRNA targets mRNAs encoding the transporter of antigenic peptides-1 (TAP1) also called ATP-binding cassette (ABC) transporter, and human leukocyte antigen (HLA) class I proteins. These targets have important roles in antigen presentation in adaptive immune response and transport of peptides to ER respectively

(97). In addition IRE1's RIDD function plays a role in some inflammatory pathways. RIDD activity can degrade TAP binding protein (TAPBP) mRNA and reduce antigen presentation (98). Small RNAs that are produced by RIDD activity can also induce IFNβ production through activation of ATP-dependent RNA helicase DDX58 (DEAD box proteins or RIGI) or mitochondrial antiviral signaling protein (MAVS) (99).

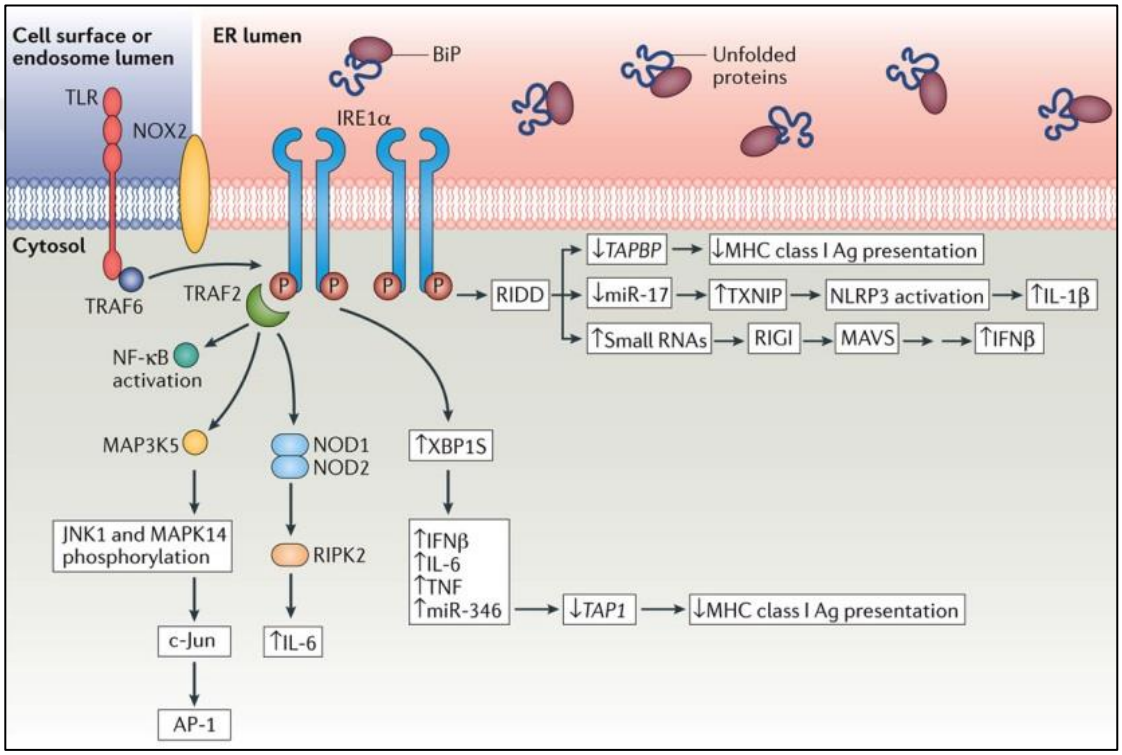

Figure 1.5. Close relation between IRE1 signaling pathways and immune response pathway

Furthermore, CHOP, induced through PERK-ATF4 signaling, can also contribute to IFNβ production. CHOP is also involved in ER stress-induced IL-23 expression in dendritic cells (84, 100).

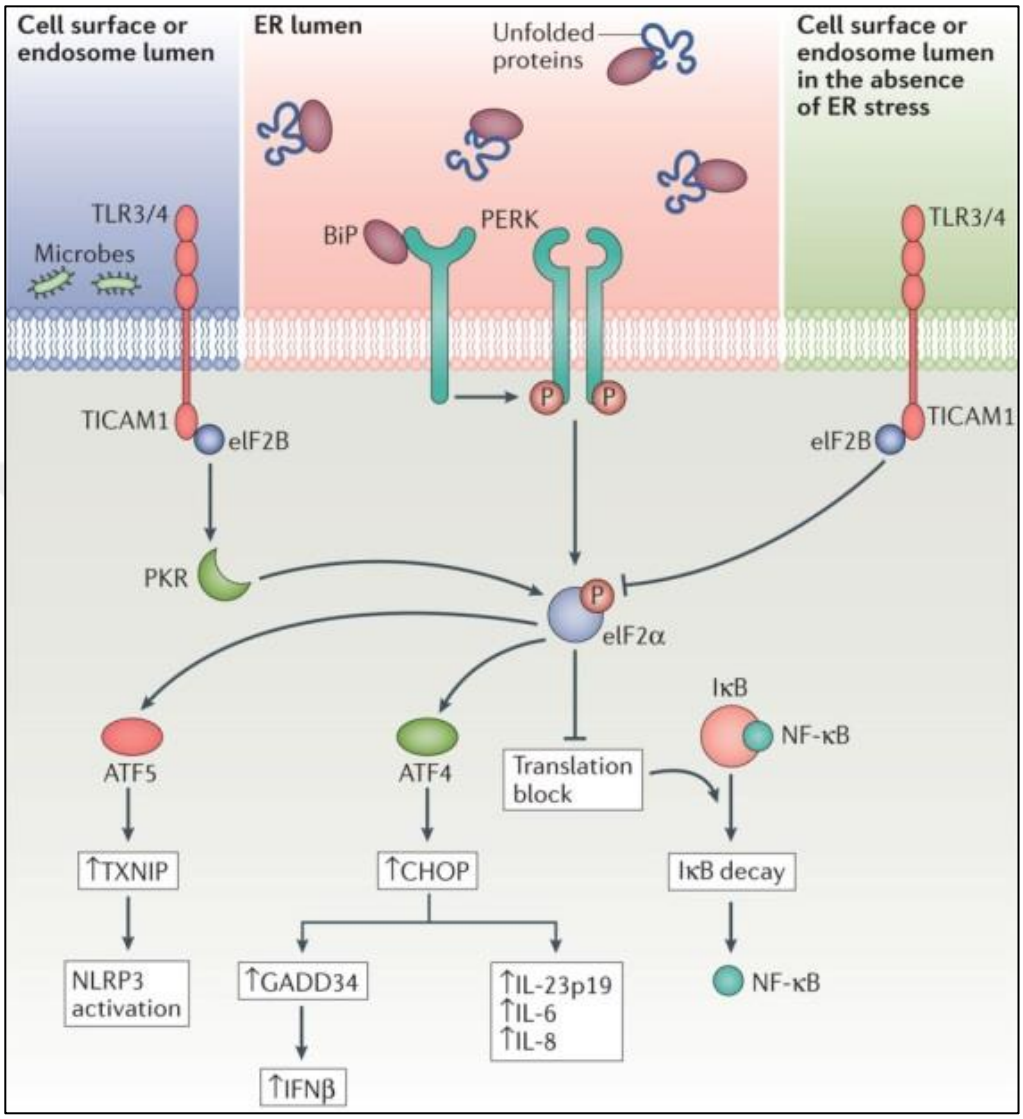

Figure 1.6. Close relation between PERK signalling pathways and immune response pathways

1.3.2. UPR Connection with Inflammasome Activation

Inflammasome Background. Pathogen-associated molecular patterns (PAMPs) and danger-associated molecular patterns (DAMPs) are recognized by germline encoded pattern recognition receptors (PPRs). The PPRs recognize a variety of stimuli and constitute an essential component of the innate immune response that controls the clearing of pathogens or damaged cells (101-103). The PRRs are expressed by cells that

serve in the immune system including macrophages, monocytes, dendritic cells, neutrophils, epithelial cells and also in airway smooth muscle (ASM) cells. Based on their genetic and functional features, PPRs can be classified into different classes. Nucleotide binding and oligomerization domain (NOD) -like receptors (NLRs), absent in melanoma-2 receptors (AIMs) and recently identified pyrin are the main PPRs that can lead to the assembly of the multi-protein inflammatory complexes, *i.e*. inflammasomes, in the cytosol (104, 105).

NLRs recognize both PAMPs and DAMPs. NLRs contain 3 main domains; an N terminal effector domain, a C-terminal leucine-rich sensor domain and a central nucleotide-binding and oligomerization domain (NBD). Based on the N-terminal domain, NLRs can be further subdivided. If the N-terminal domain includes a pyrin domain, it is called NLRP. Likewise, if it includes a caspase activation and recruitment domain (CARD), it is called NLRC. NLRs can activate the inflammasome multiprotein complex and induce an inflammatory response against cellular infection or tissue damage (104, 105). NLRP1, NLRP3 and NLRC4 are well-documented members of NLRs that assemble into an inflammasome complex in the cytosol. After the assembly of a multimeric inflammasome complex, zymogen pro-caspase-1 is recruited and cleaved. Following which, cleaved, mature caspase-1 can proteolytically process pro-IL-1β and IL-18 cytokines and induce inflammatory cell death. This pathway significantly differs from apoptosis in that it involves caspase-1-mediated cell swelling and lysis that results in the loss of membrane integrity (106-109). Bioactive IL-1β and IL-18 cytokines have important roles in both innate and adaptive inflammatory responses (108, 110, 111). They can stimulate further secretion of pro-inflammatory cytokines, leading to recruitment of more inflammatory cells to the inflamed region. These cytokines also regulate T helper (Th) cell polarization especially towards to Th1 and Th17 subtypes (110). Different NLRs are found at different locations in the cell and can be activated by different stimuli. This difference in localization can result from some tissue specific co-factors or different splicing variants of molecules that need to be studied further (112). For example, even though NLRP1 is a cytosolic receptor, it is also active in the nucleus

of neurons and lymphocytes (112). AIM2 was first defined as an IFNγ inducible protein that can oligomerize similarly to the other NLRs and form an inflammasome complex, however it was discovered that AIM2 can directly bind to nucleic acids in the cytoplasm via its hematopoietic IFN-inducible nuclear proteins with 200-amino acids (HIN200) domain and oligomerize via its nucleotide-binding and oligomerization (NACHT) domain. Also, the PTD domain of AIM2 interacts with apoptosis-associated speck-like protein containing a CARD (ASC) adaptor protein and then recruits caspase-1 zymogen for activation like the other inflammasomes (113). Bacterial ligands such as muramyl dipeptide (MDP) or anthrax lethal toxin produced by *Bacillus anthrax* activate the NLRP1 inflammasome (114). NLRC4 serves in immune defense but not by directly binding to its pathogen activators. It can be induced by a family of proteins called NLR family, apoptosis inhibitory proteins (NAIPs). NAIPs can sense their ligands and activate NLRC4. Traditional activators of NLRC4 inflammasome are bacterial flagellin or multiple proteins that belong to bacterial type 3 secretion systems (115, 116). NLRP3 is expressed by wide a variety of cell types such as granulocytes, monocytes, macrophages, dendritic cells, T and B cells, epithelial cells, osteoblasts, fibroblasts and melanoma cells. It is also activated by a broad array of ligands. NLRP3 triggers can be categorized as pathogen-associated ligands (such as cell wall components of bacteria (peptidoglycans), bacterial and viral nucleic acids, microbial toxins, nigericin (Streptomyces hygroscopicus), aerolysin (Aeromonas hydrophila), maitotoxin (Marine dinoflagellates), gramicidin (Bacillus brevis) and α-toxin (Staphylococcus aureus), environmental crystalline pollutants (such as silica, asbestos, and alum crystals), and danger-associated molecules such as ATP, serum amyloid, uric acid crystals (MSU), and ROS (117) . Also, some metabolic products such as saturated free fatty acids also lead to NLRP3 inflammasome activation (118). In experimental conditions, the NLRP3 inflammasome activation requires a priming step that leads to an increase in NLRP3 and pro-IL-1β expression levels in the cell through activation of the NF-κB pathway. For example, Lipopolysaccharide (LPS) in the cell wall components of gram-positive bacteria can provide this priming cue to the cell via binding TLR4 receptors and activating the NF-κB pathway (105, 119). After priming, there are common signaling events that are shared by the various triggers that activate NLRP3 inflammasome such as

induction of potassium (K) efflux through the ATP-gated ion channels, increase in cellular calcium levels, and increased release of ROS, DNA and cardiolipin from the mitochondria, which can be sensed by the NLRP3 resulting in its translocation from the mitochondria associated ER membranes to the cytosol (120-124). There is still a debate about the importance of these mechanisms for NLRP3 activation, because not all of these signaling events can be activated by all NLRP3 agonists.

ER Stress and Inflammasome Relationship ER stress and UPR activation are observed in obesity-induced fatty liver diseases as well as alcohol-induced liver injury. Also, inflammasome activation has been shown to contribute to the pathogenesis of the same diseases (125, 126). Emerging evidence points to a strong relationship between ER stress and inflammasome activation in liver diseases. A chemical chaperone, Tauroursodeoxycholic acid (TUDCA)-treated, genetically obese mice (ob/ob), challenged with tunicamycin to promote ER stress-associated liver injury and severe steatosis, displayed reduced signs of ER stress and inflammasome activation (125, 126). ER stress-induced progression of liver steatosis was attenuated when caspase-1 was silenced in these mice (125). Although these studies mainly focused on liver disease, they clearly showed that ER stress induced liver steatosis through the activation of the inflammasome. However, the pathways that link ER stress and inflammasome activation remain to be elucidated. For example, Tschopp's group suggested a new mechanism that links ER stress and inflammasome activation independent of classical UPR pathways but dependent on reactive oxygen species production and potassium efflux induction (127).

Another recent observation related to inflammasome activation, stated that UPR-induced thioredoxin-interacting protein (TXNIP) protein which could serve as a functional link between ER stress and inflammasome. TXNIP was discovered to be the top glucose-regulated gene in pancreatic cells and its expression increased in diabetes (128). Recently, TXNIP was shown to play a role in cellular apoptosis and insulin production. Mainly through interaction with thioredoxin in mitochondria, TXNIP regulates the redox state. All these functions make TXNIP a good candidate for therapy of diabetes (129,

130). Interestingly, in the study conducted by Papa *et al*., TXNIP levels were found to be upregulated under ER stress conditions and this effect depended on IRE1 RIDD activity. IRE1 RIDD activity can degrade the microRNA mir17, which specifically targets and suppresses TXNIP expression. TXNIP can also bind to and activate NLRP3 inflammasome components. Thus it was suggested that IRE1 could regulate inflammasome activation through TXNIP upregulation (131). Furthermore, under ER stress conditions caused by direct ER stress inducers, PERK activation also resulted in transcriptional upregulation of TXNIP. Increased TXNIP resulted in the production of mitochondrial ROS species and NLRP3 activation (132, 133). There is also another study binding IRE1 with inflammasome activation through TXNIP regulation. In this study, as a result of IRE1α-TXNIP signaling, TXNIP led to mitochondrial damage and TXNIP activated caspase-2 and Bid proteins found in mitochondria, further leading to the release of mitochondrial DNAs. Released DNA bound and activated NLRP3 inflammasome (134). On the contrary, Lebeaupin *et al.* showed that in obese mice that were challenged with LPS and tunicamycin, both separately and together, no changes in TXNIP levels occurred in liver even though ER stress led to NLRP3 inflammasome activation (126). Among the other actors that have been described with the aim of elucidating the link between ER stress and inflammasome activation is glycogen synthase kinase 3 beta (GSK-3β). A previous study showed that GSK-3β could be activated by tunicamycin and regulated IL-1β and TNF-α transcription in an IRE1-dependent manner (135). Based on these studies, ER stress relation with inflammasome activation mainly depends on NLRP3 inflammasome formation. There is also a study showing that IRE1 and PERK can regulate NLRP1 gene transcription, which is dependent on ATF4 (136). More studies are needed to clearly delineate the molecular relation between ER stress and inflammasome complexes under ER stress conditions induced through different stressors, but especially metabolic inducers.

1.4. Atherosclerosis

The global, epidemic rise in obesity and associated diseases such as insulin resistance, type 2 diabetes, fatty liver disease, and dyslipidemia are also major risk factors for atherosclerotic vascular disease (82, 137). These diseases present a major threat to public health and account for one third of deaths worldwide every year (138). The term arteriosclerosis was first introduced by Jean Lobstein, a surgeon and pathologist, in 1829 (139). Then, pathologists tied inflammatory changes to the developing atherosclerotic plaques. While Rokitansky claimed that mechanical injury and toxins are the main reasons of atherosclerosis and the following inflammation. Rudolf Virchow described for the first time the primary role that inflammation plays in atherogenesis (140, 141). In 1920, Windaus showed that cholesterol crystals and calcified connective tissue are prominent features of atherosclerotic plaques, and further studies by Anitschkow and Chaltow supported these observations by showing that atherosclerosis is indeed induced by feeding rabbits with a high cholesterol-rich diet (142, 143). Thus, these researchers identified cholesterol as one of the possible risk factors in atherosclerosis. And, in later years these atherosclerosis risk factors were expanded to include smoking, high blood pressure, high emotional stress, improper diet, diabetes and certain infections (144).

In 1993, Ross summarized in his “response to injury hypothesis” that mechanical injury, toxins and free radicals led to changes in endothelium and the initiation of atherosclerosis (145). Alternative theories by Steinberg and others postulated the “altered lipoprotein hypothesis” and “retention of modified LDL hypothesis”. In their explanations, these researchers emphasized that the retention and modification of lipoprotein in the intima of the arterial wall attracted and activated monocytes and smooth muscle cells that formed the lesions (146). However, the genetics of atherosclerosis show that it is a far more complex metabolic disease and its pathogenesis cannot be restricted simply to a lipid deposition problem (144).

1.4.1. Initiation and Progression of Atherosclerosis

Atherosclerosis is initiated with the accumulation of apoliprotein B (ApoB)-containing lipoproteins (LPs) in the intima region of arterial walls and especially in arterial branches where there is a disturbed blood flow. The core regions of ApoB-LPs are composed of neutral lipids such as triglycerides and cholesteryl fatty acyl esters and this core is surrounded by a phospholipid monolayer and proteins (147). These lipoproteins are synthesized in the liver as very low density lipoprotein (VLDL). These are converted into more dense ApoB-LPs called low density lipoproteins (LDL) with the addition of triacylglycerol in the liver which are atherogenic particles retained in the arterial intima regions (148). In arterial branching points where there is a disturbed laminal flow, these LPs are deposited on the arterial wall and transformed into various oxidized forms. After these oxidative modifications on the LPs, they behave more like a DAMP in the sense that they can activate a persistent, low-grade inflammation. With the activation of endothelial cells lining the arteries begins the recruitment of monocytes into sub-endothelial intima regions. Also, the inflammatory response induced in the plaque activates the plaque-resident smooth muscle cells (SMCs) as well as to the recruitment of other inflammatory cells such as T cells B cells, dendritic cells and mast cells (149, 150).

During this establishment period of atherosclerosis, cellular, extracellular and lipid materials accumulate in the sub-endothelial regions. After the establishment of lesions, as a protective mechanism, a fibrous cap forms over the lesions, providing a barrier between blood platelets and pro-thrombotic material in the lesions. Also, this measure helps maintain the continuity of the luminal blood flow by preventing plaque rupture. On the other hand, some types of lesions over time trigger thrombus formations and lead to serious occlusions and complications. This type of plaques is called ‘vulnerable plaques’. They usually display a lipid-filled necrotic core due to increased accumulation of apoptotic cells resulting from defective phagocytic clearance. In those regions the

fibrous cap thickness is noted to be thinner and over time the lesion's stability decrease making it prone to rupture (151-153) (Figure 1.7).

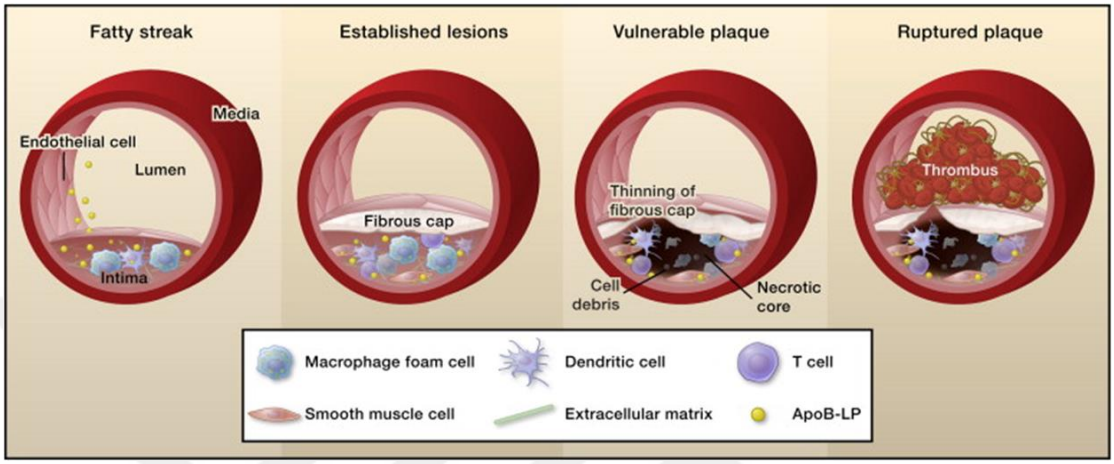

Figure 1.7. Progression of atherosclerosis in blood vessels

During atherosclerosis progression from initiation to rupture, three main cell types contribute; endothelial cells, intimal SMCs, and inflammatory cells (mainly macrophages). These cells contribute both to the progression of disease (vulnerable plaques) and eventually to rupture (154).

Endothelial cells (ECs) Atherosclerosis development occurs in a nonrandom pattern because lesions are typically located around the branched or curved areas of the blood vessels. The atherosclerosis-susceptible areas display low time-average shear stress, high oscillatory shear index and spatial gradient in shear stress. The unbranched arteries that are more protected against these forces, or exposed to uniform laminar flow, rarely develop atherosclerosis. There are observed structural, molecular and functional differences between the endothelial cells of atherosclerosis-susceptible and atherosclerosis-resistant regions of the arteries. While endothelial cells of atherosclerosis-susceptible regions have a cuboidal morphology, the endothelial cells in the atherosclerosis-resistant regions align coaxially along with the laminal flow direction and have an ellipsoidal shape. Also, the latter secrete more glycocalyx. In the branched

areas, endothelial barrier function is disturbed and the rates of cellular senescence and turnover increased (154-157). At the molecular level, there are also differences between two regions. Endothelial cells on the athero-prone regions activate the NF-κB pathway so as to prime the inflammatory signaling events. This inflammatory response further exacerbates with the retention of lipoproteins (158, 159). On the contrary, endothelial cells at the athero-resistant regions activate (Kruppel-like factor 2 (KLF2) and KLF4 gene expressions. These are two important transcription factors regulating proliferation and induced with laminar flow. There are some *in vivo* studies showing anti-athorogenic properties of these two factors. One of them conducted by Atkins *et al.* showed that there was an increase in atherosclerotic plaque area in $KLF2^{+/-}ApoE^{-/-}$ mice compared to control $ApoE^{-/-}$ (160). In another study conducted by Zhou *et al*. EC-specific KLF4 overexpression resulted in an increase in anti-inflammatory conditions in plaque (161). Thus they retained an anti-inflammatory and anti-thrombotic state in animal atherosclerotic models (154).

Smooth Muscle Cells (SMCs) The smooth muscle cells in atherosclerotic lesions are activated in response to LP retention, endothelial cell activation and inflammation, and switch their phenotypes. During atherosclerosis progression, they continue to proliferate and migrate into the lesions (162). They play important roles in vessel remodeling and plaque stabilization by producing extracellular matrix, proteoglycan and other proteins. Increase in lesion collagen enhances the fibrous cap and plaque stability, thus serving to prevent thrombosis (163, 164). Studies showed that the quiescent and fully contractile SMCs in lesions lost the expression of some genes such as smooth muscle α-actin and smooth muscle myosin heavy chain. Also some in vitro studies found that SMCs could induce the expression of macrophage markers such as cluster of differentiation (CD68), macrophage-1 antigen (Mac2) after exposure to cholesterol loading (165). Lesion areas are heterogeneous environments that contain a plethora of molecules including cytokines, inflammatory lipids, growth factors and cell debris. Many factors especially, Platelet-derived growth factor (PDGF), IL-1β, TNFα, oxidized phospholipids, found in

the plaque environment can lead to a switch in the resident SMCs phenotypes. However, more in vivo studies are needed to validate the formation of these SMC lineages (154).

Inflammatory Cells Events such as retention of LPs, activation of endothelial cells due to disturbed laminal flow can provide a trigger for the recruitment of blood monocytes into the lesion area (166). Activated endothelial cells secrete some chemoattractant proteins and also change the expression of their adhesion molecules in order to attract monocytes to the lesion area (167). The internalized monocytes differentiate into macrophages or dendritic cells with the aid of colony stimulating factor or other factors (168). Macrophages found in lesions can secrete proteoglycans that also furthers the ApoB-LP retention (169). Retained and modified LPs are ingested by lesion macrophages through their scavenger receptors. Hence, plaques macrophages become filled with lipid droplets formed in their cytoplasm and have been named 'foam cells'. Activation of lesional macrophages is a critical event that triggers inflammatory processes and leads to atherosclerosis progression, however the mechanisms of macrophage activation are not exactly known (154, 170). Nonetheless, the inflammatory receptors found on macrophages (such as TLRs or NLRs) can be activated by modified LPs and other molecules (171). Mitochondrial oxidative stress is induced by oxidized LPs and sterols and activates the NF-κB pathway, which in turn increases the expression of important chemokines (such as monocyte chemoattractant protein (MCP1) in the macrophages (172). This helps in enhancing the monocyte migration to the lesion. Furthermore, inflammasome activation is seen in atherosclerotic plaques in mice and humans (173). Studies showed that the ingestion of the retained LPs by the macrophages led to the accumulation of cholesterol crystals in these cells. Then, these crystals induced the NLRP3 inflammasome and resulted in the secretion of the inflammatory cytokine, IL-1β. Also, the released mitochondrial DNA from the damaged mitochondria could activate the NLRP3 inflammasome in the stressed macrophages (173, 174). In addition to their inflammatory roles, macrophages can promote plaque vulnerability by inducing necrosis and thinning of the fibrous cap. Macrophages can reduce collagen synthesis in the intimal SMCs or degrade various types of extracellular matrix through the secretion

of matrix-metalloproteinases. Hence, macrophages play a critical role in promoting plaque rupture (153). Various environmental conditions such as prolonged ER stress and oxidative stress promote macrophage apoptosis (175). If the phagocytic clearance (efferocytosis) is defective or insufficient, necrotic cores form in the place of these apoptotic macrophages. There is limited knowledge about the reasons leading to defective efferocytosis and mainly based on the LP-induced removal of an efferocytosis ligands, phospholipase A2, or protease-mediated degradation of efferocytosis receptors, the Mer (Mertk, Nyk, c-Eyk) receptor tyrosine kinase (MerTK) (151, 176). Furthermore, in vivo and in vitro exposure of macrophages to saturated fatty acids have been shown to prevent their ability to be effectively engulfed by apoptotic cells, but the mechanisms are not certain (177).

In addition to macrophages, other inflammatory cells play critical roles in lesion formation and progression. For example, vascular dendritic cells (DCs) are known to be found in atherosclerotic lesions (178). Independent of macrophages, these DCs can initiate an adaptive immunity through their antigen presenting functions. DCs can activate T cells and lead their differentiation into their subtypes (such as T helper cells (Th1), (Th2), Th17 and T regulatory cells (T-reg). In early atherosclerotic lesions Th1 cells are evident and mainly secrete IFN-γ and induce secretion of B-cell produced antibodies against LPs. Th1 cells show pro-atherogenic property by inducing pro-inflammatory cytokine production and B cell function regulation (179). Some in vivo studies also showed that Th2 response was also induced under hypercholesterolemia (179). However, there are some controversial studies on the role of Th2 in atherosclerosis based on the stage of atherosclerosis. Th2 cells were observed to be atheroprotective in early plaque formations and Th2 cells showed anti-atherogenic properties because they could counteract Th1 response induced IFNɣ secretion by secreting IL4. On the other hand, deficiency of IL4 secreted by Th2 led to a decrease in atherosclerosis (180-182). T-reg cells display a protective function by secreting anti-inflammatory IL-10 and TGF-β. They provide balance between Th responses and promote plaque stability affecting collagen content. (183). Natural killer (NK) cells are

another inflammatory cell type seen in early and advanced atherosclerotic lesions. The absence of NKs leads to reduction in atherosclerotic lesion formation (184). Finally, mast cells, found in lesions, have been shown to secrete pro-atherogenic cytokines such as TNF-α, IFNγ after DC connection and monitor Th cell development. (185). Also, mast cells can disturb plaque stability by secreting some proteases (183, 186, 187).

1.4.2. ER stress in Atherosclerosis

Inappropriate activation of UPR pathways are seen in especially in advanced atherosclerotic plaques (188). There are various stressors such as oxidative stress, oxysterols, modified LPs, high level intracellular cholesterol (cholesterol crystal formations) and saturated fatty acids in lesions that can stimulate UPR pathways (189). How, each of the UPR branches contribute to progression of atherosclerosis is not fully understood. There is a close relation between UPR and lipogenic pathways (190). ER stress can lead to increased lipogenesis and accumulation of lipids in hepatic cell. ER stress has also been shown to prevent proper lipoprotein secretion. Additionally, ER stress can disturb insulin signaling, stimulate glucose production and promote hyperglycemia. ER stress connects obesity, diabetes and atherosclerosis through dysregulating lipid and glucose metabolisms and the inflammatory response (73, 81, 191). The ER senses the changes of cellular lipid status and delivers this stress signal to inflammatory and apoptotic pathways (72, 75). For example, ER stress is induced by saturated fatty acids and activates adaptive immunity by stimulating major histocompatibility complex (MHC)-associated antigen presentation (192). Both innate and adaptive immunity play crucial roles in atherosclerosis progression. Thus ER may influence atherosclerosis in various ways. This role of the ER is important for the pathogenesis and progression of many metabolic diseases.

Activation of UPR is also observed in endothelial cells in lesions and in response to various metabolic and physical influences (193, 194). Especially, in the atherosclerosis-

prone regions of vessels, disturbed blood flow leads to the upregulation of ER stress transducers (195). In advanced plaque areas, the expression level of XBP1 is particularly high in ECs. When XBP1 is overexpressed in lesional ECs, the severity of atherosclerosis increases (193). In cultured human aortic ECs, tunicamycin-induced ER stress can activate the production of important cytokines like IL-6, IL-8 and MCP-1. This can be blocked by silencing XBP1 or ATF4 (194). Oxidized and glycated LDLs have been shown to induce UPR pathways through inhibition of an ER calcium pump (196, 197). Also, oxidized 1-palmitoyl-2-arachidonyl-sn-3-glycero-phosphorylcholine (oxPAPC), homocysteine, and hydrolyzed LDL (found in advanced plaques) can induce ER stress and inflammatory pathways, and promote disease progression (198-201).

There is less information about the role of ER stress in SMCs. Studies showed that ER stress induced SMC apoptosis decreased collagen production and led to the thinning of the fibrous cap, promoting plaque rupture (202). 7-ketocholesterol, unesterified cholesterol, homocysteine and glucosamine are the main inducers of ER stress in SMCs. 7-ketocholesterol and unesterified cholesterol mainly found in branched atherosclerosis-prone regions, promote apoptosis by inducing CHOP expression (203, 204).

Homocysteine also leads to the activation of sterol response element binding protein-2 (SREBP) and induce lipid accumulation in cells. Elevation of glucosamine levels in diabetes can also activate UPR in cultured aortic SMCs (205, 206).

Myoishi *et al*. showed that CHOP expression and apoptosis in macrophages increase during atherosclerosis progression in humans (207). ER stress can induce macrophage apoptosis through JNK2 activation, STAT1 and p38 mitogen activated kinase (208). In lipid loaded macrophages, cholesterol is oxidized to oxysterols which are highly toxic molecules, and then oxysterols induce ROS dependent apoptosis (209). Macrophage cell death is a pivotal event in the formation of necrotic cores (210). However further studies are needed to explain the detailed role of UPR arms in ER stress induced inflammatory

and apoptotic mechanisms and their relation with atherosclerosis initiation or progression.

1.4.3. Therapeutic Approaches in Atherosclerosis

Cardiovascular diseases are one of the leading causes of death in the world (138). Only %30 of clinical events can be treated and %10 of the vascular complications occurs in healthy individuals that don't possess any of the well-accepted risk factors (211, 212). In 2020, it is expected that cardiovascular diseases will be the number one killer in the world. Therefore, discovering better molecular targets that can be specifically targeted in therapies is of urgent need. Also, there is an increasing need for developing imaging probes and advanced imaging techniques to analyze lesion compositions in both cellular and molecular levels to guide therapies (213). Currently available therapies are mainly based on reducing hyperlipidemia and preventing thrombotic complications. However, various emerging therapies on novel targets are under investigation (214). Some of the future targeted therapies for atherosclerosis could include nutraceutical supplementation, anti-inflammatory therapies and therapies targeting UPR components (214-216).

Nutraceuticals can be classified as functional foods or dietary supplements, and are natural products. Due to their anti-inflammatory effects, they have been in use for the prevention of atherosclerosis for many years (215, 217, 218). They can provide different benefits at the various stages of atherosclerosis. For example, hydroxytyrosol (polyphenol found in olive oil), flavanols and vitamin C have showed beneficial effects in the prevention of LDL modification. There are many *in vitro* and *in vivo* studies using hydroxytyrosol as a nutraceutical in atherosclerosis (219, 220). A reduction in plaque size was observed after hydroxytyrosol treatment of rabbits fed with atherogenic diet (221). Flavanols, hydroxytyrosol, poly-unsaturated fatty acids such as Omega-3, Omega-6, Allicin provide benefits in the prevention of pro-inflammatory gene expression and monocyte recruitment in atherosclerotic lesions (215, 222). The balance between

Omega-3 and Omega-6 is very important for cardiovascular health (223). Recently, palmitolate (Omega 7) was also shown to reduce atherosclerosis (224). Allicin (H_2S donor) is mainly found in garlic and has an important function in anti-atherogenic and anti-inflammatory processes (225). H_2S donors can prevent foam cell formation in macrophages *in vitro* conditions and reduce atherosclerotic plaque size in $ApoE^{-/-}$ deficient mice that is supplemented with them, compared with control group (226, 227). Plant-derived phytoserols have similar chemical structures to cholesterols. Dietary uptake of phytoserols can reduce cholesterol uptake and show cardioprotective function (228). Vitamin C and vitamin E are also shown in some *in vivo* studies to have anti-inflammatory and anti-atherogenic effects (229, 230). In addition to these nutraceuticals, dietary fibers that are produced by the gut microbiota have shown anti-atherogenic and anti-inflammatory properties in both *in vivo* and *in vitro* studies (231). Furthermore, there are also some alternative, less-studied nutraceuticals such as, carnosine (antioxidant mainly found in meat), coenzyme Q_{10} (antioxidant), curcumin (found in turmeric), resveratrol (natural phenol found in grapes). They show strong anti-oxidant activity or anti-inflammatory activity or both activities (232-236).

Many of the emerging therapies for atherosclerosis target the inflammatory processes, because unresolved inflammation plays a critical role in atherosclerosis progression. Several new anti-inflammatory drugs are under clinical development and the most promising ones are; phospholipase A2 inhibitors, leukotriene pathway inhibitors, CCL2-CCR2 pathway inhibitors, anti-TNFα agents and IL-1β antagonists (237-242). Statins are known for their ability to decrease cholesterol synthesis; however, clinical studies now show that they also have anti-inflammatory functions. They can limit macrophage growth and disturb MMP secretion capability. Also, they inhibit T cell activation and differentiation towards Th1 (242-244). Phospholipase A2 superfamily is an important enzyme family for phospholipid modifications in LPs. They can turn LPs into highly atherogenic particles and, so targeting this enzyme can be beneficial in atherosclerosis. Unfortunately, due to the complex nature of this superfamily, clinical findings are limited (245). Arachidonate 5-lipoxygenase (5-LO) activating protein (FLAP) and 5-LO

are used as leukotriene pathway inhibitors in clinical trials. Leukotrienes (LTs) lead to accumulation of leukocytes in the inflammation area. Many animal and human studies showed that inhibition of LT pathways can provide beneficial effects in treatment (246-249). Role of CCL2-CCR2 pathway is also well-documented in atherosclerosis development. Targeting this pathway could reduce cardiovascular events in patients. However, CCR2 antagonism can also increase susceptibility to infection because of its major role in immunity (239, 250, 251). There are also some clinical trials that target IL-1β and TNFα. Indeed, anti-TNFα drugs and IL-1β antagonists can reduce inflammation and improve vascular function (241, 251).

In recent years, there has been growing attention on ER stress pathways in complex diseases. ER stress response pathways are initiated to sustain cellular homeostasis in the cells; however, prolonged or severe ER stress can engage apoptotic and inflammatory pathways (252, 253). In many stages of atherosclerosis and many plaque cell types, the expression of ER stress markers is seen and reduction of ER stress can alleviate atherosclerosis in mouse models. Furthermore, in human atherosclerotic disease, ER stress is associated with plaque vulnerability and rupture (254-256). Therefore, targeting ER stress pathways can have a therapeutic value in cardiovascular disease. One of the strategies to alleviate ER stress involves the use of chemical chaperones. For example, phenylbutyrate (PBA) and TUDCA are chemical chaperones that mimic cellular chaperones by promoting protein folding (257). PBA was shown to reduce saturated fatty acid-induced ER stress in macrophages and also reduce atherosclerosis in $ApoE^{-/-}$ mice models, however in diabetes-induced atherosclerosis mouse models, PBA was not as effective (258). TUDCA has also been used in atherosclerotic mouse models and shown to alleviate both lesional ER stress and total lesion area (257). Other emerging therapies are based on UPR modulators such as, salubrinal, guanabenz or sephin1 (specific inhibitors for Eif2α phosphatases), and SB203580 (targets CHOP mediated signaling) and SP600125 (JNK inhibitor) (259-262). Although various emerging anti-atherosclerotic therapies are considered to reduce ER stress, there are limitations and challenges in modulating the UPR. For example, the homeostatic UPR signaling can

switch from pro-survival to pro-apoptotic and the control over this decision is not fully understood at the molecular level (252). Also, it is not clear if all or some and how the different UPR arms contribute to the atherogenic process. Also, UPR activation may have beneficial effects in one cell type but detrimental ones in another. On the other hand, UPR inhibitors that are kinase inhibitors can have off-target effects as well as some side-effects. Although chaperones can restore impaired ER folding capacity under prolonged stress conditions, there are serious limitations due to their limited efficacy. High doses are needed to provide these desired therapeutic effects and it is not clear what their molecular target is in most cases (263). There are ongoing studies based on the usage of tissue specific, therapeutic agent-loaded nanoparticles. They induce inflammatory resolution in atherosclerotic plaques through anti-inflammatory cargo loaded, atherosclerotic region specific nanoparticles (264). Perhaps, this kind of an approach can be better fit to modulate a specific UPR arm in a specific lesion cell type for future atherosclerosis treatment. Ongoing studies are investigating the specific contribution and cell-type role of the activated UPR arms to disease progression. Therefore, in the future there will be more knowledge about how to best modulate the UPR signaling in cardiovascular disease.

1.5. Hypothesis and Aim of the Study

There is a strong connection between metabolism and immunity. Both overnutrition and malnutrition have immunological consequences. This connection can be called metaflammation. In this thesis I am focusing on the effect of overnutrition complications on immune response. It is known that obesity is related to aberrant immune activation and increases the risk of immune diseases. In cellular level, there are two important organelles that form a bridge between metabolic overloading and immune activation. ER and mitochondria, individually or by association, regulate immunological response under metabolic overloading. ER activates three important signaling pathways that are initiated from ER membrane and go through the nucleus to activate important transcription factors. Also under stress conditions crosstalk between ER and mitochondria can regulate important inflammatory and apoptotic pathways. However there are some missing players in nutrient overloading induced stress conditions.

IRE1, the main ER stress signaling pathway on ER membrane, is the focus of this thesis. Through its RNase and kinase domains, it plays important roles in immune activation and apoptosis under prolonged ER stress conditions. Thus, we hypothesized that we could protect the cell from metabolic stress induced inflammation by specific pharmacological modulation of IRE1 RNase function. Furthermore, we could prevent progression of metabolic disease atherosclerosis in which metabolic exposure to lipids activates ER stress and initiates inflammatory response.

As a first step, I wanted to analyze the specific role of the IRE1 RNase activity on transcriptional signature of pro-atherogenic genes and conducted RNA-seq analysis in bone marrow derived macrophage cells. Then I tested the immunological effects of IRE1 RNase domain under lipid induced ER stress conditions in both BMDM cells and human PBMCs.

Current state of literature reflected that the connection between ER stress and mitochondrial stress induced ROS production played an important role on immune activation, specifically on inflammasome activation. To further clarify the role of IRE1 RNase activity on inflammasome activation and mitochondrial ROS production under ER stress conditions, I conducted *in vitro* immunostaining experiments for detection of mitochondrial ROS production and searched new players that both regulated mtROS production and they were regulated by IRE1 RNase function.

After testing specific functions of IRE1 RNase activity *in vitro*, I decided to test whether pharmacological inhibition of IRE1 RNase activity could affect atherosclerosis progression through altering immunological state in atherosclerosis plaque structures. For this purpose I used IRE1 RNase domain specific drugs; STF-083010 and 4μ8c. $ApoE^{-/-}$ mice were used as an atherosclerotic mouse model and they were fed with high cholesterol western type diet. After the initiation of plaques, STF-083010 and 4μ8c were intraperitoneally injected into the mice. For the analysis of the results, I performed (i) immunohistochemistry stainings on both *en face* aorta and heart sections (aortic sinus part), (ii) I performed immunofluorescence staining on heart sections for the analysis of plaque composition, (iii) I also analyzed blood plasma samples for both immunological markers and lipoprotein profile, both were important for atherosclerosis progression and (iv) I further analyzed the different Th type immune response markers on splenocytes of control and drug treated animal groups.

Chapter 2.

Materials and Methods

2.1. Materials

2.1.1. Reagents

General laboratory chemicals and reagents are listed in Table 2.1

Table 2.1. Chemicals, reagents, kits used for general laboratory purposes

Product	Provider	Catalog No.
β-mercaptoethanol	Sigma-aldrich	63690
Acrylamide %40 solution(acrylamide-bisacrylamide)	Fisher scientific	BP1408-1
Amersham ECL Prime Western Blotting Detection Reagent	GE Healthcare	RPN2236
Chloroform	Sigma –Aldrich	24216
Ethanol Absolute	Sigma –Aldrich	32221
Ethylenediaminetetraacetic acid (EDTA)	AppliChem	A3562,1000
Formalin Solution 10 %	Sigma-Aldrich	HT501128-4L
DAPI	Abcam	Ab104139

Product	**Provider**	**Catalog No.**
Glycine	Glentham	GM2385
HEPES Buffer, 1M stock in normal saline	Lonza	17-737F
Ampicillin Sodium Salt	Cayman	69-52-3
Bovine Serum Albumin (BSA)	Santacruz	Sc23234
DC Protein Assay Reagents Package	Biorad	5000116
NucleoBond Xtra Midi	Macherey Nagel	740410100
PageRuler Prestained Protein Ladder,	Thermo Fisher Scientific	26620
Protease inhibitor cocktail EDTA free	Sigma	P8340-5ML
Phosphatase inhibitor cocktail3	Sigma	P0044
PVDF Transfer Membrane	Pierce–Thermo Scientific	88518
Roche Light cyler 480 SYBR Green Master Mix	Roche	4887352001
OCT compound Containing -Tissue Tek	SAKURA Tissue TEK	4583
Tris Base	Sigma	T1503
Triton X-100	AppliChem	A1388,0500
Trisure	BIOLINE	Bio 38033

2.1.2. Cell culture chemicals and reagents

Table 2.2. Chemicals, reagents, kits and media used in cell culture

Product	Provider	Catalog number
DMEM 4.5g/L Glucose w/ U1	Lonza	BE12-604F/U1/12
RPMI	Gibco	21875091
Polyethylamine	PolySciences	33966
Bovine Serum Albumin (BSA) Fatty Acid Free	Sigma	A7030-500G
Fetal bovine serum (FBS)	Gibco	10270-106
Penicillin Streptomycin 10000U/ml	Gibco	15140-122
Trypsin-Edta (0,25%) phenol red	Gibco/ Thermo Fisher	25200-056
Dimethyl sulfoxide (DMSO)	Sigma	472301
Dulbecco's Phosphate Buffered Saline (DPBS)	Gibco	14190094

2.1.3. Antibodies

Antibodies used in Western blot, immunofluorescence and FACS analysis are listed in Table 2.3.

Table 2.3. Antibodies used in study

Western Blot Antibody	**Provider**	**Catalog Number**	**Conditions**
B-Actin	Santa Cruz	sc-47778	1hr RT
Total IRE1	Cell Signaling	3294	o/n 4 ^{o}C
P-IRE1	Abcam	Ab124945	1hr RT
Caspase1	Santa Cruz	M20; sc-514	o/n 4 ^{o}C
IL-1β	Abcam	ab9722	o/n 4 ^{o}C
Goat Anti-rabbit IgG-HRP	Santa Cruz	sc2004	1hr RT
Goat Anti-mouse IgG-HRP	Santa Cruz	sc2005	1hr RT
Immunofluorescence Antibody	**Provider**	**Catalog Number**	**Conditions**
Moma-2	Abcam	ab33451	o/n 4 ^{o}C
IL-1β	Abcam	ab9722	o/n 4 ^{o}C
α-SMA	Abcam	ab5694	o/n 4 ^{o}C
anti-CD3-Alexa488	Biolegend	100212	1hr 37 ^{o}C
FACs Antibody	**Provider**	**Catalog Number**	**Conditions**
Zombie Green	BioLegend	423111	30min 4 ^{o}C
PerCP-Cy5.5-conjugated antiCD4	BD Bioscience	550954	30min 4 ^{o}C
APC-conjugated IFNγ	BD Biosciences	554413	30min 4 ^{o}C
PE-conjugated IL-17A	BD Biosciences	559502	30min 4 ^{o}C
PE-conjugated IL-4 antibodies	BD Biosciences	554389	30min 4 ^{o}C

2.1.4. Solutions

Solutions used in the study summarized in Table 2.4

Table 2.4. Solutions used in study

Buffer	**Composition**
5X Laemmli lysis buffer	10% SDS, 50% glycerol, 25% 2-mercaptoethanol, 0.02% bromphenol blue and 0.3125 M Tris HCl, pH approx. 6.8.
10X SDS Running Buffer	30g Tris-Base, 144g Glycine, 10gr SDS 1L dH_2O
10X SDS Transfer Buffer	30g Tris-Base, 144g Glycine
10X TBS	1.5 M NaCl (87.76 g), 100 mM Trizma Base adjust pH 8.0 with 1N HCl complete volume to 1 liter with ddH2O
1X TBS-T	450 ml ddH_2O, 50 ml 10x TBS, 500 µl Tween
10X PBS	80 g NaCl, 2 g KCl and 15.2 g sodium phosphate dibasic dehydrate to 1L dH_2O, pH to 7.4
HBS Buffer for Electroporation(Instead of R Buffer **)**	21 mM commercial HEPES (pH; 7.05), 137 mM NaCl,5 mM KCl,0.7 mM Na_2HPO_4,6 mM Glucose. Before using, filter and and keep at 4°C.
10% Resolving Gel	2,5 ml 40% Acrylamide mix, 2,5 ml 1.5 M Tris-HCl (pH: 8.8), 100 ul 10% SDS and 100 ul 10% Ammonium persulfate, 4 ul 0.08% TEMED; completed to 10 ml with ddH2O
5 % Stacking Gel	620 ul 40% Acrylamide mix, 630 ul 1.5 mM Tris-HCl (pH: 6.8), 50 ul 10% SDS and 50 ul 20% Ammonium persulfate, 5 ul 0.1% TEMED; completed to 5 ml with ddH2O
1.5 M Tris-HCl (pH: 6.8)	12 g Tris Base (Trizma) is dissolved with 60 ml ddH2O, pH is adjusted to 6.8 with 1 N HCl and volume is made up to 100 ml with ddH2O.
1.5 M Tris-HCl (pH: 8.8)	54.45 g Tris Base (Trizma) is dissolved in 150 ml ddH2O, pH is adjusted to 8.8 with 1 N HCl and volume is made up to 300 ml with ddH2O. It is stored at 4 °C.

Phospholysis Buffer	50 mM HEPES (pH: 7.9), 100 mM NaCl, 4 mM Tetra Sodium pyrophosphate (Na4P2O7), 10 mM EDTA, 10 mM NaF, 1% Triton, 2 mM Sodium orthovanadate (Na3VO4), 1 mM phenylmethanesulfonylfluoride (PMSF), Phosphatase Inhibitor Cocktail 3 (Sigma, P0044) and 1X Protease Inhibitor Cocktail (10μM/ ml)

2.1.5. Bacterial Strains

Plasmids encoding XBP1s (21833) and WT IRE1α (13009) were purchased from Addgene.

2.1.6. Cell lines and Their Growth Conditions

IRE1$^{-/-}$ MEFs were provided by Gokhan Hotamisligil, Harvard School of Public Health. They were grown in DMEM with %10 FBS.

BMDMs were isolated from C57BL/6 mice. They were grown in RPMI medium enriched with 15% L929 conditioned medium and 1% P/S, %10 FBS.

2.1.7. IRE1 RNase Inhibitors

STF-083010, (N-[(2-Hydroxy-1-naphthalenyl) methylene]-2-thiophenesulfonamide), IRE1 RNAse inhibitor, was purchased from SIGMA-ALDRICH (SML-0409), Santa Cruz (sc-474562) and Atamol (AT50112). It was dissolved in DMSO.

4μ8c, 7-Hydroxy-4-methyl-2-oxo-2H-1-benzopyran-8-carboxaldehyde, IRE1 RNase inhibitor, was purchased from Calbiochem (412512) and Sigma (SML0949) dissolved in DMSO.

2.2. Methods

2.2.1. Cell Culture and Treatments

Isolation of BMDM Mouse tibia and femurs were dissected, separated from muscle tissue and placed in PBS. After cutting distal ends of femurs and tibiae, the bone marrow was flushed with RPMI with a 25G needle. The bone marrow was collected into RPMI including 1% Penicillin/streptomycin (P/S) cocktail and passed through a cell strainer (BD, 352350). This was followed by centrifugation at 400 x g for 5 minutes at 4^{o}C. After centrifugation, the cells were resuspended in RPMI1640 medium containing 1% Penicillin/streptomycin (P/S) cocktail with 15% L929 conditioned medium and 10% FBS. The cells were seeded for growth on plates until differentiation into macrophages for 7 days.

Inflammasome activation We pre-treated BMDMs with 100 μM STF-083010 for 1 hour or with indicated concentrations of 4μ8c, then stimulated with 200 ng/ml ultrapure Lipopolysaccharide (LPS) for 3 hours. Then, we treated them with 1000μm palmitate-BSA for 20 hours. We used human peripheral blood mononuclear cells (PBMCs), purchased from Zenbio (Research Triangle Park, NC, USA) and grown in Lymphocyte Medium (RPMI 1640, 2mM L-Glutamine, 10% Fetal Bovine Serum, and 1% P/S) according to instructions provided by the manufacturer. We pre-treated cells with 100 μM 4μ8c before stimulation with ultrapure LPS (200 ng/ml) for 3 hours. This was followed by treatment with ethanol-BSA (control) or palmitate (PA)-BSA (500 μM).

Induction of mtROS We pre-treated BMDMs for 1 hour with 100 μM 4μ8c, followed by sequential stimulation with 200 ng/ul LPS (3 hours). Then, we treated them with 1000 μM PA/BSA or ethanol-BSA (control) for 20 hours.

2.2.2. Preparation of Palmitate-Bovine Serum Albumin Complex

Palmitate (PA) was prepared as 500 mM stock solution by dissolving it with absolute ethanol and stored at −80 °C. To obtain a working concentration, we diluted into 1% fatty acid free BSA in RPMI1640 medium (without serum) and warmed at 50°C for 30 minutes with occasional vortexing.

2.2.3. Preparation of Cholesterol Crystals

Cholesterol was prepared as 10 mg/mL stock solution in ethanol and heated to 60 °C. Then it was brought to room temperature to allow the crystallization process. After taking out the cholesterol crystals, we washed them with PBS and prepared working concentrations by suspending them in RPMI-1640 medium at 5 mg/ml. In our treatments, we used 400 μg/mL cholesterol crystals for 20 hours as described (265).

2.2.4. Quantification of Mitochondrial ROS Production (mtROS)

mtROS production was measured with MitoSOX™ Red mitochondrial superoxide indicator (M36008, Life Technologies) according to the protocol provided by the company. Representative images were acquired with a confocal microscope (Zeiss, LSM 510) and analyzed with ImageJ (National Institutes of Health).

2.2.5. Western Blot Analysis

We lysed cells in the phospholysis buffer (50 mM (4-(2-hydroxyethyl)-1-piperazineethanesulfonic acid (HEPES) pH 7.9, 100 mM sodium chloride, 10 mM ethylendiamine tetraacetic acid (EDTA), 10 mM sodium fluoride, 4 mM tetrasodium

diphosphate, 1% Triton X-100, 2 mM sodium orthovanadate, 1mM phenylmethanesulfonyl fluoride (PMSF), 1X phosphatase inhibitor cocktail and 1X protease inhibitor cocktail). We centrifuged the lysates to clear them from cellular debris. After measuring their concentrations with DC Protein Assay Reagents Package (BioRAD), we added 5X SDS loading dye. For the detection of cleaved caspase-1 (active p10 form) in the cell medium, we collected cell culture supernatants and mixed them with 2X SDS loading dye. These were then heated at 95°C for 5 minutes before loading on SDS-PAGE gels. After performing SDS-PAGE separation we transferred proteins onto PVDF membranes. For blocking and antibody incubations we used TBS with 0.1% Tween-20 (v/v) and 5% (w/v) dry milk or BSA. We visualized antibody detected bands on the PVDF membranes by using the ECL prime reagent (Amersham) on a BioRAD chemiluminescence imager.

2.2.6. Transfection

We transfected indicated plasmids into IRE1$^{-/-}$ MEFs with polyethylenimine (Sigma). Transfection was performed when cells reached 60-80% confluency. We used 2μg DNA for every 4.5x10^5 cells. For BMDMs, we used the electroporation method suggested for this cell type by the Neon electroporation system (Invitrogen MPK10096) according to protocols provided by the manufacturer.

2.2.7. RNA Interference

In the RNA silencing experiments, we used indicated siRNA reagents; 50 nM siRNA against *IRE1* (Qiagen; SI0099588), 70 nM siRNA against *XBP1* (Qiagen; SI01473227), 100nM siRNA against *LONP1* (Qiagen SI01390298) or scrambled siRNAs (Qiagen; 1027281). We treated cells with indicated reagents mentioned in cell culture and cellular treatments were done 24 hours after transfection.

2.2.8. RNA Isolation and Quantitative RT-PCR

Total RNA from cells were isolated using Trisure (Bioline) according to protocol in the reagent data sheet. We used Revert Aid First strand cDNA synthesis kit (Thermoscientific; K1691) for reverse-transcription of RNA into cDNA according to the manufacturer's protocols. qRT-PCR reactions were performed using specific primers and Roche Sybergreen on a Rotor Gene (Qiagen). The primers were shown in Table 2.5.

Table 2.5. Real Time PCR primers

Gene	Forward	Reverse
Human		
GAPDH	GACCACAGTCCATGCCATCACT	TCCACCACCCTGTTGCTGTAG
XBP1	TGCTGAGTCCGCAGCAGGTG	GCTGGCAGGCTCTGGGGAAG
CCL2	CTTCTGCGCCTGCTGTTCA	CCAGCCTACTCATTGGGATCA
IL-1β	TTACAGTGGCAATGAGGATGAC	GTCGGAGATTCGTAGCTGGAT
Mouse		
XBP1	TGAGAACCAGGAGTTAAGAACACGC	CCTGCACCTGCTGCGGAC
GAPDH	GTGAAGGTCGGTGTGAACG	GGTCGTTGATGGCAACAATCTC
CCL2	CTTCTGGGCCTGCTGTTCA	CCAGCCTACTCATTGGGATCA
IL-1β	CAACCAACAAGTGATATTCTCCATG	GATCCACACTCTCCAGCTGCA
MMP9	CTGGACAGCCAGACACTAAAG	CTCGCGGCAAGTCTTCAGAG
S100A8	AAATCACCATGCCCTCTACAAG	CCCACTTTTATCACCATCGCAA
β-ACTIN	TTCGTTGCCGGTCCACACCC	GCTTTGCACATGCCGGAGCC
GAPDH	TGAGAACCAGGAGTTAAGAACACGC	CCTGCACCTGCTGCGGAC
PDGFRB	AACCCCCTTACAGCTGTCCT	TAATCCCGTCAGCATCTTCC
SCARA3	TGCATGGATACTGACCCTGA	GCCGTGTTACCAGCTTCTTC
TXNIP	TCTTTTGAGGTGGTCTTCAACG	GCTTTGACTCGGGTAACTTCACA

ΔΔCt method was used for quantifications. We used GAPDH and β-actin transcript levels for normalization based on LifeSciences-Roche website instructions.

(http://plantbio.okstate.edu/resources/PCR_Core/Roche_RealTime%20PCR%20Application%20Manual.pdf). For fold-change calculations we used the following formula; (Primer efficiency)-ΔΔCt where ΔΔCt means ΔCt (target gene) - ΔCt (reference gene) and Ct means (threshold cycle). Results were analyzed from three or more independent experiments using the Student's t-test.

2.2.9. Mitochondrial Calcium Measurement

RHOD-2AM (Thermo Scientific) was used for Mitochondria specific calcium measurement. 5x10^5 cell / well was seeded to 12 well cell culture plates and then subsequent treatments were performed. Cells were stained with 2, 5 uM RHOD-2 AM in %10 FBS and %10 glucose containing calcium free PBS at 37^0C for 30 minutes. Cells were washed once with the same medium and then kept in 1uM EDTA containing %10 PBS for 10 minutes. Finally, they were washed with %2 FBS containing PBS. For reading in fluorescence-activated cell sorting (FACs) they were placed in % 2 FBS containing FACS buffer and signal is measured at excitation: 552nm and emission: 581 with PE filter at Beckman Coulter CytoFlex Flow Cytometry Instrument (266).

2.2.10. RNA-Sequence: Library Preparation and Sequencing

Total RNA isolation was done using Trisure (Bioline) prior to RNA-sequencing. For this purpose, control (DMSO treated) and IRE1-inhibited (with STF-083010) BMDM cells were used. After isolation, we treated the RNA samples with 20U of DNase I (New England Biolabs) to remove any genomic DNA contamination. The RNA concentrations were measured using a NanoDrop (ND-2000) Spectrophotometer. RNA quality was checked in an Agilent Technologies 2100 Bioanalyzer. Then, we depleted ribosomal

RNA from 5 micrograms of total RNA using the Ribo-Zero Gold rRNA Removal kit (Epicentre Biotechnologies) based on the manufacturer's recommendations. Sequencing libraries (for whole transcriptome analysis) were prepared using ScriptSeqTM v2 RNA-Seq Library Preparation Kit (Epicentre Biotechnologies) following the manufacturer's recommendations. After 3′-terminal tagging, the di-tagged cDNA was purified using column concentrators (DNA clean-up and concentrators, Zymo Research). The cDNA libraries were barcoded to allow sample multiplexing using ScriptSeqTM Index PCR Primers (Set 1) (Epicentre Biotechnologies). The libraries were amplified by 12 cycles of PCR and the amplified libraries were size selected and purified using 8% TBE acrylamide gels. Agilent Technologies 2100 Bioanalyzer was used for the quantification of the libraries. Up to four RNA-seq Libraries were then multiplexed in a single lane of an Illumina HiSeq2500 deep-sequencer flow cell (UCSF Center for Advanced Technologies) and sequenced using 50 bp single-end sequencing chemistry.

2.2.11. RNA Sequencing Data Processing

The FastQ/A clipper found in the FastX toolkit (http://hannonlab.cshl.edu/fastx_toolkit/) was used for the removal of the 3' adapter sequences (AGATCGGAAGAGCACACGTCTGAAC) from the sequenced libraries after de-multiplexing, and only read longer than 20 nucleotides were kept for alignment. The adapter-stripped reads were then aligned the Bowtie indices for the mouse genome reference version 10 of the University of California Santa Cruz Genome Browser (mm10), using the splice junction mapper Tophat2 v2.0.9 and the sequence aligner Bowtie 2 V2.2.3.0. Using default parameters, the transcript assembler Cufflinks V2.1.1 was then used on the list of mapped reads to assemble and quantify transcripts using an mm10 reference annotation and masking mitochondrial, rRNA, and tRNA sequences. To estimate the changes in gene expression levels, the number of sequenced reads that align to a gene of interest was then compared among biological samples using Cuffdiff (default parameters). Changes in the levels of expression of normalized Cufflinks-

quantified transcripts are expressed as FPKM/RPKM (reads per kilobase per million reads mapped) values, which are widely, used gene expression profiling by RNA-seq.

2.2.12. Flow Cytometric Analysis of Intracellular Cytokine Staining

We isolated fresh splenocytes from mouse spleens and then removed erythrocytes using a hypotonic, cell lysis buffer. We stimulated cells for 4 hours with phorbol-myristate-acetate (PMA) (50 ng/ml, Abcam) and ionomycin (1μg/ml, Abcam) in the presence of Golgistop (BD Biosciences). We stained the cells with zombie green (BioLegend) in order to discriminate live cells from dead ones. Also PerCP-Cy5.5-conjugated CD4 antibody (BD Biosciences) was used for cell surface staining followed by incubation in Cytofix/Cytoperm solution (BD Biosciences) at room temperature for 20 minutes. Then cells were washed with the permeabilization buffer. For staining of intracellular cytokines (IL-4 and IFNɣ), Allophycocyanin (APC)-conjugated) IFNγ, PE-conjugated IL-17A and PE-conjugated IL-4 antibodies (all from BD Biosciences) were used. Data were analyzed on BD Accuri C6 software.

2.2.13. Measurement of Secreted IL-1β and IL-18 and CCL2 Cytokines

We used commercial ELISA kits for detection of secreted cytokines in mouse plasma or from conditioned medium as follows; mouse IL-1β Elisa Kit (Abcam), human IL-1β Elisa Kit (Abcam), mouse IL-18 ELISA Kit (Medical & Biological Laboratories) and a mouse CCL2 Elisa Kit (Abcam).

2.2.14. Animal Study Design

For our atherosclerosis experiments, we used ApoE$^{-/-}$ (Charles River WIGA GesmbH, Sulzfeld, Germany). We put male mice (7 to 8 weeks of age) on a Western-type diet (TD88137 mod. containing 21% fat and 0.2% cholesterol) (Ssniff, Soest, Germany) for 6 weeks. Then, we started intraperitoneal injections of STF-083010 (10 mg/kg) or DMSO in 16% Cremophor EL (Sigma) saline solution as described previously (267). We continued the diet and injections for 6 weeks.

Alternatively, ApoE$^{-/-}$ mice were fed a Western diet for 8 weeks, and we began injecting 4μ8c (10 mg/kg) or DMSO in 16% Cremophor EL saline solution to the mice as described previously (134, 268) for 4 weeks while mice were continued on Western diet. We measured weights every other day. Also, we measured blood glucose concentrations only before and after treatments. At the end of the experiment, mice were anaesthetized and blood was collected by cardiac puncture. We collected the following tissues; adipose, spleen and liver, and immediately froze them in liquid nitrogen followed by storage at -80 ^{0}C. After collecting the tissues, we performed perfusion with ice-cold PBS and heparin (1000 U/ml), followed by 10% formalin solution. After this fixation step, we carefully dissected the aorta, immediately immersed in 10% formalin and stored at 4° C until analysis. After removing the heart from proximal aorta, we placed it in a tissue mold with correct orientation, and covered with OCT (Tissue-Tek) and froze in ice-cold isobutane solution, followed by storage in at -80 ^{0}C. We performed all animal experiments according to approved protocols by the experimental animal care committee at Bilkent University.

2.2.15. Staining of Cryosections

By using a cryostat (Leica CM1850), we cut 7 μm thick cryosections from the aortic roots of the frozen heart tissues and stained with; Oil red O (ChemCruz, 1320-06-5), Masson's trichrome (BioOptica 04-010802), Hemotoxylin and eosin (Mayer), anti-

MOMA-2 (1:50, ab33451; Abcam), anti-CD3-Alexa488 (1:400; Biolegend), TUNEL kit (11684795910; Roche), anti-α-SMA (1:150, ab5694; Abcam) and IL-1β antibody (1:100, ab9722, Abcam).

Immunofluorescent stainings of lesions Antibody concentrations and incubation times of used in fluorescence stainings were explained in both the materials part and above in detailed. After staining, tissues were mounted with an antifade reagent including DAPI (GR211467-2, Abcam). Representative images were taken with a Zeiss fluorescent microscope.

Immunohistochemical stainings For quantifications of lipid loaded plaques area, we stained heart tissue sections with Oil red O. Four consecutive aortic root cryosections taken from every 60 μm (in the first 180 μm) beginning at the aortic cusp were used in staining based on the previously published protocols (267). Masson's trichrome staining was used to quantify lesion collagen content according to manufacturer's protocol (Bio-Optica). For the quantification of total lesion area and necrotic core, we stained heart sections with Hematoxylin and eosin according to published protocols (224) . All quantifications were performed using ImageJ (NIH). Percentage of average cross-sectional stained area per leaflet was calculated from all three valves.

2.2.16. En Face Aorta Staining

We removed all adventitia and fat tissue from aorta carefully under a stereo-microscope (S8APO model; Leica, Berlin, Germany). After cleaning, we cut open the full aortas longitudinally and pinned them on a black wax surface. For the quantification of lipid accumulated lesion area, we stained them with Sudan IV (Sigma Aldrich 198102) as described earlier (269). We captured representative images with a stereomicroscope (Leica MC-120) attached to a HD digital camera. ImageJ software was used for the

quantification of Sudan IV–stained lesion areas and we represented the results as percent stained area relative to total aortic area according to published protocols and (269).

2.2.17. Plasma Measurements

Mouse Metabolic Phenotyping Center at the University of Cincinnati conducted all experiment for analysis of both the size distribution of lipoproteins and cholesterol or triglyceride amount in them. Fast-performance liquid chromatography (FPLC) was used for analyzing the size distribution of lipoproteins. Microtiter plate enzyme-based assay was used for the resolution of major lipoprotein classes from plasma; the columns were equilibrated in 50 mM phosphate-buffered saline. Furthermore they performed cholesterol or triglyceride assays from collected fractions of major lipoprotein classes.

2.2.18. Statistical Analysis

Values are expressed as mean ± SEM (Standard error of the mean). No samples were treated as outliers and left out of analysis. Statistical significance was evaluated using the Student's *t* test or Mann Whitney test (for *in vivo* analysis, as indicated in the figures). $P<0.05$ were considered as significant.

Chapter 3.

Results

3.1. Regulation of pro-atherogenic gene expression by IRE1's endoribonuclease activity

3.1.1. Transcriptome analysis in macrophages treated with an IRE1 endoribonuclease inhibitor

IRE1, an ER stress sensor in the UPR pathway, can regulate a wide variety of functions in the cell ranging from pro-survival to apoptosis. Studies show kinase and endoribonuclease (RNase) functions of IRE1 can initiate different downstream effects in cells (27, 270). For example, IRE1 can initiate inflammatory pathways through its kinase domain associated proteins (271, 272). A few studies also attribute a role for IRE1's RNase activity in inflammatory pathways, but these are mainly focused on the RIDD function of this domain and were found to be dependent on the regulation of TXNIP expression (133). In order to identify the full scope of IRE1's RNase function in an inflammatory cell, macrophage, I performed RNA sequencing in in bone marrow derived macrophage cells obtained from mice and treated with a specific IRE1 RNase inhibitor. To capture IRE1 regulated genes in normal conditions, I treated BMDMs for 6 hours with the IRE1 RNase inhibitor, STF-083010, and without inducing a global ER stress response. The differentially regulated genes were analyzed by RNA sequencing. I filtered all of the differentially changed genes based on p value ($p<0.05$) and the fold-change ratio (fold change>1.5). As a result, I identified 169 overexpressed genes and 135 downregulated genes upon IRE1 inhibition and when compared to control group (Figure 3.1A, Appendix A, Table A1, A2, A3, A4). I further analyzed the downregulated

genes by using Ingenuity Pathway Analysis (IPA) tool and categorized them based on their relation with disease processes. I identified many pro-atherogenic genes such as important cytokines, chemokines and their receptors were downregulated with the inhibition of IRE1 RNase activity (Figure 3.1 B).

A

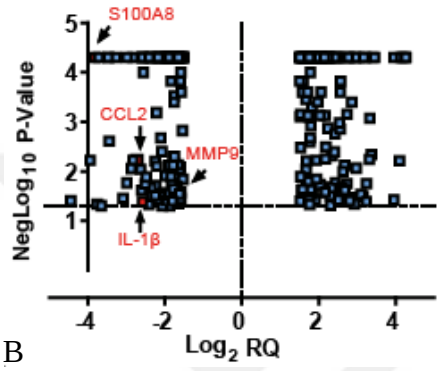

B

Symbol	Entrez Gene Name	Expression value	
		Fold Change	p-value
S100A8	s100 Calcium Binding Protein A8	-3,83	5,00E-05
CCR2	Chemokine (C-C) Motif Receptor 2	-2,98	5,00E-05
CCL2	The chemokine (C-C motif) ligand 2	-2,73	6,00E-03
IL-1β	Interleukin 1, Beta	-2,58	4,09E-02
CCR3	Chemokine (C-C) Motif Receptor 3	-2,48	1,30E-02
PLA2R1	Phospholipase A2 Receptor 1	-2,04	2,72E-02
ITGA4	Integrin, Alpha 4	-1,93	5,00E-05
MMP9	Matrix Metallopeptidase 9	-1,62	3,91E-02

Figure 3.1. IRE1 RNase activity regulates the expression of multiple pro-atherogenic genes in BMDM cells.
(A) Volcano Plot analysis of upregulated and downregulated genes. **(B)** IPA tool analysis of pro-atherogenic genes that are downregulated with IRE1 inhibition.

Next, by using quantitative reverse transcription polymerase chain reaction (qRT-PCR) method, I validated these pro-atherogenic genes in BMDMs. The results showed that inhibition of IRE1 RNase activity significantly decreased the expression of proatherogenic genes such as (A) matrix metalloprotease-9 (MMP9), (B) calgranulin A (S100A8), (C) C-C Motif Chemokine Ligand 2 (CCL2) and (D) interleukin-1β (IL-1β) ($p<0.01$, $p<0.01$, $p<0.001$, $p<0.05$, respectively) (Figure 3.2 A,B,C,D).

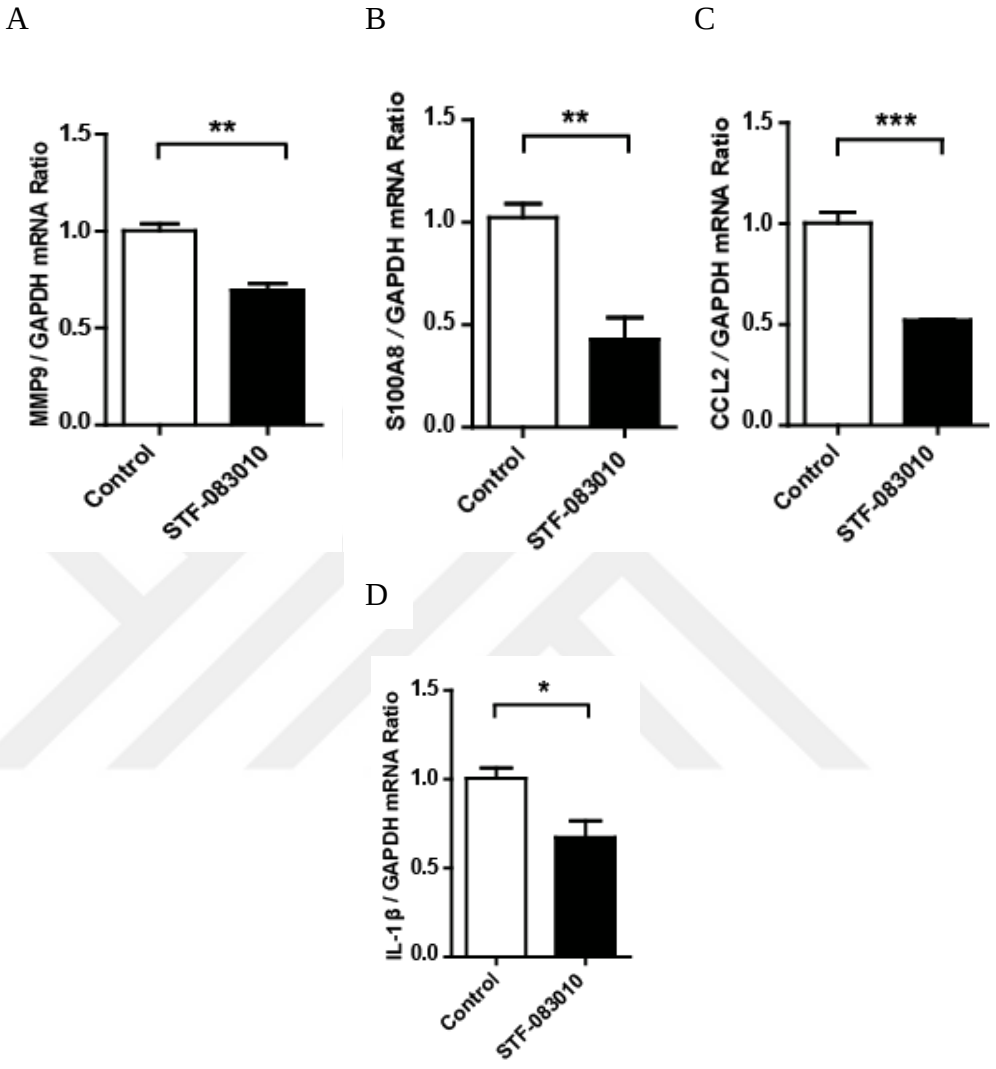

Figure 3.2. **Confirmation of pro-atherogenic gene regulation by IRE1 in STF-083010-treated BMDM cells.**
(A-D) qRT-PCR confirmation of **(A)** interleukin-1β (IL-1β), **(B)** calgranulin A (S100A8), **(C)** C-C Motif Chemokine Ligand 2 (CCL2) and **(D)** matrix metalloprotease-9 (MMP9) in BMDM cells treated with 6 hours with STF-083010 or DMSO as control. Data: mean values ± SEM; n = 3; ***p≤0.001, **p≤0.01, *p≤0.05, n.s. = not significant; Student's t test).

I further confirmed the results by performing the same experiments with a different IRE1 RNase inhibitor, 4μ8c, in BMDM cells (Figure 3.3 A, B, C, and D).

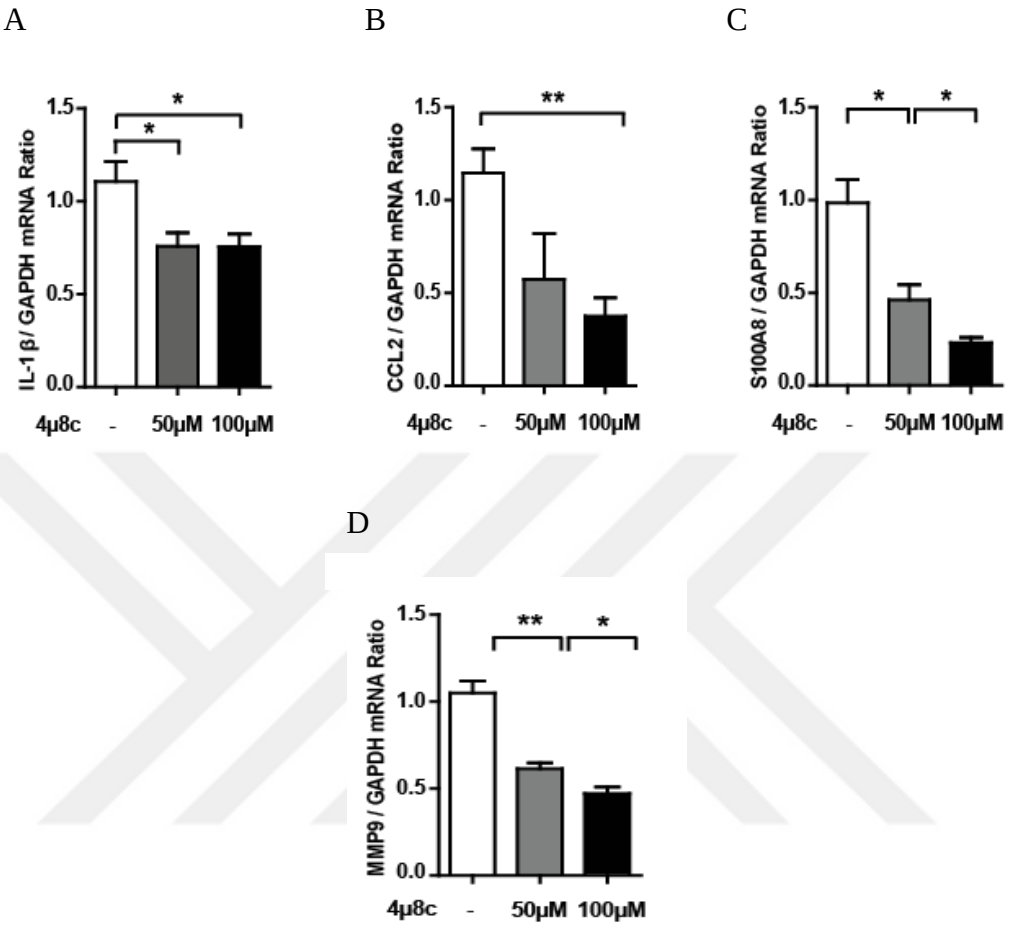

Figure 3.3. **Confirmation of pro-atherogenic gene regulation by IRE1 in 4μ8C treated BMDM cells.**
(A-D) qRT-PCR confirmation of **(A)** interleukin-1β (IL-1β), **(B)** C-C Motif Chemokine Ligand 2 (CCL2), **(C)** calgranulin A (S100A8) and **(D)** matrix metalloprotease-9 (MMP9) in BMDM cells treated with the indicated doses of 4μ8c or DMSO as a control. Data: mean values ± SEM; n = 3; ***p≤0.001, **p≤0.01, *p≤0.05, n.s. = not significant; Student's t test).

As anticipated, these RNase drugs did not have any effect on the kinase activity of IRE1 while they significantly decreased the RNase function of IRE1 (267, 273-275) (Figure 3.4 A, B and C).

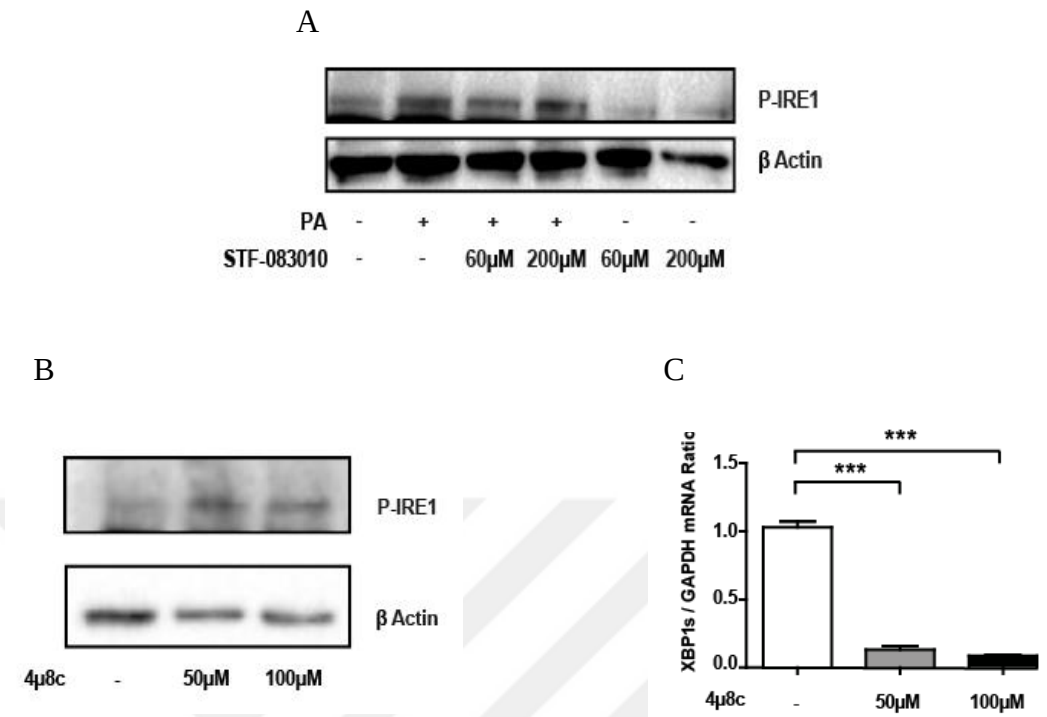

Figure 3.**4**. **IRE1 RNase inhibitors, STF-083010 and 4μ8c, successfully inhibit IRE1 RNase function without affecting IRE1 kinase function.**
(A-B) Lysates from cells treated with the indicated inhibitors were analyzed by Western blot using anti-phospho-IRE1 antibody. **(C)** Total RNA was isolated from inhibitor treated cells and sXBP1 levels were analyzed by qRT-PCR. Data: mean values ± SEM; n = 3; ***p≤0.001, **p≤0.01, *p≤0.05, n.s. = not significant; Student's t test).

3.1.2. Regulation of pro-atherogenic gene expression in IRE1 or sXBP1 overexpressing IRE$^{-/-}$ mouse embryonic fibroblasts

The splicing of XBP1 mRNA is dependent on IRE1 RNase activity (22). To assess the role of this transcription factor on the regulation of the pro-atherogenic genes that appear to be regulated by IRE1's RNase activity in BMDM, I overexpressed sXBP1 and IRE1 in the IRE1$^{-/-}$ mouse embryonic fibroblasts (MEFs). I observed overexpression of both proteins leads to a significant increase in IL-1β, CCL2 and S100A8 mRNA levels (Figure 3.5 A, B and C). For these experiments, the successful overexpression of plasmids was confirmed with qRT-PCR analysis of IRE1 and sXBP1 levels in the cells (Figure 3.5 D)

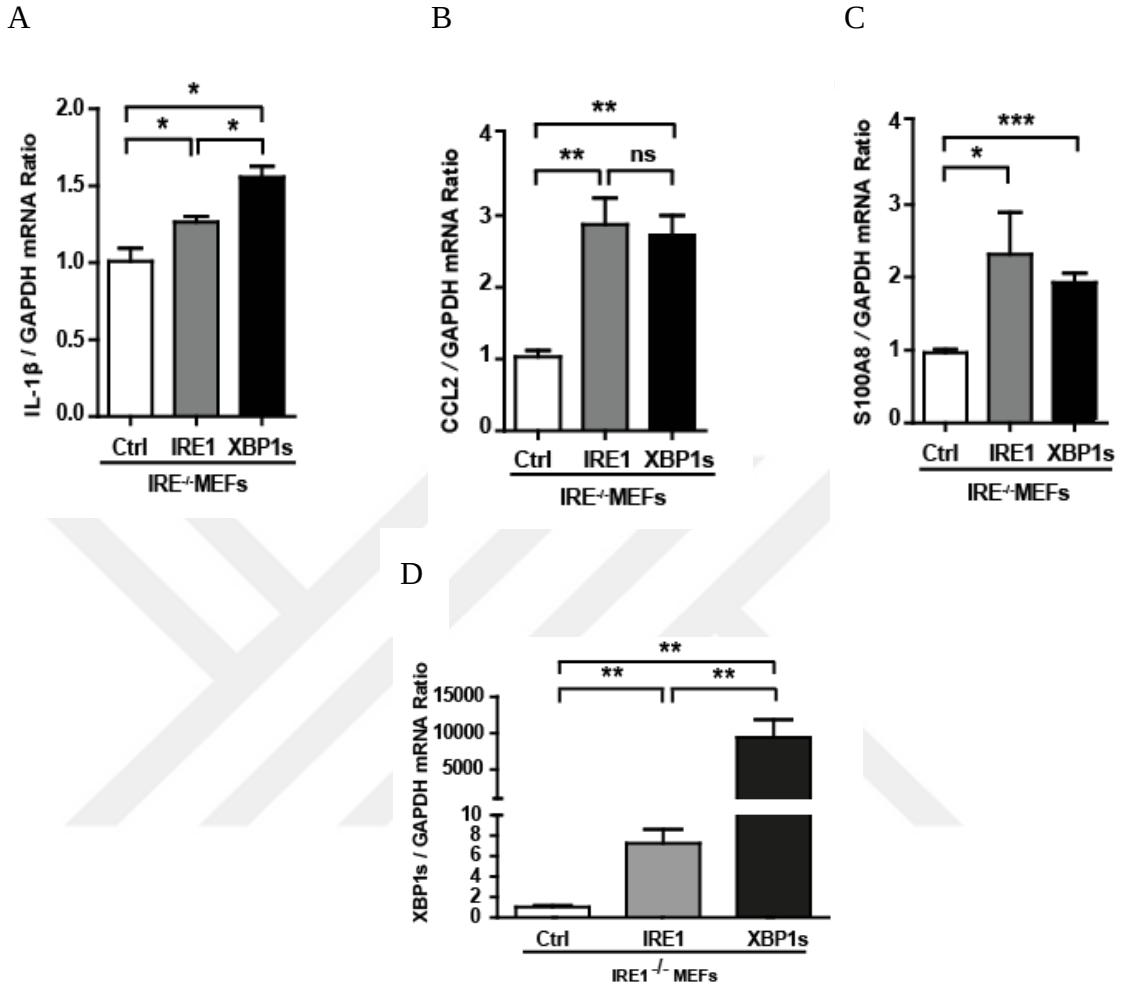

Figure 3.5. **Forced expressions of IRE1 and XBP1s in the IRE1$^{-/-}$ MEFs induce the expression of pro-atherogenic genes.**
(A-D) qRT-PCR analysis of the following genes; **(A)** IL-1β, **(B)** CCL2, **(C)** S100A8 and **(D)** XBP1s was performed on total RNA lysates obtained from IRE1, sXBP1 or vector (control) plasmid transected IRE$^{-/-}$ MEFs. Data: mean values ± SEM; n = 3; ***p≤0.001, **p≤0.01, *p≤0.05, n.s. = not significant; Student's t test).

3.2. Regulation of IL-1β and CCL2 levels under lipid induced ER stress conditions in both mouse and human macrophages.

While lipids have many essential functions such as acting as structural components of all cellular membranes and as signaling molecules, they can cause toxicity when cells devoid of a capacity for storing them are overloaded with lipids (276). The detrimental consequences of exposure to excessive amounts of lipids include increased production of reactive oxygen species (ROS), ER stress and inflammation—collectively known as lipotoxicity—and can result in apoptosis (277). Earlier studies from our laboratory as well as others showed that treatment of cultured macrophages with saturated fatty acids (SFA) such as palmitate (PA) elicits profound ER stress (118). Also, I recently showed that PA integrates into ER membranes, leading to IRE1 oligomerization, followed by XBP1 mRNA splicing (224).

Since I observed that IRE1 RNase function controls the expression of several important pro-atherogenic genes, I next sought to understand whether IRE1's RNase function is important for the regulation of pro-atherogenic genes in lipotoxic ER stress conditions in macrophages that can drive atherosclerotic disease progression.

3.2.1. Regulation of IL-1β levels under lipid-induced ER stress conditions in bone-marrow derived macrophages.

To assess the role of IRE1 RNase domain in the production of IL-1β in lipid-induced ER stress conditions, I treated LPS-primed (3 hours) BMDMs with palmitate (20 hours) in the presence or absence of IRE1 RNase inhibitors (STF-083010, 4μ8c). I showed that inhibition of IRE1 RNase activity with two different drugs can block both IL-1β mRNA production and mature IL-1β secretion from cells (Figure 3.6 A, B, C and D).

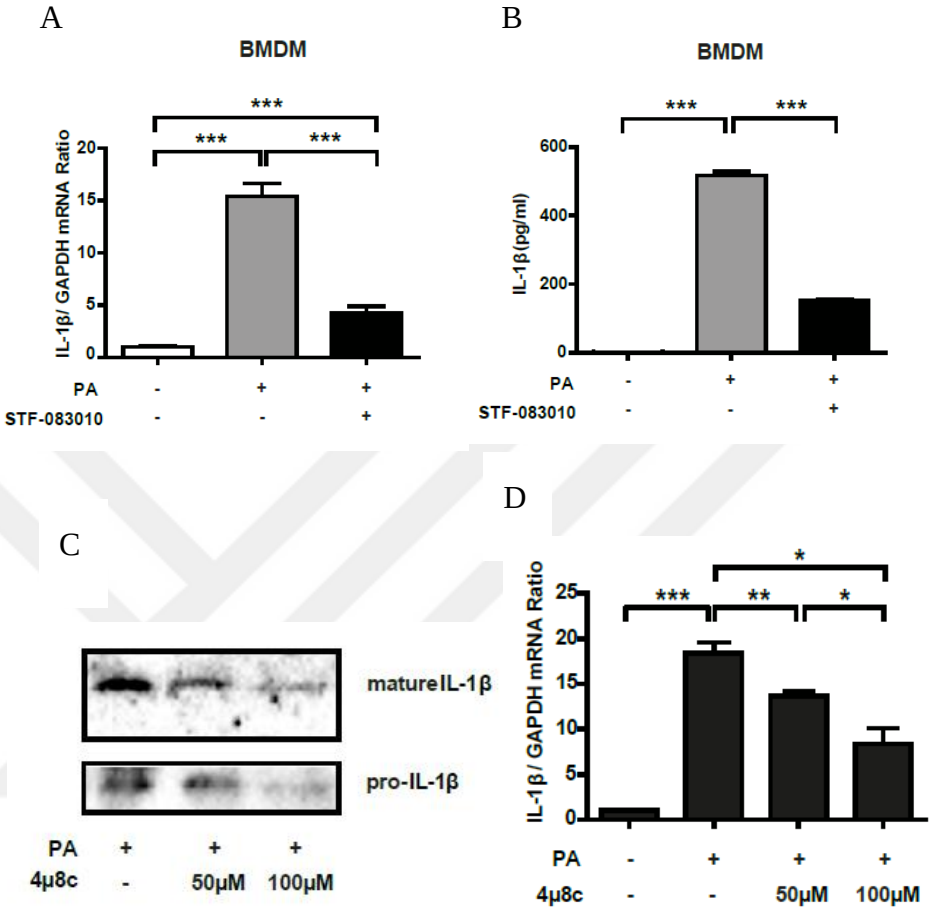

Figure 3**.6. Reduction of lipid-induced IL-1β production in BMDM cells with IRE1 inhibitors.**

(A) qRT-PCR analysis of IL-1β mRNA levels in LPS-primed, palmitate stimulated BMDM cell that were pre-treated with STF-083010 or DMSO (control). **(B)** IL-1β was measured with ELISA from the conditioned media of the treated cells in (A). **(C)** Western blot analysis of pro-IL-1β and mature IL-1β from LPS-primed, palmitate-stressed BMDM cells that were also pre-treated with or without 4μ8c. **(D)** qRT-PCR analysis of IL-1β mRNA levels from the treated cells in figure (C). Data: mean values ± SEM; n = 3; ***p≤0.001, **p≤0.01, *p≤0.05, n.s. = not significant; Student's t test).

To further confirm our results, I measured sXBP1 mRNA levels and IRE1 phosphorylation status of IRE1 RNase inhibitor-treated BMDMs with qRT-PCR and western blotting sequentially (Figure 3.7 A, B, C and D). As expected, I observed reduction in sXBP1 mRNA levels (Figure 3.7A and C) while no change in IRE1 phosphorylation was detected upon inhibitor addition (Figure 3.7B and D).

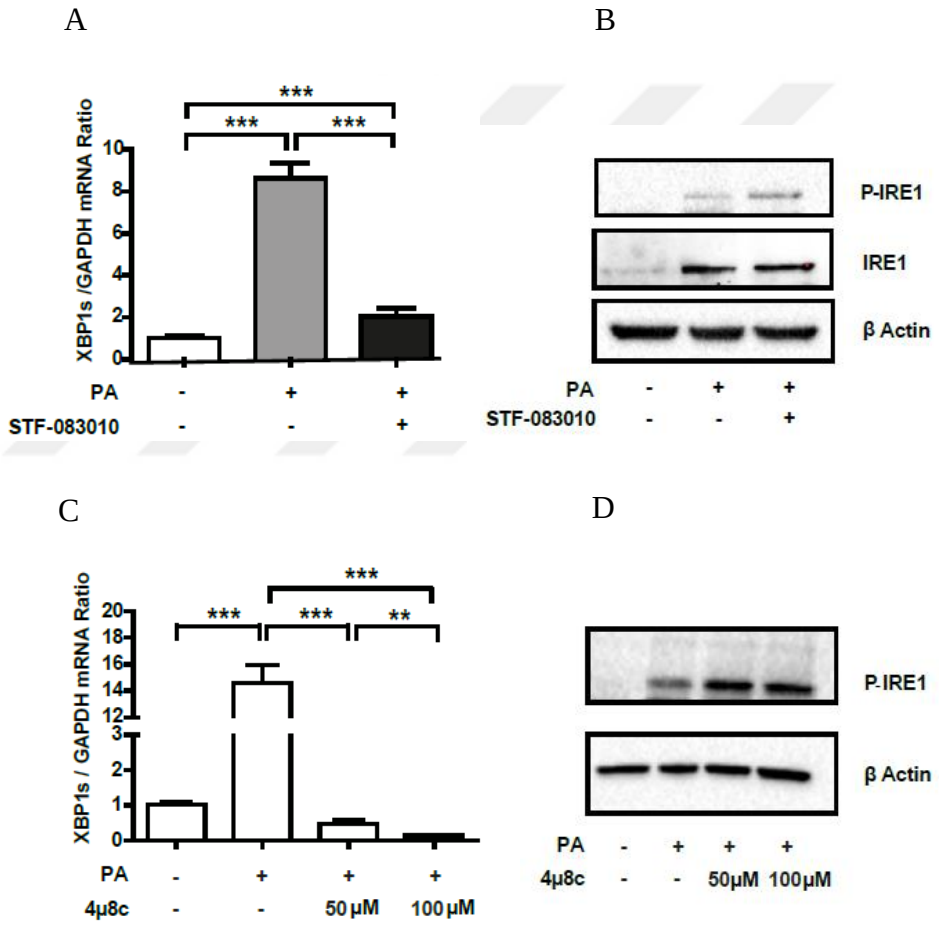

Figure 3.7. **Confirmation of STF-083010 and 4μ8c treatments in BMDM cells.** **(A)** qRT-PCR analysis of sXBP1 levels and **(B)** western blot analysis of phospho-IRE1 levels of the LPS-primed, palmitate-stressed BMDM cells that were treated with STF-083010 or DMSO (control). **(C)** qRT-PCR analysis of sXBP1 levels and **(D)** western blot analysis of P-IRE1 levels of LPS-primed, palmitate stressed BMDM cells that were treated with 4μ8c or DMSO (control). Data: mean values ± SEM; n = 3; ***p≤0.001, **p≤0.01, *p≤0.05, n.s. = not significant; Student's t test).

3.2.2. Regulation of IL-1β levels in human peripheral blood mononuclear cells (PBMC) under lipid induced ER stress.

Next, I analyzed the impact of IRE1 RNase inhibitors on secreted IL-1β levels in human peripheral blood mononuclear cells. The cells were treated as mentioned in the methods section. Confirming our BMDM findings, I observed a significant reduction in secreted IL-1β levels in PBMCs lipid-induced ER stress that are treated with IRE1 RNase inhibitor (Figure 3.8 A and B).

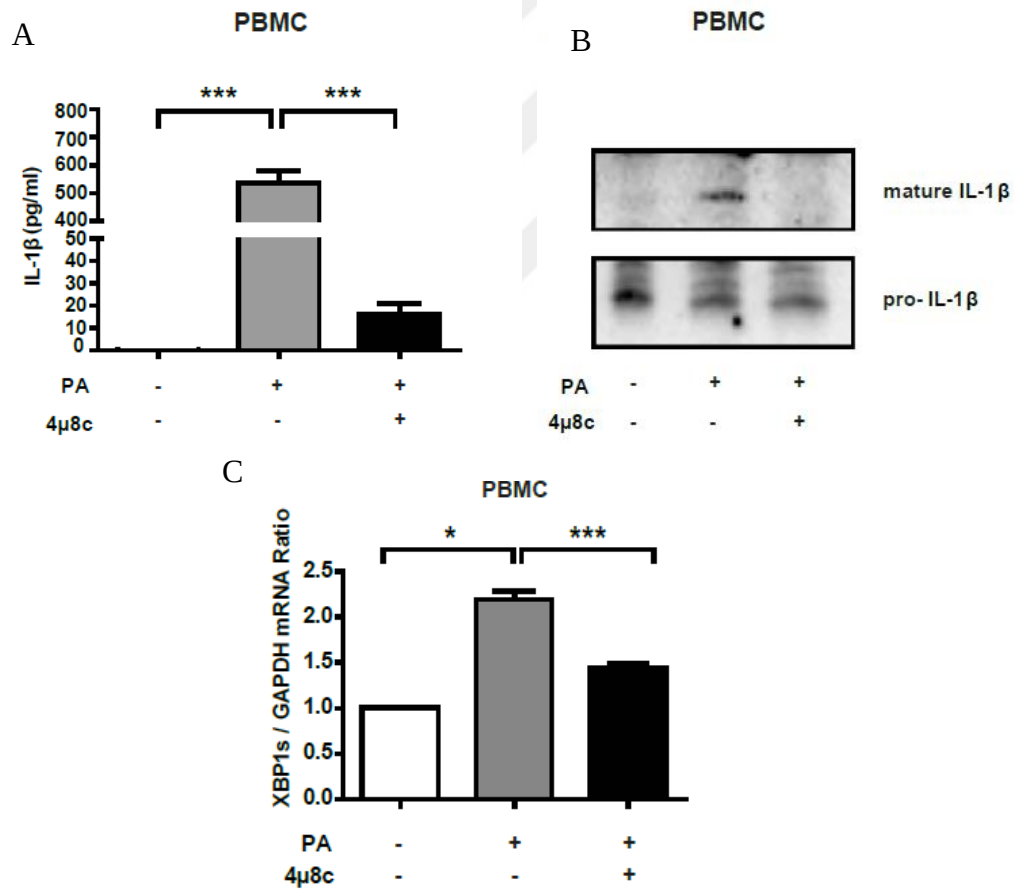

Figure 3.8. **IRE1 RNase inhibition reduces IL-1β production in lipid-stressed PBMCs.**
(A-B) Secreted IL-1β levels were measured with **(A)** ELISA and **(B)** western blot in LPS-primed, palmitate-stressed PBMC that were treated with 4μ8c. **(C)** qRT-PCR analysis of XBP1s mRNA levels in the same cells used in (A and B). Data: mean values ± SEM; n = 3; ***p≤0.001, **p≤0.01, *p≤0.05, n.s. = not significant; Student's t test)

3.2.3. The impact of IRE1 and XBP1 silencing by siRNA on lipid-induced IL-1β production in bone marrow derived macrophages

To further characterize the role of IRE1-XBP1 axis in the lipid induced IL-1β production, I silenced both IRE1 and XBP1s with specific siRNAs against them. I managed effective reduction of IRE1 mRNA (Figure 3.9 A) and spliced XBP1 (Figure 3.9 B) mRNA expression levels in the BMDM cells using these specific siRNAs. In both transfection experiments, silencing of IRE1 and sXBP1 led to reduction in both mRNA and secreted protein levels of IL-1β (Figure 3.9 C, D). These results indicate that IRE1 - XBP1s axis is directly involve in lipid-induced IL-1β production.

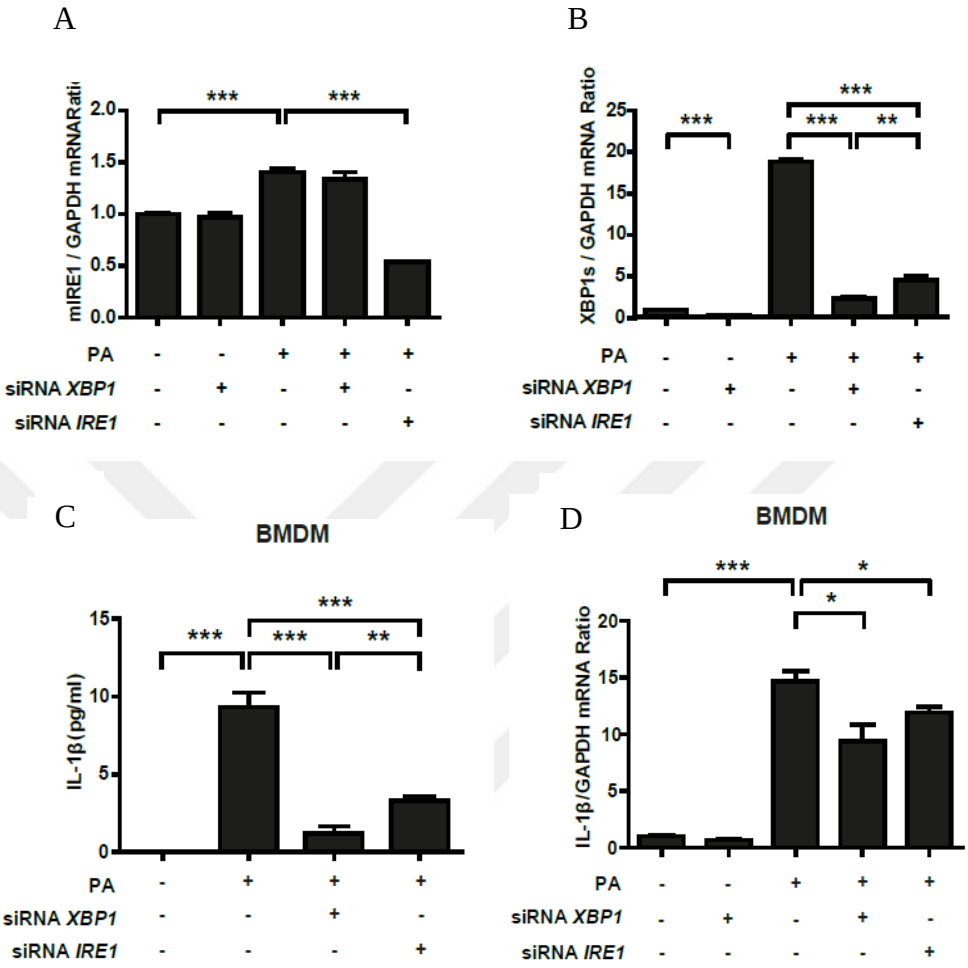

Figure 3**.9. Silencing of IRE1 and XBP1s by siRNA reduces IL-1β levels in BMDM cells.**
(A-B) qRT-PCRs analysis of **(A)** IRE1 and **(B)** XBP1s from total RNA isolated from BMDM cells treated with specific siRNAs against the same genes, respectively. **(C-D)** From the same cells **(C)** secreted IL-1β was measured from the conditioned cell medium by ELISA and **(D)** IL-1β mRNA was measured from total RNA by qRT-PCR. Data: mean values ± SEM; n = 3; ***p≤0.001, **p≤0.01, *p≤0.05, n.s. = not significant; Student's t test).

3.2.4. Regulation of CCL2 levels by IRE1 during lipid-induced ER stress in bone marrow derived macrophages.

I further analyzed the role of IRE1 in the regulation of CCL2, another important pro-atherogenic cytokine, under lipid-induced ER stress conditions in BMDMs. Inhibition of

IRE1 RNase domain with both drugs, STF-083010 and 4μ8c, prevented the production of CCL2 under lipid-induced ER stress conditions (Figure 3.10 A,B and C).

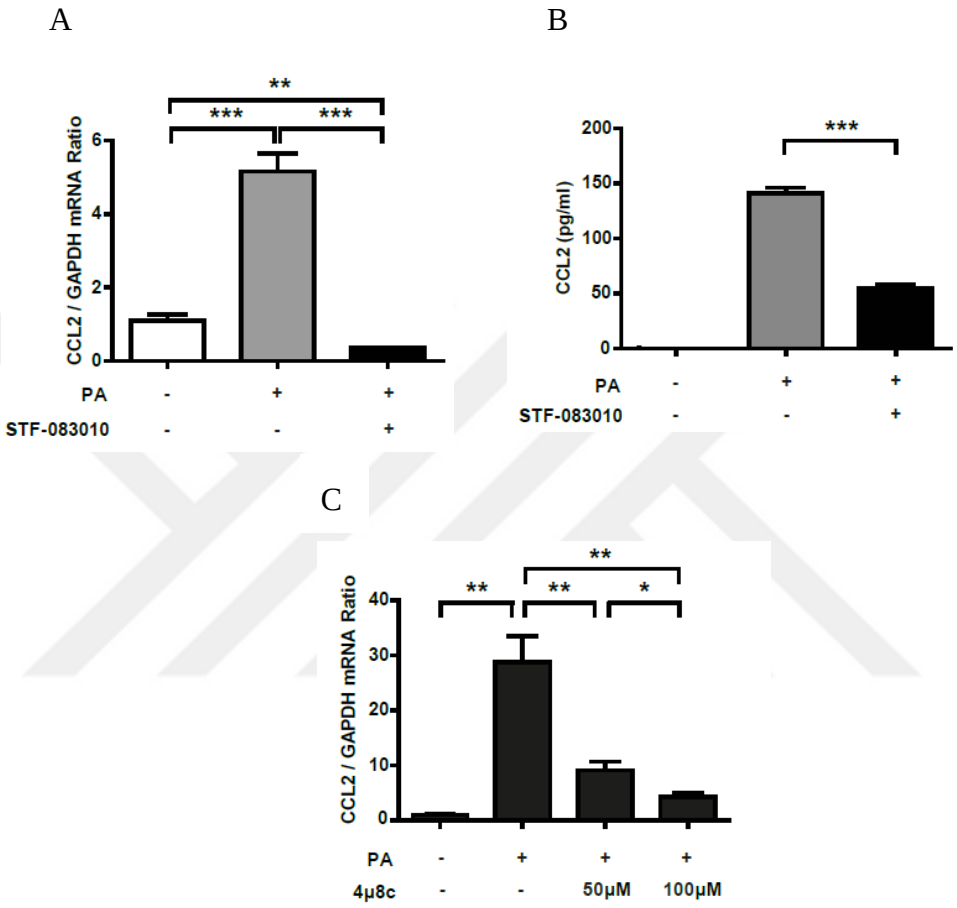

Figure 3.**10**. **IRE1 RNase inhibitors block CCL2 production in BMDM cells.**
(A-B) LPS-primed, palmitate-stimulated BMDM cells were treated STF-08030 or DMSO (control): **(A)** CCL2 mRNA levels were measured by qRT-PCR from the total RNA. **(B)** Secreted CCL2 was measured by ELISA from the conditioned medium of these cells. **(C)** LPS-primed, palmitate-stimulated BMDM cells were treated 4μ8c or DMSO (control). CCL2 mRNA was measured from the total RNA of these cells using qRT-PCR method. Data: mean values ± SEM; n = 3; ***p≤0.001, **p≤0.01, *p≤0.05, n.s. = not significant; Student's t test).

3.2.5. Regulation of CCL2 levels by IRE1 during lipid-induced ER stress in human peripheral mononuclear cells.

I also checked the level of CCL2 in lipid-stressed human PBMCs that were treated with 4μ8c. The results were in accordance with those obtained from BMDMs; there was a significant decrease in lipid-induced CCL2 mRNA levels in PBMCs after 4μ8c treatment (Figure 3.11).

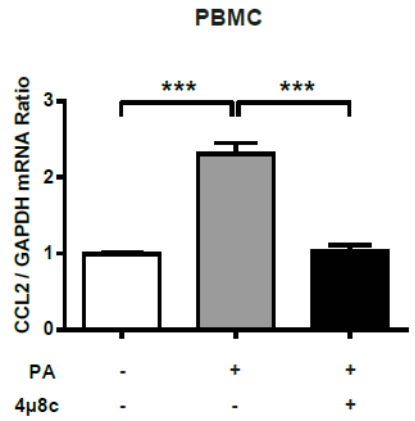

Figure 3**.11**. **4μ8c treatment blocks lipid-induced CCL2 production in PBMC cells.** CCL2 mRNA levels were measured by qRT-PCR from the total RNA lysates obtained from LPS-primed, palmitate-stimulated BMDMs that were treated 4μ8c or DMSO (control). Data: mean values ± SEM; n = 3; ***p≤0.001, **p≤0.01, *p≤0.05, n.s. = not significant; Student's t test).

3.2.6. Confirming IRE1-dependent regulation of CCL2 by suppressing the expression of IRE1 and XBP1

To confirm the role of IRE1-XBP1 signaling axis in regulating CCL2 levels during lipid-induced ER stress, I silenced BMDM cells with specific siRNAs targeting *IRE1* and *XBP1*. Reduction in the expression of both IRE1 and XBP1 resulted in suppression of lipid-induced mRNA expression and secretion of CCL2 (Figure 3.12 A and B).

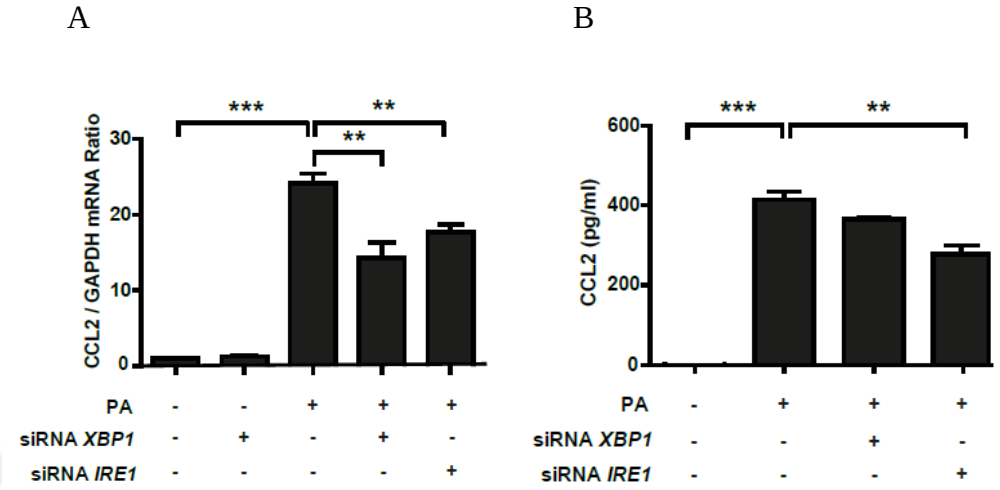

Figure 3.12. Silencing of IRE1 and XBP1 with siRNA leads to suppression of lipid-induced CCL2 levels in BMDMs.
(A-B) LPS-primed, palmitate-treated BMDMs were silenced with specific siRNAs targeting *IRE1* and *XBP1* **(A)** CCL2 mRNA was measured by q-RT-PCR from the total RNA lysates and **(B)** protein levels was measured with ELISA from the conditioned cell medium of the same cells in **(A).** Data: mean values ± SEM; n = 3; ***p≤0.001, **p≤0.01, *p≤0.05, n.s. = not significant; Student's t test).

3.3. Regulation of NLRP3 inflammasome activation with IRE1

3.3.1. The role of IRE1 in the regulation of caspase-1 activation by lipid stress

For the secretion of mature IL-1β, the inflammasome complex must be formed and activate caspase-1 enzyme by converting zymogen caspase-1 into cleaved and active form of caspase-1. Then, active caspase-1 can further cleave the pre-IL-1β to its mature and secreted form (278). Based on the evidence presented in my thesis showing inhibition of IRE1 RNase domain can suppresses both IL-1β mRNA levels and its secretion, it is plausible that IRE1 may regulate lipid-induced inflammasome activation and caspase-1 cleavage, upstream of IL-1β production and secretion.

To gain further insight, I pre-treated BMDM cells with STF-083010 or DMSO (control), prior to priming with LPS, and induced lipid stress with the addition of palmitate for indicated time and durations as in material and methods. These two stimuli, palmitate and LPS, are both needed for full activation of the inflammasome complex in BMDMs cell culture. I observed that active or cleaved caspase-1 that was secreted into cell media was decreased with the addition of STF-083010 (Figure 3.13 A). I repeated the same experiment with the other IRE1 RNase inhibitor, 4μ8c, and observed similar results (Figure 3.13 B). To further categorize the role of XBP1 in lipid-induced inflammasome activation I transfected BMDM cells with specific siRNAs targeting *IRE1* and *XBP1* genes. I observed suppression of caspase-1 cleavage in both *XBP1* and *IRE1* silenced BMDMs compared to palmitate and LPS treated samples from scrambled siRNA treated BMDMs (Figure 3.13 C).

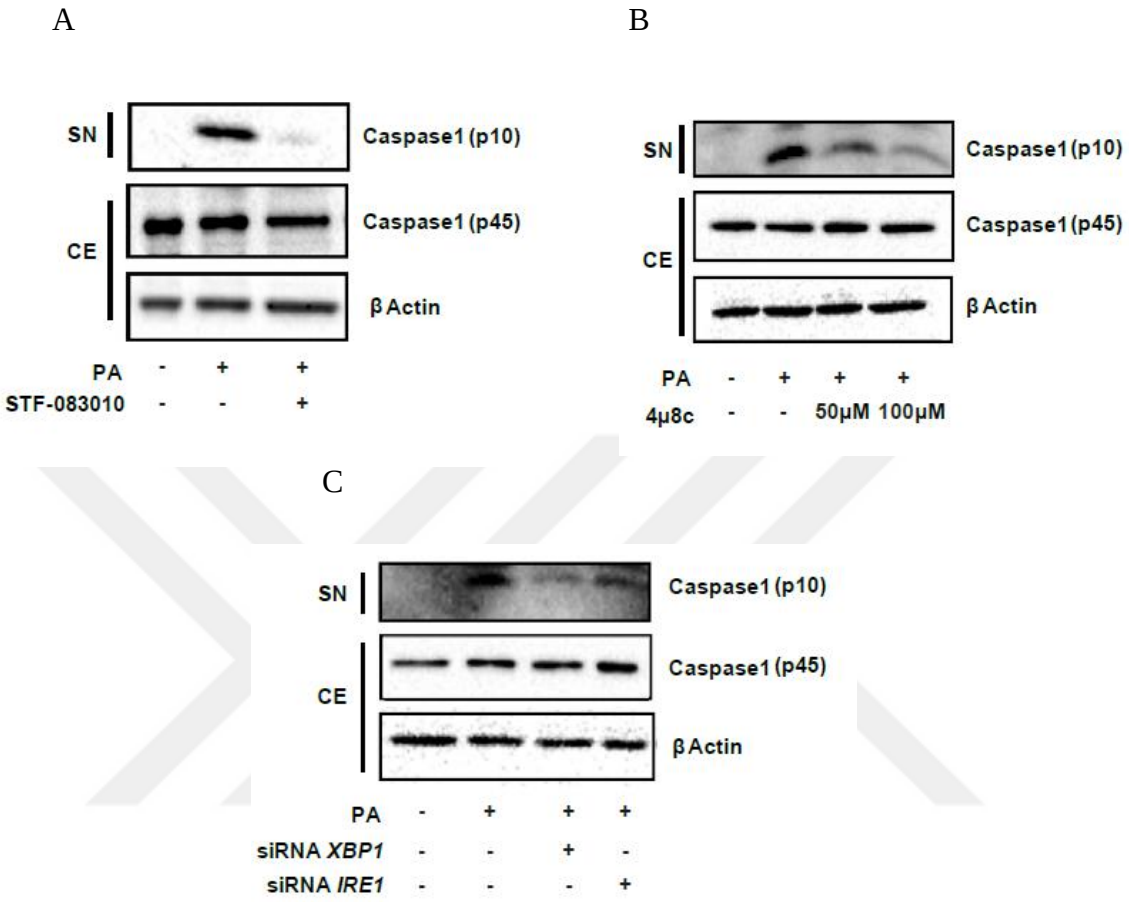

Figure 3**.13. IRE1 inhibition blocks lipid-induced activation and secretion of caspase- in BMDMs.**
(A) LPS-primed, palmitate treated BMDM cells that were treated STF-083010 or DMSO (control) and cleaved caspase1 (p10) and total caspase1 (p45) levels were detected by western blot. **(B)** LPS-primed palmitate treated BMDM cells that were treated 4μ8C or DMSO (control). Cleaved caspase1 (p10) and total caspase1 (p45) levels were detected by western blot. **(C)** BMDM cells that were transfected siRNA *XBP1* and *IRE1* were LPS-primed and stressed with palmitate and cleaved caspase1 (p10) and total caspase1 (p45) levels were detected by western blot.

3.3.2. IRE1 RNase activity specifically regulates NLRP3 inflammasome activation

Jenny P-Y Ting *et al*. identified the relation between fatty acids and inflammasome activation for the first time. They showed that saturated free fatty acids, especially palmitate, activated the NLRP3 inflammasome and promoted the secretion of IL-1β

(118). After demonstrating the role of IRE1-XBP1 axis on the lipid induced activation of NLRP3 inflammasome, I further wanted to analyze whether IRE1 plays a role in the activation of other types of inflammasomes in macrophages. LPS-primed BMDM cells were treated with aluminum salt (alum) crystals, cholesterol crystals and ATP that are known to specifically induce the NLRP3 inflammasome (279). After these treatments, as expected, I observed increase in both secreted, mature form of IL-1β and cleaved, active form of caspase-1 in cell supernatants and this increase was abolished with 4μ8c treatment (Figure 3.14A)., These results show that in addition to IRE1's role in lipid induced inflammasome activation, IRE1 RNase activity can also regulate NLRP3 inflammasome activation by different stimuli.

To examine the role of IRE1 RNase activity in the regulation of other inflammasome types, I treated LPS-primed, BMDM cells with poly (dA:dT) an inducer of AIM2 and flagellin an inducer of NLRC4 as previously described in literature (224). All treatments that activate distinct inflammasome complexes led to cleavage and activation of caspase-1 followed by the secretion of mature IL-1β. Intriguingly, IRE1 RNase inhibition didn't decrease caspase-1 cleavage while it reduced secreted, mature IL-1β. I interpret these results are due to IRE1 inhibitors' suppressive impact on IL-1β mRNA production. (Figure 3.14 B). In conclusion, IRE1 RNase activity specifically controls NLRP3 dependent caspase-1 activation by various NLRP3 inducers and does not impact the activation of other inflammasome complexes.

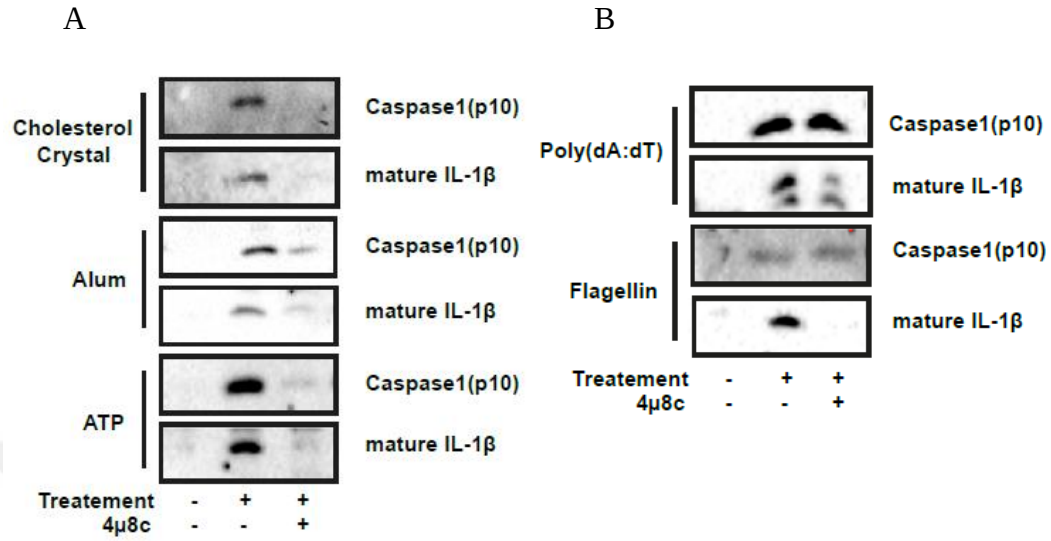

Figure 3.14. IRE1 RNase inhibition reduces NLRP3 inflammasome activation. **(A)** LPS-primed BMDMs were pre-treated with 4μ8c or DMSO and then stimulated with NLRP3 agonist (5nM ATP, 200μg/ml alum, or 400 μg/ml cholesterol crystals). From the cellular media, cleaved caspase1 (p10) and secreted mature IL-1β levels were detected by western blotting. **(B)** LPS-primed BMDMs were pre-treated with 4μ8c or DMSO and then stimulated with specific activators of other inflammasome complexes [5 μg/ml poly (dA:dT) and 1 μg/ml flagellin] according to previously published protocols. From the cellular media secreted cleaved caspase1 (p10) and secreted mature IL-1β levels were detected by western blotting. A representative blot from three independent experiments is shown.

3.3.3. Regulation of lipid-induced mitochondrial oxidative stress by IRE1-XBP1 axis

Saturated fatty acids lead to the activation of IRE1 and simultaneously induce NLRP3 inflammasome. An earlier study showed that fatty acids activated NLRP3 inflammasome through the release of ROS from the mitochondria (118, 224). Therefore, I investigated the role of IRE1 in mtROS production in response to lipid stress. I first measured mtROS production in cells that are exposed to saturated fatty acids in the presence of IRE1 RNase inhibitor 4μ8c or in control conditions (DMSO). As expected, lipid-induced stress led to a dramatic increase in the production of mtROS. This elevation was blocked in the 4μ8c pre-treated cells (Figure 3.15 A, B). In an effort to

identify the specific role of XBP1 in production of mtROS under lipid induced stress conditions, BMDM cells were transfected with siRNA specifically targeting *XBP1* gene. I observed that XBP1 knockdown blocked the elevation of mtROS in response to lipid stress (Figure 3.15 C).

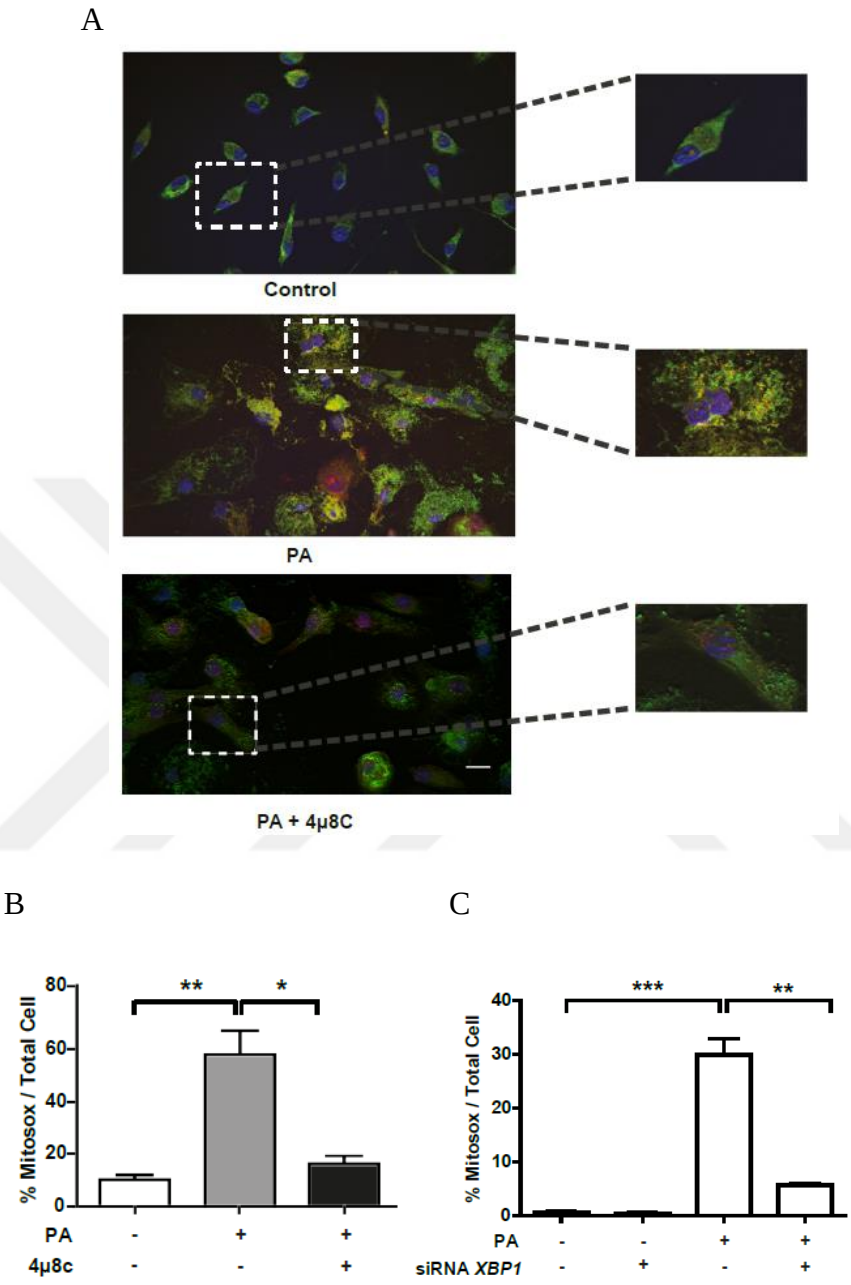

Figure 3**.15. IRE1-XBP1 axis regulates mtROS production in response to lipid stress.**

(A-B) mtROS production in lipid-induced BMDMs that were treated 4μ8c or DMSO was determined by the MitoSOX kit. **(A)** Representative figure for fluorescence staining of mtROS in BMDMs using the MitoSOX fluorescence indicator. MitoSOX fluorescence indicator was shown with red color, Mitotraker was shown in green color (Scale bar: 20μM). **(B)** Quantification of staining in (A). **(C)** Quantification of mtROS production in lipid-induced BMDMs that were transfected with siRNA targeting *IRE1* and *XBP1*. Data: mean values ± SEM; n = 3; ***p≤0.001, **p≤0.01, *p≤0.05, n.s. = not significant; Student's t test).

3.3.4. The impact of IRE1 on TXNIP induction and calcium mobilization from the ER to the mitochondria

Earlier studies showed IRE1-dependent accumulation of thioredoxin-interacting protein (TXNIP) led to activation of inflammasome in ER stress conditions (133). Therefore, I sought to examine this molecular mechanism also couples lipid-induced ER stress and NLRP3 inflammasome activation. In contrast to earlier results, which observed increase in TXNIP with chemical ER toxins, lipid-induced ER stress was accompanied with the suppression of TXNIP (Figure 3.16 A). Therefore, TXNIP induction cannot explain how lipid-induced ER stress activates NLRP3 inflammasome. Another known mechanism connecting ER stress to inflammasome activation is ER calcium mobilization into the mitochondria, which generates mtROS and activates the inflammasome (280). To analyze the role of IRE1 in Ca^{2+} mobilization under lipid stress, I measured mitochondrial calcium uptake in cells that were exposed to lipid stress in the presence of IRE1 RNase inhibitor 4μ8c. I observed that lipid-induced ER stress led to increase in mitochondrial calcium level, however, this increase could not be blocked by 4μ8c treatment (Figure 3.16 B). Combined with earlier findings reported in my thesis, these results show that IRE RNase inhibition suppresses lipid-induced mtROS production, but this reduction is not accompanied by TXNIP induction or Ca^{2+} mobilization into the mitochondria.

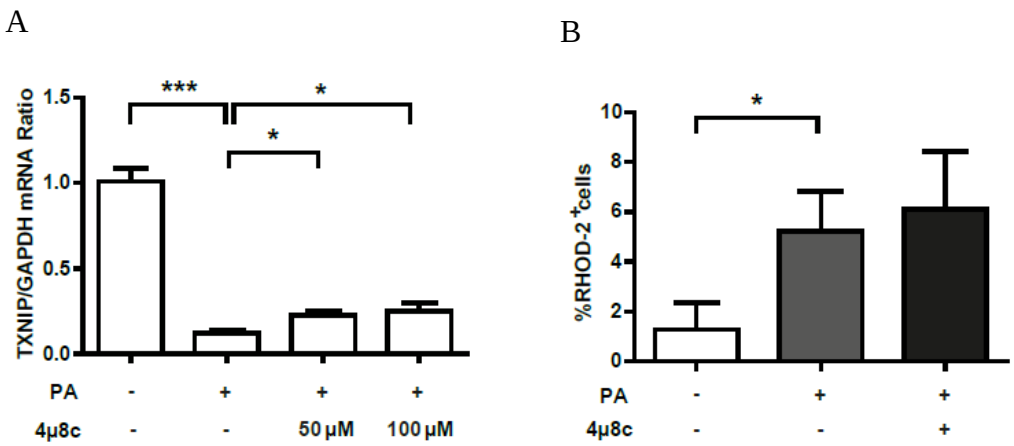

Figure 3**.16. Lipid-induced upregulation of mtROS production is independent of changes in TXNIP levels or Ca2^{+} mobilization into the mitochondria.**
(A) qRT-PCR analysis of TXNIP mRNA expression in BMDMs that were treated with 4μ8c. **(B)** Mitochondrial Ca^{2+} levels were measured in LPS-primed, palmitate-stimulated BMDMs that were treated with 4μ8c or DMSO. Data: mean values ± SEM; n = 3; ***p≤0.001, **p≤0.01, *p≤0.05, n.s. = not significant; Student's t test).

3.3.5. IRE1-dependent regulation of mitochondrial matrix protease LONP1 and mtROS production

In order to identify putative mechanisms through which IRE1 can monitor mtROS production upstream of inflammasome activation, I focused on IRE1's impact on a mitochondrial matrix protease, LONP1, which can be induced by ER stress. Thapsigargin (TG) and Brefeldin directly stimulate ER stress by leading to the accumulation of unfolded proteins in ER, albeit through different mechanisms (281). Treatment of Hela (Henrietta Lacks' 'Immortal' Cells) cells with either one of these toxins can induce LONP1 transcription (282). Furthermore, PERK is required for ER-stress induced LONP1 increase in these cells. Activation of PERK leads to inhibition of eIF2α-dependent general translation (282). But, translational inhibition does not explain how ER stress can induce transcriptional regulation of LONP1 under ER stress conditions. One of the consequences of PERK-dependent inhibition of cap-dependent translation is the activation of translation of a select group of mRNAs with a second open reading frame such as ATF4, a transcription factor that plays an important role in

mediating ER stress response (283). Indeed, a later study has demonstrated that downstream activation of transcription factors such as ATF4 and CHOP are responsible for the induction of LONP1 in ER stress conditions (284). Furthermore, it is not known if the other UPR arms can contribute to LONP1 regulation during ER stress conditions. Because, mitochondrial proteases contribute to mitochondrial homeostasis through multiple ways, I next investigated if IRE1 can impact LONP1 regulation by ER stress (282).

3.3.5.1. The impact of IRE1-XBP1 axis on the induction of LONP1 mRNA expression by lipid-induced ER stress

I first treated BMDMs with increasing doses of 4μ8c under lipid stress and evaluated changes in LONP1 mRNA expression with qRT-PCR. I observed that LONP1 expression was increased with lipid stress, but suppressed by the addition of 4μ8c in a dose-dependent manner (Figure 3.17 A). Furthermore, I showed that silencing of IRE1-XBP1 axis with specific siRNA targeting *XBP1* gene, partially blocked the expression of LONP1 mRNA (Figure 3.17 B).

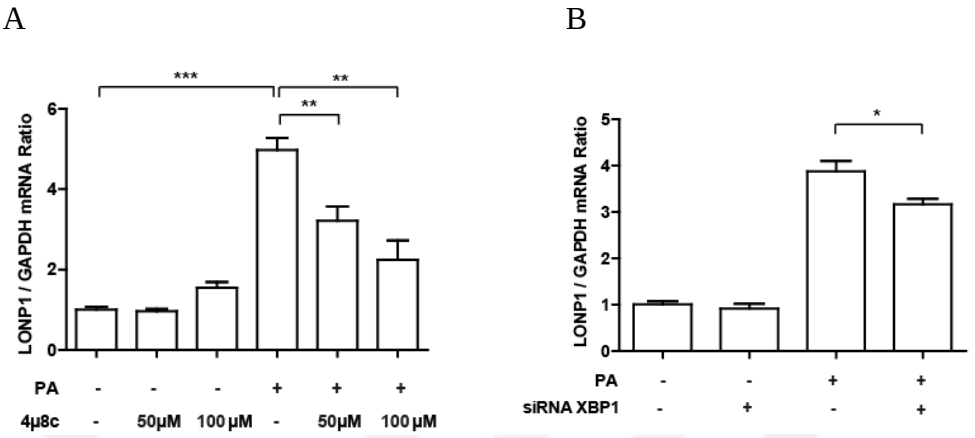

Figure 3**.17. IRE1 RNase activity regulates mitochondrial LONP1 protease level in BMDM cells.**
(A) qRT-PCR analysis of LONP1 mRNA levels from RNA lysates of LPS-primed, palmitate -stimulated mouse BMDMs that were treated with indicated doses of 4μ8c or DMSO (control). **(B)** qRT-PCR analysis of LONP1 mRNA levels from RNA lysates of LPS-primed, palmitate-stimulated mouse BMDMs that were transfected with siRNA against *IRE1* and *XBP1*. Data: mean values ± SEM; n = 3; ***p≤0.001, **p≤0.01, *p≤0.05, n.s. = not significant; Student's t test).

3.3.5.2. The impact of LONP1 on lipid-induced mtROS production

Previous studies showed that LONP1 overexpression in many cancer cell lines could induce ROS production (285). ROS are mainly produced from a dysfunction of mitochondrial electron transport chain in cells (286). Earlier studies have suggested that the induction of LONP1 could disrupt the assembly or function of these respiratory complexes, thus resulting in the generation of mitochondrial ROS.

To assess the impact of LONP1 on lipid-induced mtROS production, I transfected BMDMs with *LONP1* siRNA and then treated with palmitate to induce the production of mtROS (as described in detail in the materials and methods part of this thesis). While I observed significant increase in mtROS in palmitate-treated cells, silencing of LONP1 by a specific siRNA against this gene blocked most of the lipid-induced mtROS in BMDMs (Figure 3.18).

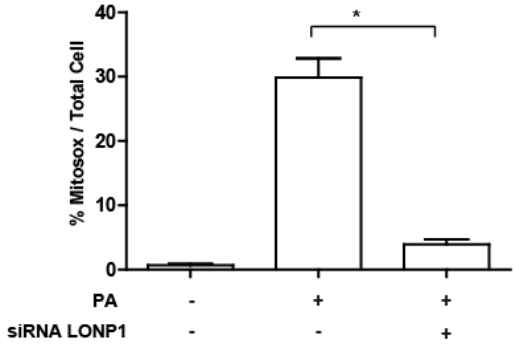

Figure 3**.18. Silencing of LONP1 reduces lipid-induced mtROS production in BMDM cells.**
BMDMs were electroporated with specific siRNA against *LONP1* and primed with LPS prior to induction of mtROS with palmitate treatment as described earlier in this thesis. mtROS was stained using MitoSOX kit and the data was analyzed as described earlier in this thesis. Data: mean values ± SEM; n = 3; ***p≤0.001, **p≤0.01, *p≤0.05, n.s. = not significant; Student's t test).

3.4. *In vivo* applications of IRE1 inhibitors in ApoE$^{-/-}$ mice

All of the evidence provided in this thesis points to a critical role of IRE1 RNase activity in lipid-induced inflammation. In addition, previous studies showed that atherosclerosis could be attenuated by reducing ER stress or with anti-inflammatory treatments (237, 238, 256, 259). Therefore, I postulated that modulation of IRE1 RNase activity with specific inhibitors can prevent atherosclerosis by limiting the effects of ER stress-induced inflammation. To prove this notion, I used ApoE$^{-/-}$ mice, which are prone to develop atherosclerosis under hypercholesterolemic, Western diet. I evaluated the effects both IRE1 RNase inhibitors; STF-083010 and 4μ8c on the ApoE$^{-/-}$ mice that were fed with a Western diet for many weeks.

3.4.1. The impact of IRE1 RNase inhibitor, STF-083010, on atherosclerosis in ApoE$^{-/-}$ mouse

ApoE$^{-/-}$ mice were challenged with hypercholesterolemic, Western diet for 12 weeks and then treated with 10mg/kg STF-083010 (in %30 Cremophore:Saline solution) by intraperitoneal injection for 6 weeks while they continued on Western diet. The specific dosage and delivery method for this drug was based on the earlier *in vivo* studies that reported the usage of STF-083010 *in vivo* (267, 287).

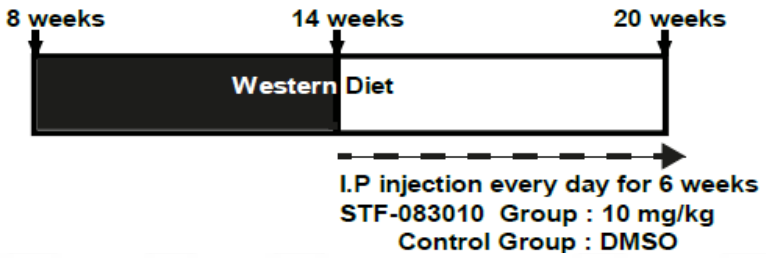

Figure 3.19. Experimental designs of STF-083010 treatment in mice

3.4.1.1. Analysis of body weight and blood glucose in animal groups

To evaluate chronic STF-083010 treatment's effect on mice, I weighed them each day and measured their blood glucose levels in the beginning and at the end of the drug treatment. I observed that the drug treated and control mice gained equal amounts of weight and they did not display any significant differences in their blood glucose levels. These results show that STF-083010 treatment does not alter weight gain that could result from an unwanted, toxic effect. Also, IRE1 RNase inhibition does not disrupt systemic glucose metabolism (Table 3.1)

Table 3.1. Body weight and blood glucose in treated animal groups

Variables	Treatment	Control	STF-083010
n		**6**	**6**
Body weight (g)	**Before**	**30.3 ± 3.5**	**28.3 ± 2.2**
	After	**33.3 ± 5.1**	**29.8 ± 2.5**
Glucose (mg/dl)	**Before**	**120.5 ± 18.5**	**134 ± 13.3**
	After	**79.0 ± 11.8**	**72.6 ± 15.1**

3.4.1.2. Regulation of XBP1 splicing and the canonical RIDD targets by STF083010 treatment *in vivo*

To test the efficacy of STF-083010 in inhibiting the IRE1 RNase activity, I isolated RNA from the spleens of mice. By using qRT-PCR method, I measured the mRNA levels of sXBP1 and the mRNA levels of several, canonical RIDD targets. I observed that STF-0830-injected mice expressed lower sXBP1 mRNA levels when compared to control mice (Figure 3.20 A). Furthermore, there was an increase in RIDD targets such as scavenger receptor class a member 3 (SCARA3) and platelet-derived growth factor receptors (PDGF-R) in the STF-083010-treated mouse spleens (Figure 3.20 B, C). On the other hand, I did not observe reduction in the phosphorylation of IRE1 in liver protein lysates demonstrating that STF-083010 did not alter IRE1's kinase activity but suppressed its RNase output (Figure 3.20 D).

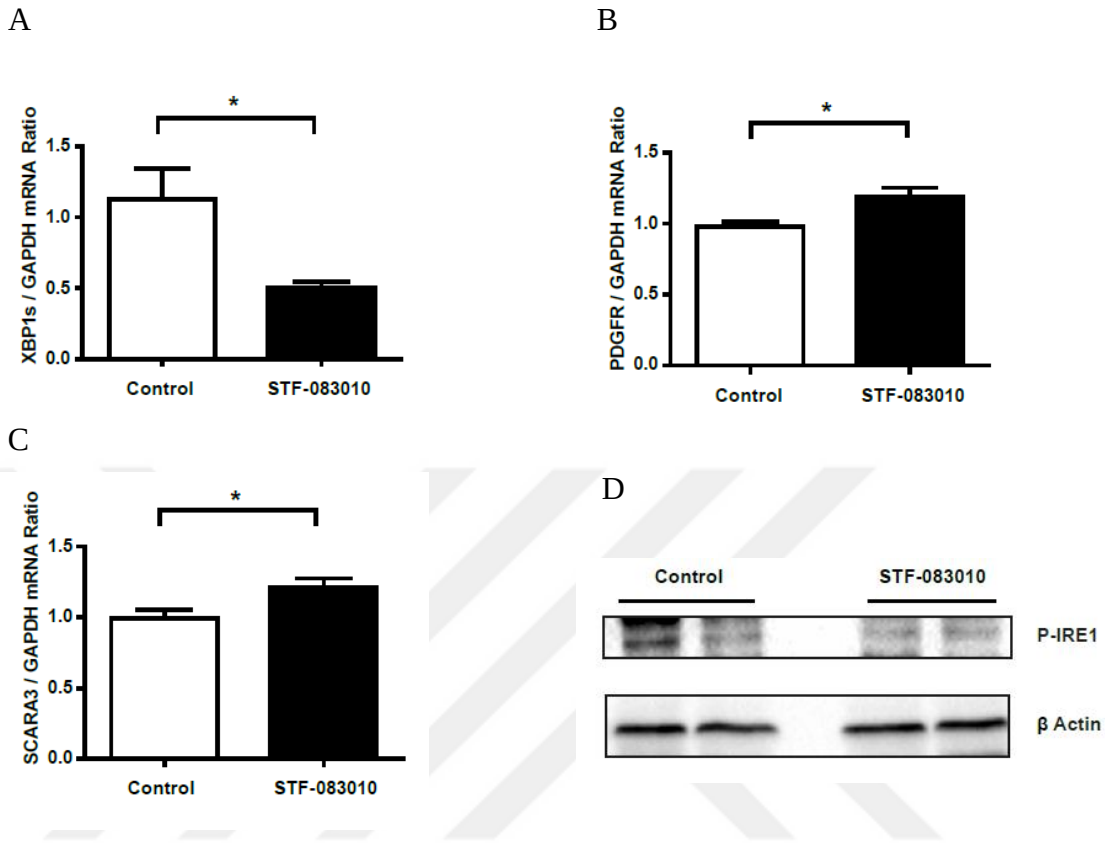

Figure 3.**20. STF-083010 treatment inhibits IRE1 RNase activity *in vivo*.**
(A,B,C) qRT-PCR analysis of IRE1 RNase targets from total RNA lysates obtained from the spleen tissues of ApoE$^{-/-}$ mice treated with STF-08301 or vehicle (control): **(A)** XBP1s, **(B)** PDGFR, and **(C)** SCARA3. **(D)** Western blot analysis of IRE1 phosphorylation levels from the liver protein lysates of same animals in **(A-C).**

3.4.1.3. Assessment of toxicity in livers from STF-083010- treated ApoE$^{-/-}$ mice

To assess the toxicity that could be related to the pharmacological inhibition of IRE1's RNase activity by STF-083010 *in vivo*, I evaluated the histopathology of the liver tissue sections (stained with hematoxylin & eosin) obtained from ApoE$^{-/-}$ mice (on Western diet) that were treated with this inhibitor or vehicle (control) . I observed increase in lipid accumulation in the control liver tissues and no morphological changes that could be associated with the drug toxicity (Figure 3.21 A). For further confirmation of the lack of liver toxicity, I performed ALT (alanine transferase) assay from plasma samples of

mice and I did not observe any ALT activity changes that could be associated with liver toxicity in relation to STF-083010 treatment in mice (Figure 3.21.B).

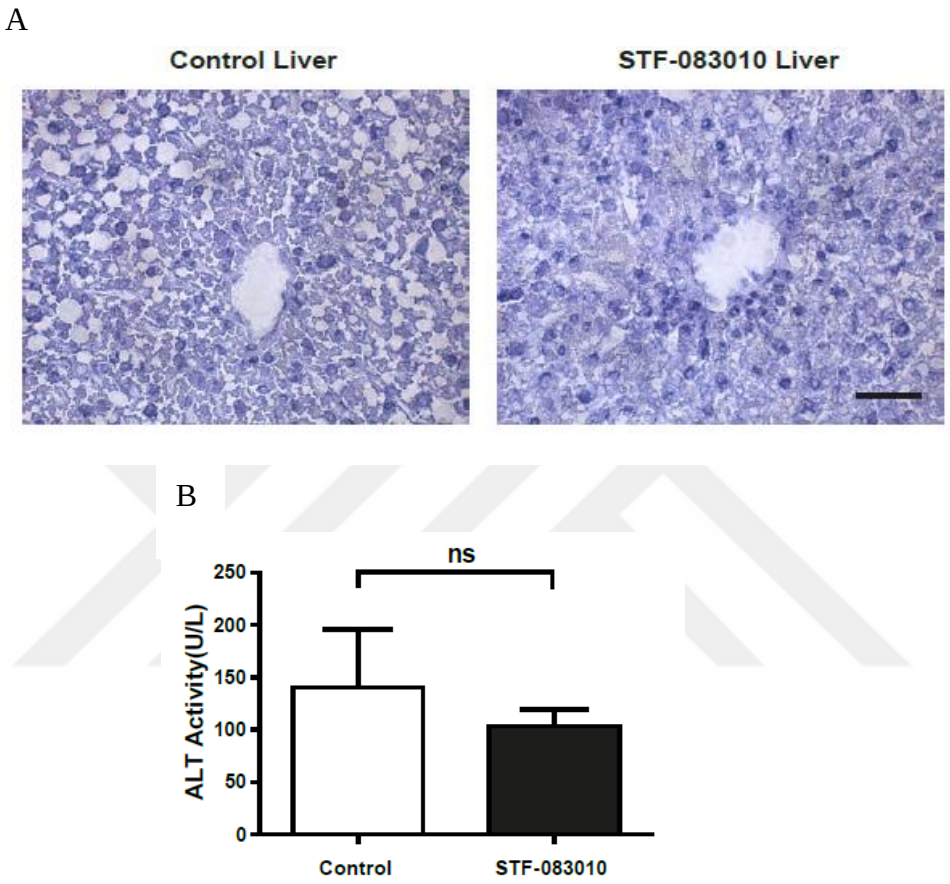

Figure 3**.21. STF-083010 treatment does not induce liver toxicity in ApoE$^{-/-}$ mice on Western diet.**
(A) Histopathological evaluation of the H & E stained liver tissue sections from STF-083010- and vehicle-treated (control) mice. **(B)** ALT assay analysis of blood plasma of STF-0830101- and vehicle-treated (control) mice.

3.4.1.4. Analysis of en face plaque area in STF-083010-treated ApoE$^{-/-}$ mice on Western diet

To evaluate the impact of STF-083010 administration on plaque development, I analyzed the plaque areas in en face aorta preparations from STF-083010- or vehicle (control)-treated ApoE$^{-/-}$ mice on Western diet. The total plaque area was calculated

from the en face aorta that was stained with Sudan IV to demonstrate the lipid-enriched lesion area (269). I observed that the plaque formations mainly accumulated in the branched regions of arteries in drug-treated and control mice and as indicated in the literature (269). I observed a significant reduction in the plaque areas of STF-083010-treated mice when compared to control mice (Figure 3.22).

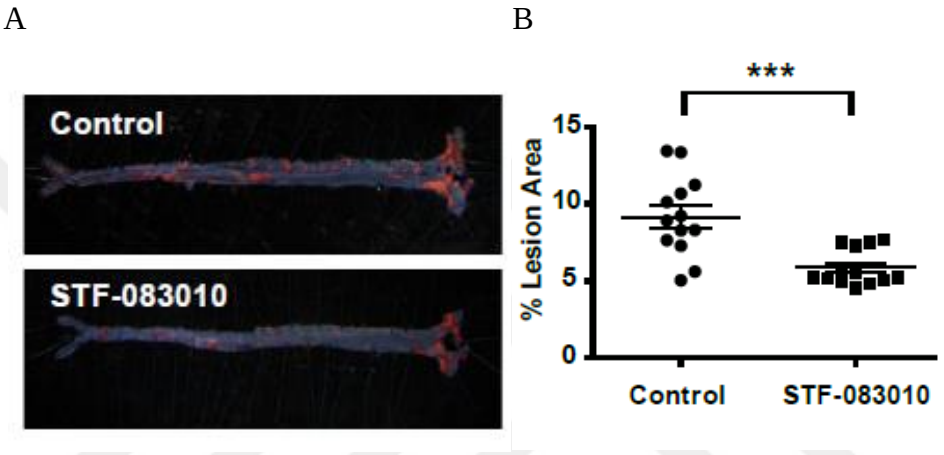

Figure 3**.22. STF-083010 treatment leads to a marked reduction in en face plaque area.**
(A) Representative images of en face aorta preparations showing red-stained (with Sudan IV) plaque area in STF-0803010- or vehicle-treated (control) ApoE$^{-/-}$ mice on Western diet. **(B)** Calculation of total plaque area (from mice in A) according to Sudan staining. . ***P $\leq$ 0.001; n=13-14.

In atherosclerosis-prone mice, aortic sinus found at the aortic root region, is the first place where lesions first become prominent. Then lesions continue to the ascending aorta (288). Therefore, methods have been developed to characterize the nature of the aortic root plaques in terms of size, volume, and composition using histochemical or immunofluorescent examination of serial sections obtained from the aortic sinus region (289, 290). By using these well-established techniques, I analyzed the sections from aortic sinus region of the hearts obtained from STF-0803010- or vehicle-treated (control) mice.

3.4.1.5. Analysis of plaque area in aortic root sections from STF-0803010-treated ApoE$^{-/-}$ mice on Western diet

To examine the aortic sinus lesion area, I cut serial sections of 7µm thickness from the beginning of the sinus area in the hearts of STF-0803010-treated or vehicle-treated (control) ApoE$^{-/-}$ mice on Western diet. I stained 4 different sections that were separated by 60µm (as described in materials and methods part or this thesis) with Oil red O stain and analyzed the total area of lipid accumulation in each of the sections. I observed that STF-083010 treatment resulted in a significant reduction of the lipid rich area in the atherosclerotic mice (Figure 3.23).

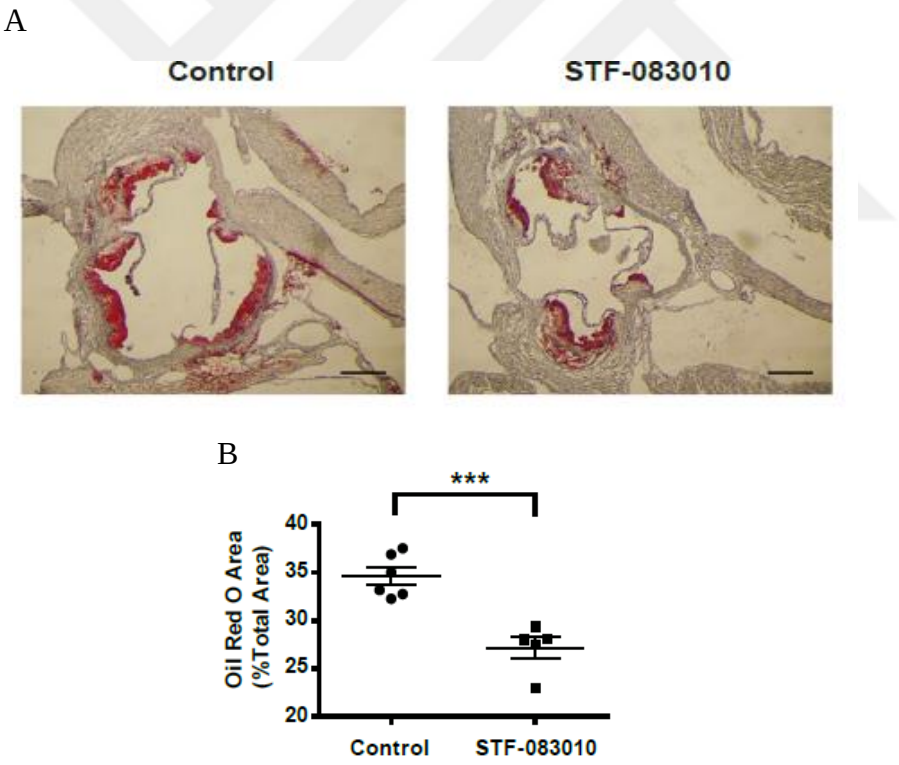

Figure 3.23. STF-083010 treatment reduces plaque area in aortic roots of ApoE$^{-/-}$ mice on Western diet.
(A) Representative images of aortic root sections from STF-0803010- or vehicle-treated ApoE$^{-/-}$ mice on Western diet that were stained with Oil RedO (Scale bar 100µm). **(B)** Calculation of plaque area from the images depicted in (A). ***P ≤ 0.001; n=5-6.

3.4.1.6. Analysis of plaque composition in aortic root sections

Atherosclerosis plaque regions are very heterogeneous in terms of their cell composition such as endothelial cells, smooth muscle cells, inflammatory cells (mainly macrophages, T cells and dendritic cells) and secreted mediators from these cells (cytokines, MMPs, DAMPs) (291). Previous studies have reported activation of the UPR occurs in many cell types in lesions is related to plaque progression (188). After observing the reduction in plaque area with STF-083010 treatment, I wanted to analyze the impact of this drug on plaque cellular composition.

3.4.1.7. The effect of STF-083010 treatment on macrophage population in aortic root sections of ApoE$^{-/-}$ mice on Western diet

Monocyte infiltration to the intima region of arteries is related to prior disruption of endothelium by factors like disturbed blood flow (particularly in the branched regions), the accumulation of lipoproteins and the accumulation of chemoattractant proteins on the transformed endothelium. The monocyte accumulation in plaque area is a major event initiating the inflammatory response dominating plaques and promoting lesion progression (151). Due to the critical role of the macrophages in inflammation in plaques, I analyzed the macrophage content in the aortic root sections obtained from STF-0803010 or vehicle-treated (control) ApoE$^{-/-}$ mice on Western diet. For this purpose I stained aortic root sections with an antibody against a protein that marks the macrophages, monocyte/macrophage marker-2 (MOMA-2). I observed a significant reduction in macrophage population in aortic root sections of STF-083010-treated mice when compared to control mice. Importantly, when sections from the same mice were stained with TUNEL assay, there were no changes in plaque apoptotic cell content (Figure 3.24). These findings suggest that the decreased macrophage number was not dependent on increased apoptosis, but likely due to the suppressive impact of IRE1

RNase inhibitors on the important macrophage chemotactic protein, CCL2, that I noted in BMDM earlier.

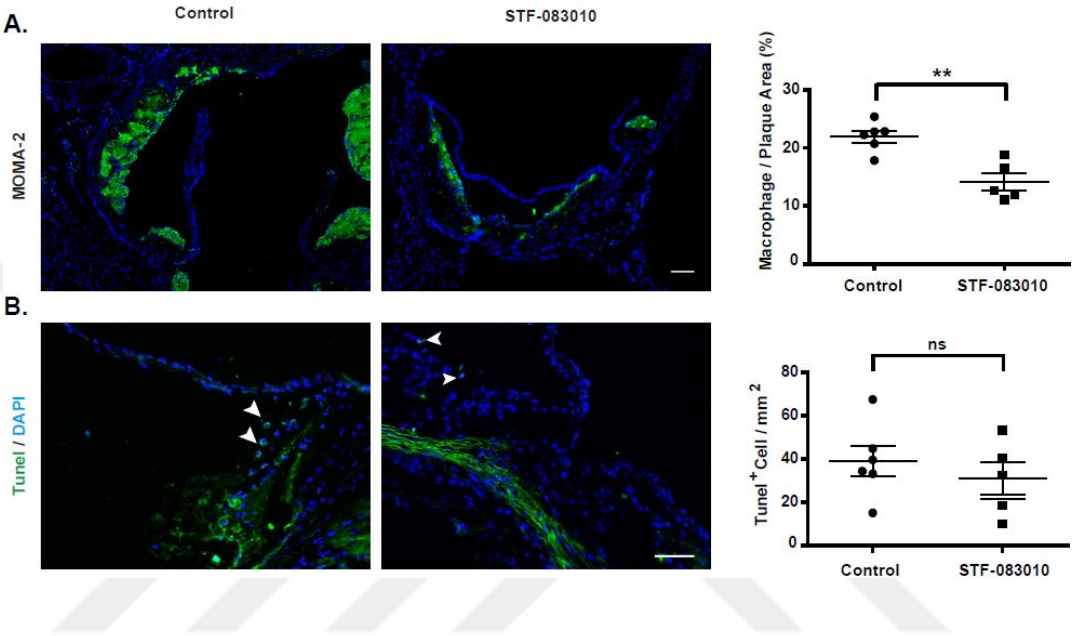

Figure 3**.24. STF-083010 treatment reduces macrophage population without altering apoptotic cell numbers in the proximal aortic root cryosections in ApoE-/- mice fed Western diet.**
(A) Representative images MOMA-2 stained aortic root sections from STF-0803010- or vehicle-treated (control) mice are shown in the *left* panel and quantification are shown in the *right* panel (Scale bar; 100µm) and **(B)** Representative images for staining with TUNEL assay of sections obtained from the same mice in A are shown in the *left* panel and quantifications shown in the *right* panel (Scale bar; 50µm) are shown. . $^{**}P \leq 0.01$; n=5.

3.4.1.8. Analysis of IL-1β levels in both aortic root sections and tissues in STF-08030-treated ApoE$^{-/-}$ mice on Western diet

Macrophages are a major contributor to the activation of immune response seen in atherosclerosis progression (151). IL-1β, which is secreted from the macrophages upon activation of the inflammasome, is one of the important immune activators in lesion progression towards vulnerable plaques. Previous studies have shown blocking the IL-1β

in ApoE$^{-/-}$ mice significantly reduced lesion area (292). I also observed significant reduction in IL-1β protein expression in heart sections of ApoE$^{-/-}$ that were treated with STF-083010 (Figure 3.25 A). Furthermore, IL-1β mRNA expression was markedly reduced with STF-083010 treatment in spleen tissues from the same mice (Figure 3.25 B).

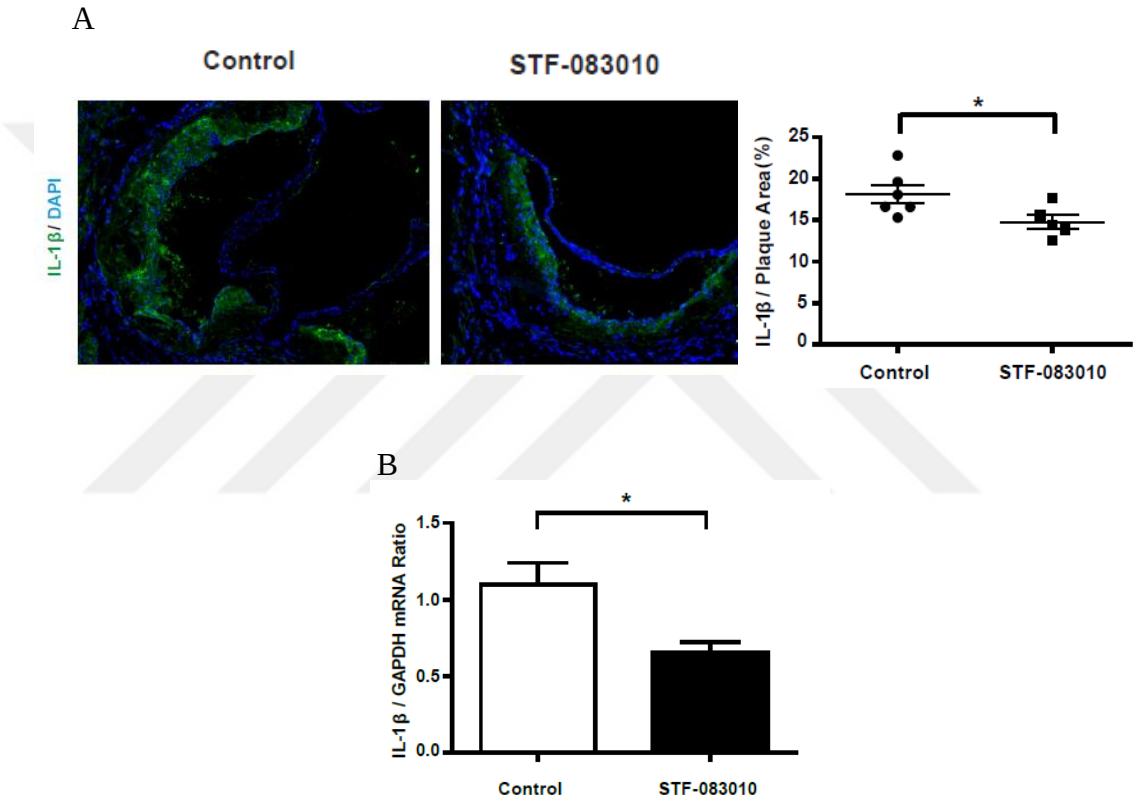

Figure 3**.25. STF-083010 treatment reduces IL-1β levels in both aortic root sections and spleen tissues.**
(A) Representative images for immunofluorescent staining for IL-1β in the aortic root sections from ApoE-/- mice treated with STF-0803010 or vehicle (control) are shown in the *left* panel and quantification is shown in the *right* panel. Scale bar: 100μm; n=5; *P ≤ 0.05. **(B)** qRT-PCR analysis of IL-1β mRNA levels in spleen obtained from the same mice in A. *P ≤ 0.05.

3.4.1.9. Analysis of collagen content and fibrous cap thickness in aortic root lesions from STF-0803010-treated ApoE$^{-/-}$ mice on Western diet

Smooth muscle cells are also one of the components of atherosclerotic lesions and they migrate to the atherosclerotic lesion area and secrete collagen that forms a fibrous cap sealing the plaque. This provides tensile strength and elasticity to plaques (163). Hence, reduced collagen amount and fibrous cap thickness are important determinants of plaque vulnerability**.** To determine whether *in vivo* inactivation of IRE1 RNase activity affects the SMCs or secretion of collagen, I stained aortic root sections obtained from STF-08030- or vehicle-treated (control) ApoE$^{-/-}$ mice with either Mason's Trichrome for collagen analysis or α-SMC actin. I observed that IRE1 RNase inhibition contributed to an increase in collagen amount without any changes in lesion SMC content (Figure 3.26 A and B. Also, I calculated fibrous cap thickness from Mason's trichrome staining, but I did not observe any changes that could be attributed to the drug treatment (Figure 3.26 C). These results suggested that the inhibition of IRE1 RNase activity could increase the tensile strength and stability of plaques through inducing more collagen secretion from lesion SMCs. However, since there was no marked increase in fibrous cap thickness with the inhibitor, the latter finding argues against this possibility.

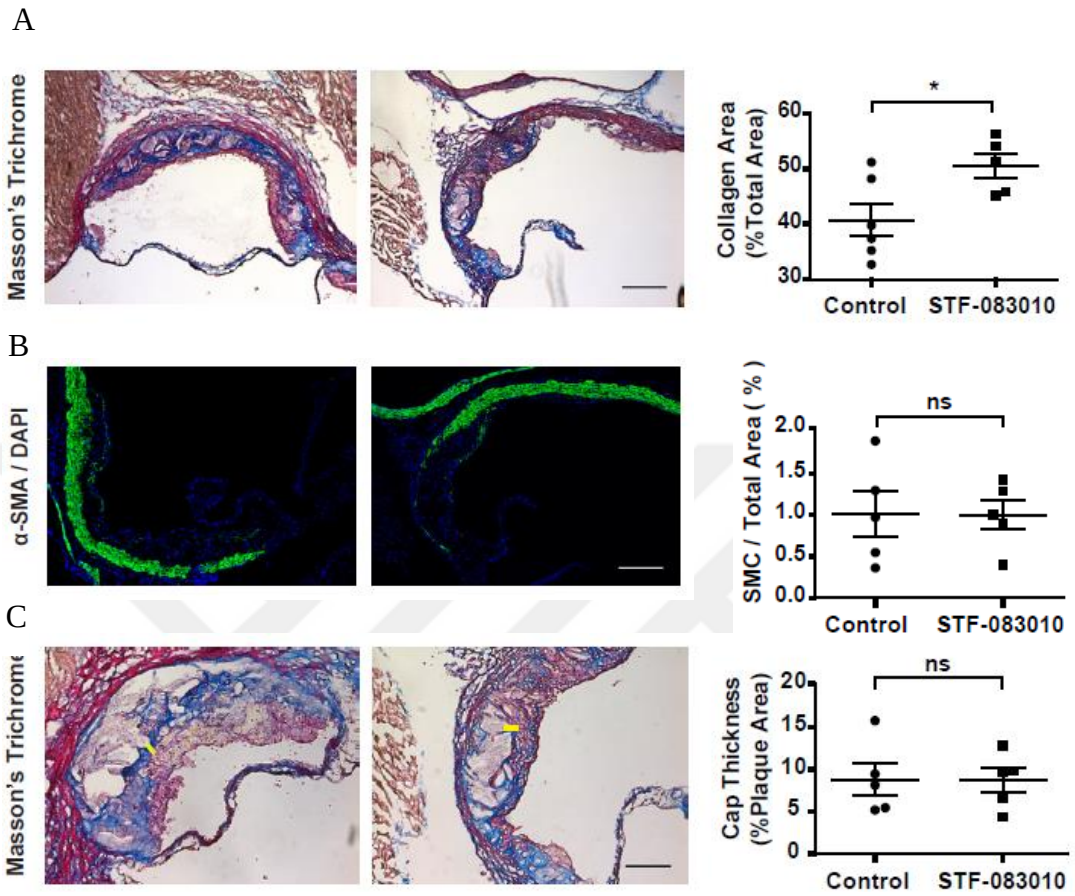

Figure 3**.26. STF-083010 treatment increases collagen content in plaques without altering SMC content and increasing fibrous cap thickness in ApoE$^{-/-}$ mice on Western diet.**

Representative images appears in the *left* and *center* panels while quantifications are depicted in the *right* panel. **(A)** Collagen area was calculated from Masson's Trichrome staining (collagen, blue; muscle fibers and cytoplasm, red). Scale bar: 200µm. **(B)** VSMC area was calculated from Anti-α smooth muscle actin staining. Scale bar: 200µm. **(C)** Fibrous cap thickness was calculated from samples in A. (Scale bar: 100 µm). ns, not significant. $^{*}P \leq 0.05$; n=5.

3.4.1.10. Analysis of total lesion area and necrotic core area in aortic root sections of STF-0803010-treated ApoE$^{-/-}$ mice on Western diet

I analyzed total lesion area and necrotic core area of aortic roots. For this purpose, I stained the tissue sections with H & E and calculated the percentage of necrotic area over total plaque area for each mouse. The results of our analysis showed IRE RNase inhibition did not affect total lesion area or necrotic core area in the aortic root sections (Figure 3.27).

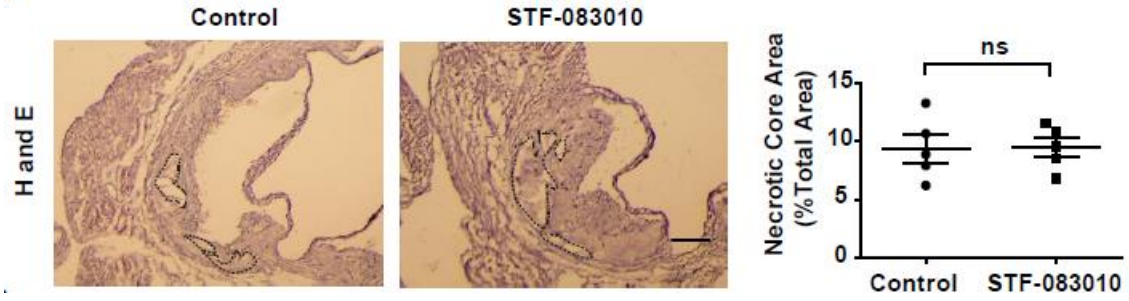

Figure 3**.27. STF-083010 treatment does not affect the size of necrotic core area in ApoE-/- mice on Western diet.**
Representative figures of aortic sections stained with H&E are shown in the *left* and quantifications appear in the *right* panel. Scale bar: 150μm. ns, not significant; n=5.

3.4.1.11. Analysis of Th-1 immune response in spleen tissues of mice

The role of T cells in the atherosclerosis progression is highly documented. Th1 cells form the majority of pathogenic T cell population infiltrating the atherosclerotic plaques. Pathogenic Th1 cells drive detrimental processes in plaques by producing IFN-γ. IFN-γ that can activate the monocytes/macrophages, inhibit vascular SMCs proliferation and block collagen production, thereby leading to thinning of fibrous cap thickness (179, 293).

To study the role of IRE1 RNase domain on Th1 cell differentiation, I collected splenocytes from STF-083010-treated and vehicle-treated (control) mice. Then, I analyzed T cell subpopulations, especially Th1, Th2 and Th17 by flow cytometry analysis. I observed that inhibition of IRE1 RNase activity reduced the number of IFN-γ producing T cell populations, which means that IRE1 RNase activity can regulate Th1 cell differentiation from the splenocytes obtained. On the other hand, I did not observe any change in Th2 and Th17 T cell subtypes suggesting the main impact of IRE1 RNase inhibition is suppression of hyperlipidemia-induced Th1 inflammatory response in $ApoE^{-/-}$ mice (Figure 3.28).

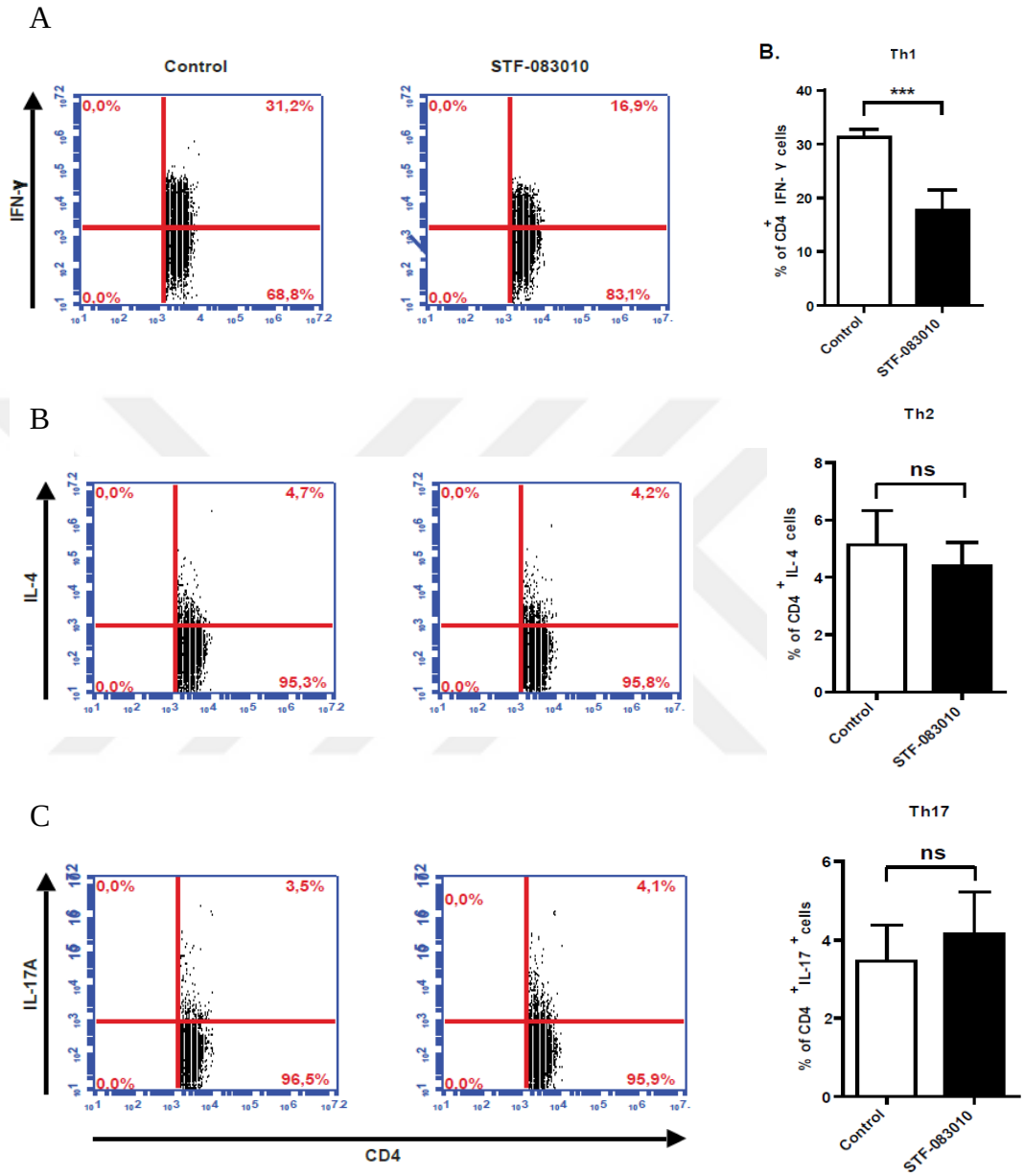

Figure 3**.28. STF-083010 treatment suppresses Th1 type immune response induced by hyperlipidemia in ApoE$^{-/-}$ mice on Western diet.**

(A-C) Flow cytometry analysis of **(A)** IFN-γ, **(B)** IL-4 and **(C)** IL-17 levels in splenocytes that were isolated from STF-0803010- or vehicle-treated (control) ApoE$^{-/-}$ mice on Western diet and activated with PMA/ionomycin. ***P ≤ 0.001; n=5 and ns, not significant).

To provide additional support to the conclusion mentioned above, I investigated the inhibitor's effect on systemic IL-18 cytokine levels by measuring it from plasma of STF-083010-treated and vehicle-treated (control) mice. IL-18 is one of the important pro-inflammatory cytokines in atherosclerosis, a product of activated inflammasome complex. It mainly affects Th1 cells by inducing IFN-γ production from them. Studies showed that plasma levels of IL-18 were increased in patients with coronary syndrome and also IL-18 was produced locally in atherosclerotic plaques (294). In parallel with the findings found in literature and the above-mentioned flow-cytometry analysis, I observed decreased IL-18 levels in plasma of animals that were treated with STF-083010 (Figure 3.29).

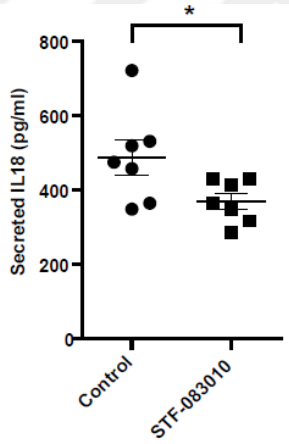

Figure 3.29. STF-083010 treatment leads to reduction in plasma IL-18 levels induced by hyperlipidemia in ApoE$^{-/-}$ mice.
The results of ELISA- based measurement of plasma IL-18 levels from STF-083010-tretaed and vehicle-treated (control) ApoE$^{-/-}$ mice on Western diet are shown. *P ≤ 0.05; n=7.

3.4.1.12. Analysis of lipoprotein profiles of STF-083010-treated ApoE$^{-/-}$ mice on Western diet

As mentioned in the introduction, lipoproteins and their modifications are important primers for the initiation and progression of atherosclerosis. Low density lipoprotein

(LDL) levels in the blood stream are closely related with atherosclerosis severity. These lipid loaded proteins can be modified and as such induce inflammation in the intima region of the blood vessels (295). I next analyzed the lipid content and their distribution into lipoprotein classes in our treatment groups by FPLC. I observed no changes in lipid content or lipoprotein class distribution in ApoE$^{-/-}$ mice treated with STF-083010 when compared to vehicle-treated (control) mice (Figure 3.30).

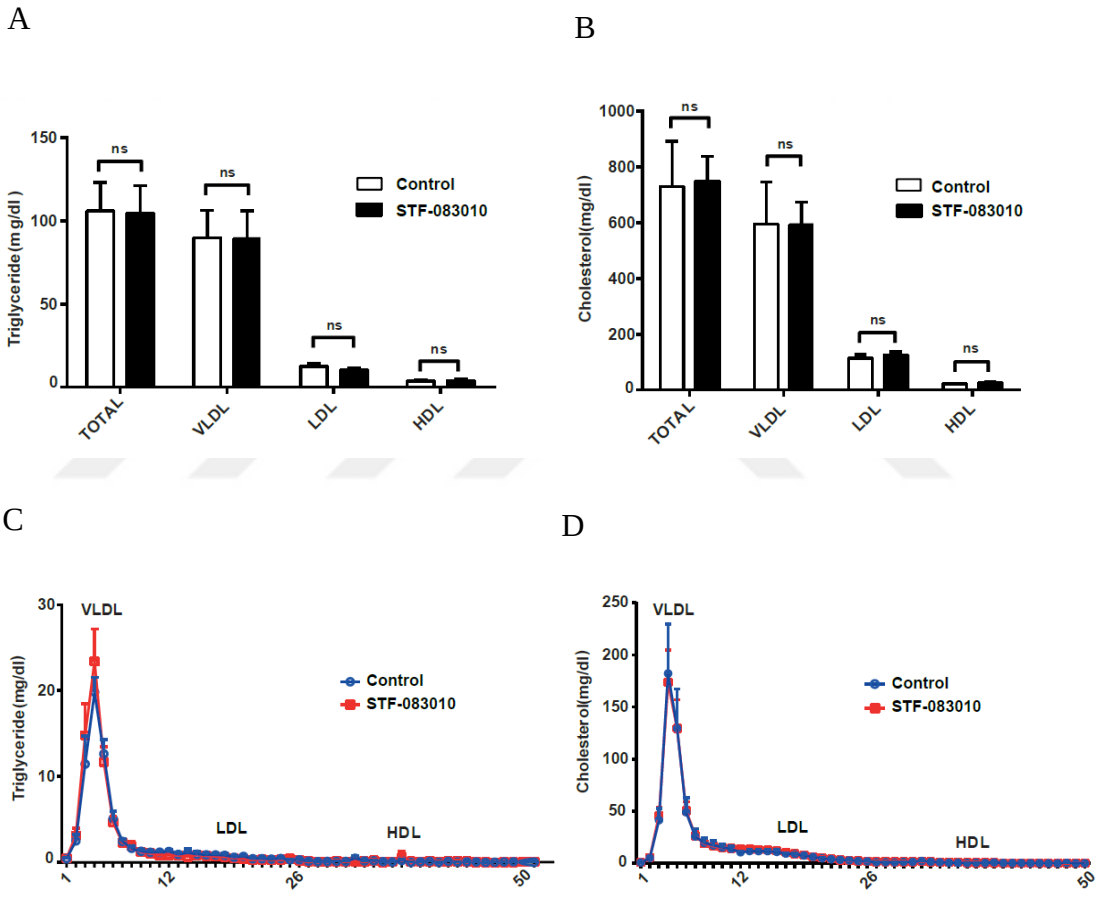

Figure 3.30. Lipoprotein profiles do not change between STF-083010-treated and vehicle-treated (control) ApoE$^{-/-}$ mice on Western diet.
(A) FPLC analysis of total triglycerides and lipoprotein triglyceride levels in control and STF-083010-treated mouse groups. **(B)** FPLC analysis of total cholesterol and lipoprotein cholesterol levels between the same mouse groups in A. **(C-D)** FPLC analysis of lipoprotein profiles of control (blue) and STF-083010-treated (red) mice blood plasma samples. ns, not significant.

Based on these results, IRE1 RNase inhibition can reduce the progression of atherosclerosis independent of correction of dyslipidemia in ApoE$^{-/-}$ mice.

3.4.2. In vivo application of 4μ8c in ApoE$^{-/-}$ mouse model of atherosclerosis

Evidences presented in this study shows that the inhibition of IRE1 RNase activity can suppress atherosclerosis progression and hyperlipidemia-driven Th1 inflammatory response. To further support our *in vivo* findings, I set up additional experiments with ApoE$^{-/-}$ mice on Western diet using a different IRE1 RNase inhibitor. I treated ApoE$^{-/-}$ mice on Western diet with 4μ8c as represented in Figure 3.31.

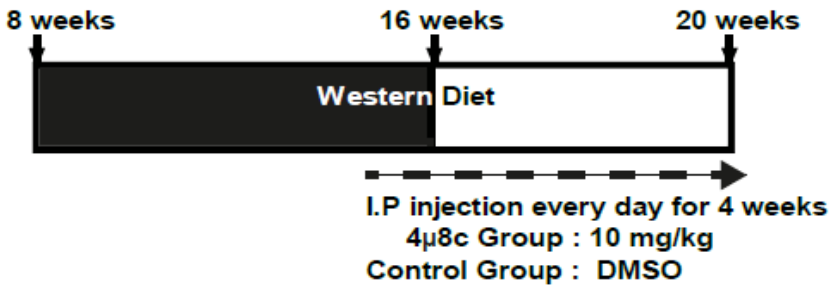

Figure 3.31. Experimental design of 4μ8c and DMSO treatments in ApoE$^{-/-}$ mice

3.4.2.1. Analysis of body weight and blood glucose in 4μ8c-treated ApoE$^{-/-}$ mice on Western diet

I first analyzed body weight and blood glucose levels of ApoE-/- mice that were treated with 4μ8c and compared to vehicle-treated (control) mice on Western diet. I observed that mice from groups gained similar weight at the end of the experiment. Also I did not see any significant differences in blood glucose levels between the groups after the treatments (Table 3.2).

Table 3.2. Body weight and blood glucose in treated animal groups

Variables	Treatment	Control	4μ8c
n		7	9
Body weight (g)	Before	28.8 ± 2.7	26.6 ± 1.9
	After	31.1 ± 2.5	28.6 ± 1.2
Glucose (mg/dl)	Before	93.9 ± 30.8	79.2 ± 19.6
	After	91.3 ± 17.0	91.9 ± 20.0

3.4.2.2. Evaluating the impact of *in vivo* 4μ8c treatment on IRE1 RNase and kinase activities

In order to determine the impact of IRE1 RNase inhibitor on its target, I analyzed the effect of 4μ8c on XBP1 splicing and IRE1 phosphorylation. As expected, 4μ8c led to a significant but partial inhibition of XBP1 mRNA splicing showing it could engage its target IRE1 RNase activity, but it did not alter phosphorylation status of IRE1 protein (Figure 3.32 A and B).

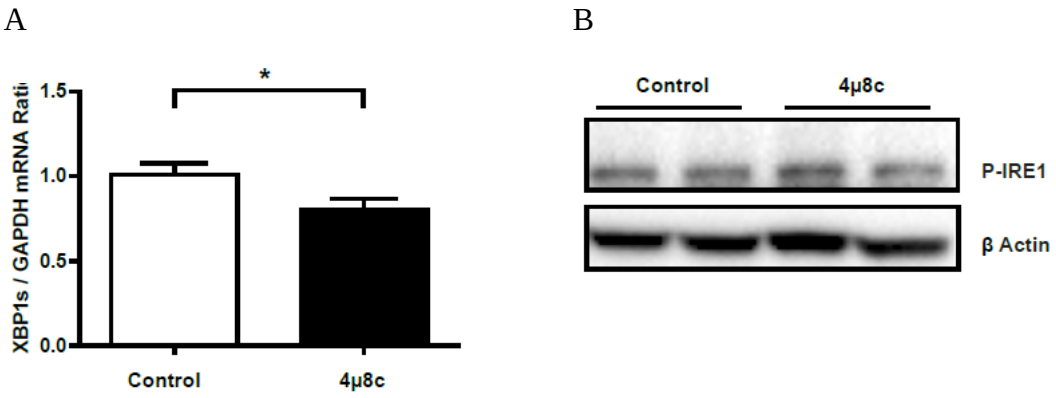

Figure 3.**32. 4μ8c treatment inhibits IRE1 RNase activity *in vivo*.**
(A) qRT-PCR analysis of spliced version of XBP1 mRNA from 4μ8c-treated and vehicle-treated (control) mice. **(B)** Western blot analysis of phospho-IRE1protein from the liver protein lysates of the same mice in A. *P ≤ 0.05.

3.4.2.3. Assessment of liver toxicity that could be related to *in vivo* 4μ8c treatment in ApoE$^{-/-}$ mice on Western diet

I analyzed histopathology of liver sections stained with H&E and ALT assay performed from plasma of ApoE$^{-/-}$ mice on Western diet that were treated with 4μ8c or vehicle (control). There were no histopathological changes that could be attributed to a 4μ8c-toxicity in the livers of these mice nor differences between ALT assay enzymatic measurements between the groups (Figure 3.33).

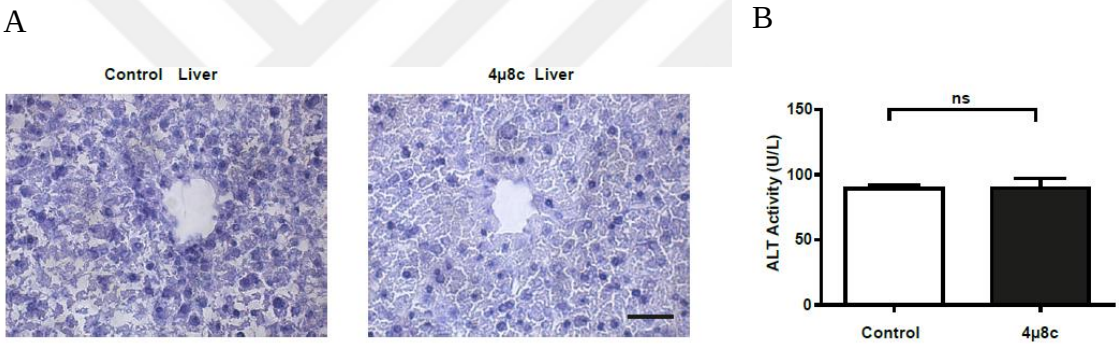

Figure 3**.33. 4μ8c treatment is not toxic in liver tissues of ApoE$^{-/-}$ mice on Western diet.**
(A) Representative figures from H&E stained liver tissue sections from ApoE-/- mice treated with 4μ8c or vehicle (control) during Western diet. **(B)** ALT assay analysis of plasma from the same mice in A. ns, not significant.

3.4.2.4. Analysis of en face plaque area

To further examine the effect of 4μ8c on atherosclerotic plaque progression, I analyzed total plaque area from en face aorta preparations. I observed that total atherosclerotic lesion area (relevant to entire aortic area) was significantly reduced in 4μ8c-treated group when compared with control group (Figure 3.34).

A B

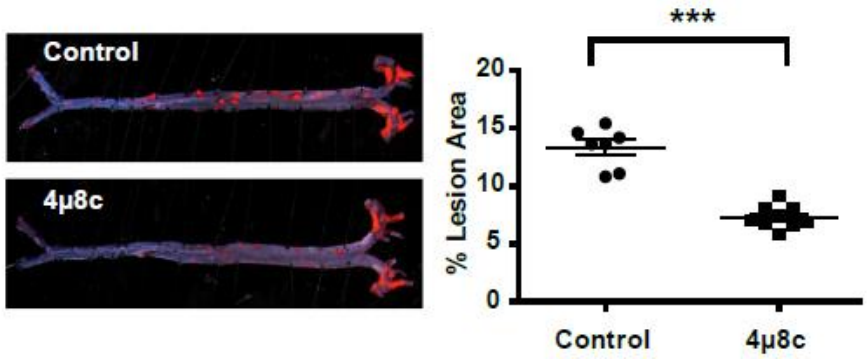

Figure 3**.34. 4μ8c treatment leads to reduction in en face plaque area.**
(A) Representative images of en face aortas stained with Sudan IV to depict lipid-rich plaque area (red) are shown. **(B)** Quantification of plaque area in A. ***P ≤ 0.001; n=13-14.

3.4.2.5. Analysis of plaque area in aortic root sections of 4μ8c-treated ApoE$^{-/-}$ mice on Western diet

After observing the reduction in en face aorta, I next analyzed the lesion area in the aortic root sections of ApoE$^{-/-}$ mice on Western diet that were treated with 4μ8c or vehicle (control). I stained lipid rich plaque regions with Oil red O stain and observed that this IRE1 RNase inhibitor significantly reduced plaque area in aortic root sections.

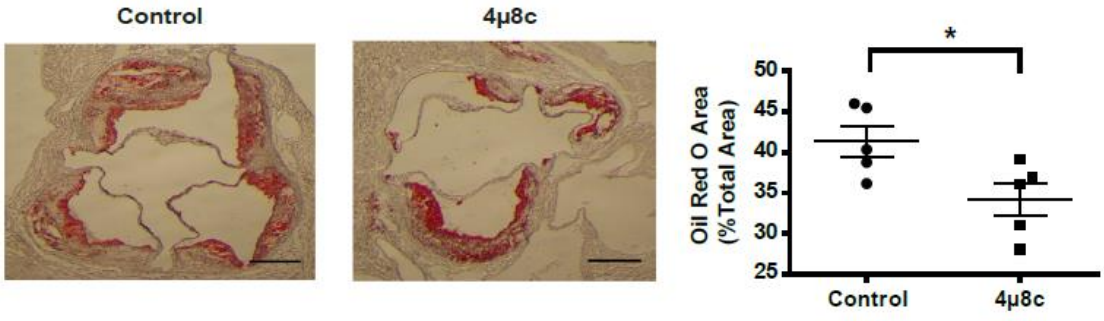

Figure 3.35. 4μ8c treatment reduces plaque area in aortic roots of ApoE$^{-/-}$ mice on Western diet.
Representative figures of aortic sections stained with Oil Red O stain are shown in *left* and quantifications appear in the *right*. Scale bar: 150μm. ns, not significant; n=5.

3.4.2.6. Analysis of IL-1β expression levels in bone marrow of 4μ8c-treated ApoE$^{-/-}$ mice on Western diet

Results obtained from both *in vitro* and *in vivo* studies using 4μ8c showed that IRE1 RNase inhibition reduced the mRNA expression of IL-1β in macrophages. Hence, I checked the bone marrow tissue taken from both 4μ8c- and DMSO-treated ApoE$^{-/-}$ mice that were fed with a Western diet at the end of the experiment and analyzed IL-1β mRNA expression by qRT-PCR. I observed that 4μ8c led to a significant decrease in IL-1β mRNA expression in bone marrow of mice (Figure 3.36).

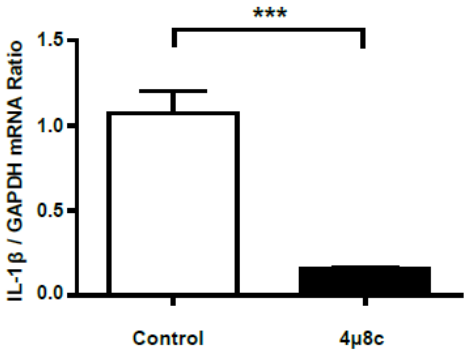

Figure 3.36. 4μ8c treatment leads to a signficant reduction in IL-1β mRNA expression in bone marrow of ApoE$^{-/-}$ mice on Western diet.
qRT-PCR analysis of IL-1β expression from bone marrow of 4μ8c- or vehicle-treated (control) ApoE$^{-/-}$ mice on Western diet is shown. ***$P \leq 0.001$

Chapter 4.

Discussion

There are many fundamental ways in which both cells and organisms interact with their environment and sustain life. Two of these ways are obtaining nutrients to meet their energy needs and defending against infections. The ability to fight pathogens and store energy can result in a significant survival advantage for the organism (296). Evolutionarily, many immunological and metabolic pathways are highly conserved from *C. elegans* to Drosophila (297). Additionally, mounting an immune response requires high energy. For example, energy consumption in our body increases 7–13% under fever conditions. Each 1°C increase in body temperature costs to 9.4×10^6 joules which is a near equivalent of a 70 kg person walking 45 km (298). In the case of sepsis, our metabolism rate increases 30–60% (299). Phagocytosis costs 7.9×10^5 joules during infection (298). Thus, it is not surprising that immune response and metabolic pathways are closely linked and interdependent. Many important cellular factors such as hormones, cytokines, signaling molecules, transcription factors, and bioactive lipids have effects on both immune and metabolic systems. For example leptin is an important polypeptide, secreted from adipocytes ant it acts as an endocrine signal and monitor a wide variety of functions in the cell. While it regulates energy expenditures and storage, it is also involved in both innate and adaptive immune responses (300). Sphingosine-1-phosphate is an important natural bioactive lipid. It is found in the composition of the sphingomyelin membranes. It behaves like a secondary messenger activating Ras-Erk and PI3K-Akt pathways. In addition to its metabolic roles, it participates to T cell regulation and development (301). Furthermore, these two systems can regulate and support each other in many ways. For example, in the early reaction against pathogens

or injury (also known as Acute Phase Response), mobilization of lipids such as cholesterol, supports the immune response (302). Also in this phase, the catabolic metabolism is stimulated instead of the anabolic metabolism, because immune reactions are energetically costly (302). To sustain good health and proper immune function, an optimal metabolic or nutritional balance is crucial (191). Evidence shows that both malnutrition and overnutrition can disturb immune function. For example, epidemiological studies show that nutrient deficiency aggravates some types of infections such as pneumonia, bacterial or viral diarrhea, measles and tuberculosis by impairing a variety of immune responses including cell-mediated immunity, phagocyte function, cytokine production, antibody response and the complement system. Nutrient deficiency, especially starvation, is the most common example of immunodeficiency (303, 304). However, to constrain the relation between immunity and metabolism to malnutrition does not sufficiently help explain the cellular and metabolic processes that are tightly and consistently integrated in normal circumstances.

The epidemic increase in obesity and related metabolic problems in the world has swung the pendulum in opposite direction (305). A wealth of evidence shows that maintaining heathy weight is as critical as malnutrition on the proper functioning of the immune system. With overnutrition, a new set of problems and complications has arisen. For example, obesity-dependent and inappropriate activation of the immune and inflammatory responses has been causally associated with insulin resistance, diabetes and cardiovascular diseases. Studies show metabolic overloading (such as in obesity) can activate inflammatory pathways and lead to an atypical form of inflammation that is low grade, chronic and involves both immune and metabolic cells (306, 307). This metabolically-driven inflammation has also come to be known as metaflammation. TNF alpha was one of the first identified inflammatory molecules that increases with obesity and connects the dysregulated immune response to insulin resistance. In addition to being elevated in human adipose tissue and circulation, this pro-inflammatory cytokine was shown to be over-produced from the adipose tissue of obese mice, and its ablation resulted in suppression of obesity-induced insulin resistance in those mice (308, 309).

Also, obesity can lead to the elevation of many other pro-inflammatory molecules such as interleukin 6 (IL-6), macrophage colony-stimulating factor(M-CSF), soluble Tumor Necrosis Factor receptor (TNFR), interleukin 18 (IL-18) and Monocyte chemoattractant protein-1(MCP1;CCL2) (307). Based on numerous subsequent studies, it has become clear that obesity-dependent metabolic stress can activate multiple inflammatory pathways that are not dependent on the presence of a pathogen.

In recent years, studies have also shown that metabolic stress can impair the function of two important intracellular organelles, the ER and mitochondria, and alter their anabolic and catabolic functions, respectively. Metabolic stress-induced dysfunction of ER and mitochondria can lead to release of ROS from these organelles and initiate some key inflammatory pathways under overnutrition conditions (297). Metabolic homeostasis is mainly dependent on these organelles. Mitochondria, known as the cellular 'power plants', produce energy from nutrients in the form of ATP (310). In addition, mitochondria are cellular sources of ROS and mitochondria-initiated pathways directly control cell death (311, 312). Many genetic or environmental factors, nutrients, hormones, exercise and aging can alter mitochondrial activity and thus influence cell survival or proliferation (313). For example, nutrient excess could lead to the accumulation of oxidized substrates like fatty acids, linked to the overproduction of ROS and finally, result in the disruption of mitochondrial function (314). Subsequently, mitochondria-generated DAMPs and ROS can lead to activation of the inflammasome complex and secretion of pro-inflammatory cytokines (123). Mitochondria dysfunction and aberrant inflammasome activation is associated with many metabolic diseases such as insulin resistance, diabetes, fatty liver and cardiovascular diseases (310, 315-317). ER is the other key organelle, that when stressed by nutrient excess can promote metaflammation (297). While the ER performs many cellular tasks such as protein folding, lipid synthesis and calcium storage, it also plays the role of a bridge between cellular metabolism and immune response (318). Like mitochondria, ER dysfunction is also observed in mice and human obesity, diabetes and atherosclerosis, and its reduction by genetic or chemical means have resulted in suppression of these diseases in mice

models (93, 191, 258). The studies described in the introduction part of my thesis establish a clear relationship between ER stress and inflammation as well as the key role of ER stress in the pathogenesis of many metabolic diseases, especially atherosclerosis. Currently, many research laboratories have focused their attention to identify the molecular details of ER stress-induced inflammation in an attempt to discover specific and novel therapeutic approaches for metabolic syndrome (188, 319). My studies identified one of the underlying links between ER stress and inflammation to be IRE1-regulated changes in mitochondrial oxidative stress response to lipids and inflammasome activation.

IRE1 can modulate a variety of pathways and cellular responses through its kinase and RNase domains (22). While some studies showed that IRE1's kinase function leads to activation of some important pro-inflammatory pathways, an understanding of the role of the IRE1 RNase domain in inflammation has been limited (272). A recent study has shown that under extreme toxin-induced ER stresses, IRE1's RNase domain, through decay of specific pre-microRNAs, can alter inflammasome activation (131). In my studies, however, I investigated the RNA substrates of IRE1 RNase activity in non-stress conditions in macrophages by using two specific inhibitors of IRE1 RNase activity, STF-083010 and 4μ8C. Surprisingly, I discovered that IRE1 targets the genes of a variety of inflammatory cytokines and receptors as well as many pro-atherogenic genes. Under normal conditions, IRE1-XBP1 signaling helps maintain the expression of these genes and when stressed by lipids, IRE1's RNase activity leads to induction in these mRNAs. Furthermore, using these inhibitors in vivo, I demonstrated that inhibition of IRE1's RNase activity uncouples hyperlipidemic stress from the induction of inflammasome-produced cytokines such as IL-1β and IL-18 in $ApoE^{-/-}$ mice on a Western diet. Therefore, the results of my studies place IRE1 at the interface of metabolism and inflammation during the course of atherosclerotic disease development.

In this study, I investigated the role of IRE1 RNase activity on transcriptome in BMDM cells using RNA-Seq. Specifically; I analyzed differentially expressed mRNAs at early

time points after inhibition of IRE1 RNase function. The intention here was to observe the direct impact of IRE1 inhibition on gene regulation. By using Ingenuity Pathway Analysis (IPA) tool, I categorized the affected genes according to their association with disease pathways. These classifications revealed that IRE1 RNase activity regulates both upregulation and downregulation of important genes in macrophages. For example, I identified that IRE1 RNase inhibition significantly downregulated many pro-atherogenic genes related to inflammatory pathways including IL-1β, CCL2 (chemokine receptor 2), MMP9 (Matrix metallopeptidase 9) and S100A8 (S100 calcium-binding protein A8) and confirmed these results with overexpression studies (using IRE1 or sXBP1) in $IRE^{-/-}$ MEF cells. In addition, my pathway analysis revealed that IRE1 also regulates key cholesterol metabolic genes such as acetyl-Coenzyme A acetyltransferase 2, pyruvate dehydrogenase kinase, isoenzyme 1 (*PDK1*), fatty acid desaturase 2 (*FADS2*) and key genes for mitochondria such as ATP-binding cassette, sub-family A (*ABC1*), member 8b (*ABCA8B*), sestrin 1(*SESN1*), glutaredoxin (*GLRX*). However, I have not completed extensive validation experiments for these interesting genes.

All three arms of the UPR are activated by both environmental and physiological stressors (252). Saturated fatty acids (SFA) are one of the major stressors causing activation of UPR in many cell types that are sensitive to perturbations of ER function such as B cell, macrophages, hepatocytes, adipocytes and pancreatic beta cells (320). Fat-rich diets contain high amounts of saturated fatty acids such as palmitate, and lead to accumulation of immune cells in metabolic tissues like adipose tissue and underneath the endothelium lining blood vessels (321, 322). When immune cells such as macrophages or dendritic cells are treated with saturated fatty acids, they are transformed to a pro-inflammatory mode and begin secreting highly inflammatory and atherogenic cytokines (323, 324). Furthermore, it was shown that the flux of SFAs in phosphatidylcholine (PC) is critical for the triggering of UPR, especially IRE1 activation (325). Hence, I investigated whether IRE1 could impact SFA-induced inflammation in macrophages. The outcome of my studies showed that IRE1-XBP1 signaling was required for SFA-induced IL-1β and CCL2 production and validated my central

hypothesis. Furthermore, I sought to understand the mechanism by which IRE1 activation and inflammatory response are linked. IL-1β secretion is regulated by the inflammasome. Earlier studies have shown that IRE1's RNase domain is involved in inflammasome activation in severe ER stress conditions induced by ER toxins such as tunicamycin and thapsigargin (133), but there were no reported observations linking IRE1 to metabolically-induced inflammasome activation. Hence, I investigated the role of IRE1's RNase domain on the activation of inflammasome by lipids. The collective data presented in my thesis demonstrates that IRE1-XBP1 axis can indeed modulate inflammasome activation under lipid induced ER stress conditions. To further delineate, whether IRE1 has a major impact on all of some of the inflammasomes, I used multiple specific inflammasome complex activators to induce the inflammasome in conjunction with IRE1 RNase inhibition. IRE1 RNase inhibition did not block absent in melanoma 2 (AIM2) and NLR Family CARD Domain Containing 4 (NLRC4) inflammasome activation (as demonstrated by caspase-1 cleavage) induced by poly (dA:dT) and flagellin, respectively, but IRE1 RNase inhibition still reduced the secretion of IL-1β under these conditions. This was expected, because findings from my RNAseq analysis and confirmatory experiments demonstrated that IRE1-XBP1 signaling regulates the expression of pro-IL-1β. In summary, the findings presented in my thesis demonstrate that IRE1 RNase activity specifically affects NLRP3 inflammasome activation.

To understand the connection between ER stress and inflammasome activation, I analyzed the release of ROS from mitochondria in lipid-stressed macrophages. SFA-induced ER stress and also the release of ROS from mitochondria (mtROS), a potent NLRP3 activator (134). Furthermore, suppression of IRE1 RNase activity blocked saturated fatty acid (SFA)-induced mtROS generation in the macrophages. Our results implied that the IRE1 –XBP1 axis plays a role in NLRP3 activation by affecting lipid induced mitochondrial ROS production.

There are close physical and functional interactions between mitochondria and endoplasmic reticulum (326, 327). Both organelles try to maintain cellular metabolism

and homeostasis, and this co-operation is impacted by stress conditions (326, 327). ER stress, through several mechanisms, can affect mitochondrial function and the production of reactive oxygen species. One mechanism involves the increased transfer of calcium from ER to mitochondria. This calcium transfer disturbs the mitochondrial functions and leads to generation of ROS from the mitochondria (328, 329). A critical molecule, thioredoxin interacting protein (TXNIP), provides another connection between ER and mitochondria under stress conditions. ER toxins such as tunicamycin have been shown to induce TXNIP, which is a regulator of redox reactions in mitochondria, and increases mtROS production and the activation of NLRP3 inflammasome (134, 330). Furthermore, another study showed IRE1 RNase activity can induce NLRP3 inflammasome activation in viral infection through the regulation of TXNIP (134). According to the data presented in my thesis, IRE1 RNase domain inhibition did not alter calcium levels in mitochondria or TXNIP expression during lipid-induced ER stress. Thus, lipid-induced IRE1 RNase activity regulates NLRP3 inflammasome activation independent of TXNIP accumulation or Ca^{2+} transfer to the mitochondria. These findings prompted us to search for a new mechanism by which ER stress and mitochondrial ROS production can be coupled during lipid overloading.

Recent studies on mitochondrial biology began to reveal the complexities of a group of mitochondrial proteins, the mitochondrial proteases. Their expression is upregulated in mammalian cells under conditions that induce mitochondrial stress (331). Hence, the stress is transmitted from the mitochondria to the nucleus (282). The mitochondrial proteases conduct a wide variety of functions from protein quality, integrity, mitochondrial biogenesis, mitophagy and apoptosis (332). Their functional impairment is associated with aging and many metabolic disorders (332). It has been shown that ER stress is one of the inducers of a particular mitochondrial matrix Lon protease, LONP1, which I tested as a candidate link between ER stress and mitochondrial oxidative stress (285, 333). In an earlier study, the ER-stress induced upregulation of LONP1 was found to be PERK-dependent (282). Hence, I first confirmed that LONP1 mRNA is induced by lipid stress in macrophages. Then, I showed that palmitate-induced LONP1 expression is

dependent on IRE1's RNase activity as well as its direct target, the transcription factor XBP1. Furthermore, it has been shown by an earlier study that LONP1 overexpression leads to induction of mtROS production in cancer cell lines. The results of my studies demonstrated that saturated fatty acid-induced an increased in mtROS production and inflammasome activation was blocked by a specific siRNA against LONP1 or small molecule LONP1 inhibitor. Although the detailed studies will be needed for how XBP1 induces LONP1 expression, my results suggest LONP1 provides a mechanism by which the ER can impact mitochondria resulting in dramatic changes in mtROS production.

.

Recent findings showing increased expression of UPR markers in multiple cell types and many stages of atherosclerosis, suggest that modulating the UPR and specifically the IRE1 RNase activity could have an important impact on atherosclerosis progression (188, 334). Many cardiovascular risk factors such as hyperglycemia, hypercholesterolemia and saturated fatty acids can trigger ER stress (25, 335, 336). Several strategies have been developed to manage atherosclerosis based on enhancing ER functions. One of these strategies is the administration of molecular chaperones such as PBA or TUDCA which have been shown to reduce general ER stress and increase insulin sensitivity in obese mice (258, 337). One of the caveats in this strategy is the need for high doses in order for these chemical chaperons to have therapeutic effects. Additionally they may have non-specific, off target effects (257). In fact, it's not clear what the specific molecular targets of these chemical chaperones are in vivo (338). Another strategy involves the targeting of ER stress-related apoptotic pathways, especially CHOP that is downstream of the PERK arm (339). Currently, no specific strategies exist for targeting the immunometabolic functions of ER because it has remained unclear how ER stress engages immunological or metabolic pathways (340). Thus, my study, by providing a mechanism by which how ER stress engages inflammatory signaling, also provides a therapeutic molecular target in the UPR that can be modified for the treatment of a chronic disease such as atherosclerosis.

The outcome of my studies has shown that IRE1 RNase domain inhibition with two different, specific small molecule inhibitors, STF-083010 and 4μ8C, can reduce atherosclerosis progression. Importantly, administration of STF-083010 did not lead to any changes in lipoprotein and lipid profiles of these mice. This indicates that the reduction in plaque size is independent of a correction of dyslipidemia. Detailed investigation of the lesions showed that the inhibition of IRE1 RNase function alters cellular composition of plaques mainly by reducing the pro-inflammatory foamy macrophage content but without altering apoptotic cell counts. Based on our in vitro data, which showed that IRE1-XBP1 signaling regulates CCL2 induction by lipids, the observed reduction in macrophage accumulation in plaque area may stem from the suppression of CCL2 by the IRE1 RNase inhibitors. Alternatively, IRE1 RNase inhibition-induced changes in the phagocytosis of dead macrophages (efferocytosis) could account for the reduction in macrophage counts in the lesions. More detailed studies will be needed to elucidate the reasons of macrophage reduction in plaque area by IRE1 RNase inhibitors.

Furthermore, I observed a significant increase in the collagen content of plaques from the IRE1 RNase inhibitor treated mice. However, I did not observe any difference in the number of lesional vascular smooth muscle cells (VSMCs) in the inhibitor-treated mice compared with control mice. Increase in the lesion collagen content provides tensile strength and elasticity to the plaques and helps prevent plaque rupture. This increase in collagen could be related to enhanced ER function resulting in augmented collagen folding and secretion, or it could be due to reduced cleavage by matrix metalloproteases (MMPs), which my data showed was another target of IRE1 RNase function in macrophages. It is also plausible that the inhibition of RIDD-dependent collagen degradation could lead to increase in collagen. Collagen, type VI, α1 (Col6) was observed as RIDD target in the study conducted by Hollien *et.al*. (35). All these possibilities need to be investigated further.

I observed reduction in both IL-1β protein levels in plaques and IL-1β expression in tissues. These observations support my in vitro findings in macrophages showing that IRE1 RNase inhibition can reduce the levels of important pro-inflammatory cytokine IL-1β. These findings are of clinical importance due to ongoing atherosclerosis clinical trials based on IL-1β antagonism (292).

In addition to macrophages T cells play an important role in the progression of atherosclerosis (341). Th1 and Th17 cell populations have been shown to drive atherosclerosis progression, whereas Th2 is shown to be suppressive (341, 342). IL-1β and IL-18, produced as a result of inflammasome activity, can promote atherosclerosis. IL-1β drives Th17 differentiation whereas IL-18 promotes Th1 differentiation (341, 343). In my studies, treatment of mice with STF-083010 reduced IL-1β in plaques and IL-18 levels in plasma. In parallel with the reduced IL-1β levels, STF-083010 led to a decrease in Th1 cell population. Treg cell populations also are important cell types in atherosclerosis due to their anti-atherogenic effects (344). While, I did not conduct any experiment to show the changes of Treg cell population in my mice, previous studies have found that IRE1 inhibition did not affect the Treg cell population (345).

The study design and the findings presented in this thesis addressed an important question regarding the contribution of IRE1 arm of the UPR signaling network to metaflammation and atherogenesis. My data shows that IRE1 RNase activity is essential for lipid-induced pro-atherogenic gene expression in vitro and in vivo. Also modulation of IRE1 RNase activity with small inhibitors can reduce plaque size and block atherosclerosis progression.

Chapter 5.

Future Perspectives

The critical role of ER stress in the progression of atherosclerosis has been stated for many years and many strategies have been developed to reduce ER stress (258, 338). In various studies, expression of UPR components, especially IRE1, was found to be upregulated (193). In this thesis, for the first time, my findings help translated the earlier observations into a strategy that is amenable to therapeutic translation. Although UPR components, mediating inflammation related pathways are expressed in many cell types, they can show different functions in different cell types (256, 259, 319). Thus selective targeting of these drugs into specific organs or cells is crucial to overcome unintended toxicity. For example, specific nanoparticles have been developed for the controlled delivery of anti-inflammatory cytokine IL-10 into particularly atherosclerotic lesions (264). This kind of targeted nanoparticle-based method can be developed to increase the specificity of drugs. For our case, macrophage specific applications of IRE1 RNase inhibitors may be more beneficial in disease progression. The intraperitoneal injection method, I used in this study, affects the whole body so higher doses of inhibitor are required compared to targeted methods. In our method, due to their chemical composition, drugs can easily be removed from the body because they have short half-lives are short (268, 346). This also limits application of this kind of drugs in clinics. Nonetheless, new drugs, targeting specifically IRE RNase domain, that are long lasting with low toxicity can be developed based on our study. There are some approaches targeting inflammatory mediators in atherosclerosis. Although they can be successful in the short-term, their prolonged use can lead to an increase in acute inflammation and a propensity for immune system deficiencies (214, 347). Thus, targeting ER stress related

inflammation is more advantageous. In the future, identification of new specific drug targets in UPR signaling pathways and inflammation related downstream components is all-important.

On the other hand, in literature, there are many missing parts in the activation and regulation of UPR pathways. We must think about both sides of the coin. While UPR pathways in the beginning of stress activate pro-survival pathways, under prolonged stress conditions, more inflammatory and apoptotic pathways are activated. The exact regulation of these pathways is not yet known (348). New protein partners of UPR components must be elucidated. For example the only known kinase substrate of IRE1 kinase domain is itself. Under different stress conditions IRE1 can associate with different partners and activate different signaling pathways. We do not have any information about whether there is any protein that associate with IRE1 and modulate its assembly and RNase function under stress conditions (22, 349, 350). Also further RNAseq studies can be performed to detect changes in transcription profiles under different stress condition and their dependency on XBP1(S) transcription factor.

Furthermore, elucidating the specific role of IRE1 RNase activity in other cell types (VSMCs and epithelial cells) that play important roles in atherosclerosis progression is crucial (351). MMP9 was found to be regulated by IRE1 RNase function in BMDMs. We can perform further experiments to find out the role of the IRE1 RNase domain in regulation of matrix metalloproteinases that are mainly secreted from VSMCs and have crucial importance in plaque stability (352). Pathways between IRE1 RNase activity and MMP9 can be potent targets for future drug investigations.

Although I showed a new function for IRE1 RNase domain in the transmission of stress from ER to mitochondria through the regulation of LONP1 (mitochondrial protease), I did not explain the mechanistic details of this interaction. I only showed that lipid induced upregulation of LONP1 is dependent on IRE1 RNase activity and also silencing

of LONP1 led to a decrease in inflammasome activation. Further experiments are needed to prove the relation between IRE1-LONP1 and inflammasome activation. Future experiments can focus on mitochondrial protease targets of LONP1. One of the targets of LONP1 is PINK which is an important protein in mitophagy (353). Based on the findings in this study, the inhibition of IRE1 RNase activity and the resultant reduction of LONP1 could be paralleled with an increase of PINK protein. This in effect could induce mitophagy in cells. Mitophagy is important pathway for the removal of ROS production and reduction of inflammasome activation (354, 355). This could be the basis for a mechanistic explanation to the role of IRE1 RNase domain in inflammasome activation and constitute a subject for upcoming scientific projects.

Bibliography

1. Westrate LM, Lee JE, Prinz WA, & Voeltz GK (2015) Form follows function: the importance of endoplasmic reticulum shape. *Annu Rev Biochem* 84:791-811.
2. Schwarz DS & Blower MD (2016) The endoplasmic reticulum: structure, function and response to cellular signaling. *Cellular and molecular life sciences : CMLS* 73:79-94.
3. Fagone P & Jackowski S (2009) Membrane phospholipid synthesis and endoplasmic reticulum function. *J Lipid Res* 50 Suppl:S311-316.
4. Braakman I & Hebert DN (2013) Protein Folding in the Endoplasmic Reticulum. *Cold Spring Harbor perspectives in biology* 5(5).
5. Araki K & Nagata K (2011) Protein Folding and Quality Control in the ER. *Cold Spring Harbor perspectives in biology* 3(11).
6. Vance JE (1990) Phospholipid synthesis in a membrane fraction associated with mitochondria. *J Biol Chem* 265(13):7248-7256.
7. Rowland AA & Voeltz GK (Endoplasmic reticulum-mitochondria contacts: function of the junction. *Nat Rev Mol Cell Biol* 13(10):607-625.
8. Basseri S & Austin RC (2008) ER stress and lipogenesis: a slippery slope toward hepatic steatosis. *Dev Cell* 15(6):795-796.
9. Basseri S & Austin RC (2012) Endoplasmic Reticulum Stress and Lipid Metabolism: Mechanisms and Therapeutic Potential. *Biochemistry Research International* 2012:13.
10. Vallim T & Salter A (2010) Regulation of hepatic gene expression by saturated fatty acids. *Prostaglandins, Leukotrienes, and Essential Fatty Acids* 82(4-6):211-218.
11. Jaffe LF (1983) Sources of calcium in egg activation: a review and hypothesis. *Developmental biology* 99(2):265-276.
12. Clapham DE (Calcium Signaling. *Cell* 131(6):1047-1058.
13. Gilkey JC, Jaffe LF, Ridgway EB, & Reynolds GT (1978) A free calcium wave traverses the activating egg of the medaka, Oryzias latipes. *J Cell Biol* 76(2):448-466.
14. Krols M, Bultynck G, & Janssens S (2016) ER–Mitochondria contact sites: A new regulator of cellular calcium flux comes into play. *The Journal of Cell Biology* 214(4):367-370.
15. Cardenas C, *et al.* (2010) Essential regulation of cell bioenergetics by constitutive InsP3 receptor Ca2+ transfer to mitochondria. *Cell* 142(2):270-283.

16. Booth David M, Enyedi B, Geiszt M, Várnai P, & Hajnóczky G (2016) Redox Nanodomains Are Induced by and Control Calcium Signaling at the ER-Mitochondrial Interface. *Molecular Cell* 63(2):240-248.

17. Vembar SS & Brodsky JL (2008) One step at a time: endoplasmic reticulum-associated degradation. *Nature reviews. Molecular cell biology* 9(12):944-957.

18. McGuckin MA, Eri RD, Das I, Lourie R, & Florin TH (2010) ER stress and the unfolded protein response in intestinal inflammation. *American Journal of Physiology - Gastrointestinal and Liver Physiology* 298(6):G820-G832.

19. Taouji S, Wolf S, & Chevet E (2013) Chapter Seventeen - Oligomerization in Endoplasmic Reticulum Stress Signaling. *Progress in Molecular Biology and Translational Science*, eds Jesús G & Francisco C (Academic Press), Vol Volume 117, pp 465-484.

20. Hetz C (2012) The unfolded protein response: controlling cell fate decisions under ER stress and beyond. *Nat Rev Mol Cell Biol* 13(2):89-102.

21. Hetz C, Martinon F, Rodriguez D, & Glimcher LH (2011) The unfolded protein response: integrating stress signals through the stress sensor IRE1alpha. *Physiol Rev* 91.

22. Ron D & Walter P (2007) Signal integration in the endoplasmic reticulum unfolded protein response. *Nat Rev Mol Cell Biol* 8(7):519-529.

23. Tabas I & Ron D (2011) Integrating the mechanisms of apoptosis induced by endoplasmic reticulum stress. *Nature cell biology* 13.

24. Yoshida H, Matsui T, Yamamoto A, Okada T, & Mori K (2001) XBP1 mRNA is induced by ATF6 and spliced by IRE1 in response to ER stress to produce a highly active transcription factor. *Cell* 107.

25. Wang S & Kaufman RJ (2012) The impact of the unfolded protein response on human disease. *J Cell Biol* 197(7):857-867.

26. Walter P & Ron D (2011) The unfolded protein response: from stress pathway to homeostatic regulation. *Science* 334.

27. Chen Y & Brandizzi F (2013) IRE1: ER stress sensor and cell fate executor. *Trends in cell biology* 23(11):547-555.

28. Yoshida H, Matsui T, Yamamoto A, Okada T, & Mori K (2001) XBP1 mRNA is induced by ATF6 and spliced by IRE1 in response to ER stress to produce a highly active transcription factor. *Cell* 107(7):881-891.

29. Lee AH, Iwakoshi NN, & Glimcher LH (2003) XBP-1 regulates a subset of endoplasmic reticulum resident chaperone genes in the unfolded protein response. *Mol Cell Biol* 23(21):7448-7459.

30. Acosta-Alvear D, *et al.* (2007) XBP1 controls diverse cell type- and condition-specific transcriptional regulatory networks. *Mol Cell* 27(1):53-66.

31. Sriburi R, Jackowski S, Mori K, & Brewer JW (2004) XBP1: a link between the unfolded protein response, lipid biosynthesis, and biogenesis of the endoplasmic reticulum. *J Cell Biol* 167(1):35-41.

32. Uemura A, *et al.* (2013) UBC9 regulates the stability of XBP1, a key transcription factor controlling the ER stress response. *Cell structure and function* 38(1):67-79.

33. Yanagitani K, Kimata Y, Kadokura H, & Kohno K (2011) Translational pausing ensures membrane targeting and cytoplasmic splicing of XBP1u mRNA. *Science* 331(6017):586-589.

34. Yoshida H, Oku M, Suzuki M, & Mori K (2006) pXBP1(U) encoded in XBP1 pre-mRNA negatively regulates unfolded protein response activator pXBP1(S) in mammalian ER stress response. *J Cell Biol* 172(4):565-575.

35. Hollien J, *et al.* (2009) Regulated Ire1-dependent decay of messenger RNAs in mammalian cells. *J Cell Biol* 186(3):323-331.

36. Hollien J & Weissman JS (2006) Decay of endoplasmic reticulum-localized mRNAs during the unfolded protein response. *Science* 313(5783):104-107.

37. Maurel M, Chevet E, Tavernier J, & Gerlo S (2014) Getting RIDD of RNA: IRE1 in cell fate regulation. *Trends in biochemical sciences* 39(5):245-254.

38. Upton JP, *et al.* (2012) IRE1alpha Cleaves Select microRNAs during ER Stress to Derepress Translation of Proapoptotic Caspase-2. *Science*.

39. Korennykh AV, *et al.* (2009) The unfolded protein response signals through high-order assembly of Ire1. *Nature* 457(7230):687-693.

40. Urano F, *et al.* (2000) Coupling of stress in the ER to activation of JNK protein kinases by transmembrane protein kinase IRE1. *Science* 287(5453):664-666.

41. Tam AB, Mercado EL, Hoffmann A, & Niwa M (2012) ER stress activates NF-kappaB by integrating functions of basal IKK activity, IRE1 and PERK. *PLoS One* 7(10):e45078.

42. Harding HP, Zhang Y, Bertolotti A, Zeng H, & Ron D (2000) Perk is essential for translational regulation and cell survival during the unfolded protein response. *Mol Cell* 5(5):897-904.

43. Harding HP, Zhang Y, & Ron D (1999) Protein translation and folding are coupled by an endoplasmic-reticulum-resident kinase. *Nature* 397.

44. Liu Z, Lv Y, Zhao N, Guan G, & Wang J (2015) Protein kinase R-like ER kinase and its role in endoplasmic reticulum stress-decided cell fate. *Cell Death Dis* 6:e1822.

45. Akai R, Hosoda A, Yoshino M, & Iwawaki T (2015) Constitutive role of GADD34 and CReP in cancellation of phospho-eIF2alpha-dependent translational attenuation and insulin biosynthesis in pancreatic beta cells. *Genes to cells : devoted to molecular & cellular mechanisms* 20(11):871-886.

46. Cullinan SB, *et al.* (2003) Nrf2 Is a Direct PERK Substrate and Effector of PERK-Dependent Cell Survival. *Mol Cell Biol* 23(20):7198-7209.

47. Haze K, Yoshida H, Yanagi H, Yura T, & Mori K (1999) Mammalian transcription factor ATF6 is synthesized as a transmembrane protein and activated by proteolysis in response to endplasmic reticulum stress. *Mol Biol Cell* 10.

48. Shen J, Chen X, Hendershot L, & Prywes R (2002) ER stress regulation of ATF6 localization by dissociation of BiP/GRP78 binding and unmasking of Golgi localization signals. *Dev Cell* 3(1):99-111.

49. Chen X, Shen J, & Prywes R (2002) The luminal domain of ATF6 senses endoplasmic reticulum (ER) stress and causes translocation of ATF6 from the ER to the Golgi. *J Biol Chem* 277(15):13045-13052.

50. Ye J, *et al.* (2000) ER stress induces cleavage of membrane-bound ATF6 by the same proteases that process SREBPs. *Mol Cell* 6(6):1355-1364.

51. Yamamoto K, *et al.* (2007) Transcriptional induction of mammalian ER quality control proteins is mediated by single or combined action of ATF6alpha and XBP1. *Dev Cell* 13(3):365-376.

52. Adachi Y, *et al.* (2008) ATF6 is a transcription factor specializing in the regulation of quality control proteins in the endoplasmic reticulum. *Cell structure and function* 33(1):75-89.

53. Bommiasamy H, *et al.* (2009) ATF6alpha induces XBP1-independent expansion of the endoplasmic reticulum. *J Cell Sci* 122(Pt 10):1626-1636.

54. Belmont PJ, *et al.* (2010) Roles for endoplasmic reticulum-associated degradation and the novel endoplasmic reticulum stress response gene Derlin-3 in the ischemic heart. *Circ Res* 106(2):307-316.

55. Hirsch I, Weiwad M, Prell E, & Ferrari DM (2014) ERp29 deficiency affects sensitivity to apoptosis via impairment of the ATF6-CHOP pathway of stress response. *Apoptosis : an international journal on programmed cell death* 19(5):801-815.

56. Wu J, *et al.* (2007) ATF6alpha optimizes long-term endoplasmic reticulum function to protect cells from chronic stress. *Dev Cell* 13(3):351-364.

57. Yamazaki H, *et al.* (2009) Activation of the Akt-NF-kappaB pathway by subtilase cytotoxin through the ATF6 branch of the unfolded protein response. *J Immunol* 183(2):1480-1487.

58. Janssens S, Pulendran B, & Lambrecht BN (2014) Emerging functions of the unfolded protein response in immunity. *Nat Immunol* 15(10):910-919.

59. Hollien J (2013) Evolution of the unfolded protein response. *Biochimica et Biophysica Acta (BBA) - Molecular Cell Research* 1833(11):2458-2463.

60. Kimmig P, *et al.* (2012) The unfolded protein response in fission yeast modulates stability of select mRNAs to maintain protein homeostasis. *eLife* 1.

61. Askew DS (2014) Endoplasmic reticulum stress and fungal pathogenesis converge. *Virulence* 5(2):331-333.

62. Nagashima Y, *et al.* (2011) Arabidopsis IRE1 catalyses unconventional splicing of bZIP60 mRNA to produce the active transcription factor. *Scientific Reports* 1:29.

63. Moreno AA, *et al.* (2012) IRE1/bZIP60-mediated unfolded protein response plays distinct roles in plant immunity and abiotic stress responses. *PLoS One* 7(2):e31944.

64. Jelitto-Van Dooren EP, Vidal S, & Denecke J (1999) Anticipating endoplasmic reticulum stress. A novel early response before pathogenesis-related gene induction. *The Plant Cell* 11(10):1935-1944.

65. Shen X, *et al.* (2001) Complementary signaling pathways regulate the unfolded protein response and are required for C. elegans development. *Cell* 107(7):893-903.

66. Richardson CE, Kooistra T, & Kim DH (2010) An essential role for XBP-1 in host protection against immune activation in C. elegans. *Nature* 463(7284):1092-1095.

67. Hinnebusch AG & Lorsch JR (2012) The mechanism of eukaryotic translation initiation: new insights and challenges. *Cold Spring Harbor perspectives in biology* 4(10).

68. Feng B, *et al.* (2003) The endoplasmic reticulum is the site of cholesterol-induced cytotoxicity in macrophages. *Nat Cell Biol* 5(9):781-792.

69. Maedler K, *et al.* (2002) Glucose-induced beta cell production of IL-1beta contributes to glucotoxicity in human pancreatic islets. *J Clin Invest* 110(6):851-860.

70. Kharroubi I, *et al.* (2004) Free fatty acids and cytokines induce pancreatic beta-cell apoptosis by different mechanisms: role of nuclear factor-kappaB and endoplasmic reticulum stress. *Endocrinology* 145(11):5087-5096.

71. Yamamuro A, Yoshioka Y, Ogita K, & Maeda S (2006) Involvement of endoplasmic reticulum stress on the cell death induced by 6-hydroxydopamine in human neuroblastoma SH-SY5Y cells. *Neurochemical research* 31(5):657-664.

72. Zhang K & Kaufman RJ (2008) From endoplasmic-reticulum stress to the inflammatory response. *Nature* 454(7203):455-462.

73. Hotamisligil GS (2006) Inflammation and metabolic disorders. *Nature* 444(7121):860-867.

74. Cao SS & Kaufman RJ (2014) Endoplasmic Reticulum Stress and Oxidative Stress in Cell Fate Decision and Human Disease. *Antioxidants & redox signaling* 21(3):396-413.

75. Chaudhari N, Talwar P, Parimisetty A, Lefebvre d'Hellencourt C, & Ravanan P (2014) A Molecular Web: Endoplasmic Reticulum Stress, Inflammation, and Oxidative Stress. *Frontiers in Cellular Neuroscience* 8.

76. Raturi A & Simmen T (2013) Where the endoplasmic reticulum and the mitochondrion tie the knot: the mitochondria-associated membrane (MAM). *Biochim Biophys Acta* 1833(1):213-224.

77. Flis VV & Daum G (2013) Lipid Transport between the Endoplasmic Reticulum and Mitochondria. *Cold Spring Harbor perspectives in biology* 5(6).

78. Kaufman RJ (2002) Orchestrating the unfolded protein response in health and disease. *J Clin Invest* 110(10):1389-1398.

79. Lindholm D, Wootz H, & Korhonen L (2006) ER stress and neurodegenerative diseases. *Cell Death Differ* 13(3):385-392.

80. Hotamisligil GS (2008) Inflammation and endoplasmic reticulum stress in obesity and diabetes. *Int J Obes (Lond)* 32 Suppl 7:S52-54.

81. Hotamisligil GS (2010) Endoplasmic reticulum stress and the inflammatory basis of metabolic disease. *Cell* 140(6):900-917.

82. Hotamisligil GS (2010) Endoplasmic reticulum stress and atherosclerosis. *Nat Med* 16(4):396-399.

83. Hasnain SZ, Lourie R, Das I, Chen ACH, & McGuckin MA (2012) The interplay between endoplasmic reticulum stress and inflammation. *Immunol Cell Biol* 90(3):260-270.

84. Navid F & Colbert RA (2017) Causes and consequences of endoplasmic reticulum stress in rheumatic disease. *Nat Rev Rheumatol* 13(1):25-40.

85. Kaneko M, Niinuma Y, & Nomura Y (2003) Activation signal of nuclear factor-kappa B in response to endoplasmic reticulum stress is transduced via IRE1 and tumor necrosis factor receptor-associated factor 2. *Biological & pharmaceutical bulletin* 26(7):931-935.

86. Raha S & Robinson BH (2000) Mitochondria, oxygen free radicals, disease and ageing. *Trends in biochemical sciences* 25(10):502-508.

87. Rius J, *et al.* (2008) NF-kappaB links innate immunity to the hypoxic response through transcriptional regulation of HIF-1alpha. *Nature* 453(7196):807-811.

88. Lawrence T (2009) The Nuclear Factor NF-κB Pathway in Inflammation. *Cold Spring Harbor perspectives in biology* 1(6).

89. Pahl HL & Baeuerle PA (1996) Activation of NF-kappa B by ER stress requires both Ca2+ and reactive oxygen intermediates as messengers. *FEBS letters* 392(2):129-136.

90. Jiang HY, *et al.* (2003) Phosphorylation of the alpha subunit of eukaryotic initiation factor 2 is required for activation of NF-kappaB in response to diverse cellular stresses. *Mol Cell Biol* 23(16):5651-5663.

91. Rao J, *et al.* (2014) ATF6 Mediates a Pro-inflammatory Synergy between ER Stress and TLR Activation in the Pathogenesis of Liver Ischemia Reperfusion Injury. *American journal of transplantation : official journal of the American Society of Transplantation and the American Society of Transplant Surgeons* 14(7):1552-1561.

92. Keestra-Gounder AM, *et al.* (2016) NOD1 and NOD2 signalling links ER stress with inflammation. *Nature* 532(7599):394-397.

93. Ozcan U, *et al.* (2004) Endoplasmic reticulum stress links obesity, insulin action, and type 2 diabetes. *Science* 306(5695):457-461.

94. Urano F, *et al.* (2000) Coupling of stress in the ER to activation of JNK protein kinases by transmembrane protein kinase IRE1. *Science* 287.

95. Smith JA, *et al.* (2008) Endoplasmic reticulum stress and the unfolded protein response are linked to synergistic IFN-beta induction via X-box binding protein 1. *European journal of immunology* 38(5):1194-1203.

96. Martinon F, Chen X, Lee AH, & Glimcher LH (2010) TLR activation of the transcription factor XBP1 regulates innate immune responses in macrophages. *Nat Immunol* 11(5):411-418.

97. Bartoszewski R, *et al.* (2011) The Unfolded Protein Response (UPR)-activated Transcription Factor X-box-binding Protein 1 (XBP1) Induces MicroRNA-346 Expression That Targets the Human Antigen Peptide Transporter 1 (TAP1) mRNA and Governs Immune Regulatory Genes. *J Biol Chem* 286(48):41862-41870.

98. Osorio F, *et al.* (2014) The unfolded-protein-response sensor IRE-1alpha regulates the function of CD8alpha+ dendritic cells. *Nat Immunol* 15(3):248-257.

99. Cho JA, *et al.* (2013) The unfolded protein response element IRE1alpha senses bacterial proteins invading the ER to activate RIG-I and innate immune signaling. *Cell host & microbe* 13(5):558-569.

100. Goodall JC, *et al.* (2010) Endoplasmic reticulum stress-induced transcription factor, CHOP, is crucial for dendritic cell IL-23 expression. *Proceedings of the National Academy of Sciences of the United States of America* 107(41):17698-17703.

101. Chen GY & Nunez G (2010) Sterile inflammation: sensing and reacting to damage. *Nat Rev Immunol* 10(12):826-837.

102. Horvath GL, Schrum JE, De Nardo CM, & Latz E (2011) Intracellular sensing of microbes and danger signals by the inflammasomes. *Immunological reviews* 243(1):119-135.

103. Lamkanfi M & Dixit VM (2014) Mechanisms and functions of inflammasomes. *Cell* 157(5):1013-1022.

104. Ting JP, *et al.* (2008) The NLR gene family: a standard nomenclature. *Immunity* 28(3):285-287.

105. Sharma D & Kanneganti T-D (2016) The cell biology of inflammasomes: Mechanisms of inflammasome activation and regulation. *The Journal of Cell Biology* 213(6):617-629.

106. Shao W, Yeretssian G, Doiron K, Hussain SN, & Saleh M (2007) The caspase-1 digestome identifies the glycolysis pathway as a target during infection and septic shock. *J Biol Chem* 282(50):36321-36329.

107. Thornberry NA, *et al.* (1992) A novel heterodimeric cysteine protease is required for interleukin-1 beta processing in monocytes. *Nature* 356(6372):768-774.

108. Gu Y, *et al.* (1997) Activation of interferon-gamma inducing factor mediated by interleukin-1beta converting enzyme. *Science* 275(5297):206-209.

109. Miao EA, Rajan JV, & Aderem A (2011) Caspase-1-induced pyroptotic cell death. *Immunological reviews* 243(1):206-214.

110. Dinarello CA (1999) IL-18: A TH1 -inducing, proinflammatory cytokine and new member of the IL-1 family. *Journal of Allergy and Clinical Immunology* 103(1):11-24.

111. Dinarello CA (1996) Biologic basis for interleukin-1 in disease. *Blood* 87(6):2095-2147.

112. Kummer JA, *et al.* (2007) Inflammasome Components NALP 1 and 3 Show Distinct but Separate Expression Profiles in Human Tissues Suggesting a Site-specific Role in the Inflammatory Response. *Journal of Histochemistry & Cytochemistry* 55(5):443-452.

113. Hornung V, *et al.* (2009) AIM2 recognizes cytosolic dsDNA and forms a caspase-1-activating inflammasome with ASC. *Nature* 458(7237):514-518.

114. Faustin B, *et al.* (2007) Reconstituted NALP1 Inflammasome Reveals Two-Step Mechanism of Caspase-1 Activation. *Molecular Cell* 25(5):713-724.

115. Vance RE (2015) The NAIP/NLRC4 inflammasomes. *Curr Opin Immunol* 32:84-89.

116. Tenthorey JL, Kofoed EM, Daugherty MD, Malik HS, & Vance RE (2014) Molecular basis for specific recognition of bacterial ligands by NAIP/NLRC4 inflammasomes. *Mol Cell* 54(1):17-29.

117. Man SM & Kanneganti TD (2015) Regulation of inflammasome activation. *Immunological reviews* 265(1):6-21.

118. Wen H, *et al.* (2011) Fatty acid-induced NLRP3-PYCARD inflammasome activation interferes with insulin signaling. *Nature immunology* 12(5):408-415.

119. Bauernfeind FG, *et al.* (2009) Cutting edge: NF-kappaB activating pattern recognition and cytokine receptors license NLRP3 inflammasome activation by regulating NLRP3 expression. *J Immunol* 183(2):787-791.

120. Cruz CM, *et al.* (2007) ATP activates a reactive oxygen species-dependent oxidative stress response and secretion of proinflammatory cytokines in macrophages. *J Biol Chem* 282(5):2871-2879.

121. Petrilli V, *et al.* (2007) Activation of the NALP3 inflammasome is triggered by low intracellular potassium concentration. *Cell Death Differ* 14(9):1583-1589.

122. Dostert C, *et al.* (2008) Innate immune activation through Nalp3 inflammasome sensing of asbestos and silica. *Science* 320(5876):674-677.

123. Zhou R, Yazdi AS, Menu P, & Tschopp J (2011) A role for mitochondria in NLRP3 inflammasome activation. *Nature* 469(7329):221-225.

124. Murakami T, *et al.* (2012) Critical role for calcium mobilization in activation of the NLRP3 inflammasome. *Proceedings of the National Academy of Sciences of the United States of America* 109(28):11282-11287.

125. Zhang J, Zhang K, Li Z, & Guo B (2016) ER Stress-induced Inflammasome Activation Contributes to Hepatic Inflammation and Steatosis. *Journal of clinical & cellular immunology* 7(5).

126. Lebeaupin C, *et al.* (2015) ER stress induces NLRP3 inflammasome activation and hepatocyte death. *Cell Death Dis* 6(9):e1879-.

127. Menu P, *et al.* (2012) ER stress activates the NLRP3 inflammasome via an UPR-independent pathway. *Cell Death Dis* 3:e261.

128. Shalev A, *et al.* (2002) Oligonucleotide microarray analysis of intact human pancreatic islets: identification of glucose-responsive genes and a highly regulated TGFβ signaling pathway. *Endocrinology* 143(9):3695-3695.

129. Chen J, Fontes G, Saxena G, Poitout V, & Shalev A (2010) Lack of TXNIP Protects Against Mitochondria-Mediated Apoptosis but Not Against Fatty Acid–Induced ER Stress–Mediated β-Cell Death. *Diabetes* 59(2):440-447.

130. Shalev A (2014) Minireview: Thioredoxin-Interacting Protein: Regulation and Function in the Pancreatic β-Cell. *Molecular Endocrinology* 28(8):1211-1220.

131. Lerner AG, *et al.* (2012) IRE1α induces thioredoxin-interacting protein to activate the NLRP3 inflammasome and promote programmed cell death under irremediable ER stress. *Cell metabolism* 16(2):250-264.

132. Oslowski CM, *et al.* (2012) Thioredoxin-interacting protein mediates ER stress-induced beta-cell death through initiation of the inflammasome. *Cell Metab* 16.

133. Lerner AG, *et al.* (2012) IRE1alpha induces thioredoxin-interacting protein to activate the NLRP3 inflammasome and promote programmed cell death under irremediable ER stress. *Cell Metab* 16(2):250-264.

134. Bronner DN, *et al.* (2015) Endoplasmic Reticulum Stress Activates the Inflammasome via NLRP3- and Caspase-2-Driven Mitochondrial Damage. *Immunity* 43(3):451-462.

135. Kim S, *et al.* (2015) Endoplasmic Reticulum Stress–Induced IRE1α Activation Mediates Cross-Talk of GSK-3β and XBP-1 To Regulate Inflammatory Cytokine Production. *The Journal of Immunology* 194(9):4498-4506.

136. D'Osualdo A, *et al.* (2015) Transcription Factor ATF4 Induces NLRP1 Inflammasome Expression during Endoplasmic Reticulum Stress. *PLoS One* 10(6):e0130635.

137. Klingenberg R & Hansson GK (2009) Treating inflammation in atherosclerotic cardiovascular disease: emerging therapies. *European heart journal* 30(23):2838-2844.

138. Lopez AD, Mathers CD, Ezzati M, Jamison DT, & Murray CJL (Global and regional burden of disease and risk factors, 2001: systematic analysis of population health data. *The Lancet* 367(9524):1747-1757.

139. Lobstein JF (1833) *Traité d'anatomie pathologique* (Levrault).

140. von Rokitansky KF (1855) *A manual of pathological anatomy* (Blanchard & Lea).

141. Virchow R (1863) *Cellular Pathology as Based Upon Physiological and Pathological Histology* (JB Lippincott).

142. Windaus At (1910) Über den Gehalt normaler und atheromatöser Aorten an Cholesterin und Cholesterinestern. *Hoppe-Seyler´ s Zeitschrift für physiologische Chemie* 67(2):174-176.

143. Anitschkow N, Chalatow S, Müller C, & Duguid J (1913) Ueber experimentelle Cholesterinsteatose und ihre Bedeutehung einiger pathologischer Prozesse. *Centrbl Allg Pathol Pathol Anat* 24:1-9.

144. Mayerl C, *et al.* (2006) Atherosclerosis research from past to present--on the track of two pathologists with opposing views, Carl von Rokitansky and Rudolf Virchow. *Virchows Archiv : an international journal of pathology* 449(1):96-103.

145. Ross R (1993) The pathogenesis of atherosclerosis: a perspective for the 1990s. *Nature* 362(6423):801.

146. Steinberg D & Witztum JL (1990) Lipoproteins and atherogenesis. Current concepts. *Jama* 264(23):3047-3052.

147. Weber C & Noels H (2011) Atherosclerosis: current pathogenesis and therapeutic options. *Nat Med* 17(11):1410-1422.

148. Tiwari S & Siddiqi SA (2012) Intracellular Trafficking and Secretion of Very Low Density Lipoproteins. *Arteriosclerosis, thrombosis, and vascular biology* 32(5):1079-1086.

149. Libby P (2008) The molecular mechanisms of the thrombotic complications of atherosclerosis. *J Intern Med* 263(5):517-527.

150. Williams KJ & Tabas I (1995) The response-to-retention hypothesis of early atherogenesis. *Arterioscler Thromb Vasc Biol* 15(5):551-561.

151. Moore KJ & Tabas I (2011) Macrophages in the pathogenesis of atherosclerosis. *Cell* 145(3):341-355.

152. Hansson GK & Hermansson A (2011) The immune system in atherosclerosis. *Nat Immunol* 12(3):204-212.

153. Virmani R, Burke AP, Kolodgie FD, & Farb A (2002) Vulnerable plaque: the pathology of unstable coronary lesions. *Journal of interventional cardiology* 15(6):439-446.

154. Tabas I, García-Cardeña G, & Owens GK (2015) Recent insights into the cellular biology of atherosclerosis. *J Cell Biol* 209(1):13-22.

155. Gimbrone MA & García-Cardeña G (2013) Vascular endothelium, hemodynamics, and the pathobiology of atherosclerosis. *Cardiovascular pathology : the official journal of the Society for Cardiovascular Pathology* 22(1):9-15.

156. Koo A, Dewey CF, & García-Cardeña G (2013) Hemodynamic shear stress characteristic of atherosclerosis-resistant regions promotes glycocalyx formation in cultured endothelial cells. *American Journal of Physiology - Cell Physiology* 304(2):C137-146.

157. Mc GH, Jr., Geer JC, & Holman RL (1957) Sites of vascular vulnerability in dogs demonstrated by Evans blue. *AMA Arch Pathol* 64(3):303-311.

158. Dai G, *et al.* (2004) Distinct endothelial phenotypes evoked by arterial waveforms derived from atherosclerosis-susceptible and -resistant regions of human vasculature. *Proceedings of the National Academy of Sciences of the United States of America* 101(41):14871-14876.

159. Hajra L, *et al.* (2000) The NF-κB signal transduction pathway in aortic endothelial cells is primed for activation in regions predisposed to atherosclerotic lesion formation. *Proceedings of the National Academy of Sciences of the United States of America* 97(16):9052-9057.

160. Atkins GB, *et al.* (2008) Hemizygous Deficiency of Kruppel-like Factor 2 Augments Experimental Atherosclerosis. *Circ Res* 103(7):690-693.

161. Zhou G (2012) Endothelial Kruppel-like factor 4 protects against atherothrombosis in mice. 122(12):4727-4731.

162. Alexander MR & Owens GK (2012) Epigenetic control of smooth muscle cell differentiation and phenotypic switching in vascular development and disease. *Annual review of physiology* 74:13-40.

163. Rudijanto A (2007) The role of vascular smooth muscle cells on the pathogenesis of atherosclerosis. *Acta medica Indonesiana* 39(2):86-93.

164. Bennett MR, Sinha S, & Owens GK (2016) Vascular smooth muscle cells in atherosclerosis. *Circ Res* 118(4):692-702.

165. Rong JX, Shapiro M, Trogan E, & Fisher EA (2003) Transdifferentiation of mouse aortic smooth muscle cells to a macrophage-like state after cholesterol loading. *Proceedings of the National Academy of Sciences of the United States of America* 100(23):13531-13536.

166. Dutta P, *et al.* (2012) Myocardial infarction accelerates atherosclerosis. *Nature* 487(7407):325-329.

167. Gu L, *et al.* (1998) Absence of monocyte chemoattractant protein-1 reduces atherosclerosis in low density lipoprotein receptor-deficient mice. *Mol Cell* 2(2):275-281.

168. Rajavashisth T, *et al.* (1998) Heterozygous osteopetrotic (op) mutation reduces atherosclerosis in LDL receptor- deficient mice. *J Clin Invest* 101(12):2702-2710.

169. Srinivasan SR, Radhakrishnamurthy B, Vijayagopal P, & Berenson GS (1991) Proteoglycans, lipoproteins, and atherosclerosis. *Advances in experimental medicine and biology* 285:373-381.

170. Gerrity RG (1981) The role of the monocyte in atherogenesis: I. Transition of blood-borne monocytes into foam cells in fatty lesions. *The American journal of pathology* 103(2):181-190.

171. Febbraio M, *et al.* (2000) Targeted disruption of the class B scavenger receptor CD36 protects against atherosclerotic lesion development in mice. *J Clin Invest* 105(8):1049-1056.

172. Wang Y, Wang GZ, Rabinovitch PS, & Tabas I (2014) Mitochondrial Oxidative Stress Promotes Atherosclerosis and Nuclear Factor-κB–Mediated Inflammation in Macrophages *Circulation Research* 114(3):421-433.

173. Duewell P, *et al.* (2010) NLRP3 inflammasomes are required for atherogenesis and activated by cholesterol crystals. *Nature* 464(7293):1357-1361.

174. Duewell P, *et al.* (2010) NLRP3 inflamasomes are required for atherogenesis and activated by cholesterol crystals that form early in disease. *Nature* 464(7293):1357-1361.

175. Kirkham P (2007) Oxidative stress and macrophage function: a failure to resolve the inflammatory response. *Biochemical Society transactions* 35(Pt 2):284-287.

176. Sather S, *et al.* (2007) A soluble form of the Mer receptor tyrosine kinase inhibits macrophage clearance of apoptotic cells and platelet aggregation. *Blood* 109(3):1026-1033.

177. Garbin U, *et al.* (2013) Expansion of necrotic core and shedding of Mertk receptor in human carotid plaques: a role for oxidized polyunsaturated fatty acids? *Cardiovascular research* 97(1):125-133.

178. Bobryshev YV & Lord RS (1995) Ultrastructural recognition of cells with dendritic cell morphology in human aortic intima. Contacting interactions of Vascular Dendritic Cells in athero-resistant and athero-prone areas of the normal aorta. *Archives of histology and cytology* 58(3):307-322.

179. Zhou X, Paulsson G, Stemme S, & Hansson GK (1998) Hypercholesterolemia is associated with a T helper (Th) 1/Th2 switch of the autoimmune response in atherosclerotic apo E-knockout mice. *J Clin Invest* 101(8):1717-1725.

180. Huber SA, Sakkinen P, David C, Newell M, & Tracy R (2001) T helper–cell phenotype regulates atherosclerosis in mice under conditions of mild hypercholesterolemia. *Circulation* 103(21):2610-2616.

181. King VL, Szilvassy SJ, & Daugherty A (2002) Interleukin-4 deficiency decreases atherosclerotic lesion formation in a site-specific manner in female LDL receptor−/− mice. *Arteriosclerosis, thrombosis, and vascular biology* 22(3):456-461.

182. Mallat Z, Taleb S, Ait-Oufella H, & Tedgui A (2009) The role of adaptive T cell immunity in atherosclerosis. *Journal of lipid research* 50(Supplement):S364-S369.

183. Galkina E & Ley K (2009) Immune and Inflammatory Mechanisms of Atherosclerosis. *Annu Rev Immunol* 27:165-197.

184. Whitman SC & Ramsamy TA (2006) Participatory role of natural killer and natural killer T cells in atherosclerosis: lessons learned from in vivo mouse studies. *Canadian journal of physiology and pharmacology* 84(1):67-75.

185. Alcaide P, *et al.* (2007) Dendritic cell expression of the transcription factor T-bet regulates mast cell progenitor homing to mucosal tissue. *J Exp Med* 204(2):431-439.

186. Sun J, *et al.* (2007) Mast cells promote atherosclerosis by releasing proinflammatory cytokines. *Nat Med* 13(6):719-724.

187. Lindstedt KA, Mäyränpää MI, & Kovanen PT (2007) Mast cells in vulnerable atherosclerotic plaques – a view to a kill. *J Cell Mol Med* 11(4):739-758.

188. Zhou AX & Tabas I (2013) The UPR in atherosclerosis. *Semin Immunopathol* 35(3):321-332.

189. Maxfield FR & Tabas I (2005) Role of cholesterol and lipid organization in disease. *Nature* 438(7068):612-621.

190. Zheng Z, Zhang C, & Zhang K (2010) Role of unfolded protein response in lipogenesis. *World Journal of Hepatology* 2(6):203-207.

191. Hotamisligil GS & Erbay E (2008) Nutrient sensing and inflammation in metabolic diseases. *Nat Rev Immunol* 8(12):923-934.

192. Shaikh SR, *et al.* (2008) Differential Effects of a Saturated and a Monounsaturated Fatty Acid on MHC Class I Antigen Presentation. *Scandinavian journal of immunology* 68(1):30-42.

193. Zeng L, *et al.* (2009) Sustained activation of XBP1 splicing leads to endothelial apoptosis and atherosclerosis development in response to disturbed flow. *Proc Natl Acad Sci U S A* 106(20):8326-8331.

194. Gargalovic PS, *et al.* (2006) The unfolded protein response is an important regulator of inflammatory genes in endothelial cells. *Arterioscler Thromb Vasc Biol* 26(11):2490-2496.

195. Zeng L, *et al.* (2009) Sustained activation of XBP1 splicing leads to endothelial apoptosis and atherosclerosis development in response to disturbed flow. *Proceedings of the National Academy of Sciences of the United States of America* 106(20):8326-8331.

196. Hansson GK (2005) Inflammation, atherosclerosis, and coronary artery disease. *The New England journal of medicine* 352(16):1685-1695.

197. Muller C, *et al.* (2013) Protein disulfide isomerase modification and inhibition contribute to ER stress and apoptosis induced by oxidized low density lipoproteins. *Antioxidants & redox signaling* 18(7):731-742.

198. Kim JB, *et al.* (2011) Paraoxonase-2 modulates stress response of endothelial cells to oxidized phospholipids and a bacterial quorum-sensing molecule. *Arteriosclerosis, thrombosis, and vascular biology* 31(11):2624-2633.

199. Gargalovic PS, *et al.* (2006) Identification of inflammatory gene modules based on variations of human endothelial cell responses to oxidized lipids. *Proceedings of the National Academy of Sciences of the United States of America* 103(34):12741-12746.

200. Zhang C, *et al.* (2001) Homocysteine Induces Programmed Cell Death in Human Vascular Endothelial Cells through Activation of the Unfolded Protein Response. *Journal of Biological Chemistry* 276(38):35867-35874.

201. Gora S, *et al.* (2010) Phospholipolyzed LDL induces an inflammatory response in endothelial cells through endoplasmic reticulum stress signaling. *The FASEB Journal* 24(9):3284-3297.

202. Clarke MCH, *et al.* (2006) Apoptosis of vascular smooth muscle cells induces features of plaque vulnerability in atherosclerosis. *Nat Med* 12(9):1075-1080.

203. Salmeron J, *et al.* (1997) Dietary fiber, glycemic load, and risk of non-insulin-dependent diabetes mellitus in women. *Jama* 277(6):472-477.

204. Kedi X, Ming Y, Yongping W, Yi Y, & Xiaoxiang Z (2009) Free cholesterol overloading induced smooth muscle cells death and activated both ER- and mitochondrial-dependent death pathway. *Atherosclerosis* 207(1):123-130.

205. Werstuck GH, *et al.* (2001) Homocysteine-induced endoplasmic reticulum stress causes dysregulation of the cholesterol and triglyceride biosynthetic pathways. *J Clin Invest* 107(10):1263-1273.

206. Werstuck GH, *et al.* (2006) Glucosamine-Induced Endoplasmic Reticulum Dysfunction Is Associated With Accelerated Atherosclerosis in a Hyperglycemic Mouse Model. *Diabetes* 55(1):93-101.

207. Myoishi M, *et al.* (2007) Increased endoplasmic reticulum stress in atherosclerotic plaques associated with acute coronary syndrome. *Circulation* 116(11):1226-1233.

208. Scull CM & Tabas I (2011) Mechanisms of ER Stress-induced Apoptosis in Atherosclerosis. *Arteriosclerosis, thrombosis, and vascular biology* 31(12):2792-2797.

209. Feng B, *et al.* (2003) The endoplasmic reticulum is the site of cholesterol-induced cytotoxicity in macrophages. *Nature cell biology* 5(9):781-792.

210. Seimon T & Tabas I (2009) Mechanisms and consequences of macrophage apoptosis in atherosclerosis. *J Lipid Res* 50 Suppl:S382-387.

211. Baigent C, Keech A, Kearney P, & Blackwell L (2005) Efficacy and safety of cholesterol-lowering treatment: prospective meta-analysis of data from 90 056 participants in 14 randomised trials of statins. *The Lancet* 366(9493):1267.

212. Greenland P, *et al.* (2003) Major risk factors as antecedents of fatal and nonfatal coronary heart disease events. *Jama* 290(7):891-897.

213. Klingenberg R & Hansson GK (2009) Treating inflammation in atherosclerotic cardiovascular disease: emerging therapies. *European heart journal* 30(23):2838-2844.

214. Charo IF & Taub R (2011) Anti-inflammatory therapeutics for the treatment of atherosclerosis. *Nature reviews. Drug discovery* 10(5):365-376.

215. Moss JWE & Ramji DP (2016) Nutraceutical therapies for atherosclerosis. *Nature reviews. Cardiology* 13(9):513-532.

216. Minamino T, Komuro I, & Kitakaze M (2010) Endoplasmic reticulum stress as a therapeutic target in cardiovascular disease. *Circ Res* 107(9):1071-1082.

217. Granados-Principal S, Quiles JL, Ramirez-Tortosa CL, Sanchez-Rovira P, & Ramirez-Tortosa MC (2010) Hydroxytyrosol: from laboratory investigations to future clinical trials. *Nutrition reviews* 68(4):191-206.

218. Scoditti E, *et al.* (2012) Mediterranean diet polyphenols reduce inflammatory angiogenesis through MMP-9 and COX-2 inhibition in human vascular endothelial cells: A potentially protective mechanism in atherosclerotic vascular disease and cancer. *Archives of Biochemistry and Biophysics* 527(2):81-89.

219. Gorinstein S, *et al.* (2002) Olive oils improve lipid metabolism and increase antioxidant potential in rats fed diets containing cholesterol. *Journal of agricultural and food chemistry* 50(21):6102-6108.

220. Dell'Agli M, *et al.* (2006) Minor components of olive oil modulate proatherogenic adhesion molecules involved in endothelial activation. *Journal of agricultural and food chemistry* 54(9):3259-3264.

221. Gonzalez-Santiago M, *et al.* (2006) One-month administration of hydroxytyrosol, a phenolic antioxidant present in olive oil, to hyperlipemic rabbits improves blood lipid profile, antioxidant status and reduces atherosclerosis development. *Atherosclerosis* 188(1):35-42.

222. Slavin JL & Lloyd B (2012) Health benefits of fruits and vegetables. *Advances in nutrition (Bethesda, Md.)* 3(4):506-516.

223. Das UN (2008) Essential fatty acids and their metabolites could function as endogenous HMG-CoA reductase and ACE enzyme inhibitors, anti-arrhythmic, anti-hypertensive, anti-atherosclerotic, anti-inflammatory, cytoprotective, and cardioprotective molecules. *Lipids Health Dis* 7:37.

224. Çimen I, *et al.* (2016) Prevention of atherosclerosis by bioactive palmitoleate through suppression of organelle stress and inflammasome activation. *Science Translational Medicine* 8(358):358ra126-358ra126.

225. Wang R (2012) Physiological Implications of Hydrogen Sulfide: A Whiff Exploration That Blossomed. *Physiological Reviews* 92(2):791-896.

226. Zhao ZZ, *et al.* (2011) Hydrogen sulfide inhibits macrophage-derived foam cell formation. *Experimental biology and medicine (Maywood, N.J.)* 236(2):169-176.

227. Lee DY, *et al.* (2012) Anti-Inflammatory Activity of Sulfur-Containing Compounds from Garlic. *Journal of Medicinal Food* 15(11):992-999.

228. Katan MB, *et al.* (2003) Efficacy and Safety of Plant Stanols and Sterols in the Management of Blood Cholesterol Levels. *Mayo Clinic Proceedings* 78(8):965-978.

229. Osganian SK, *et al.* (2003) Vitamin C and risk of coronary heart disease in women. *Journal of the American College of Cardiology* 42(2):246-252.

230. Averill MM, *et al.* (2009) Dietary Antioxidants and Genistein Do Not Inhibit the Progression of Established Atherosclerotic Lesions in Older Apo E Deficient Mice. *Atherosclerosis* 203(1):82-88.

231. Liu S, *et al.* (2002) A prospective study of dietary fiber intake and risk of cardiovascular disease among women. *Journal of the American College of Cardiology* 39(1):49-56.

232. Rashid I, van Reyk DM, & Davies MJ (2007) Carnosine and its constituents inhibit glycation of low-density lipoproteins that promotes foam cell formation in vitro. *FEBS letters* 581(5):1067-1070.

233. Ghirlanda G, *et al.* (1993) Evidence of Plasma CoQ10-Lowering Effect by HMG-CoA Reductase Inhibitors: A Double-Blind, Placebo-Controlled Study. *The Journal of Clinical Pharmacology* 33(3):226-229.

234. Wang D, *et al.* (2014) Coenzyme Q10 Promotes Macrophage Cholesterol Efflux by Regulation of the Activator Protein-1/MicroRNA-378/ATP-Binding Cassette Transporter G1–Signaling Pathway. *Arteriosclerosis, Thrombosis, and Vascular Biology*.

235. Abe Y, Hashimoto SHU, & Horie T (1999) Curcumın ınhıbıtıon of ınflammatory cytokıne productıon by human perıpheral blood monocytes and alveolar macrophages. *Pharmacological Research* 39(1):41-47.

236. Voloshyna I, Hai O, Littlefield MJ, Carsons S, & Reiss AB (2013) Resveratrol mediates anti-atherogenic effects on cholesterol flux in human macrophages and

endothelium via PPARγ and adenosine. *European Journal of Pharmacology* 698(1–3):299-309.

237. Rosenson RS (2009) Future role for selective phospholipase A2 inhibitors in the prevention of atherosclerotic cardiovascular disease. *Cardiovascular drugs and therapy* 23(1):93-101.

238. De Caterina R & Zampolli A (2004) From asthma to atherosclerosis—5-lipoxygenase, leukotrienes, and inflammation. *New England Journal of Medicine* 350(1):4-7.

239. Gilbert J, *et al.* (2011) Effect of CC chemokine receptor 2 CCR2 blockade on serum C-reactive protein in individuals at atherosclerotic risk and with a single nucleotide polymorphism of the monocyte chemoattractant protein-1 promoter region. *The American journal of cardiology* 107(6):906-911.

240. Popa C, *et al.* (2005) Influence of anti-tumour necrosis factor therapy on cardiovascular risk factors in patients with active rheumatoid arthritis. *Annals of the rheumatic diseases* 64(2):303-305.

241. Fearon WF & Fearon DT (2008) Inflammation and Cardiovascular Disease. (Am Heart Assoc).

242. Zapolska-Downar D, Siennicka A, Kaczmarczyk M, Kołodziej B, & Naruszewicz M (2004) Simvastatin modulates TNFα-induced adhesion molecules expression in human endothelial cells. *Life sciences* 75(11):1287-1302.

243. Aikawa M, *et al.* (2001) An HMG-CoA reductase inhibitor, cerivastatin, suppresses growth of macrophages expressing matrix metalloproteinases and tissue factor in vivo and in vitro. *Circulation* 103(2):276-283.

244. Steffens S & Mach F (2004) Anti-inflammatory properties of statins. *Seminars in vascular medicine*, (Copyright© 2004 by Thieme Medical Publishers, Inc., 333 Seventh Avenue, New York, NY 10001, USA.), pp 417-422.

245. Suckling K (2010) Phospholipase A2s: Developing drug targets for atherosclerosis. *Atherosclerosis* 212(2):357-366.

246. Tabibiazar R, *et al.* (2005) Signature patterns of gene expression in mouse atherosclerosis and their correlation to human coronary disease. *Physiological genomics* 22(2):213-226.

247. Lötzer K, Funk CD, & Habenicht AJ (2005) The 5-lipoxygenase pathway in arterial wall biology and atherosclerosis. *Biochimica et Biophysica Acta (BBA)-Molecular and Cell Biology of Lipids* 1736(1):30-37.

248. Hakonarson H, *et al.* (2005) Effects of a 5-lipoxygenase–activating protein inhibitor on biomarkers associated with risk of myocardial infarction: a randomized trial. *Jama* 293(18):2245-2256.

249. Tardif J-C, *et al.* (2010) Treatment with 5-lipoxygenase inhibitor VIA-2291 (Atreleuton) in patients with recent acute coronary syndrome. *Circulation: Cardiovascular Imaging*:CIRCIMAGING. 110.937169.

250. Koenen RR, *et al.* (2009) Disrupting functional interactions between platelet chemokines inhibits atherosclerosis in hyperlipidemic mice. *Nature medicine* 15(1):97-103.

251. Serbina NV & Pamer EG (2006) Monocyte emigration from bone marrow during bacterial infection requires signals mediated by chemokine receptor CCR2. *Nature immunology* 7(3):311-317.

252. Ron D & Walter P (2007) Signal integration in the endoplasmic reticulum unfolded protein response. *Nature reviews Molecular cell biology* 8(7):519-529.

253. Todd DJ, Lee A-H, & Glimcher LH (2008) The endoplasmic reticulum stress response in immunity and autoimmunity. *Nature reviews immunology* 8(9):663-674.

254. Myoishi M, *et al.* (2007) Increased endoplasmic reticulum stress in atherosclerotic plaques associated with acute coronary syndrome. *Circulation* 116(11):1226-1233.

255. Zhou J, Lhoták Š, Hilditch BA, & Austin RC (2005) Activation of the unfolded protein response occurs at all stages of atherosclerotic lesion development in apolipoprotein E–deficient mice. *Circulation* 111(14):1814-1821.

256. Tabas I (2010) The role of endoplasmic reticulum stress in the progression of atherosclerosis. *Circulation research* 107(7):839-850.

257. Engin F & Hotamisligil G (2010) Restoring endoplasmic reticulum function by chemical chaperones: an emerging therapeutic approach for metabolic diseases. *Diabetes, Obesity and Metabolism* 12(s2):108-115.

258. Özcan U, *et al.* (2006) Chemical chaperones reduce ER stress and restore glucose homeostasis in a mouse model of type 2 diabetes. *Science* 313(5790):1137-1140.

259. Fu HY, *et al.* (2010) Ablation of C/EBP homologous protein attenuates endoplasmic reticulum–mediated apoptosis and cardiac dysfunction induced by pressure overload. *Circulation* 122(4):361-369.

260. Cheng W, Wang B, & Shyu K (2009) Regulation of GADD153 induced by mechanical stress in cardiomyocytes. *European journal of clinical investigation* 39(11):960-971.

261. Das I, *et al.* (2015) Preventing proteostasis diseases by selective inhibition of a phosphatase regulatory subunit. *Science* 348(6231):239-242.

262. Chen Y-J, Tan BC-M, Cheng Y-Y, Chen J-S, & Lee S-C (2009) Differential regulation of CHOP translation by phosphorylated eIF4E under stress conditions. *Nucleic acids research*:gkp1034.

263. Zhou AX & Tabas I (2013) The UPR in atherosclerosis. *Seminars in immunopathology*, (Springer), pp 321-332.

264. Kamaly N, *et al.* (2016) Targeted interleukin-10 nanotherapeutics developed with a microfluidic chip enhance resolution of inflammation in advanced atherosclerosis. *ACS nano* 10(5):5280-5292.

265. Freigang S, *et al.* (2011) NRF2 is essential for cholesterol crystal-induced inflammasome activation and exacerbation of atherosclerosis. *European journal of immunology* 41(7):2040-2051.

266. Zhang D & Armstrong JS (2006) Bax and the mitochondrial permeability transition cooperate in the release of cytochrome c during endoplasmic reticulum-stress-induced apoptosis. *Cell Death Differ* 14(4):703-715.

267. Papandreou I, *et al.* (2011) Identification of an Ire1alpha endonuclease specific inhibitor with cytotoxic activity against human multiple myeloma. *Blood* 117(4):1311-1314.

268. Qiu Q, *et al.* (2013) Toll-like receptor-mediated IRE1alpha activation as a therapeutic target for inflammatory arthritis. *Embo j* 32(18):2477-2490.

269. Furuhashi M, *et al.* (2007) Treatment of diabetes and atherosclerosis by inhibiting fatty-acid-binding protein aP2. *Nature* 447(7147):959-965.

270. Walter P & Ron D (2011) The unfolded protein response: from stress pathway to homeostatic regulation. *Science* 334(6059):1081-1086.

271. Garg AD, *et al.* (2012) ER stress-induced inflammation: does it aid or impede disease progression? *Trends in molecular medicine* 18(10):589-598.

272. Tam AB, Mercado EL, Hoffmann A, & Niwa M (2012) ER stress activates NF-κB by integrating functions of basal IKK activity, IRE1 and PERK. *PloS one* 7(10):e45078.

273. Qiu Q, *et al.* (2013) Toll-like receptor-mediated IRE1α activation as a therapeutic target for inflammatory arthritis. *The EMBO journal* 32(18):2477-2490.

274. Cross BC, *et al.* (2012) The molecular basis for selective inhibition of unconventional mRNA splicing by an IRE1-binding small molecule. *Proceedings of the National Academy of Sciences* 109(15):E869-E878.

275. Wu T, *et al.* (2014) Hrd1 suppresses Nrf2-mediated cellular protection during liver cirrhosis. *Genes & development* 28(7):708-722.

276. Schaffer JE (2003) Lipotoxicity: when tissues overeat. *Curr Opin Lipidol* 14(3):281-287.

277. Borradaile NM, *et al.* (2006) Disruption of endoplasmic reticulum structure and integrity in lipotoxic cell death. *J Lipid Res* 47(12):2726-2737.

278. Lopez-Castejon G & Brough D (2011) Understanding the mechanism of IL-1β secretion. *Cytokine & growth factor reviews* 22(4):189-195.

279. Tőzsér J & Benkő S (2016) Natural Compounds as Regulators of NLRP3 Inflammasome-Mediated IL-1β Production. *Mediators of Inflammation* 2016.

280. Timmins JM, *et al.* (2009) Calcium/calmodulin-dependent protein kinase II links ER stress with Fas and mitochondrial apoptosis pathways. *J Clin Invest*.

281. Oslowski CM & Urano F (2011) Measuring ER stress and the unfolded protein response using mammalian tissue culture system. *Methods in enzymology* 490:71.

282. Hori O, *et al.* (2002) Transmission of cell stress from endoplasmic reticulum to mitochondria. *The Journal of cell biology* 157(7):1151-1160.

283. Lu PD, Harding HP, & Ron D (2004) Translation reinitiation at alternative open reading frames regulates gene expression in an integrated stress response. *J Cell Biol* 167(1):27-33.

284. Han J, *et al.* (2013) ER-stress-induced transcriptional regulation increases protein synthesis leading to cell death. *Nat Cell Biol* 15(5):481-490.

285. Nie X, *et al.* (2013) Down-regulating overexpressed human Lon in cervical cancer suppresses cell proliferation and bioenergetics. *PLoS One* 8(11):e81084.

286. Murphy MP (2009) How mitochondria produce reactive oxygen species. *Biochemical Journal* 417(1):1-13.

287. Bronner DN, *et al.* (2015) Endoplasmic Reticulum stress activates the inflammasome via NLRP3-caspase-2 driven mitochondrial damage. *Immunity* 43(3):451-462.

288. Kolpakov V, *et al.* (1996) Atherosclerosis-prone branch regions in human aorta: microarchitecture and cell composition of intima. *Atherosclerosis* 122(2):173-189.

289. Mohanta S, Yin C, Weber C, Hu D, & Habenicht AJ (2016) Aorta atherosclerosis lesion analysis in hyperlipidemic mice. *Bio-protocol* 6(11).

290. Pedretti M, *et al.* (2010) Comparative immunohistochemical staining of atherosclerotic plaques using F16, F8 and L19: Three clinical-grade fully human antibodies. *Atherosclerosis* 208(2):382-389.

291. Moore KJ & Tabas I (2011) The cellular biology of macrophages in atherosclerosis. *Cell* 145(3):341.

292. Bhaskar V, *et al.* (2011) Monoclonal antibodies targeting IL-1 beta reduce biomarkers of atherosclerosis in vitro and inhibit atherosclerotic plaque formation in Apolipoprotein E-deficient mice. *Atherosclerosis* 216(2):313-320.

293. Ovchinnikova O, *et al.* (2009) T-cell activation leads to reduced collagen maturation in atherosclerotic plaques of ApoE−/− mice. *The American journal of pathology* 174(2):693-700.

294. Nakanishi K, Yoshimoto T, Tsutsui H, & Okamura H (2001) Interleukin-18 regulates both Th1 and Th2 responses. *Annual review of immunology* 19(1):423-474.

295. Gofman JW, *et al.* (1950) The role of lipids and lipoproteins in atherosclerosis. *Science (Washington)* 111:166-186.

296. Hotamisligil GS & Erbay E (2008) Nutrient sensing and inflammation in metabolic diseases. *Nature Reviews Immunology* 8(12):923-934.

297. Hotamisligil GS (2006) Inflammation and metabolic disorders. *Nature* 444(7121):860-867.

298. Romanyukha AA, Rudnev SG, & Sidorov IA (2006) Energy cost of infection burden: An approach to understanding the dynamics of host–pathogen interactions. *Journal of theoretical biology* 241(1):1-13.

299. Maier SF, Watkins LR, & Fleshner M (1994) Psychoneuroimmunology: The interface between behavior, brain, and immunity. *American Psychologist* 49(12):1004.

300. Lago R, Gómez R, Lago F, Gómez-Reino J, & Gualillo O (2008) Leptin beyond body weight regulation—current concepts concerning its role in immune function and inflammation. *Cellular immunology* 252(1):139-145.

301. Chi H (2011) Sphingosine-1-phosphate and immune regulation: trafficking and beyond. *Trends in pharmacological sciences* 32(1):16-24.

302. Khovidhunkit W, *et al.* (2004) Effects of infection and inflammation on lipid and lipoprotein metabolism: mechanisms and consequences to the host. *The Journal of Lipid Research* 45(7):1169-1196.

303. Chandra RK (1996) Nutrition, immunity and infection: from basic knowledge of dietary manipulation of immune responses to practical application of ameliorating suffering and improving survival. *Proceedings of the National Academy of Sciences* 93(25):14304-14307.

304. Blackburn GL (2001) Pasteur's Quadrant and malnutrition. *Nature* 409(6818):397-401.

305. Cummings DE & Schwartz MW (2003) Genetics and pathophysiology of human obesity. *Annual review of Medicine* 54(1):453-471.

306. Hotamisligil G (2004) Inflammation, TNFalpha, and insulin resistance. *Diabetes mellitus: a fundamental and clinical text*:953-962.

307. Wellen KE & Hotamisligil GS (2005) Inflammation, stress, and diabetes. *The Journal of clinical investigation* 115(5):1111-1119.

308. Hotamisligil GS, Shargill NS, & Spiegelman BM (1993) Adipose Expression of Tumor Necrosis Factor- : Direct Role in Obesity-Linked Insulin Resistance. *Scıence-New york Then Washıngton-* 259:87-87.

309. Sethi JK & Hotamisligil GS (1999) The role of TNFα in adipocyte metabolism. *Seminars in cell & developmental biology*, (Elsevier), pp 19-29.

310. Hu F & Liu F (2011) Mitochondrial stress: a bridge between mitochondrial dysfunction and metabolic diseases? *Cellular signalling* 23(10):1528-1533.

311. Li X, *et al.* (2013) Targeting mitochondrial reactive oxygen species as novel therapy for inflammatory diseases and cancers. *Journal of hematology & oncology* 6(1):19.

312. Bernardi P, Scorrano L, Colonna R, Petronilli V, & Di Lisa F (1999) Mitochondria and cell death. *European Journal of Biochemistry* 264(3):687-701.

313. Sivitz WI & Yorek MA (2010) Mitochondrial dysfunction in diabetes: from molecular mechanisms to functional significance and therapeutic opportunities. *Antioxidants & redox signaling* 12(4):537-577.

314. Gupte AA, Lyon CJ, & Hsueh WA (2013) Nuclear factor (erythroid-derived 2)-like-2 factor (Nrf2), a key regulator of the antioxidant response to protect against atherosclerosis and nonalcoholic steatohepatitis. *Current diabetes reports* 13(3):362-371.

315. Shulman GI (2000) Cellular mechanisms of insulin resistance. *J Clin Invest* 106(2):171-176.

316. Pessayre D (2007) Role of mitochondria in non-alcoholic fatty liver disease. *Journal of gastroenterology and hepatology* 22(s1):S20-S27.

317. Ballinger SW (2005) Mitochondrial dysfunction in cardiovascular disease. *Free Radical Biology and Medicine* 38(10):1278-1295.

318. Schröder M & Kaufman RJ (2005) The mammalian unfolded protein response. *Annu. Rev. Biochem.* 74:739-789.

319. Hotamisligil GS (2010) Endoplasmic reticulum stress and atherosclerosis. *Nature medicine* 16(4):396-399.

320. Cao J, *et al.* (2012) Saturated fatty acid induction of endoplasmic reticulum stress and apoptosis in human liver cells via the PERK/ATF4/CHOP signaling pathway. *Molecular and cellular biochemistry* 364(1-2):115-129.

321. Kennedy A, Martinez K, Chuang C-C, LaPoint K, & McIntosh M (2009) Saturated fatty acid-mediated inflammation and insulin resistance in adipose tissue: mechanisms of action and implications. *The Journal of nutrition* 139(1):1-4.

322. Surmi BK & Hasty AH (2008) Macrophage infiltration into adipose tissue: initiation, propagation and remodeling. *Future lipidology* 3(5):545-556.

323. Håversen L, Danielsson KN, Fogelstrand L, & Wiklund O (2009) Induction of proinflammatory cytokines by long-chain saturated fatty acids in human macrophages. *Atherosclerosis* 202(2):382-393.

324. Weatherill AR, *et al.* (2005) Saturated and polyunsaturated fatty acids reciprocally modulate dendritic cell functions mediated through TLR4. *The Journal of Immunology* 174(9):5390-5397.

325. Robblee MM, *et al.* (Saturated Fatty Acids Engage an IRE1a-Dependent Pathway to Activate the NLRP3 Inflammasome in Myeloid Cells.

326. Marchi S, Patergnani S, & Pinton P (2014) The endoplasmic reticulum–mitochondria connection: one touch, multiple functions. *Biochimica et Biophysica Acta (BBA)-Bioenergetics* 1837(4):461-469.

327. Giorgi C, De Stefani D, Bononi A, Rizzuto R, & Pinton P (2009) Structural and functional link between the mitochondrial network and the endoplasmic reticulum. *The international journal of biochemistry & cell biology* 41(10):1817-1827.

328. Zeeshan HMA, Lee GH, Kim H-R, & Chae H-J (2016) Endoplasmic reticulum stress and associated ROS. *International journal of molecular sciences* 17(3):327.

329. Zhang K & Kaufman RJ (2008) From endoplasmic-reticulum stress to the inflammatory response. *Nature* 454(7203):455-462.

330. Lerner AG, *et al.* (IRE1alpha induces thioredoxin-interacting protein to activate the NLRP3 inflammasome and promote programmed cell death under irremediable ER stress. *Cell Metab* 16(2):250-264.

331. Gibellini L, *et al.* (2016) Mitochondrial proteases as emerging pharmacological targets. *Current pharmaceutical design* 22(18):2679-2688.

332. Quirós PM, Langer T, & López-Otín C (2015) New roles for mitochondrial proteases in health, ageing and disease. *Nature reviews Molecular cell biology* 16(6):345-359.

333. Ngo JK & Davies KJ (2009) Mitochondrial Lon protease is a human stress protein. *Free Radical Biology and Medicine* 46(8):1042-1048.

334. Zhou J, Lhotak S, Hilditch BA, & Austin RC (2005) Activation of the unfolded protein response occurs at all stages of atherosclerotic lesion development in apolipoprotein E-deficient mice. *Circulation* 111(14):1814-1821.

335. Back SH & Kaufman RJ (2012) Endoplasmic reticulum stress and type 2 diabetes. *Annual review of biochemistry* 81:767-793.

336. Bornfeldt KE & Tabas I (2011) Insulin resistance, hyperglycemia, and atherosclerosis. *Cell metabolism* 14(5):575-585.

337. Erbay E, *et al.* (2009) Reducing endoplasmic reticulum stress through a macrophage lipid chaperone alleviates atherosclerosis. *Nature medicine* 15(12):1383-1391.

338. Engin F & Hotamisligil GS (2010) Restoring endoplasmic reticulum function by chemical chaperones: an emerging therapeutic approach for metabolic diseases. *Diabetes Obes Metab* 12 Suppl 2:108-115.

339. Thorp E, *et al.* (2009) Reduced apoptosis and plaque necrosis in advanced atherosclerotic lesions of Apoe-/- and Ldlr-/- mice lacking CHOP. *Cell Metab* 9(5):474-481.

340. Unanue ER & Urano F (2014) Endoplasmic reticulum: an interface between the immune system and metabolism. *Diabetes* 63(1):48-49.

341. Huber SA, Sakkinen P, David C, Newell MK, & Tracy RP (2001) T helper-cell phenotype regulates atherosclerosis in mice under conditions of mild hypercholesterolemia. *Circulation* 103(21):2610-2616.

342. Chen S, Crother TR, & Arditi M (2010) Emerging role of IL-17 in atherosclerosis. *Journal of innate immunity* 2(4):325-333.

343. Gerdes N, *et al.* (2002) Expression of interleukin (IL)-18 and functional IL-18 receptor on human vascular endothelial cells, smooth muscle cells, and macrophages. *Journal of Experimental Medicine* 195(2):245-257.

344. Pastrana JL, *et al.* (2012) Regulatory T cells and Atherosclerosis. *Journal of clinical & experimental cardiology* 2012(Suppl 12):002.

345. Kemp KL, *et al.* (2013) The serine-threonine kinase inositol-requiring enzyme 1α (IRE1α) promotes IL-4 production in T helper cells. *Journal of Biological Chemistry* 288(46):33272-33282.

346. Zhang L, Nosak C, Sollazzo P, Odisho T, & Volchuk A (2014) IRE1 inhibition perturbs the unfolded protein response in a pancreatic β-cell line expressing mutant proinsulin, but does not sensitize the cells to apoptosis. *BMC cell biology* 15(1):29.

347. Linda H, *et al.* (2009) Progressive multifocal leukoencephalopathy after natalizumab monotherapy. *The New England journal of medicine* 361(11):1081-1087.

348. Duan X, Qi Y, & Tang C (2009) Endoplasmic reticulum stress and cardiovascular diseases. *Geriatr Cardiol* 6:49-55.

349. Gardner BM, Pincus D, Gotthardt K, Gallagher CM, & Walter P (2013) Endoplasmic Reticulum Stress Sensing in the Unfolded Protein Response. *Cold Spring Harbor Perspectives in Biology* 5(3):a013169.

350. Kimata Y, *et al.* (2007) Two regulatory steps of ER-stress sensor Ire1 involving its cluster formation and interaction with unfolded proteins. *The Journal of Cell Biology* 179(1):75-86.

351. Libby P, Ridker PM, & Hansson GK (2011) Progress and challenges in translating the biology of atherosclerosis. *Nature* 473(7347):317-325.

352. Rogowicz A, Zozulinska D, & Wierusz-Wysocka B (2007) The role of matrix metalloproteinases in the development of vascular complications of diabetes mellitus-clinical implications. *Polskie Archiwum Medycyny Wewnętrznej* 117(3):43.

353. Jin SM & Youle RJ (2013) The accumulation of misfolded proteins in the mitochondrial matrix is sensed by PINK1 to induce PARK2/Parkin-mediated mitophagy of polarized mitochondria. *Autophagy* 9(11):1750-1757.

354. Kurihara Y, *et al.* (2012) Mitophagy plays an essential role in reducing mitochondrial production of reactive oxygen species and mutation of

mitochondrial DNA by maintaining mitochondrial quantity and quality in yeast. *The Journal of biological chemistry* 287(5):3265-3272.

355. Minton K (2016) Inflammasome: Anti-inflammatory effect of mitophagy. *Nat Rev Immunol* 16(4):206-206.

Appendices

Appendix A

Table A1. Top 25 up-regulated genes with STF-083010 treatment in mouse BMDM cells

Gene	Description	Fold change	p-Value
Gem	GTP binding protein (gene overexpressed in skeletal muscle)	5,28	0,0197
Aqp9	aquaporin 9	4,26	5,00E-05
Slc7a11	solute carrier family 7 (cationic amino acid transporter, y+ system), member 11	4,25	5,00E-05
Chac1	ChaC, cation transport regulator-like 1	4,20	5,00E-05
Trib3	tribbles homolog 3	4,14	5,00E-05
Dclk1	doublecortin-like kinase 1	4,10	0,0061
Slc1a4	solute carrier family 1 (glutamate/neutral amino acid transporter), member 4	3,96	5,00E-05
Stx1a	syntaxin 1A (brain)	3,96	0,03755
Soat2	sterol O-acyltransferase 2	3,45	5,00E-05
Ifrd1	interferon-related developmental regulator 1	3,39	5,00E-05
Trim46	tripartite motif-containing 46	3,37	0,00455
Dnmt3l	similar to DNA cytosine-5 methyltransferase 3-like protein	3,33	0,00085

Gene	Description	Fold change	p-Value
Zfp827	zinc finger protein 827	3,32	0,0057
Bcar1	breast cancer anti-estrogen resistance 1	3,24	0,01765
Fzd4	frizzled homolog 4 (Drosophila)	3,24	0,04035
Tmeff1	transmembrane protein with EGF-like and two follistatin-like domains 1	3,22	5,00E-05
Slc7a5	similar to solute carrier family 7	3,17	5,00E-05
Efcab5	EF-hand calcium binding domain 5	3,15	0,03165
Gm13889	predicted gene 13889	3,10	0,02935
Matn2	matrilin 2	3,06	5,00E-05
Aplp1	amyloid beta (A4) precursor-like protein 1	2,98	0,0086
Asns	asparagine synthetase	2,96	5,00E-05
Ddit3	DNA-damage inducible transcript 3	2,94	5,00E-05
Riiad1	Regulatory Subunit Of Type II PKA R-Subunit (RIIa) Domain Containing 1	2,93	0,04555
Map6	Microtubule-Associated Protein 6	2,86	0,0004

Table A2. Top 25 down-regulated genes with STF-083010 treatment in mouse BMDM cells

Gene	Description	Fold change	p-Value
Plxnb3	plexin B3	-4,45	0,03955
Smpd3	sphingomyelin phosphodiesterase 3, neutral	-3,94	0,006
S100a8	S100 calcium binding protein A8 (calgranulin A)	-3,83	5,00E-05
Fpr2	formyl peptide receptor 2	-3,76	0,0461
S100a9	S100 calcium binding protein A9 (calgranulin B)	-3,72	5,00E-05
Cd177	CD177 antigen	-3,66	0,04935
Cx3cr1	chemokine (C-X3-C) receptor 1	-3,48	5,00E-05
Chil3	chitinase-like 3	-3,46	5,00E-05
Rhobtb1	Rho-related BTB domain containing 1	-3,45	0,00245
Hpgd	hydroxyprostaglandin dehydrogenase 15 (NAD)	-3,28	5,00E-05
Syne1	synaptic nuclear envelope 1	-3,09	0,03485
Gpr34	G protein-coupled receptor 34	-2,99	0,0171
Ccr2	chemokine (C-C motif) receptor 2	-2,99	5,00E-05
Sult1a1	sulfotransferase family 1A, phenol-preferring, member 1	-2,88	0,00875
Ltf	lactotransferrin	-2,84	5,00E-05
Gm5086	predicted gene 5086	-2,83	0,00595
Ccl2	chemokine (C-C motif) ligand 2	-2,73	0,006
Cd69	CD69 antigen	-2,63	0,0091
Idi1	isopentenyl-diphosphate delta isomerase	-2,61	0,02395

Gene	Description	Fold change	p-Value
Ms4a6b	membrane-spanning 4-domains, subfamily A, member 6B	-2,60	5,00E-05
Il1b	interleukin 1 beta	-2,59	0,0409
Ccnd1	cyclin D1	-2,58	5,00E-05
Sesn1	sestrin 1	-2,57	5,00E-05
Rab3il1	RAB3A interacting protein (rabin3)-like 1	-2,57	5,00E-05
Gm1966	GTPase, very large interferon inducible 1	-2,57	0,0001

Table A3. Down-regulated genes with stf-083010 treatment in mouse BMDM cells (P<0.05; Fold change≤ 1.5)

gene	log2(fold change)	P value
Plxnb3	-4.44764	0.03955
Smpd3	-3.94316	0.006
S100a8	-3.82977	0.00005
Fpr2	-3.76381	0.0461
S100a9	-3.72286	0.00005
Cd177	-3.65563	0.04935
Cx3cr1	-3.47787	0.00005
Chil3	-3.45585	0.00005
Rhobtb1	-3.44936	0.00245
Hpgd	-3.27722	0.00005
Syne1	-3.08616	0.03485
Gpr34	-2.98719	0.0171
Ccr2	-2.98566	0.00005
Sult1a1	-2.87828	0.00875
Ltf	-2.83511	0.00005
Gm5086	-2.82563	0.00595
Ccl2	-2.73314	0.006
Cd69	-2.63158	0.0091

gene	log2(fold change)	P value
Idi1	-2.60711	0.02395
Ms4a6b	-2.60444	0.00005
Il1b	-2.58506	0.0409
Ccnd1	-2.57725	0.00005
Sesn1	-2.57127	0.00005
Rab3il1	-2.56647	0.00005
Gm1966	-2.56539	0.0001
Gpr160	-2.51227	0.01795
Fgl2	-2.48424	0.00005
Ccr3	-2.48336	0.01305
F830016B08Rik	-2.41656	0.0469
Ngp	-2.41329	0.00005
Lcn2	-2.36067	0.02125
Tmem176a	-2.35849	0.00005
Bco2	-2.33413	0.0312
Fgd2	-2.32753	0.00005
Maf	-2.27498	0.00005
Rnase6	-2.25026	0.00625
Camp	-2.24925	0.03105
Slit1	-2.23478	0.01935

gene	log2(fold change)	P value
Dok2	-2.22353	0.00005
Lifr	-2.22126	0.00065
Hp	-2.20974	0.0078
Nxpe4	-2.19556	0.0373
Tagap	-2.18866	0.03035
F630028O10Rik	-2.16789	0.00005
Fads2	-2.16111	0.00005
Cmklr1	-2.1531	0.00005
Tmem176b	-2.14868	0.00005
Ankle1	-2.11712	0.03085
Gpr155	-2.11133	0.00005
Iigp1	-2.10541	0.0021
Fgr	-2.07653	0.004
Sncaip	-2.06901	0.0492
Clec4a1	-2.05649	0.00005
Pla2r1	-2.04743	0.0272
Hsd17b7	-1.99196	0.00005
Cp	-1.99082	0.01225
Mir99ahg	-1.98521	0.00005
Abcg3	-1.98438	0.0279

gene	log2(fold change)	P value
F13a1	-1.97845	0.00005
Ccbl1	-1.95616	0.0387
Pot1b	-1.94355	0.00005
Plxdc2	-1.94111	0.00005
Itga4	-1.93477	0.00005
Pald1	-1.9109	0.00005
Ms4a6c	-1.91002	0.00005
Tspyl4	-1.90064	0.0076
Ehd4	-1.89296	0.00005
Fpr1	-1.89188	0.0296
Tifab	-1.89107	0.00005
Aldh1l1	-1.88674	0.00005
40602	-1.88042	0.00005
Cd79b	-1.87561	0.0497
Slco2b1	-1.86158	0.00005
Palld	-1.84558	0.0126
Ppfia4	-1.84332	0.00005
Olfm1	-1.84172	0.00015
Mef2c	-1.84072	0.00005
Abca9	-1.83888	0.00005

gene	log2(fold change)	P value
Frmd4b	-1.8272	0.00005
Chn2	-1.81978	0.01815
Chst7	-1.80693	0.0399
Adam19	-1.80141	0.00005
Zfp36l1	-1.7944	0.00005
Sema4a	-1.79349	0.0051
Dhcr24	-1.78857	0.00005
Lpar5	-1.7885	0.00755
Ms4a4c	-1.77669	0.02055
Kif9	-1.77459	0.02245
Tlr1	-1.77378	0.00005
Emilin1	-1.76825	0.00005
Kif20a	-1.7593	0.00725
Gprc5c	-1.75867	0.0003
Gpr162	-1.75739	0.0004
Disc1	-1.75728	0.0241
Tlr9	-1.75552	0.005
Nlrp1c-ps	-1.74391	0.00005
Dab2	-1.73316	0.00005
Arhgap15	-1.72586	0.00005

gene	log2(fold change)	P value
Rasgrp3	-1.72348	0.00005
Zfp119a	-1.72306	0.0293
Npl	-1.71991	0.0123
Clec4a3	-1.71461	0.00005
Etv5	-1.71288	0.0206
Bzrap1	-1.68346	0.0199
Arhgap4	-1.682	0.00005
Map2k6	-1.6761	0.02985
Dcstamp	-1.67151	0.04085
Ift80	-1.65694	0.00735
Tlr8	-1.65013	0.00005
Clec10a	-1.64722	0.0446
Lrmp	-1.64162	0.00005
Sorl1	-1.63625	0.00005
Fcgr1	-1.6347	0.00005
Rnf150	-1.63399	0.00005
Gas7	-1.63371	0.00005
Ophn1	-1.6329	0.00005
Rab39	-1.62177	0.02885
Mmp9	-1.62102	0.0391

gene	log2(fold change)	P value
Clec4b1	-1.61534	0.0407
Gm14446	-1.60541	0.00905
I830012O16Rik	-1.60288	0.00825
Cysltr1	-1.59952	0.00015
Thsd1	-1.59224	0.0354
Gm5512,Rmnd1	-1.59196	0.02645
Nlrp1b	-1.58864	0.00005
Glrx	-1.5832	0.0001
Gm5431	-1.57082	0.00025
Ptpro	-1.55734	0.00005
Gbp9	-1.54544	0.0015
Arhgap19	-1.53929	0.00005
Fam26f	-1.53522	0.01445
Pid1	-1.52583	0.00005
Slamf9	-1.52383	0.00005
Sla	-1.51354	0.00005
Gpr65	-1.50821	0.00005

Table A4. Up-regulated genes with stf-083010 treatment in mouse BMDM cells (P<0.05; Fold change ≥ 1.5)

gene	log2(fold change)	P value
Gem	5.28278	0.0197
Aqp9	4.26347	0.00005
Slc7a11	4.24918	0.00005
Chac1	4.19526	0.00005
Trib3	4.13576	0.00005
Dclk1	4.10127	0.0061
Slc1a4	3.95788	0.00005
Stx1a	3.95533	0.03755
Soat2	3.45083	0.00005
Ifrd1	3.39259	0.00005
Trim46	3.36948	0.00455
Dnmt3l	3.32889	0.00085
Zfp827	3.31926	0.0057
Bcar1	3.24321	0.01765
Fzd4	3.23602	0.04035
Tmeff1	3.21715	0.00005
Slc7a5	3.17413	0.00005
Efcab5	3.15013	0.03165

gene	log2(fold change)	P value
Gm13889	3.09609	0.02935
Matn2	3.05605	0.00005
Aplp1	2.97531	0.0086
Asns	2.95982	0.00005
Ddit3	2.94324	0.00005
Riiad1	2.92652	0.04555
Map6	2.85911	0.0004
Fgfbp3	2.81398	0.04065
Cdr2l	2.80969	0.0337
Mmp10	2.80742	0.03915
Serpinb9b	2.80164	0.00005
Gdf15	2.77544	0.00005
Ednrb	2.74677	0.00005
Dusp8	2.74046	0.0007
Hao1	2.73616	0.01775
Slc7a1	2.68925	0.00005
Timm8a1	2.67968	0.024
Tgm1	2.67678	0.00755
Gdap1l1	2.66195	0.0271
Cd5	2.62948	0.0101

gene	log2(fold change)	P value
Cmtm8	2.61491	0.0207
Stamos	2.59835	0.02765
Myo1b	2.56664	0.00015
Tnfrsf12a	2.56599	0.00025
Rapgef3	2.55992	0.0014
Rhou	2.54032	0.00105
Sema6c	2.51592	0.0375
Procr	2.50874	0.00005
Wfdc18	2.48881	0.03435
Gadd45a	2.48809	0.00005
Sqstm1	2.47551	0.00005
Slc25a33	2.43559	0.00005
Zfp112	2.43476	0.017
Abca8b	2.43399	0.00005
Gng4	2.42574	0.00175
Mthfd2	2.42187	0.00005
Clic5	2.40535	0.00405
Ltb	2.35245	0.0234
Osbp2	2.34282	0.0048
Tarm1	2.33254	0.02175

gene	log2(fold change)	P value
Mfsd4	2.30784	0.0481
Foxd2	2.30594	0.03065
Phgdh	2.29362	0.00005
Csf1	2.28538	0.00005
Hilpda	2.26825	0.00005
Osgin1	2.25189	0.00005
Ankrd23	2.2428	0.00135
Atp6v1g2	2.21715	0.02105
Rassf8	2.20563	0.00005
Rhov	2.18938	0.00005
Nupr1	2.18563	0.00005
Srxn1	2.18475	0.00005
Atf5	2.18269	0.0032
Olr1	2.17238	0.00565
Prss46	2.16951	0.0263
Bach2	2.16697	0.00075
Spint1	2.16064	0.0265
Nqo1	2.14674	0.00005
Atf4	2.13663	0.00005
Ext1	2.11097	0.00005

gene	log2(fold change)	P value
Cxcl2	2.09783	0.00005
Plin2	2.09593	0.00005
Slc22a4	2.06689	0.00005
Ppap2b	2.06084	0.00025
Amz1	2.05757	0.00005
Ppp1r15a	2.03232	0.00005
Zbtb46	2.03115	0.0186
Brdt	2.02987	0.00075
Cdkn1c	2.0124	0.00005
Nfil3	1.99707	0.00005
Ankrd13b	1.97289	0.0004
Arhgap28	1.95536	0.00005
Proser3	1.9437	0.01425
Rin1	1.93689	0.006
Maff	1.92669	0.00005
Tenc1	1.91092	0.03765
Hspa9	1.88909	0.00005
Fbxo32	1.8813	0.00005
Gsta3	1.87721	0.00005
Slc3a2	1.87669	0.00005

gene	log2(fold change)	P value
Traf1	1.85727	0.00005
Cyp1b1	1.82884	0.0244
Galnt3	1.82414	0.02765
Chchd10	1.82361	0.0005
Cipc	1.80882	0.00005
Arid5a	1.80796	0.00005
Rgs1	1.8062	0.00005
Klf9	1.80604	0.00005
Tmem140	1.8029	0.00005
Abca5	1.80017	0.0012
Acot2	1.79927	0.00005
Atp6v0a4,D630045J12Rik	1.79748	0.02315
Serpinf1	1.79412	0.0402
Aars	1.79383	0.00005
Fam46c	1.79337	0.00005
Akap2	1.78699	0.0001
Slc38a2	1.78161	0.00005
D16Ertd472e	1.77723	0.0021
Vash2	1.77157	0.00255
Sema3c	1.76547	0.0463

gene	log2(fold change)	P value
Clec4e	1.76059	0.00005
Cgnl1	1.75589	0.00005
Slc9b2	1.75418	0.03795
Cacna1b	1.7535	0.0008
Hbegf	1.74754	0.04075
Samd8	1.738	0.00005
Zbtb10	1.73345	0.00005
Rps6ka2	1.73332	0.00005
Il7r	1.73242	0.00005
Zfp93	1.73073	0.01595
Kdr	1.72567	0.022
Tmem158	1.72286	0.00075
Irg1	1.71371	0.00005
Tacc2	1.71066	0.00025
Serpinb9	1.70973	0.00005
Micall1	1.69293	0.00005
40610	1.68716	0.0183
Dusp9	1.68262	0.00615
Galnt6	1.68183	0.00005
Dusp18	1.67331	0.00915

gene	log2(fold change)	P value
AA467197	1.66707	0.00035
Lonrf1	1.66077	0.00005
Optn	1.65924	0.00005
Gclc	1.65863	0.00005
Rcan1	1.65552	0.00005
Stx3	1.65371	0.00005
Klf11	1.65346	0.00005
Pdgfa	1.64352	0.00005
Eif4ebp1	1.64082	0.00005
Ptgir	1.61006	0.00005
Txnrd1	1.60562	0.00005
Plcxd2	1.59377	0.00015
Tmem178	1.58801	0.03465
Tgm2	1.58534	0.00005
Serpinb1b	1.58505	0.0395
Tnfrsf22	1.58106	0.023
C77080	1.58094	0.00025
Stx11	1.57712	0.00005
Polr3d	1.5717	0.00005
Edaradd	1.55832	0.02395

gene	log2(fold change)	P value
Rilpl1	1.54099	0.00005
Sars	1.5346	0.00005
Runx2	1.53071	0.0033
Gpatch4	1.52972	0.0007
Myo6	1.52781	0.01275
Top1mt	1.52115	0.0008
Pmepa1	1.51505	0.04005
Tspan13	1.51436	0.00005
Ccrl2	1.51275	0.00005
Ercc6	1.51146	0.00005
Klf4	1.50854	0.00015

Copy Right Permissions and Curriculum vitae

NATURE PUBLISHING GROUP LICENSE TERMS AND CONDITIONS

May 19, 2017

This Agreement between ozlem tufanlı ("You") and Nature Publishing Group ("Nature Publishing Group") consists of your license details and the terms and conditions provided by Nature Publishing Group and Copyright Clearance Center.

License Number	4112381273268
License date	May 19, 2017
Licensed Content Publisher	Nature Publishing Group
Licensed Content Publication	Nature
Licensed Content Title	From endoplasmic-reticulum stress to the inflammatory response
Licensed Content Author	Kezhong Zhang and Randal J. Kaufman
Licensed Content Date	Jul 23, 2008
Licensed Content Volume	454
Licensed Content Issue	7203
Type of Use	reuse in a dissertation / thesis
Requestor type	academic/educational
Format	print and electronic
Portion	figures/tables/illustrations
Number of figures/tables/illustrations	1
High-res required	no
Figures	Figure 6. The 'ER-stress–inflammation' loop in specialized cells
Author of this NPG article	no
Your reference number	
Title of your thesis / dissertation	From endoplasmic-reticulum stress to the inflammatory response.
Expected completion date	Jun 2017
Estimated size (number of pages)	200
Requestor Location	ozlem tufanlı bilkent university main campus 79. dormitory room15 ankara, 06800 Turkey Attn: ozlem tufanlı

NATURE PUBLISHING GROUP LICENSE
TERMS AND CONDITIONS

May 19, 2017

This Agreement between ozlem tufanlı ("You") and Nature Publishing Group ("Nature Publishing Group") consists of your license details and the terms and conditions provided by Nature Publishing Group and Copyright Clearance Center.

License Number	4112390601942
License date	May 19, 2017
Licensed Content Publisher	Nature Publishing Group
Licensed Content Publication	Nature Immunology
Licensed Content Title	Emerging functions of the unfolded protein response in immunity
Licensed Content Author	Sophie Janssens, Bali Pulendran, Bart N Lambrecht
Licensed Content Date	Sep 18, 2014
Licensed Content Volume	15
Licensed Content Issue	10
Type of Use	reuse in a dissertation / thesis
Requestor type	academic/educational
Format	print and electronic
Portion	figures/tables/illustrations
Number of figures/tables/illustrations	1
High-res required	no
Figures	Figure 2 Evolution of the UPR shows conserved functions in immune responses
Author of this NPG article	no
Your reference number	
Title of your thesis / dissertation	From endoplasmic-reticulum stress to the inflammatory response.
Expected completion date	Jun 2017
Estimated size (number of pages)	200
Requestor Location	ozlem tufanlı bilkent university main campus 79. dormitory room15 ankara, 06800 Turkey

Print This Page

THE AMERICAN ASSOCIATION FOR THE ADVANCEMENT OF SCIENCE LICENSE TERMS AND CONDITIONS

May 19, 2017

This Agreement between ozlem tufanlı ("You") and The American Association for the Advancement of Science ("The American Association for the Advancement of Science") consists of your license details and the terms and conditions provided by The American Association for the Advancement of Science and Copyright Clearance Center.

License Number	4112400463387
License date	May 19, 2017
Licensed Content Publisher	The American Association for the Advancement of Science
Licensed Content Publication	Science
Licensed Content Title	The Unfolded Protein Response: From Stress Pathway to Homeostatic Regulation
Licensed Content Author	Peter Walter,David Ron
Licensed Content Date	Nov 25, 2011
Licensed Content Volume	334
Licensed Content Issue	6059
Volume number	334
Issue number	6059
Type of Use	Thesis / Dissertation
Requestor type	Scientist/individual at a research institution
Format	Print and electronic
Portion	Figure
Number of figures/tables	2
Order reference number	
Title of your thesis / dissertation	From endoplasmic-reticulum stress to the inflammatory response.
Expected completion date	Jun 2017
Estimated size(pages)	200
Requestor Location	ozlem tufanlı bilkent university main campus 79. dormitory room15 ankara, 06800 Turkey Attn: ozlem tufanlı
Billing Type	Invoice

Print This Page

NATURE PUBLISHING GROUP LICENSE
TERMS AND CONDITIONS

May 19, 2017

This Agreement between ozlem tufanlı ("You") and Nature Publishing Group ("Nature Publishing Group") consists of your license details and the terms and conditions provided by Nature Publishing Group and Copyright Clearance Center.

License Number	4112401054400
License date	May 19, 2017
Licensed Content Publisher	Nature Publishing Group
Licensed Content Publication	Nature Reviews Rheumatology
Licensed Content Title	Causes and consequences of endoplasmic reticulum stress in rheumatic disease
Licensed Content Author	Fatemeh Navid, Robert A. Colbert
Licensed Content Date	Dec 1, 2016
Licensed Content Volume	13
Licensed Content Issue	1
Type of Use	reuse in a dissertation / thesis
Requestor type	academic/educational
Format	print and electronic
Portion	figures/tables/illustrations
Number of figures/tables/illustrations	2
High-res required	no
Figures	Figure 2: IRE1α signalling pathways interact with immune response pathways Figure 3: PERK signalling pathways interact with immune response pathways.
Author of this NPG article	no
Your reference number	
Title of your thesis / dissertation	From endoplasmic-reticulum stress to the inflammatory response.
Expected completion date	Jun 2017
Estimated size (number of pages)	200
Requestor Location	ozlem tufanlı bilkent university main campus 79. dormitory room15

Print This Page

ELSEVIER LICENSE
TERMS AND CONDITIONS

May 19, 2017

This Agreement between ozlem tufanlı ("You") and Elsevier ("Elsevier") consists of your license details and the terms and conditions provided by Elsevier and Copyright Clearance Center.

License Number	4112401477174
License date	May 19, 2017
Licensed Content Publisher	Elsevier
Licensed Content Publication	Cell
Licensed Content Title	Macrophages in the Pathogenesis of Atherosclerosis
Licensed Content Author	Kathryn J. Moore,Ira Tabas
Licensed Content Date	29 April 2011
Licensed Content Volume	145
Licensed Content Issue	3
Licensed Content Pages	15
Start Page	341
End Page	355
Type of Use	reuse in a thesis/dissertation
Intended publisher of new work	other
Portion	figures/tables/illustrations
Number of figures/tables/illustrations	1
Format	both print and electronic
Are you the author of this Elsevier article?	No
Will you be translating?	No
Order reference number	
Original figure numbers	Figure 1 Progression of an Atherosclerotic Lesion
Title of your thesis/dissertation	From endoplasmic-reticulum stress to the inflammatory response.
Expected completion date	Jun 2017
Estimated size (number of pages)	200
Elsevier VAT number	GB 494 6272 12
Requestor Location	ozlem tufanlı bilkent university main campus

Print This Page

BILKENT UNIVERSITY• DEPARTMENT OF MOELCULAR BIOLOGY AND GENETICS•
FACULTY OF SCIENCE, BBUILDING•
ANKARA, TURKEY•
PHONE: +90-(312) 290 2491•
E-MAIL: TUFANLI@BILKENT.EDU.TR•

ÖZLEM TUFANLI

ACADEMIC POSITIONS

PhD **(**combined MSc + PhD program**)** 2010 - 2017

Department of Molecular Biology and Genetics Bilkent University

Ankara, Turkey

EDUCATION

Bachelor's Degree 2005 – 2010

Middle East Technical University, Biology Department

(Education Language is English). CGPA 3.33/4.00

(Honor student, 3rd degree in class)

High School 2004

Bornova Anatolia High-School

Izmir, Turkey. CGPA: 4.94/5.00

ACADEMIC TRAINING

PhD student at Bilkent University 2010-2016

Project: Lipotoxic endoplasmic reticulum stress in cardiometabolic syndrome:

Novel mechanisms and therapeutic targets

Supported through the Intensified Cooperation Grant between Turkey and Germany from the Scientific and Technological Research Council of Turkey

(Collaborator: Christian Weber, Ludwig Maximillians University).

Training in Ludwig Maximillians University Medical Center 2015

(Prof. Dr. Andreas Schober Lab.)

I practiced in situ hybridization, laser microdissection, paraffin embedding, sectioning of heart tissue and immunofluorescent staining of heart tissue sections and analysis of them.

(Supported by Scientific and Technological Research Council of Turkey)

Working on the project: 2010-2016

Delineation of lipotoxic endoplasmic stress pathway and identification of pro-atherogenic cytokines that are regulated by endoribonuclease activity of IRE1

(Collaborator Peter Walter University of California San Francisco, HHMI)

We performed RNASeq experiments and validation of genes

Contribution to the project on: 2014-2016

The impact of bioactive lipokines on atherosclerosis

Supported by European commission

(Collaboration with Gokhan S. Hotamisligil,Harvard School of Public Health.

Training in Ludwig Maximillians Universitat Medical Center 2013

(Prof. Dr. Christian Weber lab.)

I worked on Carotid Artery Ligation Experiments

Working on the project: 2010-2013

Molecular mechanisms and identification of IRE1 alpha associated proteins

I used chemical genetics methods and immunoprecipitation techniques.

UNDERGRADUATE PART

Undergraduate Project 2007-2008

Effect of Prenatal Exposure to Diclofenac Sodium on behaviors' of Juvenile Wistar Rats

Under supervision of Prof. Dr. Ewa Jakubowska-Doğru

Internship 2006

Yeditepe University, Genetics and Bioengineering Dept. Istanbul

Under supervision of Prof. Dr. Gamze T. Köse.

Internship 2006

Ankara Biotechnology Laboratory, Ankara University

Under supervison of Assist. Prof. Dr. Hilal Özdag.

Internship 2005

Molecular Medicine Laboratory, Çapa Medical Faculty, Istanbul

TEACHING EXPERIENCE

Teaching Assistant, Bilkent University 2010-2011

Biochemistry (MBG311) Student Laboratory

Teaching Assistant, Bilkent University 2011-2012

Genetics (MBG210) Student Laboratory

Teaching Assistant, BilkentUniversity 2013-2014

Molecular Biology of the Gene (MBG 324) Student Laboratory

TeachingAssistant,BilkentUniversity 2015-2016

Molecular Biology of the Cell (MBG 320) Student Laboratory

PROFESSIONAL ORGANIZATIONS AND SOCIETIES

Turkish Molecular Biology Association

ORAL PRESENTATIONS

Molecular Biology Society Winter Retreat, Bilkent University 2015

Role of IRE1 in Inflammation and Atherosclerosis

Unam Graduate Seminars 2017

Targeting IRE1 with Small Molecules Counteracts Progression of Atherosclerosis

POSTER PRESENTATIONS

Unfolded proteins: from basic to bedside, Stocholm, Sweden 2016
Targeting IRE1's Endoribonuclease Activity With Small Molecules For The Treatment of Atherosclerosis

FEBS EMBO Paris, France. 2014
The role of macrophage inositol requiring enzyme-1 in lipid-induced inflammation.
(Supported by FEBS EMBO organization)

Nanoday National Nanotechnology Research Centre Bilkent University, 2014
Characterization of PERK-directed Endoplasmic Reticulum Stress Response to Lipids

XIII. National Congress of Medical Biology and Genetics, Turkey 2013
Identification of differentially expressed microRNAs and analysis of the regulated genes by them during lipotoxic endoplasmic reticulum stress.

EMBO YIP PhD. Course Heidelberg, Germany 2012
Chemical genetic approach for the elucidation of signal transduction by IRE1 kinase

EMBO Young Scientists' Forum, Istanbul. 2012
Identification of novel Perk substrates during metabolic stress

COURSE ATTENDED

EMBO Young Investigator, PhD. Course, Heidelberg, Germany 2012
EMBL-EBI Bioinformatic Roadshow, Sabancı University 2011
Laboratory Animal Usage Course, Bilkent University 2010

SOCIAL PROJECT AND SPORTS EVENTS

Volunteer at Educational Volunteers Society during 3 year. (http://www.tegv.org/en)
(I conducted many activities with children such as Journey to Myself, Science and I, I read I play, Thinking Children.)

3rd degree (intermediate level) in tennis tournament at Bilkent University

PUBLICATIONS

* Nadir M, Tufanli O, Erbay E and Atalay A. (2016) Identification of Differentially Expressed MicroRNAs during Lipotoxic Endoplasmic Reticulum Stres. Turkish Journal of Biochemistry

* Çimen I., Kocatürk B., Koyuncu S., Tufanlı Ö., Onat U.I., Yildirim A. D., Apaydın O., Demirsoy S., Aykut Z. G., Nguyen U.T., Watkins S. M., Hotamışlıgil G.S., Erbay E. (2016) Prevention of Atherosclerosis by Bioactive Palmitoleate Through Suppression of Organelle Stress and Inflammasome Activation. Science Translational Medicine

Ozlem Tufanli, Pelin Telkoparan Akillilar, Diego Acosta-Alvear, Begum Kocaturk, Umut Inci Onat, Syed Muhammad Hamid, Ismail Çimen, Peter Walter, Christian Weber, and Ebru Erbay (2016) Targeting IRE1 with small molecules counteracts progression of atherosclerosis, PNAS.

CrossMark click for updates

Targeting IRE1 with small molecules counteracts progression of atherosclerosis

Ozlem Tufanli[a,b], Pelin Telkoparan Akillilar[a,b,1], Diego Acosta-Alvear[c,d,2], Begum Kocaturk[a,b], Umut Inci Onat[a,b], Syed Muhammad Hamid[a,b], Ismail Çimen[a,b,3], Peter Walter[c,d,4], Christian Weber[e,f], and Ebru Erbay[a,b,4]

[a]Department of Molecular Biology and Genetics, Bilkent University, Ankara 06800, Turkey; [b]National Nanotechnology Center, Bilkent University, Ankara 06800, Turkey; [c]Howard Hughes Medical Institute, University of California, San Francisco, CA 94143; [d]Department of Biochemistry and Biophysics, University of California, San Francisco, CA 94143; [e]Institute for Cardiovascular Prevention, Ludwig Maximilian University, Munich 80336, Germany; and [f]German Centre for Cardiovascular Research, Munich Heart Alliance, Munich 80336, Germany

Contributed by Peter Walter, December 28, 2016 (sent for review November 22, 2016; reviewed by Anne Bertolotti and Ira Tabas)

Metaflammation, an atypical, metabolically induced, chronic low-grade inflammation, plays an important role in the development of obesity, diabetes, and atherosclerosis. An important primer for metaflammation is the persistent metabolic overloading of the endoplasmic reticulum (ER), leading to its functional impairment. Activation of the unfolded protein response (UPR), a homeostatic regulatory network that responds to ER stress, is a hallmark of all stages of atherosclerotic plaque formation. The most conserved ER-resident UPR regulator, the kinase/endoribonuclease inositol-requiring enzyme 1 (IRE1), is activated in lipid-laden macrophages that infiltrate the atherosclerotic lesions. Using RNA sequencing in macrophages, we discovered that IRE1 regulates the expression of many proatherogenic genes, including several important cytokines and chemokines. We show that IRE1 inhibitors uncouple lipid-induced ER stress from inflammasome activation in both mouse and human macrophages. In vivo, these IRE1 inhibitors led to a significant decrease in hyperlipidemia-induced IL-1β and IL-18 production, lowered T-helper type-1 immune responses, and reduced atherosclerotic plaque size without altering the plasma lipid profiles in apolipoprotein E-deficient mice. These results show that pharmacologic modulation of IRE1 counteracts metaflammation and alleviates atherosclerosis.

endoplasmic reticulum stress | unfolded protein response | metaflammation | lipotoxicity | atherosclerosis

Complex molecular interactions between environment, diet, and genetics that take place at the metabolic and immune interface provoke a low-grade, chronic inflammatory response—metaflammation—that engages cells of the immune system (macrophages, neutrophils, and lymphocytes) and metabolic tissues (adipocytes, hepatocytes, and pancreatic cells) (1). An important primer for metaflammation is chronic metabolic overloading of organelles, such as the endoplasmic reticulum (ER) and mitochondria, which results in impairment of their functions (2).

The ER serves essential cellular functions that include the synthesis and folding of secreted and transmembrane proteins, calcium storage, and lipid synthesis for membrane biogenesis or energy storage. Disruption of any of these functions leads to ER stress and the subsequent activation of an elaborate network of adaptive responses, collectively known as the unfolded protein response (UPR) (3). The UPR reestablishes homeostasis through both transcriptional and translational layers of control. The UPR signals through three mechanistically distinct branches that are initiated by the ER-resident protein folding sensors inositol-requiring enzyme 1 (IRE1), protein kinase RNA-like endoplasmic reticulum kinase (PERK), and activating transcription factor 6 (ATF6) (3).

IRE1 controls the phylogenetically most conserved branch of the UPR found from fungi to metazoans. It has an ER-lumenal sensor domain that recognizes unfolded peptides and cytosolic kinase and endoribonuclease (RNase) domains that relay the information to downstream effectors (3). On sensing unfolded proteins, IRE1 oligomerizes and *trans*-autophosphorylates, thereby activating its RNase function. Metazoan IRE1 possesses two functional outputs dependent on its RNase activity. (*i*) It initiates a nonconventional splicing reaction that processes the mRNA encoding X-box binding protein-1 (*Xbp1*) to allow the translation of its active form, XBP1s, a potent transcription factor that, together with ATF6, drives expression of numerous genes, including those encoding ER-resident chaperones and ER-associated protein degradation machinery (3). (*ii*) IRE1 selectively degrades ER-bound mRNAs in a process known as regulated inositol-requiring enzyme 1-dependent decay (RIDD) to alleviate ER load (4). By these mechanisms, UPR activation reinstates homeostasis.

Increased ER stress and activation of the UPR are well-documented in atherosclerosis (5). Many metabolic cardiovascular risk factors observed in obesity, including hyperglycemia, hypercholesterolemia, and elevated saturated fats, can induce ER stress in all stages of atherogenesis, the process leading to the development of atherosclerotic plaques. During atherogenesis, a maladaptive inflammatory response is initiated by the deposition of cholesterol-rich lipoproteins in the subendothelial layer of arterial walls (6). Signs of ER stress are most prominent in the atherosclerosis-prone regions of vascular lesions, such as the branching points of arteries, and typically observed in macrophages—among other immune cells—infiltrating these regions (7, 8). Chronic, irremediable ER stress triggers apoptosis in macrophages, contributing to the growth of the necrotic core

Significance

Endoplasmic reticulum (ER) stress is linked to the development of complex metabolic diseases, including diabetes, obesity, and atherosclerosis. Irremediable ER stress can push the unfolded protein response (UPR) toward proinflammatory and proapoptotic signaling. The need to dissociate the adaptive UPR responses from its destructive outputs has become a major challenge for therapeutic strategies aimed at mitigating ER stress that is often observed in chronic diseases. Our findings show that inositol-requiring enzyme 1 (IRE1) plays a critical role in metaflammation and that administering IRE1-specific inhibitors to hyperlipidemic mice counteracts atherosclerosis progression.

Author contributions: P.W., C.W., and E.E. designed research; O.T., P.T.A., D.A.-A., B.K., U.I.O., S.M.H., and I.Ç. performed research; O.T., P.T.A., D.A.-A., B.K., U.I.O., S.M.H., I.Ç., P.W., C.W., and E.E. analyzed data; and O.T. and E.E. wrote the paper.

Reviewers: A.B., MRC Laboratory of Molecular Biology; and I.T., Columbia University.

The authors declare no conflict of interest.

Freely available online through the PNAS open access option.

[1]Present address: Department of Medical Biology, Yuksek Ihtisas University, Ankara 06520, Turkey.

[2]Present address: Department of Molecular, Cellular and Developmental Biology, University of California, Santa Barbara, CA 93106.

[3]Present address: Institute for Cardiovascular Prevention, Ludwig Maximilian University, Munich 80336, Germany.

[4]To whom correspondence may be addressed. Email: peter@walterlab.ucsf.edu or eerbay@bilkent.edu.tr.

This article contains supporting information online at www.pnas.org/lookup/suppl/doi:10.1073/pnas.1621188114/-/DCSupplemental.

that is observed in atherosclerotic plaques, which leads to a subsequent reduction in plaque stability, promoting their rupture (5).

Work over the last decade has pinpointed ER stress as a driving force for atherosclerosis progression (5, 7–10). For example, inhibiting the apoptotic signaling downstream of ER stress through genetic deletion of the proapoptotic transcription factor CCAAT box binding enhancer homologous protein (CHOP) or the signal transducer c-jun N-terminal kinase (JNK) blocks atherosclerosis progression (5, 11–13). Moreover, modulation of ER stress by using chemical chaperones alleviates atherosclerosis, further supporting the idea that therapeutic modulation of ER function is a promising avenue to combat atherosclerosis (14–16). Precedence for this notion is provided by pharmacological approaches to improve ER function—and thereby, limit ER stress—that include autophagy inducers, antioxidants, and regulators of ER calcium homeostasis (17–19).

Recent drug discovery efforts have opened the door to approaches that entail selective modulation of UPR signaling. This quest has led to the identification of several new small molecules that target the enzymatic activities of specific UPR regulators (19–23). Specifically, blocking IRE1 or XBP1s function has been shown to be beneficial for restraining tumor progression in mouse models (21, 24), highlighting that the specific targeting of the UPR can have beneficial impact in disease.

Several lines of evidence support the notion that selective pharmacological targeting of IRE1 is a desirable therapeutic approach for treatment of atherosclerosis. First, a profound increase in IRE1 phosphorylation and XBP1s expression is observed in atherosclerotic plaques of mice and humans (8, 10). Second, mechanical sheer stresses activate IRE1, whereas cardiovascular disease risk factors, such as oxidized phospholipids and homocysteine, induce both IRE1 and PERK (5, 25–29). Third, experimentally sustained *Xbp1* mRNA splicing in the vessel wall promotes atherosclerosis, whereas its ablation ameliorates hypercholesterolemia in obese or apolipoprotein E-deficient ($ApoE^{-/-}$) mice (10, 30). Two small molecules, STF-083010 and 4μ8C, which selectively inhibit IRE1's RNase function, have been used in cells and animals to produce favorable therapeutic outcomes in other disease settings: STF-083010 reduced growth of multiple myeloma (21, 24, 31, 32), and 4μ8c suppressed inflammation in a murine arthritis model (33). The action of both compounds is well-understood mechanistically. Both form a Schiff base with a specific lysine positioned in the active site of the IRE1 RNase domain, blocking its function, and both show no overt toxicity when administered systemically (21, 32, 33). Thus, we reasoned that these drugs might have therapeutic applicability in atherosclerosis.

Here, we investigated the direct contribution of IRE1 to lipid-induced inflammation and atherosclerotic disease progression by administering these two IRE1 inhibitors to macrophages and $ApoE^{-/-}$ mice on a Western-type (high-fat and high-cholesterol) diet. Our results substantiate the concept that specific pharmacological modulation of IRE1 counteracts metaflammation and yields therapeutic gains in atherosclerotic disease, warranting additional validation in human disease.

Results

Proatherogenic Genes Are Regulated by IRE1. To understand the contributions of IRE1 in atherogenesis, we first analyzed the impact of its inhibition on the transcriptome of macrophages using RNA sequencing (RNA-seq). ER poisons, such as tunicamycin, which inhibits protein *N*-linked glycosylation in the ER lumen, or thapsigargin, which disrupts ER calcium reuptake, activate all UPR branches simultaneously, impeding the dissection of the signaling contributions of individual UPR branches. By refraining from using these pleiotropic drugs, we aimed to identify the specific IRE1-regulated gene expression changes. To this end, we probed the transcriptional response to acute inhibition of IRE1 using STF-083010 in primary mouse bone marrow-derived macrophages (BMDMs) (34, 35). We analyzed differentially regulated mRNAs at early time points (6 hours) after IRE1 inhibition to distinguish immediately responsive genes from those with expression that may be altered as part of an adaptive response to chronic inhibition. Using an arbitrary cutoff of 1.5-fold, we observed increased expression of 169 genes and decreased expression of 135 genes on IRE1 inhibition (Fig. 1*A*, Dataset S1, and Tables S1 and S2) ($P < 0.05$). To categorize the affected genes functionally according to their association with disease processes, we used the Ingenuity Pathway Analysis (IPA) tool (36). IPA identified the down-regulation of many important proatherogenic genes, including cytokines, chemokines, and chemokine receptors, on inhibition of the steady-state IRE1 activity (Fig. 1*B*).

We next validated our findings using quantitative (q)RT-PCR. In these experiments, we observed a significant reduction in the mRNA levels of *Il-1β*, C-C motif chemokine ligand 2 (*Ccl2*), calgranulin A (*S100a8*), and matrix metalloprotease-9 (*Mmp9*) ($P < 0.05$, $P < 0.001$, $P < 0.01$, and $P < 0.01$, respectively) after IRE1 inhibition with either STF-083010 or 4μ8c (Fig. 1 *C–E* and Fig. S1 *A–E*). Both of these drugs were used at concentrations that do not compromise cell viability or induce any other toxicity (21, 34, 35, 37–40). Consistent with earlier reports, these IRE1 inhibitors had no effect on the kinase function of IRE1 (Fig. S1 *F–H*), confirming that the identified proatherogetic genes are regulated by IRE1's RNase activity.

Because IRE1 is rate-limiting for the production of XBP1s, we next assessed if XBP1s regulates the expression of these proatherogenic genes. To this end, we forced expressed XBP1s or restored IRE1 function in inositol-requiring enzyme 1-deficient ($IRE1^{-/-}$) mouse embryonic fibroblasts (MEFs) (Fig. S1*I*). Both experiments showed a marked induction of *Il-1β, Ccl2,* and *S100a8* mRNA levels (Fig. 1 *F–H*). Together, our findings confirm that the IRE1-XBP1 signaling branch of the UPR maintains the expression of key proatherogenic cytokines and chemokines in macrophages.

Induction of IL-1β and CCL2 Depends on IRE1 During Lipotoxicity. Our finding that IRE1 maintains the expression of several important proatherogenic genes in macrophages suggests that, when induced by metabolic stress, heightened IRE1 activity could drive the atherosclerotic process. One important activating signal for the UPR in macrophages is exposure to excessive amounts of lipids, which elicits toxicity (14, 28, 41). This lipotoxicity results in increased production of reactive oxygen species (ROS), ER stress, and inflammation, and it can result in apoptosis (41).

Based on these observations, we next investigated if lipid-induced IRE1 activation plays a role in IL-1β induction. Inhibition of IRE1 with STF-083010 led to a significant block in lipid-induced *Il-1β* mRNA production and secretion from BMDMs (Fig. 2 *A* and *B* and Fig. S2 *A* and *B*). As expected, inhibition of IRE1 activity with 4μ8c showed the same effects (Fig. S2 *C–F*). To further delineate the role of IRE1 and XBP1s in the regulation of IL-1β, we transfected BMDMs with a specific siRNA. We found that transfection of siRNAs against *Ire1α* (the ubiquitously expressed IRE1 homolog) or *Xbp1* resulted in a significant reduction in lipid-induced *Il-1β* mRNA production and IL-1β secretion in BMDMs [Fig. 2 *C* and *D* ($P < 0.05$, $P < 0.05$, $P < 0.001$, and $P < 0.001$) and Fig. S2 *G* and *H*]. Moreover, treatment of human peripheral blood monocytes (PBMCs) with lipids induced IL-1β secretion, which was blocked by preincubation with 4μ8c (Fig. 2 *E* and *F* and Fig. S2*I*). These findings show that IRE1-XBP1 signaling plays an important role in *Il-1β* mRNA up-regulation and secretion from both mouse and human macrophages.

We also investigated if the proatherogenic chemokine CCL2 is regulated by IRE1 under lipotoxic ER stress conditions. Both STF-083010 and 4μ8c treatments of BMDMs resulted in complete inhibition of lipid-induced *Ccl2* mRNA production and protein secretion (Fig. S3 *A–C*). Consistent with this observation, siRNAs against *Ire1α* or *Xbp1* also suppressed lipid-induced CCL2 production and secretion in BMDMs (Fig. S3 *D* and *E*). Moreover, 4μ8c blocked lipid-induced CCL2 production in human PBMCs (Fig. S3*F*). Collectively, these data show that IRE1 is important for the inflammatory response to lipids and the

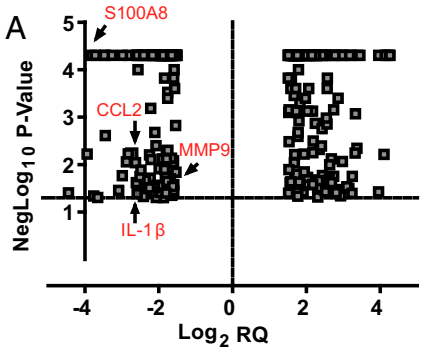

B

Symbol	Entrez Gene Name	Expression value	
		Fold Change	p-value
S100A8	s100 Calcium Binding Protein A8	-3,83	5,00E-05
CCR2	Chemokine (C-C) Motif Receptor 2	-2,98	5,00E-05
CCL2	The chemokine (C-C motif) ligand 2	-2,73	6,00E-03
IL-1β	Interleukin 1, Beta	-2,58	4,09E-02
CCR3	Chemokine (C-C) Motif Receptor 3	-2,48	1,30E-02
PLA2R1	Phospholipase A2 Receptor 1	-2,04	2,72E-02
ITGA4	Integrin, Alpha 4	-1,93	5,00E-05
MMP9	Matrix Metallopeptidase 9	-1,62	3,91E-02

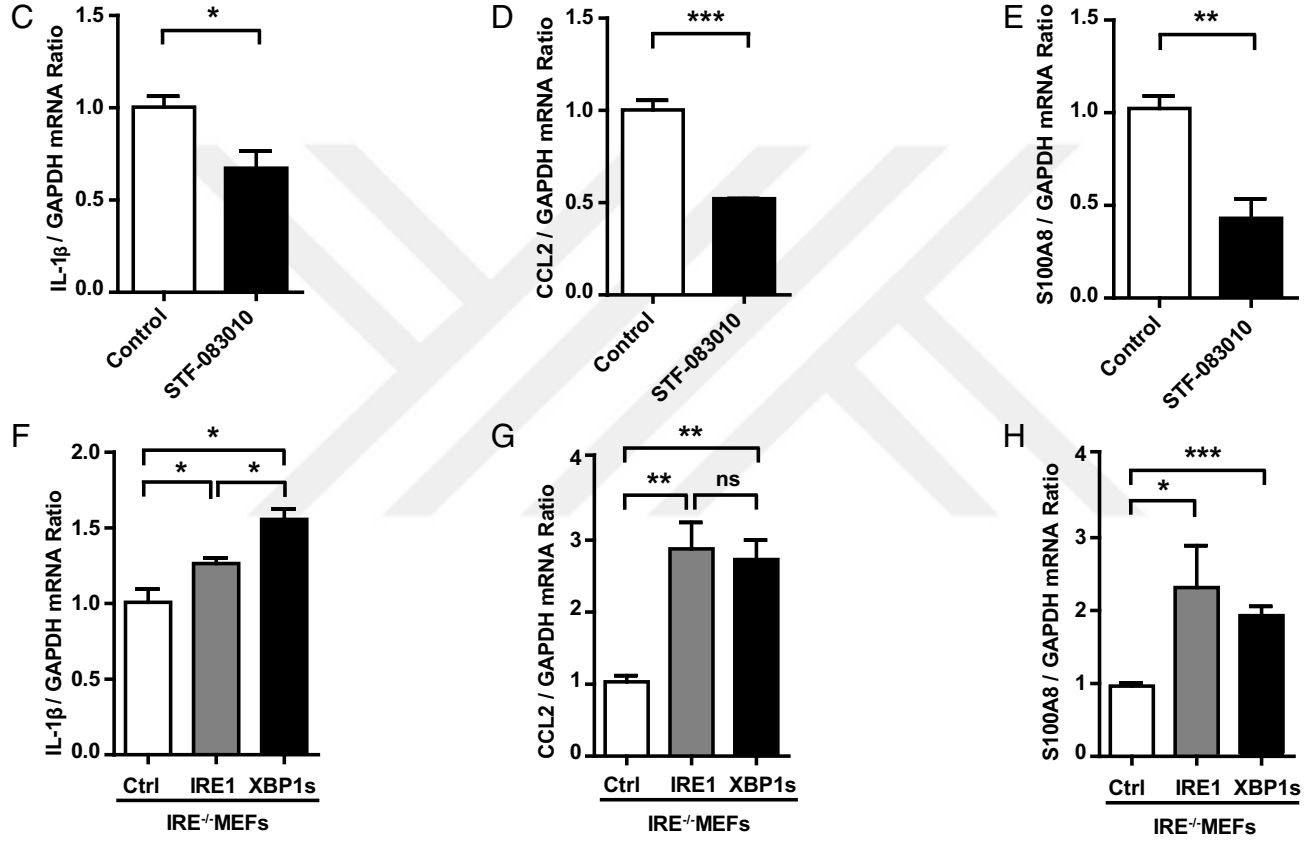

Fig. 1. IRE1 regulates the expression of proatherogenic genes. (*A*) RNA-seq analysis in BMDMs treated with 60 μM STF-083010 or DMSO (control) for 6 hours. Volcano plot of differentially expressed mRNAs. (*B*) Analysis of atherosclerosis-related mRNAs using the IPA tool (details are in the text). (*C–E*) Confirmation of IRE1-dependent atherogenic gene regulation in mouse BMDMs treated with STF-083010 or DMSO (control) by qRT-PCR. (*F–H*) qRT-PCR analysis of atherogenic gene expression in IRE1$^{-/-}$ MEFs on forced expression of XBP1s or restoring IRE1's function. Data: mean values ± SEM; $n = 3$. Student's *t* test. Ctrl, control; ns, not significant. $^{*}P \leq 0.05$; $^{**}P \leq 0.01$; $^{***}P \leq 0.001$.

production of proatherogenic cytokines in both mouse and human macrophages.

Inflammasome Activation Depends on IRE1 During Lipotoxicity. Because IRE1 inhibition leads to a strong suppression of IL-1β secretion, we reasoned that IRE1 may contribute to the lipid-induced activation of the Nod-like receptor family, pyrin domain-containing protein-3 (NLRP3) inflammasome, a multicomponent platform that contains caspase-1 and induces the caspase-1–dependent secretion of the proinflammatory cytokines IL-1β and IL-18 (42, 43). Previous studies showed that ER stress induces inflammasome activation through several mechanisms, including calcium mobilization and the release of reactive oxygen species from damaged mitochondria (mtROS) (44). Because earlier studies from our laboratory and the laboratories of others showed that treatment of macrophages with saturated fatty acids activates IRE1 and because these lipids specifically activated the NLRP3 inflammasome through inducing mtROS production, we sought to investigate this connection further (42, 43, 45). To this end, we first measured mtROS production in cells exposed to lipotoxic stress in the presence of IRE1 inhibitors. We observed that lipid-induced ER stress in BMDMs resulted in a dramatic elevation of mtROS, which was completely blocked by 4μ8c treatment as well as XBP1 knockdown (Fig. 3 *A* and *B* and Fig. S4*A*).

The impact of IRE1 signaling on inflammasome activation has been postulated to be mediated by the IRE1-dependent accumulation of the thioredoxin-interacting protein (TXNIP), a thioredoxin inhibitor with increased levels that promote activation of the NLRP3 inflammasome (35). In stark contrast to these earlier findings, which used cells treated with canonical ER poisons, lipid-induced ER stress led to a profound suppression of

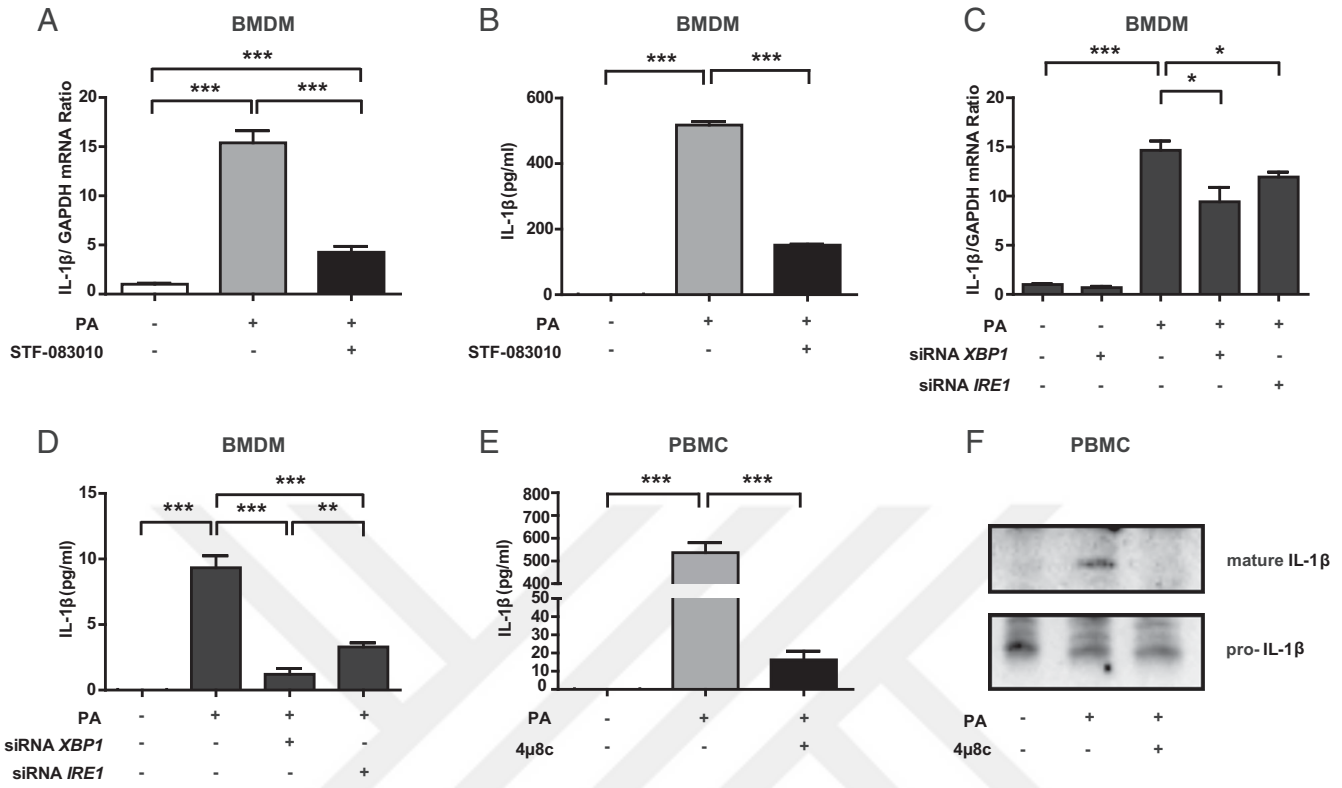

Fig. 2. IRE1 regulates lipid-induced IL-1β secretion in mouse and human macrophages. *Il-1β* (*A*) mRNA and (*B*) protein levels measured from LPS-primed and PA-stimulated mouse BMDMs treated with 150 μM STF-083010 or DMSO (control) by qRT-PCR and ELISA, respectively. *Il-1β* (*C*) mRNA and (*D*) protein levels measured from LPS-primed and PA-stimulated mouse BMDMs transfected with siRNAs against *Ire1α* or *Xbp1* by qRT-PCR and ELISA, respectively. (*E*) Secreted IL-1β from LPS-primed, PA-stimulated human PBMCs treated or not treated with 100 μM 4μ8c measured by ELISA. (*F*) Same as *E* but protein levels were measured by immunoblotting to show the immature and processed forms of the cytokine (representative image of three independent blots). Statistics are the same as in Fig. 1. $*P \leq 0.05$; $**P \leq 0.01$; $***P \leq 0.001$.

TXNIP in macrophages, which was partially blocked by inhibiting IRE1 (Fig. S4*B*). Another mechanism by which ER stress can induce mitochondrial oxidative stress and activation of the NLRP3 inflammasome complex is through calcium mobilization (46). Indeed, we observed that palmitic acid (PA) leads to a significant increase (threefold) of calcium levels in the mitochondria, but this increase could not be prevented by IRE1 inhibition (Fig. S4*C*). Moreover, lipid-induced ER stress also induced procaspase-1 maturation (indicated by the appearance of the p10 fragment), an effect that was reduced by treatment with IRE1 inhibitors or siRNA-mediated silencing of *Ire1α* and *Xbp1* (Fig. 3*C* and Fig. S4 *D* and *E*). Taken together, these results indicate that IRE1 plays a crucial role in perpetuating mtROS production and NLRP3 inflammasome activation in cells experiencing lipotoxic ER stress but that this effect is independent of TXNIP induction and calcium mobilization.

We further investigated if IRE1 affects the activation of the NLRP3 inflammasome by other stimuli or the activation of different inflammasome complexes by specific inducers. Although IRE1 inhibition blocked NLRP3 inflammasome activation, cleavage of caspase-1, and secretion of IL-1β by various different NLRP3 inflammasome inducers (including ATP, Alum, and cholesterol crystals) (Fig. 3*D*), it did not alter the activation of other inflammasome complexes, such as NLR family CARD domain-containing protein 4 by flagellin or absent in melanoma 2 by poly(deoxyadenylic-deoxythymidylic acid) [poly(dA:dT)] as evident by no changes in caspase-1 cleavage (Fig. 3*E*). Because IRE1-XBP1 controls *Il-1β* mRNA production, we observed reduction in secreted IL-1β protein levels in all of the treatments (Fig. 3 *D* and *E*). Finally, together with our results showing that IRE1 induces IL-1β, our data show that IRE1 plays a major role in controlling IL-1β signaling both transcriptionally and by promotion of its maturation via the activation of the NLRP3 inflammasome.

Pharmacological Inhibition of IRE1 Combats Atherosclerosis. The evidence presented above in conjunction with previous results showing that restoring or improving ER function alleviates atherosclerosis (14, 17, 47) suggest that inhibiting IRE1 may impair atherosclerosis progression. Therefore, we postulated that administration of IRE1 modulators might have beneficial effects by limiting the inflammatory signaling associated with elevated ER stress in a mouse model of atherosclerosis. To test this notion, we challenged $ApoE^{-/-}$ mice with a Western diet (12 weeks) and then treated them daily with STF-083010 by intraperitoneal (i.p.) injection (6 weeks) (Fig. 4*A*). Although limited pharmacodynamic data are available for the IRE1 inhibitors that we used, target engagement has been shown in cells and tissues (21, 39). We based our in vivo drug dosage and delivery on earlier in vivo studies that successfully administered the IRE1 modulators without toxicity (21, 24, 31). Furthermore, we confirmed target engagement in tissues by assessing drug-induced suppression of *Xbp1* mRNA splicing and RIDD activities by observing a significant reduction in the spliced *Xbp1* mRNA ($P < 0.05$) and a modest increase in canonical RIDD target mRNAs ($P < 0.05$) (Fig. S5 *A*–*C*). Importantly, the IRE inhibitor that we used did not alter IRE1 phosphorylation in vivo (Fig. S5*D*). Furthermore, we detected no differences in body weights, blood glucose levels, liver morphology, plasma alanine amino transferase (ALT) activity, and cholesterol profiles between the STF-083010–treated and control groups (Figs. S5 *E* and *F* and S6 and Table S3). However, the analysis of en face aorta preparations showed that chronic administration of STF-083010 led to a significant decrease (35.8%; $P < 0.001$) in atherosclerotic lesions compared with the control

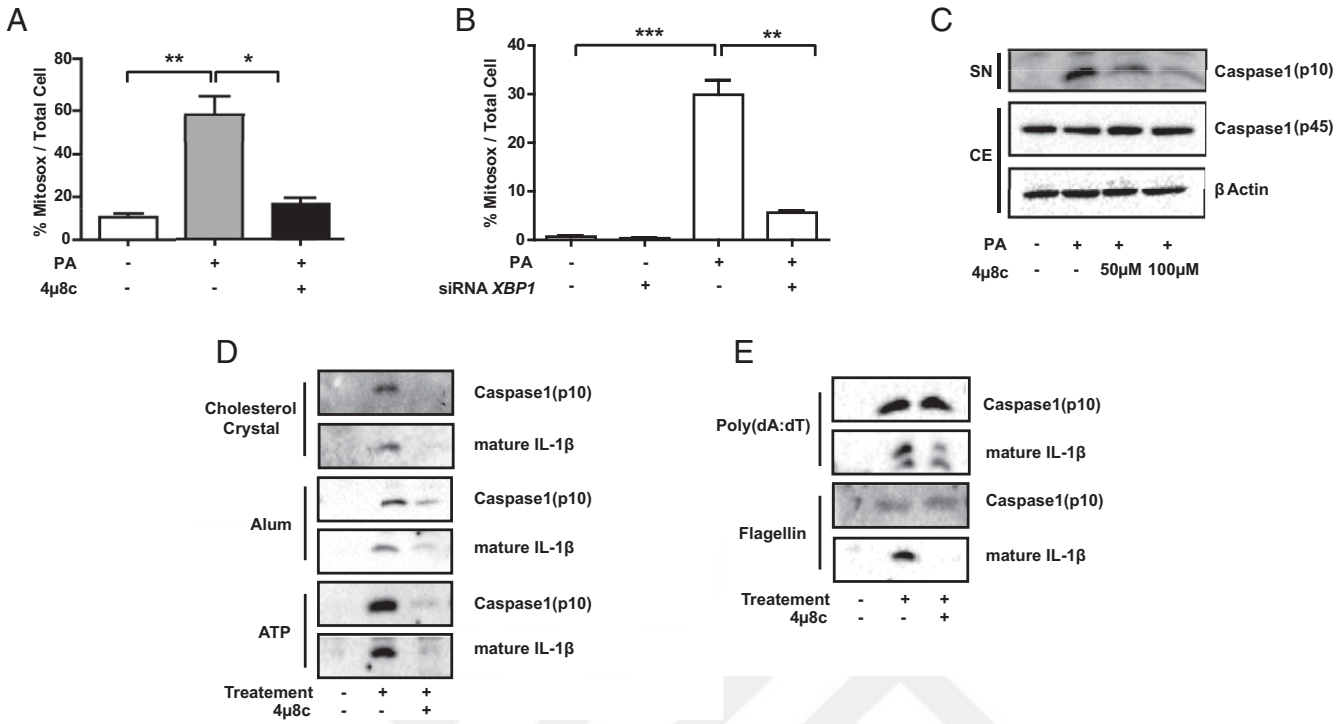

Fig. 3. IRE1 inhibitors block lipid-induced mtROS release and inflammasome activation. (*A* and *B*) mtROS production was measured in LPS-primed, PA-stimulated mouse BMDMs after (*A*) 100 μM 4μ8c or DMSO (control) treatment or (*B*) transfection with scrambled or *Xbp1*-specific siRNAs. (*C–E*) Immunoblots of the levels of the zymogen (p45) and mature (p10) forms of caspase-1 in LPS-primed mouse BMDMs pretreated with 4μ8c (at the indicated doses) or DMSO (control) and stimulated with (*C*) PA, (*D*) other NLRP3 agonists (5 nM ATP, 200 μg/mL alum, or 400 μg/mL cholesterol crystals), or (*E*) specific activators of other inflammasome complexes [5 μg/mL poly(dA:dT) and 1 μg/mL flagellin] according to previously published protocols (described in detail in *Experimental Procedures*). Blots shown are representative of three independent experiments. Statistics are the same as in Fig. 1. CE, cell extract; SN, supernatant. $*P \leq 0.05$; $**P \leq 0.01$; $***P \leq 0.001$.

group (Fig. 4*B*). Furthermore, when we evaluated the impact of STF-0803010 on plaque development in the aortic root, we observed a significant reduction (21.4%; $P < 0.001$) in the foam cell area (visualized by Oil Red O staining) in the inhibitor-treated group compared with control mice (Fig. 4*C*).

Analogous experiments using 4μ8c in the same animal model [using previously published doses that showed no toxicity (33, 37, 40, 48)] produced similar results (Fig. 4 *D–F*): 4μ8c treatment led to a significant reduction (45.2%; $P < 0.001$) in atherosclerotic lesion area in en face aorta preparations (Fig. 4*E*) and a significant reduction in the spliced *Xbp1* mRNA (Fig. S7*A*) ($P < 0.05$) but no change in IRE1 phosphorylation in the spleens (Fig. S7*B*). Furthermore, 4μ8c treatment led to a reduced foam cell area (Fig. 4*F*) without overt differences in body weight, blood glucose levels (Table S4), liver morphology, and plasma ALT activity between the inhibitor-treated and control mice (Fig. S7 *C* and *D*). These in vivo findings show that pharmacological inhibition of IRE1 can effectively mitigate plaque development in mice.

Pharmacological Inhibition of IRE1 Alters Plaque Composition. Endothelial cells, vascular smooth muscle cells (VSMCs), and immune cells, such as lymphocytes, dendritic cells, neutrophils, and macrophages, play important roles in the development of atherosclerotic plaques in the arterial wall. The UPR is activated in many of these cell types and at all stages of atherosclerotic plaque development. This increase in ER stress is also associated with plaque progression, vulnerability to rupture, and acute coronary syndrome in humans (7). Given that IRE1 inhibitors alleviated atherosclerosis in ApoE$^{-/-}$ mice, we next analyzed the impact of these inhibitors on the cellular composition of the lesions. STF-083010 treatment led to a significant reduction (35%; $P < 0.01$) in macrophages [as visualized by monocyte/macrophage marker-2 (MOMA-2) staining] infiltrating the aortic root plaques (Fig. 5*A*). This reduction in macrophage numbers was not the product of increased apoptosis as determined by TUNEL (in situ cell death detection) assays in macrophage-enriched areas of the plaques (Fig. 5*B*). Furthermore, there were no differences in the necrotic core area between the treatment and control groups (Fig. S8*A*). During plaque formation, VSMCs migrate from adventitia to intima, secreting collagen and sealing the fibrous cap of the plaque. The analysis of the lesions in STF-083010–treated mice (with Masson's Trichrome staining) showed that there is a significant increase in collagen content that is responsible for tensile strength and elasticity of the plaques (22%; $P < 0.05$) without changes in the numbers of the VSMCs infiltrating the lesions (Fig. S8 *B* and *D*). However, we did not observe significant differences in the fibrous cap thickness between the treatment and control groups (Fig. S8*C*) Finally, STF-083010 treatment did not alter CD3$^+$ T-cell numbers in the adventia/lesions (Fig. S8*E*). Taken together, these results indicate that the major consequences of IRE1 inhibition include a reduction in macrophages and an increase in collagen deposition in atherosclerotic plaques.

Last, we sought in vivo evidence for the observed inhibition of IL-1β by IRE1 inhibition in macrophages (Figs. 1 and 2). We observed that STF-083010 treatment reduced the expression of IL-1β in the aortic root lesions stained with a specific antibody against IL-1β (Fig. 5*C*). Together, these results validate our earlier in vitro findings and show that the antiatherogenic effect of IRE1 inhibitors involves a blockage of inflammation in the lesions.

IRE1 Inhibitors Suppress Hyperlipidemia-Induced Th-1 Immune Responses. Atherosclerosis initiation and progression depend on both innate and adaptive immunity pathways. T cells orchestrate adaptive immunity, whereas macrophages bridge innate and adaptive immune processes that contribute to lesion development. Th cells form the majority of lymphocytes in the atherosclerotic

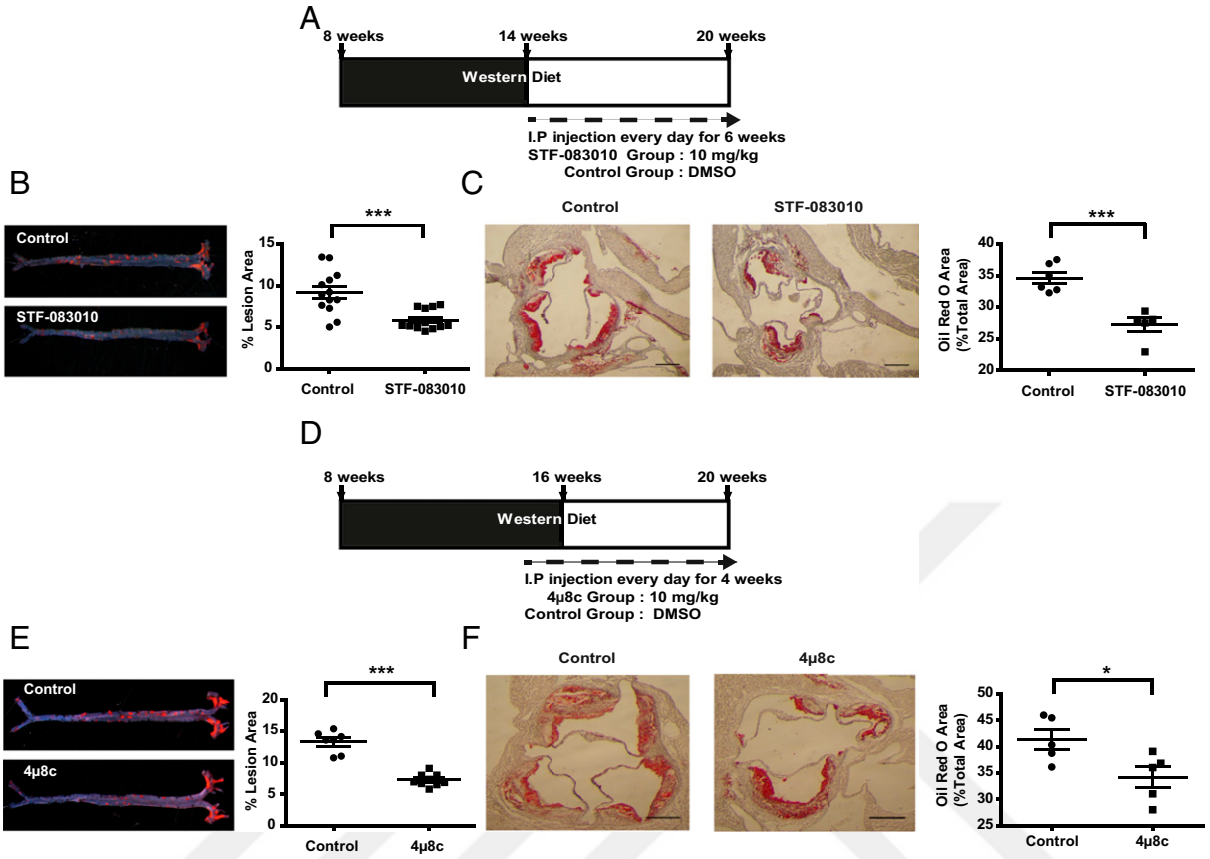

Fig. 4. IRE1 inhibitors reduce plaque area in a mouse model of atherosclerosis. (*A*) Experimental design in ApoE$^{-/-}$ mice using STF-083010 (10 mg/kg per day). (*B*) En face aorta analysis of atherosclerotic plaques in ApoE$^{-/-}$ mice. (*Left*) Sudan IV staining of atherosclerotic plaques. (*Right*) Quantification of plaque area (n = 13–14). (*C*) Analysis of aortic sinus plaque area in the animals in *A* and *B*. (*Left* and *Center*) Oil Red O staining of aorta cross-sections. (*Right*) Quantification of plaque area (n = 5–6). (*D–F*) Experimental design and data for analogous experiments in ApoE$^{-/-}$ mice using 4μ8c (10 mg/kg per day; *E*, n = 7–9; *F*, n = 5). Statistics are the same as in Fig. 1. (Scale bar: 350 μm.) *$P \leq 0.05$; ***$P \leq 0.001$.

plaques. Th-1 cells are proinflammatory, produce high amounts of IFN-γ, and contribute to the progression of atherosclerosis. Two other types of lymphocytes implicated in atherosclerosis progression include Th-2 cells, which produce IL-4, and Th-17 cells, which produce IL-17 (49–51). The inflammasome-induced cytokines IL-18 and IL-1β play an important role in the polarization of Th-1 and Th-17 responses (52). Because inhibition of IRE1 suppressed inflammasome activation (Fig. 3*C* and Fig. S4 *D* and *E*) and IL-1β production in lipid-challenged macrophages (Fig. 2) as well as lesions and tissues (Fig. 5*C* and Fig. S9 *A* and *B*), we next assessed the impact of IRE1 inhibition on systemic IL-18 levels and Th cell differentiation in hyperlipidemic mice. ApoE$^{-/-}$ mice (on Western diet) that were treated with STF-083010 displayed a significant decrease in plasma IL-18 levels (Fig. 6*A*) ($P < 0.05$) and a marked reduction in the secretion of IFN-γ—but not IL-4 or IL-17—from splenocytes ($P < 0.001$) (Fig. 6 *B–D* and Fig. S9 *C–E*). We did not observe changes in the overall T-cell counts in atherosclerotic lesions after STF-083010 treatment (Fig. S8*E*), indicating that decreased lymphokine production is intrinsic to intracellular signaling and does not result from a decline in the infiltrating immune cells that produce them. In conclusion, the reduced inflammasome activity in these mice (as measured by IL-1β and IL-18 levels in Figs. 5*C* and 6*A*) after STF-083010 treatment correlates with the suppression of the Th-1 inflammatory response that is known to promote atherosclerosis development.

Discussion

Studies in mice and humans suggest that chronic ER stress plays an important role in atherosclerosis progression. Therefore, pharmacological manipulation of the UPR—the network of signaling pathways that respond to ER stress—represents a promising therapeutic approach to manage atherosclerosis (7, 14, 53). The recent discovery of highly selective UPR modulators provides unique opportunities to investigate the contribution of individual UPR branches to the pathogenesis of this disease. Using small molecules that target IRE1, we showed that modulating IRE1 signaling counteracts atherosclerotic plaque formation in mouse models.

First, IRE1 inhibition altered plaque cellular composition mainly by reducing the numbers of macrophages in the atherosclerotic lesions without altering apoptosis. We infer that this effect is likely to stem from reduction in CCL2, a strong macrophage chemoattractant, consistent with our observations in macrophages treated with IRE1 inhibitors. Alternatively, IRE1 modulators could impact macrophage clearance from lesions by phagocytosis of dying cells. We observed no change in the apoptotic cell counts in lesions, arguing against this possibility. Nevertheless, more detailed future studies are required to discriminate between these two possibilities.

Second, IRE1 inhibitor-treated mice displayed an increased collagen content in atherosclerotic lesions, which imparts tensile strength and elasticity to the plaques (54). However, we did not observe an increase in fibrous cap thickness on IRE1 inhibitor treatment. Because we observed no differences in the number of VSMCs in the lesions, the increased collagen deposition may be related to increased collagen folding and secretion, which is consequential to enhanced ER function coupled to reduced cleavage by MMPs. In fact, early in our study, we observed that MMP9 is regulated by IRE1, whereas another study reported RIDD-dependent

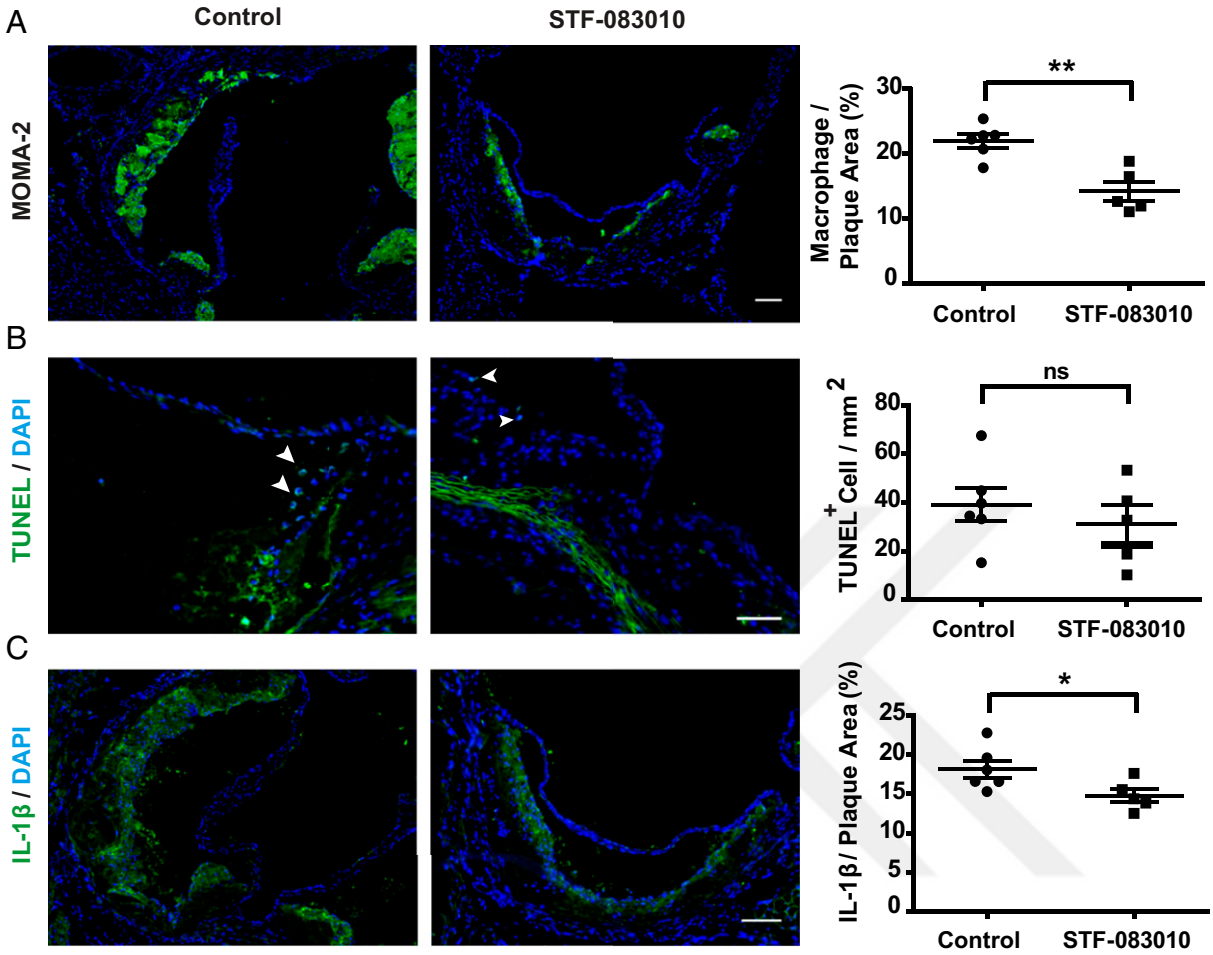

Fig. 5. IRE1 inhibitors alter plaque composition and inflammation. Immunohistochemical and TUNEL assay analyses of proximal aorta cryosections from ApoE$^{-/-}$ mice (Fig. 4) treated with an IRE1 inhibitor. In each case, a representative image is shown in *Left* and *Center*, and the quantification of the data appears on in *Right*. (*A*) MOMA-2. (Scale bar: 100 μm.) (*B*) TUNEL assay (apoptotic cells are shown with arrowheads). (Scale bar: 50 μm.) (*C*) IL-1β. (Scale bar: 100 μm.) Statistics are the same as in Fig. 1. ns, not significant. *$P \leq 0.05$; **$P \leq 0.01$.

collagen degradation during ER stress (55). Both observations lend support to our findings and substantiate our hypotheses.

Third, the results from our RNA-seq analyses in macrophages that were treated with IRE1 inhibitors strongly hinted at IRE1's involvement in the production of several proatherogenic cytokines, chemokines, and their receptors, including IL-1β, CCL2, and chemokine receptor 2. Indeed, IRE1, through XBP1s, regulates *Il-1β* and *Ccl2* mRNA induction in lipid-stressed macrophages. Moreover, oxidative stress can activate NF-κB and production of CCL2, resulting in the recruitment of monocytes to a growing plaque (7).

Fourth, cholesterol crystals, saturated fatty acids, and ROS accumulate in plaque areas and provide activation signals for activation of the NLRP3 inflammasome and subsequent secretion of IL-1β and IL-18 (44). These cytokines generate Th-1–type immune responses that promote plaque progression and unstable lesions (52). Treatment of macrophages with the IRE1 inhibitors suppressed lipid-induced mtROS production, activation of the NLRP3 inflammasome, and subsequent IL-1β secretion. Our results, therefore, implicate IRE1 activation in the perpetuation of lipid-induced mitochondrial oxidative stress upstream of NLRP3 inflammasome activation, but our data show that this effect is independent of TXNIP induction or calcium mobilization (35, 44). Macrophage mitochondrial oxidative stress plays an important role in atherogenesis by amplifying inflammation (56). Our results reveal that IRE1 is crucial for the regulation of mtROS generation during lipid-induced ER stress; however, future detailed studies will be needed to uncover how this is achieved by IRE1. In addition to our findings in cells, we confirmed the inhibitory effect of IRE1 inhibitors on hypercholesterolemia-induced IL-1β and IL-18 production in vivo in plaques and plasma, respectively. Consistent with these observations, treatment with IRE1 inhibitors led to a marked suppression of hyperlipidemia-induced Th-1 immune responses in these mice. We observed no differences in T-cell numbers in adventia/lesions between the IRE1 inhibitor treatment and control groups, and previous studies have shown the IRE1 inhibitor used in this study does not affect Treg cells (33, 37). Collectively, these findings show that prevention of inflammasome-associated cytokine production by IRE1 inhibitors in vivo has dramatic effects on counteracting atherosclerotic disease progression. Our findings correlating suppression of IL-1β with atheroprotection are timely in view of a major ongoing clinical trial on the effect of an anti–IL-1β trial in coronary artery disease (by Cantos). Although our data show a clear impact of IRE1 inhibition on macrophage inflammatory functions, activation of the UPR also occurs in many other lesion-resident cell types. Thus, our results do not exclude the possibility that the antiatherogenic effects of IRE1 inhibition could also involve other lesion-resident cell types that contribute to atherogenesis.

Fifth, the reduction in plaque inflammation and size occurred independent of a correction of elevated plasma lipid levels in IRE1 inhibitor-treated ApoE$^{-/-}$ mice. This notion contrasts with results of a previous study, in which mice bearing a liver-specific deletion

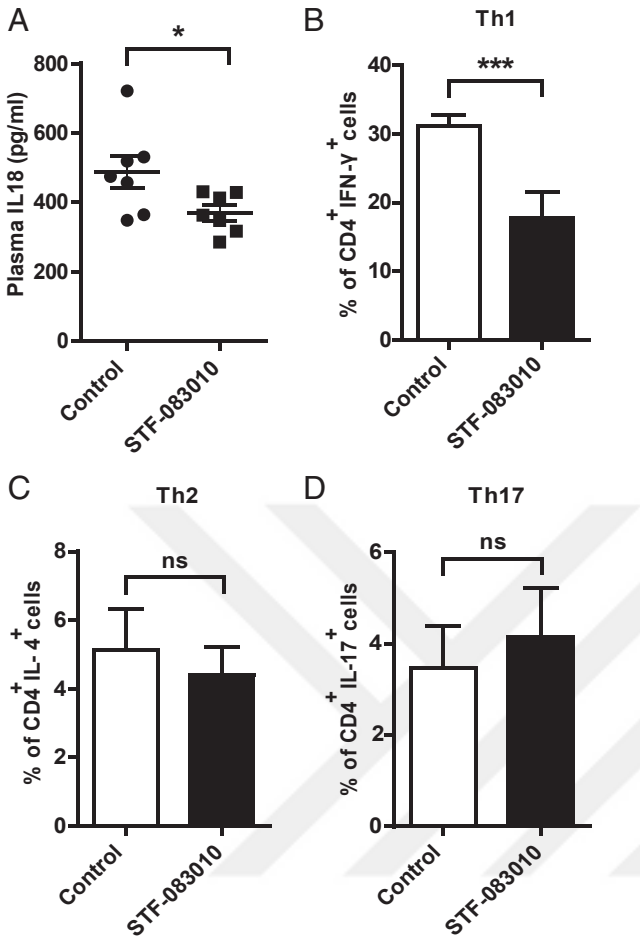

Fig. 6. IRE1 inhibitors suppress hyperlipidemia-induced Th-1 immune responses and IL-18 cytokine levels. (*A*) Plasma IL-18 in ApoE$^{-/-}$ mice (Fig. 4) treated with an IRE1 inhibitor was measured by ELISA ($n = 7$). (*B–D*) Flow cytometry analysis of IFN-γ, IL-4, and IL-17 in splenocytes from ApoE$^{-/-}$ mice treated with IRE1 inhibitor and activated with PMA/ionomycin ($n = 5$). Statistics are the same as in Fig. 1. ns, not significant. *$P \leq 0.05$; ***$P \leq 0.001$.

of *Xbp1* displayed a profound reduction in plasma cholesterol and triglyceride levels (57). However, it is important to note that this apparent disparity may exclusively result from feedback activation of IRE1 on genetic loss of *Xbp1* (57). Notably, additional siRNA-mediated IRE1 depletion partially reverted the hypolipidemic phenotype in vivo, hinting at an RIDD-dependent function that controls lipid metabolism (30). Furthermore, we did not observe feedback activation of IRE1 or any signs of liver toxicity with the IRE1 modulators. Because XBP1s promotes the transcriptional up-regulation of a lipogenic gene program, these findings could be interpreted to mean that the splicing and RIDD outputs of IRE1 have opposing effects on lipid metabolism (30). Although most of the direct targets of XBP1 participating in triglyceride and sterol lipogenic programs were also identified as RIDD substrates in this study (ref. 30, figure 3), IRE1 (through its RIDD modality) seems to be able to reduce the steady-state expression of a larger number of lipogenic genes independent of XBP1, hinting at a complex lipogenic regulatory program that depends on the interplay between XBP1 and IRE1 signaling (30, 57). Thus, the reduction in plaque size that we observed in our study is likely to result from IRE1 inhibitor-mediated antiinflammatory changes and not to result from the product of changes in lipid metabolism.

Although we have seen important gains in mitigating atherosclerosis by pharmacologically targeting IRE1 in our experimental models, it is important to note that the other UPR branches, particularly the PERK-CHOP branch, are also induced as atherosclerosis progresses and seem to be instrumental for macrophage apoptosis (5, 11). Previous studies focusing on the engagement of apoptotic pathways initiated by the UPR (such as those mediated by CHOP and JNK) showed that mice deficient for these apoptotic effectors are protected from atherosclerosis (5, 11–13). Independent of CHOP or JNK engagement, here, we found that modulating IRE1 signaling in vivo with small molecule IRE1 inhibitors modifies a different branch of UPR signaling that impinges on metaflammation and alters the course of atherosclerosis. These results support the notion that it may be possible to uncouple metabolically induced ER stress from inflammation by calibrating UPR signaling, thereby improving the clinical outcome of atherosclerosis. With the advent of specific inhibitors that can target different UPR branches, exploring the efficacy of combinatorial UPR calibration in this chronic disease setting becomes a promising endeavor.

Experimental Procedures

A list of primers used in the study can be found in Dataset S1.

Reagents and Plasmids. IRE1$^{-/-}$ MEFs were provided by Gokhan Hotamişligil, Harvard School of Public Health, Cambridge, MA. BMDMs were isolated from C57BL/6 mice. Plasmids encoding XBP1s (21833) and WT IRE1α (13009) were purchased from Addgene. L-Glutamine, DMEM, PBS, HBSS, penicillin/streptomycin (P/S), FBS, and Roswell Park Memorial Institute (RPMI)-1640 medium were obtained from Thermo Scientific or HyClone (GE Healthcare Life Sciences). Trypsin, ampicillin, kanamycin, Bradford assay reagents, ultrapure LPS, PA (palmitic acid), phosphatase inhibitor mixture, and STF-083010 were purchased from Sigma-Aldrich; 4μ8c was purchased from Calbiochem. Primary antibodies used for immunoblotting were purchased from the following suppliers: anti-IRE1 phospho-S724 antibody (ab48187; Abcam), IL-1β (ab9722; Abcam), IRE1α rabbit mAb (3294; Cell Signaling), β-Actin (sc-47778; Santa Cruz Biotechnology), β-actin (sc-9104; Santa Cruz Biotechnology), Caspase-1 (M20; sc-514; Santa Cruz Biotechnology), and IL-1β (AF-401-NA; R&D Systems). ECL Prime Western Blot Detection Kit was purchased from Amersham Pharmacia. ALT assay (MAK052) was from Sigma-Aldrich.

Preparation of PA-BSA Complex. PA was dissolved in absolute ethanol to yield a stock concentration of 500 mM and stored at −80 °C. Stock PA was diluted to the working concentration and suspended with 1% fatty acid-free BSA in RPMI-1640 medium (without serum) by mixing at 50 °C for 30 min.

Preparation of Cholesterol Crystal. The 10-mg/mL cholesterol solution was prepared in ethanol, heated to 60 °C, brought to room temperature to allow for crystallization, washed with PBS, and resuspended in RPMI-1640 medium at 5 mg/mL; 400-μg/mL cholesterol crystals were used for treating the cells (for 20 hours) as described (58).

Cell Culture and Treatments.

Isolation of BMDMs. Bone marrows were collected from the tibia and femurs of mice into RPMI-1640 medium containing 1% P/S. After filtering through a cell strainer (352350; BD Biosciences), the cells were centrifuged at 400 × *g* for 5 min and resuspended in RPMI-1640 medium enriched with 15% (vol/vol) L929 conditioned medium and 1% P/S followed by seeding for growth and differentiation into macrophages on Petri dishes for 7 d.

Inflammasome activation. BMDMs were pretreated (1 h) with 150 μM STF-083010 or the indicated concentrations of 4μ8c followed by stimulation with ultrapure LPS (200 ng/mL) for 3 hours and then, followed by treatment with PA-BSA (1,000 μM) for 20 hours. Human PBMCs were purchased from Zenbio and grown in lymphocyte medium (RPMI-1640, 2 mM L-glutamine, 10% (vol/vol) FBS, 1% P/S) according to the instructions provided by the manufacturer. Cells were pretreated with 100 μM 4μ8c before stimulation with ultrapure LPS (200 ng/mL) for 3 hours. These incubations were followed by treatment with ethanol-BSA (control) or PA-BSA (500 μM). LPS-primed BMDMs were treated with various inflammasome inducers, including 5 nM ATP (Sigma-Aldrich), 200 μg/mL Imject Alum (Thermo Scientific), and 1 μg/mL Flagellin (Invivogen) either alone or in combination with 100 μM 4μ8c. Lipofectamine 3000 was used for poly(dA:dT) DNA (5 μg/mL) transfection as described (43).

Induction of mtROS. BMDMs were pretreated (1 h) with 100 μM 4μ8c followed by sequential stimulation with 200 ng/mL LPS (3 hours) and then, PA-BSA (1,000 μM) or vehicle (ethanol)-BSA (control) for 20 hours.

Western Blot Analysis. Cells were lysed in lysis buffer [50 mM Hepes, pH 7.9, 100 mM sodium chloride, 10 mM EDTA, 10 mM sodium fluoride, 4 mM tetrasodium diphosphate, 1% Triton X-100, 2 mM sodium orthovanadate, 1 mM PMSF (phenylmethylsulfonyl), 1× phosphatase inhibitor mixture (Sigma-Aldrich), 1× protease inhibitor mixture (Sigma-Aldrich)]. Lysates were cleared by brief centrifugation followed by the addition of 5× SDS loading dye. For the detection of cleaved caspase-1 (active p10 form) in the cell medium, cell culture supernatants were collected, mixed with 5× SDS loading dye, and heated at 95 °C for 5 min before loading on SDS/PAGE gels. Proteins were subjected to SDS/PAGE separation and transferred onto PVDF membranes. Blocking and antibody incubation were carried out in TBS (Tris-buffered saline) with 0.1% (vol/vol) Tween-20 and 5% (wt/vol) dry milk or BSA and visualized by ECL in a BioRad Imager.

Transfection. IRE1$^{-/-}$ MEFs that reached 60–80% confluency were transfected with the indicated plasmids (2 μg DNA for every 4.5 × 10^5 cells) and polyethylenimine (Sigma-Aldrich), and BMDMs were electroporated using a Neon Electroporator (Invitrogen) according to the protocols provided by the manufacturer.

RNAi. BMDMs were transfected with 50 nM siRNA against *ire1* (SI0099588; Qiagen), 70 nM siRNA against *Xbp1* (SI01473227; Qiagen), or scrambled siRNAs (1027281; Qiagen); 24 hours after transfection, the cells were treated with indicated reagents.

RNA Isolation and qRT-PCR. Trisure (Bioline) was used to isolate total RNA from cells and reverse-transcribed using the RevertAid First Strand cDNA Synthesis Kit (K1691; Thermo Scientific) according to the manufacturer's protocols. cDNAs were amplified using specific primers on a Rotor Gene (Qiagen) real-time PCR instrument. Roche SYBR Green was used for qRT-PCR. Quantifications were performed using the ΔΔCt (threshold cycle) method, and gene expression levels were normalized to *Gapdh* transcript levels using the following expression: (primer efficiency)$^{-\Delta\Delta Ct}$, where ΔΔCt means ΔCt (target gene) − ΔCt (reference gene). We analyzed the results from three or more independent experiments using the Student's *t* test.

RNA-Seq Library Preparation and Sequencing. Total RNA was isolated from control and IRE1-inhibited (with STF-083010) BMDM samples using Trisure (Bioline). To remove genomic DNA contamination, the RNA samples were treated with 20 U DNase I (New England Biolabs). rRNA was depleted from 5 μg total RNA using Ribo-Zero Gold rRNA Removal Kit (Epicentre Biotechnologies) following the manufacturer's recommendations. Sequencing libraries for whole-transcriptome analysis were prepared using the ScriptSeq v2 RNA-Seq Library Preparation Kit (Epicentre Biotechnologies) following the manufacturer's recommendations. After 3′-terminal tagging, the di-tagged cDNA was purified using column concentrators (DNA clean-up and concentrators; Zymo Research). The cDNA libraries were bar-coded to allow sample multiplexing using ScriptSeqTM Index PCR Primers (Epicentre Biotechnologies). The libraries were amplified by 12 cycles of PCR, and the amplified libraries were size-selected and purified using 8% TBE (Tris/borate/EDTA) acrylamide gels. The libraries were quantified using Agilent Technologies 2100 Bioanalyzer. Up to four RNA-seq libraries were then multiplexed in a single lane of an Illumina HiSeq2500 Deep-Sequencer Flow Cell (University of California, San Francisco Center for Advanced Technologies) and sequenced using 50-bp single-end sequencing chemistry.

RNA Sequencing Data Processing. The 3′ adapter sequences (AGATCGGAAGAGCACACGTCTGAAC) were removed from the sequenced libraries using the FastQ/A clipper found in the FastX Toolkit (hannonlab.cshl.edu/fastx_toolkit/) after d-multiplexing, and only reads longer than 20 nt were kept for alignment. The adapter-stripped reads were then aligned with the Bowtie indices for the mouse genome reference version 10 of the University of California, Santa Cruz Genome Browser (mm10) using the splice junction mapper Tophat2 v2.0.9 and the sequence aligner Bowtie 2 V2.2.3.0 with default parameters. The transcript assembler Cufflinks V2.1.1 was then used on the list of mapped reads to assemble and quantify transcripts using an mm10 reference annotation and masking mitochondrial, rRNA, and tRNA sequences. To estimate the changes in gene expression levels, the number of sequenced reads that align to a gene of interest was then compared among biological samples using Cuffdiff (default parameters). Changes in the levels of expression of normalized Cufflinks-quantified transcripts are expressed as fragments per kilobase of transcript per million mapped reads (FPKM).

Flow Cytometric Analysis of Intracellular Cytokine Staining. Fresh splenocytes were prepared from mice spleen, and erythrocytes were removed using RBC (red blood cell) lysis buffer as described earlier (43). Cells were stimulated for 4 hours with phorbol-myristate-acetate (PMA; 50 ng/mL; Abcam) and ionomycin (1 μg/mL; Abcam) in the presence of Golgi stop (BD Biosciences). Live cells were discriminated from dead ones by using Zombie Green (Bio Legend). Cell surfaces were stained with PerCP-Cy5.5–conjugated anti-CD4 antibody (BD Biosciences) followed by incubation in Cytofix/Cytoperm Solution (BD Biosciences) at room temperature for 15 min. Then, intracellular cytokines were stained with allophycocyanin (APC)-conjugated IFN-γ, phycoerythrin (PE)-conjugated IL-17A, and PE-conjugated IL-4 antibodies (all from BD Biosciences). Data were analyzed on BD Accuri C6 software.

Measurement of Secreted IL-1β and IL-18 and CCL2 Cytokines. An IL-1β Elisa Kit (Abcam) was used for detecting IL-1β; a Mouse IL-18 ELISA Kit (Medical & Biological Laboratories) and a Mouse CCL2 Elisa Kit (Abcam) were used for detecting the cytokines in mouse plasma or conditioned medium, respectively, as indicated according to the manufacturer's instructions.

Plasma Measurements. FPLC was used for analyzing the size distribution of lipoproteins. All measurements were carried out at the Mouse Metabolic Phenotyping Center at the University of Cincinnati. For the resolution of major lipoprotein classes from plasma; the columns were equilibrated in 50 mM PBS. Using a microtiter plate enzyme-based assay, the major lipoprotein classes were measured in cholesterol or triglyceride assays from collected fractions.

Staining of Cryosections. Cryosections (7-μm thick) were cut from the aortic root of the frozen heart tissue with a cryostat (Leica CM1850) and stained with Oil Red O, anti–MOMA-2 (monocyte/macrophage marker) (ab33451; Abcam), anti–CD3-Alexa488 (1:400; Biolegend), TUNEL Kit (11684795910; Roche), anti–α-SMA (ab5694; Abcam), and IL-1β antibody (ab9722; Abcam). Immunofluorescent staining was mounted with an antifade reagent including DAPI (GR211467-2; Abcam). Representative images were taken with a Zeiss Fluorescent Microscope. Collagen content of the lesions and fibrous cap thickness were determined in Masson's Trichrome-stained lesions (as per the manufacturer's protocol; Bio-Optica). Fibrous cap thickness was calculated according to the published protocol (59). Heart tissue sections were stained with Oil Red O stain for plaque area quantifications and H&E for necrotic core quantification in accord with previously published protocols (43). All quantifications were performed using ImageJ (NIH). Percentage of average cross-sectional stained area per leaflet was calculated from all three valves.

Atherosclerotic Lesion Analysis. Aortas were pinned on a black wax surface, and atherosclerotic lesions were analyzed in the aortic arch and descending aorta by Sudan IV staining as described earlier (43). Areas were quantified using ImageJ and expressed as the percentages of the total aorta area.

Quantification of mtROS. mtROS production was measured with MitoSOX Red Mitochondrial Superoxide Indicator (M36008; Life Technologies) according to the protocol provided by the company. Representative images were acquired with a confocal microscope (LSM 510; Zeiss) and analyzed with ImageJ.

Mitochondrial Calcium Measurement. RHOD-2 AM (cell-permeable fluorescent calcium indicator) (Thermo Scientific) was used for mitochondria-specific calcium measurement according to previously published protocols (60).

Mice and Treatments. ApoE$^{-/-}$ mice in a C57BL/6 background (Charles River WIGA GmbH) were used in atherosclerosis experiments. Starting from 8 weeks of age, male mice were fed a Western diet (TD88137 mod. containing 21% fat and 0.2% cholesterol; Ssniff) for 6 weeks. Then, the mice were injected with STF-083010 (10 mg/kg) or DMSO, both given in 16% (vol/vol) Cremophor EL (Sigma-Aldrich) saline solution via i.p. injections as described previously, for 6 more weeks while mice were continued on the Western diet (21). The other ApoE$^{-/-}$ mice that were used in atherosclerosis experiments were fed a Western diet for 8 weeks. Then, they were injected with 4μ8c (10 mg/kg) or DMSO, both given in 16% (vol/vol) Cremophor EL saline solution via i.p. injections as described previously (33), for 4 more weeks while mice were continued on Western diet. Weights were measured every other day, whereas blood glucose concentrations were measured before and after treatments. At the end of the experiment, mice were anesthetized, and blood was collected by cardiac puncture. Bone marrow, spleen, and liver tissues were collected, frozen immediately into liquid nitrogen, and stored at −80 °C. Perfusion was performed with ice-cold PBS and heparin (1,000 U/mL) followed by 10% formalin solution (Sigma). After fixation, the aorta was

dissected intact, immersed immediately in 10% formalin, and stored at 4 °C until analysis. The heart was removed at the proximal aorta, placed into a tissue mold, covered with OCT (optimal cutting temperature compound) (Tissue-Tek), frozen in cold isobutene solution, and stored at −80 °C. All animal experiments were performed according to protocols approved by the Experimental Animal Care Committee at Bilkent University.

Statistical Analysis. Values are expressed as mean ± SEM. No samples were treated as outliers and left out of analysis. Statistical significance was evaluated using the Student's *t* test or the Mann–Whitney test (for in vivo analysis as indicated in the figures). $P < 0.05$ was considered as significant.

ACKNOWLEDGMENTS. We thank Gokhan S. Hotamisligil (Harvard University) for providing IRE1$^{-/-}$ MEFs, Esther Lutgens and Dirk Lievens for technical advice on bone marrow-derived macrophages (BMDMs), Buket Gültekin for administrative help, and Mojtaba Beyramzadeh for technical assistance with atherosclerosis studies. This work was funded, in part, by Scientific and Technological Research Council of Turkey (TUBITAK)-German Federal Ministry of Education and Research (BMBF) Intensified Cooperation Grant 110S293 (to C.W. and E.E.), TUBITAK Grant 113Z023 (to E.E.), and European Research Council (ERC) Starting Grant 336643 (to E.E.). D.A.-A. was supported by an Irvington Postdoctoral Fellowship from the Cancer Research Institute. P.W. is an Investigator of the Howard Hughes Medical Institute.

1. Wellen KE, Hotamisligil GS (2005) Inflammation, stress, and diabetes. *J Clin Invest* 115(5):1111–1119.
2. Hotamisligil GS (2010) Endoplasmic reticulum stress and the inflammatory basis of metabolic disease. *Cell* 140(6):900–917.
3. Walter P, Ron D (2011) The unfolded protein response: From stress pathway to homeostatic regulation. *Science* 334(6059):1081–1086.
4. Hollien J, et al. (2009) Regulated Ire1-dependent decay of messenger RNAs in mammalian cells. *J Cell Biol* 186(3):323–331.
5. Zhou AX, Tabas I (2013) The UPR in atherosclerosis. *Semin Immunopathol* 35(3): 321–332.
6. Williams KJ, Tabas I (1995) The response-to-retention hypothesis of early atherogenesis. *Arterioscler Thromb Vasc Biol* 15(5):551–561.
7. Tabas I (2010) The role of endoplasmic reticulum stress in the progression of atherosclerosis. *Circ Res* 107(7):839–850.
8. Myoishi M, et al. (2007) Increased endoplasmic reticulum stress in atherosclerotic plaques associated with acute coronary syndrome. *Circulation* 116(11):1226–1233.
9. McAlpine CS, Werstuck GH (2013) The development and progression of atherosclerosis: Evidence supporting a role for endoplasmic reticulum (ER) stress signaling. *Cardiovasc Hematol Disord Drug Targets* 13(2):158–164.
10. Zeng L, et al. (2009) Sustained activation of XBP1 splicing leads to endothelial apoptosis and atherosclerosis development in response to disturbed flow. *Proc Natl Acad Sci USA* 106(20):8326–8331.
11. Thorp E, et al. (2009) Reduced apoptosis and plaque necrosis in advanced atherosclerotic lesions of Apoe-/- and Ldlr-/- mice lacking CHOP. *Cell Metab* 9(5):474–481.
12. Ricci R, et al. (2004) Requirement of JNK2 for scavenger receptor A-mediated foam cell formation in atherogenesis. *Science* 306(5701):1558–1561.
13. Babaev VR, et al. (2016) Jnk1 deficiency in hematopoietic cells suppresses macrophage apoptosis and increases atherosclerosis in low-density lipoprotein receptor null mice. *Arterioscler Thromb Vasc Biol* 36(6):1122–1131.
14. Erbay E, et al. (2009) Reducing endoplasmic reticulum stress through a macrophage lipid chaperone alleviates atherosclerosis. *Nat Med* 15(12):1383–1391.
15. Ishimura S, et al. (2014) Reduction of endoplasmic reticulum stress inhibits neointima formation after vascular injury. *Sci Rep* 4:6943.
16. Wang B, et al. (2014) The modulation of endoplasmic reticulum stress by chemical chaperone upregulates immune negative cytokine IL-35 in apolipoprotein E-deficient mice. *PLoS One* 9(1):e87787.
17. Engin F, Hotamisligil GS (2010) Restoring endoplasmic reticulum function by chemical chaperones: An emerging therapeutic approach for metabolic diseases. *Diabetes Obes Metab* 12(Suppl 2):108–115.
18. Ong DS, Kelly JW (2011) Chemical and/or biological therapeutic strategies to ameliorate protein misfolding diseases. *Curr Opin Cell Biol* 23(2):231–238.
19. Hetz C, Chevet E, Harding HP (2013) Targeting the unfolded protein response in disease. *Nat Rev Drug Discov* 12(9):703–719.
20. Atkins C, et al. (2013) Characterization of a novel PERK kinase inhibitor with antitumor and antiangiogenic activity. *Cancer Res* 73(6):1993–2002.
21. Papandreou I, et al. (2011) Identification of an Ire1alpha endonuclease specific inhibitor with cytotoxic activity against human multiple myeloma. *Blood* 117(4): 1311–1314.
22. Sidrauski C, et al. (2013) Pharmacological brake-release of mRNA translation enhances cognitive memory. *eLife* 2:e00498.
23. Das I, et al. (2015) Preventing proteostasis diseases by selective inhibition of a phosphatase regulatory subunit. *Science* 348(6231):239–242.
24. Mimura N, et al. (2012) Blockade of XBP1 splicing by inhibition of IRE1α is a promising therapeutic option in multiple myeloma. *Blood* 119(24):5772–5781.
25. Gargalovic PS, et al. (2006) The unfolded protein response is an important regulator of inflammatory genes in endothelial cells. *Arterioscler Thromb Vasc Biol* 26(11):2490–2496.
26. Gora S, et al. (2010) Phospholipolyzed LDL induces an inflammatory response in endothelial cells through endoplasmic reticulum stress signaling. *FASEB J* 24(9):3284–3297.
27. Outinen PA, et al. (1999) Homocysteine-induced endoplasmic reticulum stress and growth arrest leads to specific changes in gene expression in human vascular endothelial cells. *Blood* 94(3):959–967.
28. Feng B, et al. (2003) The endoplasmic reticulum is the site of cholesterol-induced cytotoxicity in macrophages. *Nat Cell Biol* 5(9):781–792.
29. Zhou J, Lhoták S, Hilditch BA, Austin RC (2005) Activation of the unfolded protein response occurs at all stages of atherosclerotic lesion development in apolipoprotein E-deficient mice. *Circulation* 111(14):1814–1821.
30. So JS, et al. (2012) Silencing of lipid metabolism genes through IRE1α-mediated mRNA decay lowers plasma lipids in mice. *Cell Metab* 16(4):487–499.
31. Volkmann K, et al. (2011) Potent and selective inhibitors of the inositol-requiring enzyme 1 endoribonuclease. *J Biol Chem* 286(14):12743–12755.
32. Cross BC, et al. (2012) The molecular basis for selective inhibition of unconventional mRNA splicing by an IRE1-binding small molecule. *Proc Natl Acad Sci USA* 109(15): E869–E878.
33. Qiu Q, et al. (2013) Toll-like receptor-mediated IRE1α activation as a therapeutic target for inflammatory arthritis. *EMBO J* 32(18):2477–2490.
34. Upton JP, et al. (2012) IRE1α cleaves select microRNAs during ER stress to derepress translation of proapoptotic Caspase-2. *Science* 338(6108):818–822.
35. Lerner AG, et al. (2012) IRE1α induces thioredoxin-interacting protein to activate the NLRP3 inflammasome and promote programmed cell death under irremediable ER stress. *Cell Metab* 16(2):250–264.
36. Krämer A, Green J, Pollard J, Jr, Tugendreich S (2014) Causal analysis approaches in Ingenuity Pathway Analysis. *Bioinformatics* 30(4):523–530.
37. Kemp KL, et al. (2013) The serine-threonine kinase inositol-requiring enzyme 1α (IRE1α) promotes IL-4 production in T helper cells. *J Biol Chem* 288(46):33272–33282.
38. Bright MD, Itzhak DN, Wardell CP, Morgan GJ, Davies FE (2015) Cleavage of BLOC1S1 mRNA by IRE1 is sequence specific, temporally separate from XBP1 splicing, and dispensable for cell viability under acute endoplasmic reticulum stress. *Mol Cell Biol* 35(12):2186–2202.
39. Cross BC, et al. (2012) The molecular basis for selective inhibition of unconventional mRNA splicing by an IRE1-binding small molecule. *Proc Natl Acad Sci USA* 109(15): E869–E878.
40. Zhang L, Nosak C, Sollazzo P, Odisho T, Volchuk A (2014) IRE1 inhibition perturbs the unfolded protein response in a pancreatic β-cell line expressing mutant proinsulin, but does not sensitize the cells to apoptosis. *BMC Cell Biol* 15:29.
41. Schaffer JE (2003) Lipotoxicity: When tissues overeat. *Curr Opin Lipidol* 14(3):281–287.
42. Wen H, et al. (2011) Fatty acid-induced NLRP3-ASC inflammasome activation interferes with insulin signaling. *Nat Immunol* 12(5):408–415.
43. Çimen I, et al. (2016) Prevention of atherosclerosis by bioactive palmitoleate through suppression of organelle stress and inflammasome activation. *Sci Transl Med* 8(358): 358ra126.
44. Guo H, Callaway JB, Ting JP (2015) Inflammasomes: Mechanism of action, role in disease, and therapeutics. *Nat Med* 21(7):677–687.
45. Robblee MM, et al. (2016) Saturated fatty acids engage an IRE1α-dependent pathway to activate the NLRP3 inflammasome in myeloid cells. *Cell Reports* 14(11):2611–2623.
46. Murakami T, et al. (2012) Critical role for calcium mobilization in activation of the NLRP3 inflammasome. *Proc Natl Acad Sci USA* 109(28):11282–11287.
47. Kraskiewicz H, FitzGerald U (2012) InterfERing with endoplasmic reticulum stress. *Trends Pharmacol Sci* 33(2):53–63.
48. Wu T, et al. (2014) Hrd1 suppresses Nrf2-mediated cellular protection during liver cirrhosis. *Genes Dev* 28(7):708–722.
49. Zhou X, Paulsson G, Stemme S, Hansson GK (1998) Hypercholesterolemia is associated with a T helper (Th) 1/Th2 switch of the autoimmune response in atherosclerotic apo E-knockout mice. *J Clin Invest* 101(8):1717–1725.
50. Whitman SC, Ravisankar P, Daugherty A (2002) IFN-gamma deficiency exerts gender-specific effects on atherogenesis in apolipoprotein E-/- mice. *J Interferon Cytokine Res* 22(6):661–670.
51. Huber SA, Sakkinen P, David C, Newell MK, Tracy RP (2001) T helper-cell phenotype regulates atherosclerosis in mice under conditions of mild hypercholesterolemia. *Circulation* 103(21):2610–2616.
52. Ait-Oufella H, Taleb S, Mallat Z, Tedgui A (2011) Recent advances on the role of cytokines in atherosclerosis. *Arterioscler Thromb Vasc Biol* 31(5):969–979.
53. Austin RC (2009) The unfolded protein response in health and disease. *Antioxid Redox Signal* 11(9):2279–2287.
54. Adiguzel E, Ahmad PJ, Franco C, Bendeck MP (2009) Collagens in the progression and complications of atherosclerosis. *Vasc Med* 14(1):73–89.
55. Hollien J, Weissman JS (2006) Decay of endoplasmic reticulum-localized mRNAs during the unfolded protein response. *Science* 313(5783):104–107.
56. Wang Y, Wang GZ, Rabinovitch PS, Tabas I (2014) Macrophage mitochondrial oxidative stress promotes atherosclerosis and nuclear factor-κB-mediated inflammation in macrophages. *Circ Res* 114(3):421–433.
57. Lee AH, Scapa EF, Cohen DE, Glimcher LH (2008) Regulation of hepatic lipogenesis by the transcription factor XBP1. *Science* 320(5882):1492–1496.
58. Freigang S, et al. (2011) Nrf2 is essential for cholesterol crystal-induced inflammasome activation and exacerbation of atherosclerosis. *Eur J Immunol* 41(7):2040–2051.
59. Fredman G, et al. (2016) An imbalance between specialized pro-resolving lipid mediators and pro-inflammatory leukotrienes promotes instability of atherosclerotic plaques. *Nat Commun* 7:12859.
60. Zhang D, Armstrong JS (2007) Bax and the mitochondrial permeability transition cooperate in the release of cytochrome c during endoplasmic reticulum-stress-induced apoptosis. *Cell Death Differ* 14(4):703–715.

Supporting Information

Tufanli et al. 10.1073/pnas.1621188114

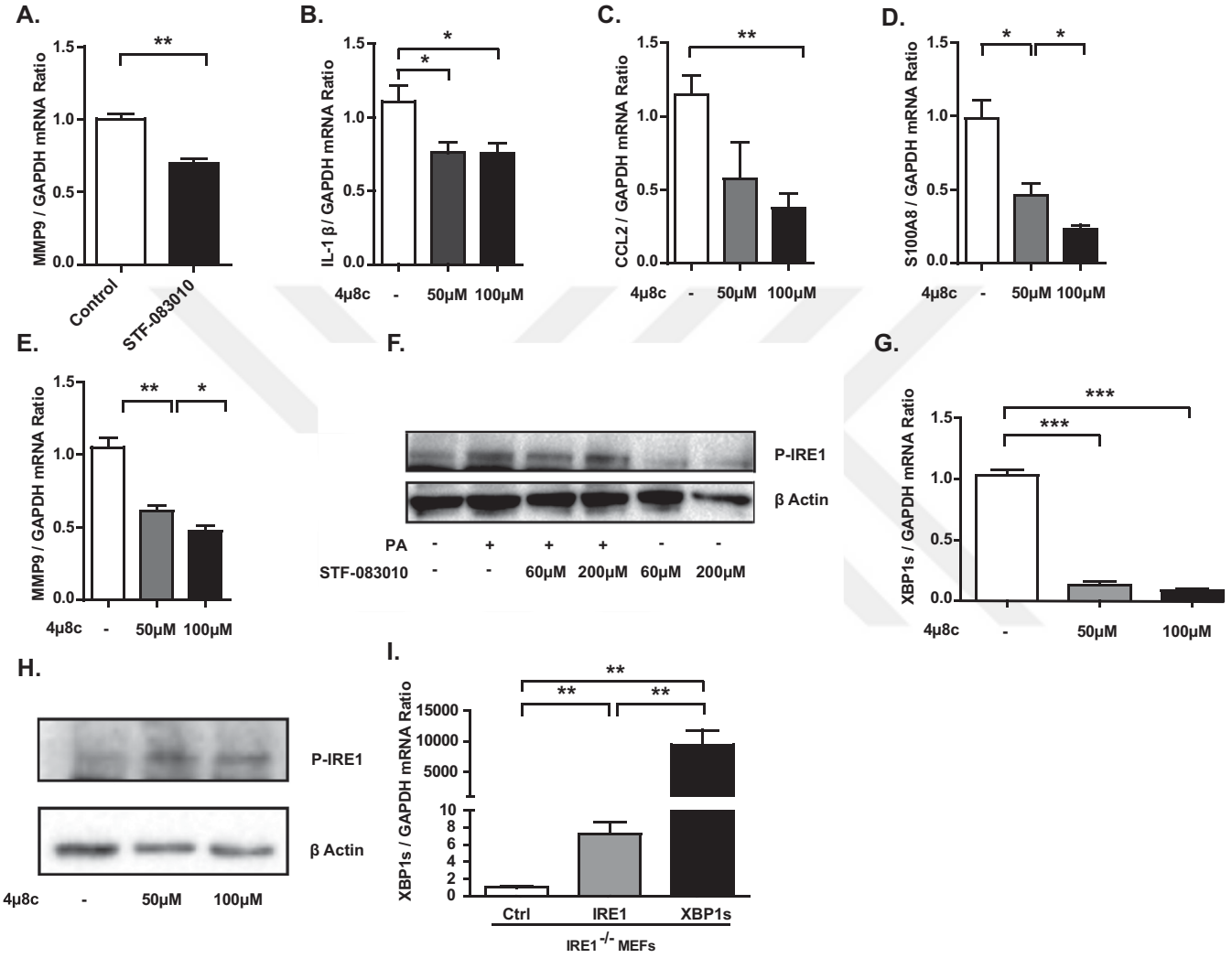

Fig. S1. Modulation of IRE1 signaling by various methods: validation and impact on various proatherogenic genes. (*A*) qRT-PCR analysis of *Mmp9* mRNA levels in mouse BMDMs treated with 60 μM STF-083010 or DMSO (control). (*B–E*) qRT-PCR analysis of *Il-1β, Ccl2, S100a8,* and *Mmp9* mRNA levels in mouse BMDMs treated with 4μ8c (at the indicated doses) or DMSO (control). (*F*) Validation of results in *A* and Fig. 1 *A–E*. IRE1 phosphorylation was detected by Western blot in lysates of PA-stimulated BMDMs treated with STF-083010 or DMSO (control). (*G* and *H*) Validation of results in *B–E*. (*G*) qRT-PCR analysis of spliced *Xbp1* mRNA levels in mouse BMDMs treated with increasing doses of 4μ8C. (*H*) Western blot analysis of IRE1 phosphorylation in BMDMs after IRE1 inhibition with 4μ8c. (*I*) Validation of results in Fig. 1 *F–H*. qRT-PCR analysis of spliced *Xbp1* mRNA levels in IRE1$^{-/-}$ MEFs transfected with plasmids encoding IRE1 or XBP1s. Statistics are the same as in Fig. 1. *$P \leq 0.05$; **$P \leq 0.01$; ***$P \leq 0.001$.

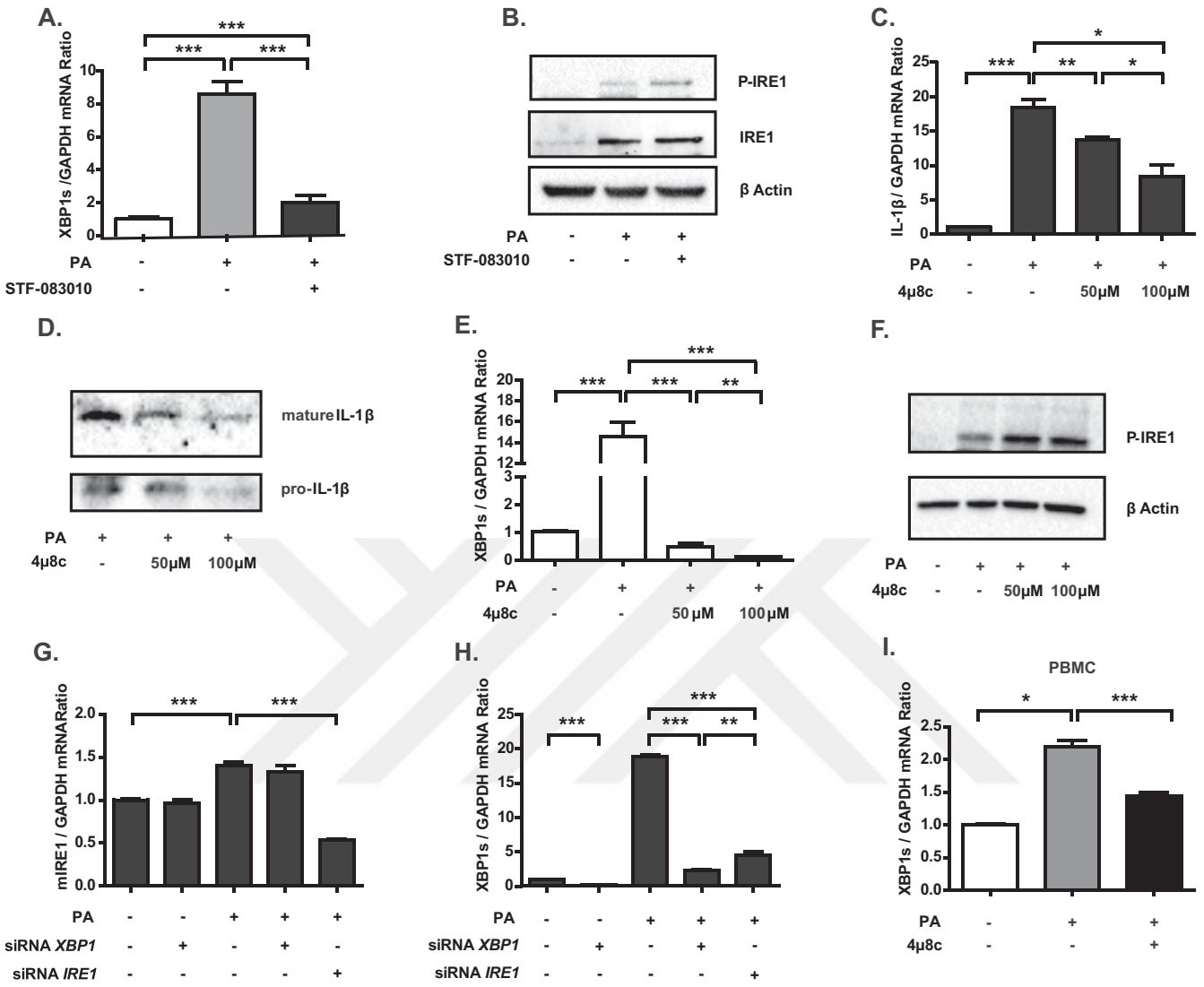

Fig. S2. Inhibition of IRE1 by various methods in lipid-stressed macrophages: validation of its impact on IL-1β. (*A* and *B*) Validation of results in Fig. 2 *A* and *B*. (*A*) qRT-PCR analysis of spliced *Xbp1* mRNA levels in LPS-primed, PA-stimulated mouse BMDMs treated with 150 μM STF-083010 or DMSO (control). (*B*) Western Blot analysis of p-IRE in LPS-primed, PA-stimulated mouse BMDMs treated with 150 μM STF-083010 or DMSO (control). (*C–F*) Inhibition of IRE1 RNase activity by 4μ8c and its impact on IL-1β. (*C*) qRT-PCR analysis of *Il-1β* mRNA levels in LPS-primed, PA-stimulated mouse BMDMs treated with 4μ8c (at the indicated doses). (*D*) Western blot analysis of secreted mature IL-1β from LPS-primed, PA-stimulated BMDMs treated with 4μ8c (at the indicated doses) or DMSO (control). (*E*) qRT-PCR analysis of spliced *Xbp1* mRNA levels in LPS-primed, PA-stimulated mouse BMDMs treated with 4μ8c (at the indicated doses) or DMSO (control). (*F*) Western blot analysis of IRE1 phosphorylation in LPS-primed, PA-stimulated mouse BMDMs treated with 4μ8c (at the indicated doses) or DMSO (control). (*G* and *H*) Validation of *Ire1α* and *Xbp1* knockdown in Figs. 2 *C* and *D* and 3*B*. qRT-PCR analysis of (*G*) *Ire1α* or (*H*) spliced *Xbp1* mRNA levels in LPS-primed, PA-stimulated mouse BMDMs transfected with siRNAs against *Ire1α* or *Xbp1*. (*I*) Validation of results in Fig. 2 *E* and *F*. qRT-PCR analysis of spliced *Xbp1* mRNA levels in LPS-primed human PBMCs treated with PA or a combination of PA and 4μ8c. Statistics are the same as in Fig. 1. **P* ≤ 0.05; ***P* ≤ 0.01; ****P* ≤ 0.001.

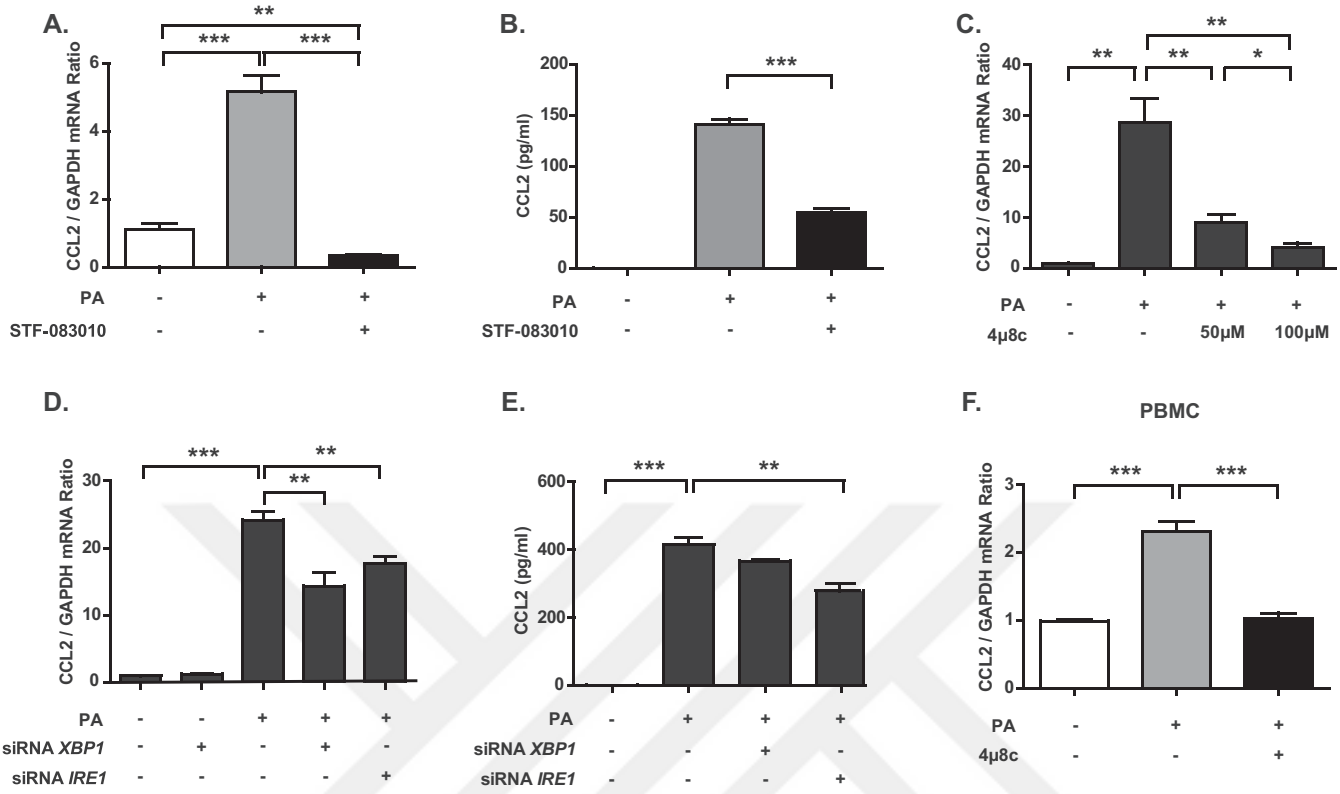

Fig. S3. IRE1 regulates lipid-induced CCL2 production in macrophages. (*A*) qRT-PCR analysis of *Ccl2* mRNA levels in LPS-primed, PA-stimulated BMDMs that were treated with 150 μM STF-083010 or DMSO (control). (*B*) ELISA measurements of secreted CCL2 from the conditioned medium used to culture the cells in *A*. (*C* and *D*) qRT-PCR analysis of *Ccl2* mRNA levels in LPS-primed, PA-stimulated BMDMs that were (*C*) treated with 4μ8c (at the indicated doses) or DMSO (control) or (*D*) transfected with siRNAs against *Ire1α* or *Xbp1*. (*E*) ELISA measurements of secreted CCL2 from the cells in *D*. (*F*) qRT-PCR analysis of *Ccl2* mRNA levels in LPS-primed, PA-stimulated human PBMCs treated with 4μ8c (at the indicated doses) or DMSO (control). Statistics are the same as in Fig. 1. $*P \leq 0.05$; $**P \leq 0.01$; $***P \leq 0.001$.

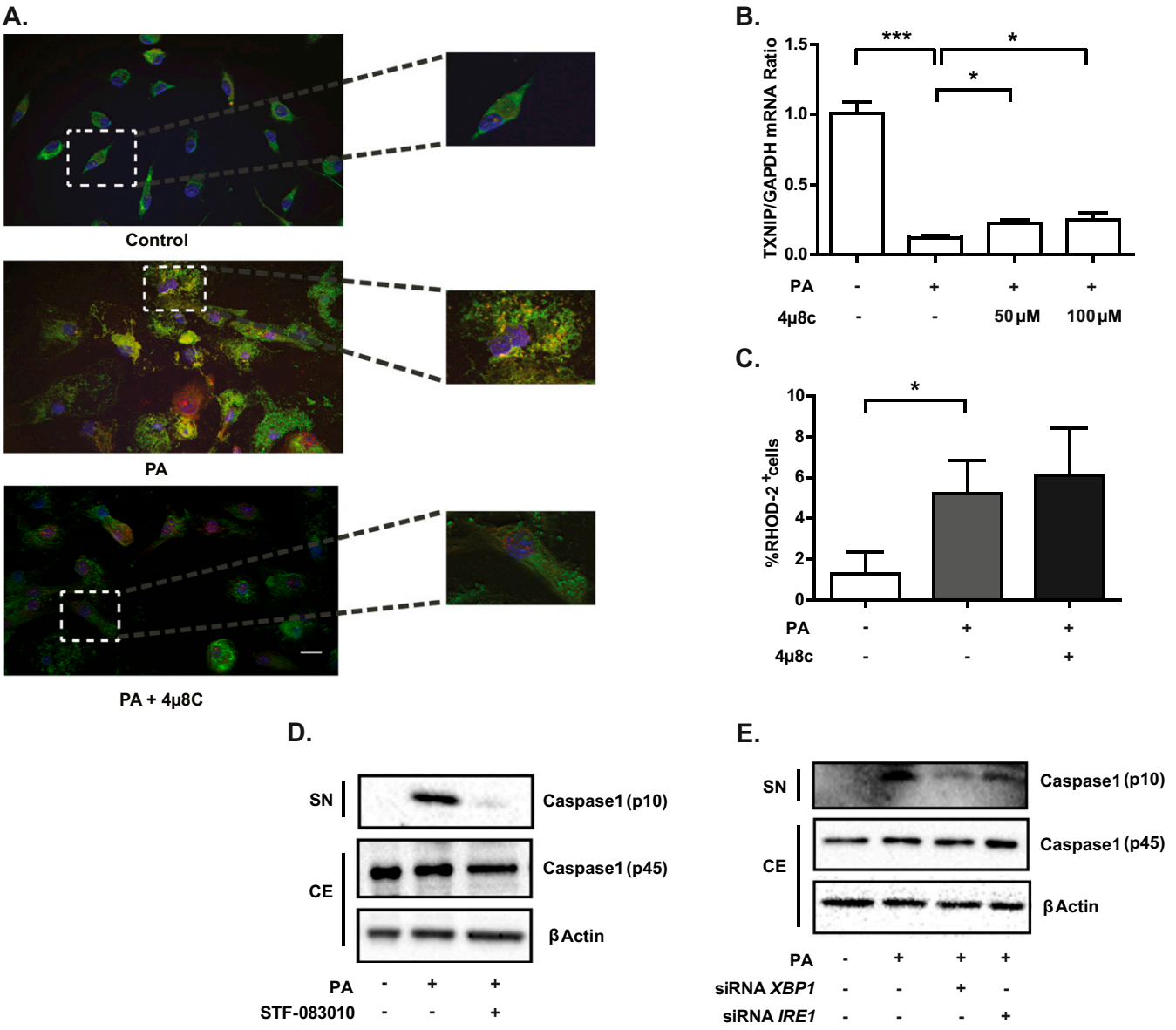

Fig. S4. IRE1 perpetuates mtROS production and inflammasome activation. (*A*) Representative confocal microscopy images of mtROS production in BMDMs (Fig. 3*A*). MitoSOX fluorescence indicator (red) and Mitotracker (green) are shown. mtROS (yellow) levels are quantified and depicted in the graph in Fig. 3*A*. (Scale bar: 20 μm.) (*B* and *C*) PA-stimulated BMDMs treated with the indicated doses of 4μ8c (at the indicated doses) or DMSO (control) were analyzed with (*B*) qRT-PCR for *Txnip* mRNA and (*C*) calcium uptake. (*D* and *E*) Western blot analysis of caspase-1 activation in LPS-primed, PA-stimulated mouse BMDMs (*D*) treated with 150 μM STF-083010 or DMSO (control) or (*E*) transfected with siRNAs against *Ire1α* or *Xbp1* Procaspase-1 (p45) and cleaved caspase-1 (p10) levels are indicated. Statistics are the same as in Fig. 1. CE, cell extract. SN, supernatant. $*P \leq 0.05$; $***P \leq 0.001$.

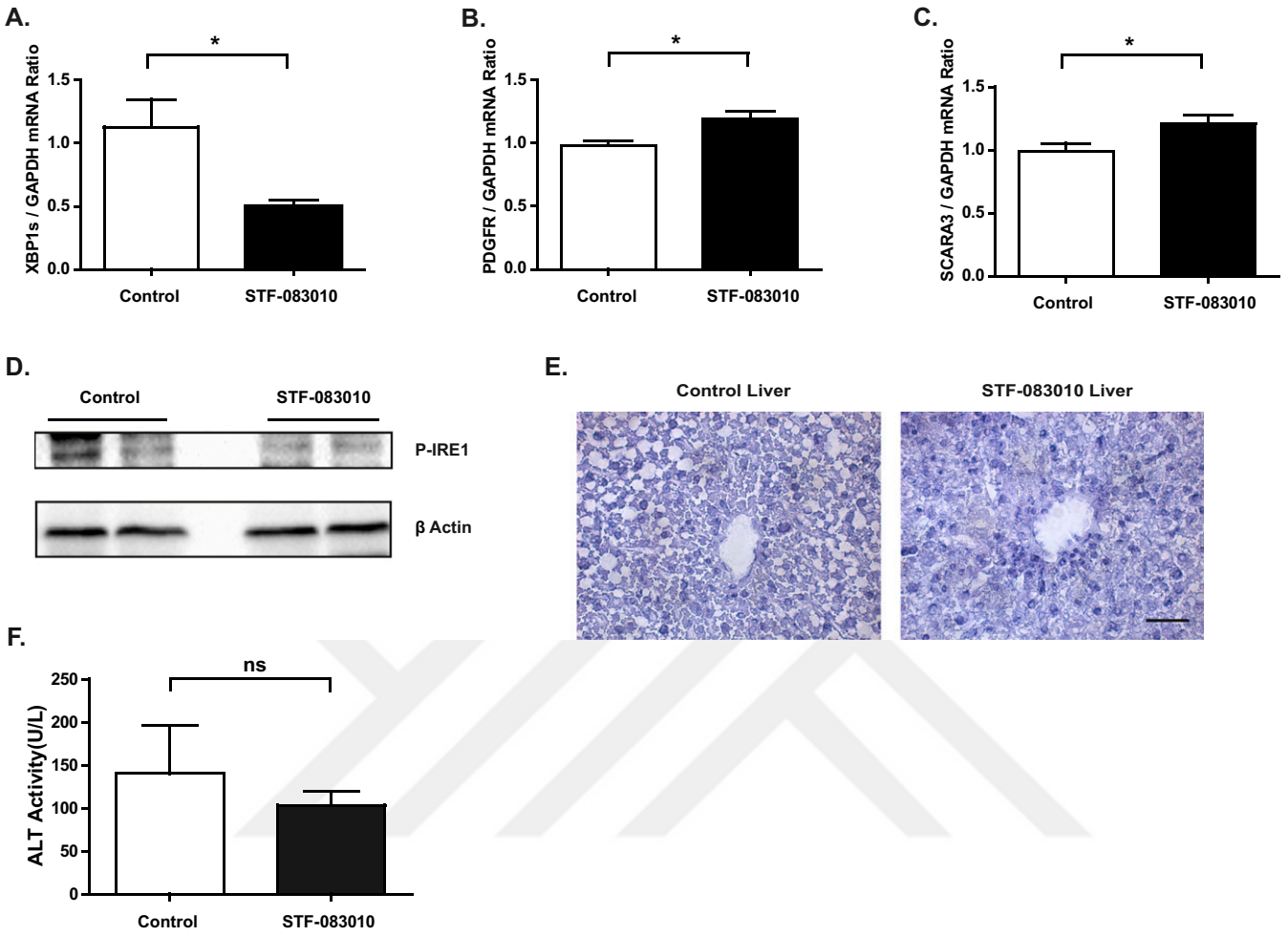

Fig. S5. Treatment of ApoE$^{-/-}$ mice with IRE1 inhibitors suppresses *Xbp1* mRNA splicing and degradation of canonical RIDD targets. (*A*) qRT-PCR analysis of spliced *Xbp1* mRNA levels from spleen tissue of ApoE$^{-/-}$ mice that were fed a Western diet for 12 weeks and treated with STF-083010 (10 mg/kg per day) or vehicle (control) for 6 weeks. (*B* and *C*) qRT-PCR analysis of the mRNA levels of reported RIDD targets in the same tissues as in *A*. (*D*) Liver protein lysates from the same mice as in *A* were analyzed for the phosphorylated form of IRE1 by Western blotting. (*E*) H&E staining of the livers from the same mice in *A*. (Scale bar: 50 μm.) (*F*) Plasma ALT activity measurements from the same mice in *A*. Statistics are the same as in Fig. 1. ns, Not significant. *$P \leq 0.05$.

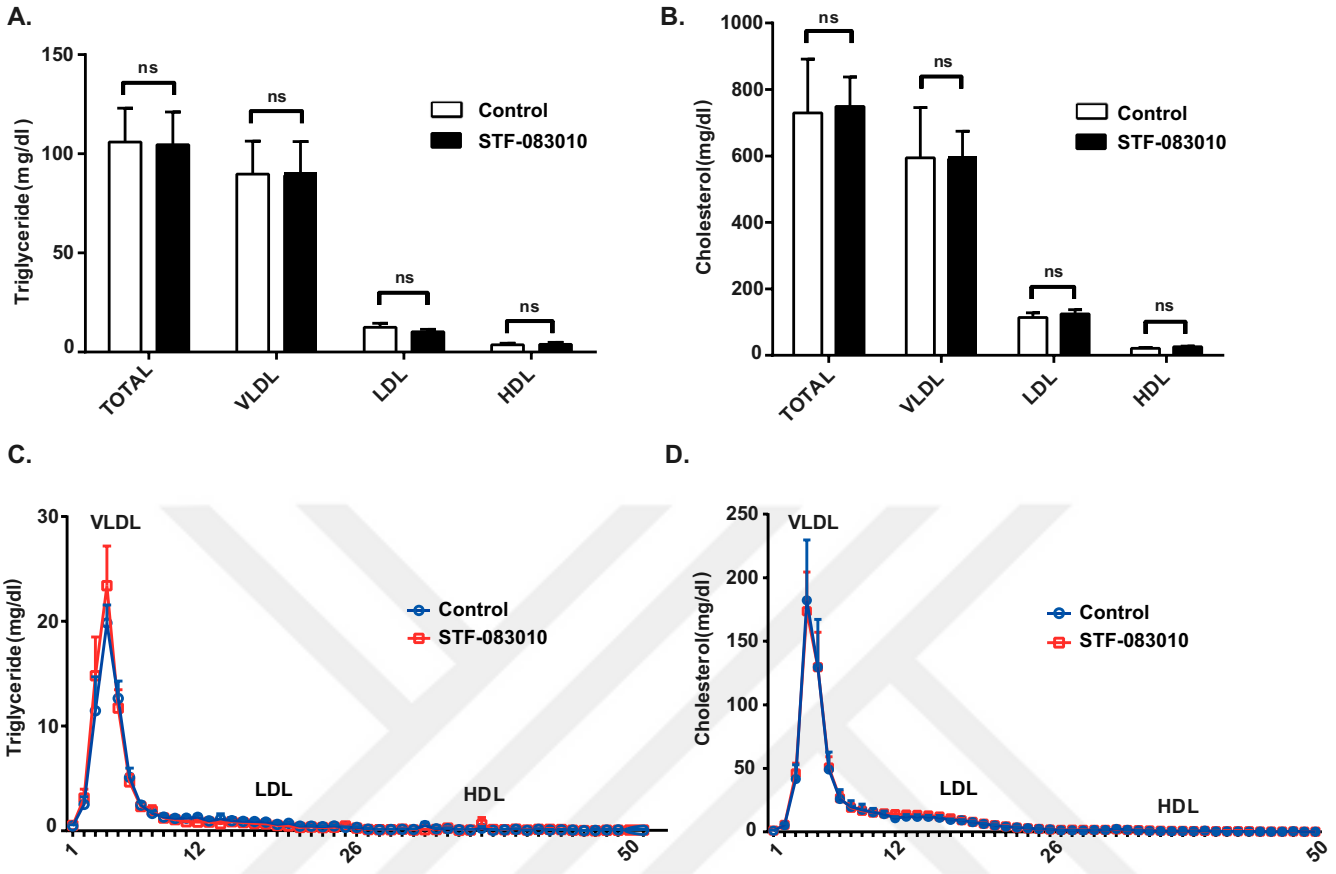

Fig. S6. Lipid and lipoprotein profiles do not change in animals treated with IRE1 inhibitors. (*A*) Total plasma triglyceride and lipoprotein [very LDL (VLDL), LDL, and HDL] triglyceride levels in STF-083010– and vehicle-treated groups. (*B*) Total plasma cholesterol and lipoprotein (VLDL, LDL, and HDL) cholesterol levels in STF-083010– and vehicle-treated groups. (*C* and *D*) Lipoprotein profiles in control (blue) and STF-083010–treated (red) ApoE$^{-/-}$ mice. Statistics are the same as in Fig. 1. ns, not significant.

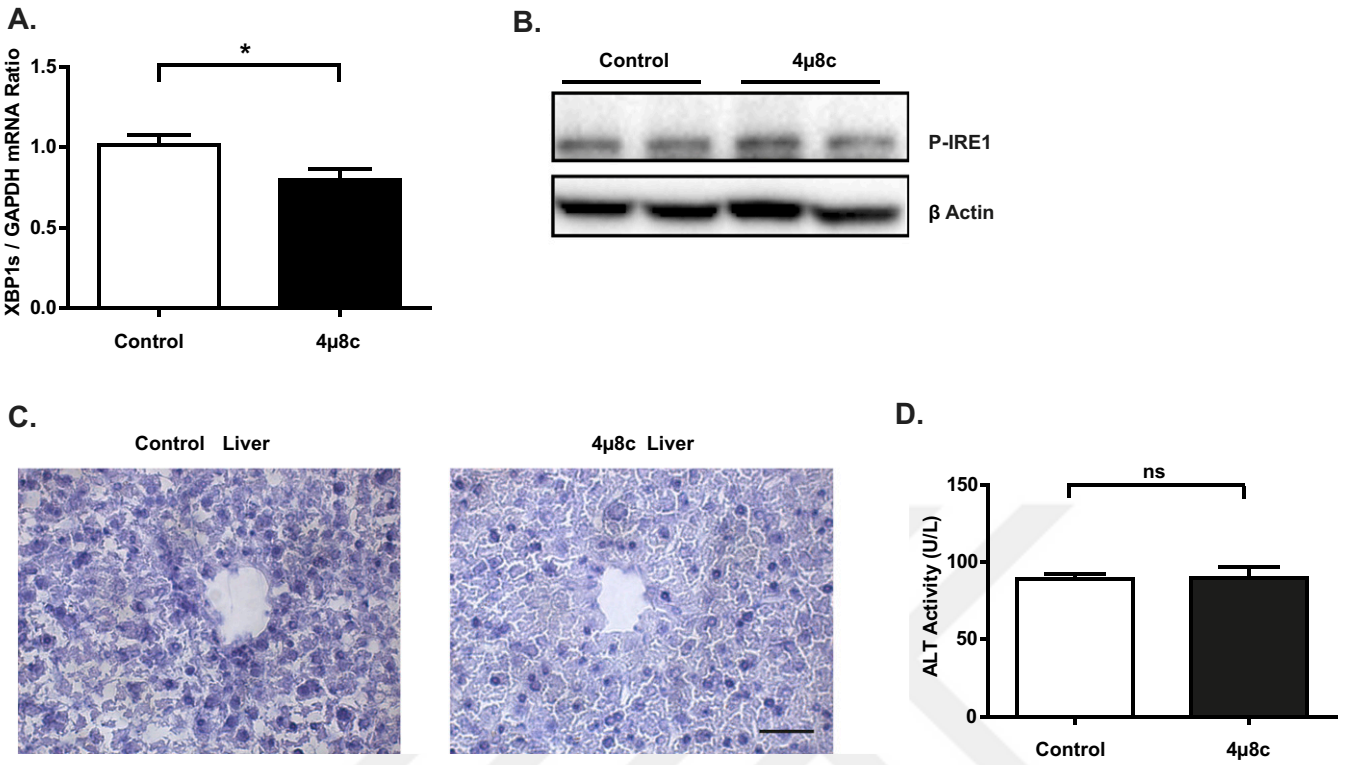

Fig. S7. Suppression of *Xbp1* mRNA splicing by IRE1 inhibitors in vivo. (*A*) qRT-PCR analysis of spliced *Xbp1* mRNA levels in spleen of ApoE$^{-/-}$ mice that were fed a Western diet for 12 weeks and treated with 4μ8c (10 mg/kg per day) or vehicle (control) for 4 weeks. (*B*) Liver protein lysates from the same mice as in *A* were analyzed for the phosphorylated form of IRE1 by Western blotting. (*C*) H&E staining of the livers from the same mice in *A*. (Scale bar: 50 μm.) (*D*) Plasma ALT activity measurements from the same mice in *A*. Statistics are the same as in Fig. 1. ns, not significant. *$P \leq 0.05$.

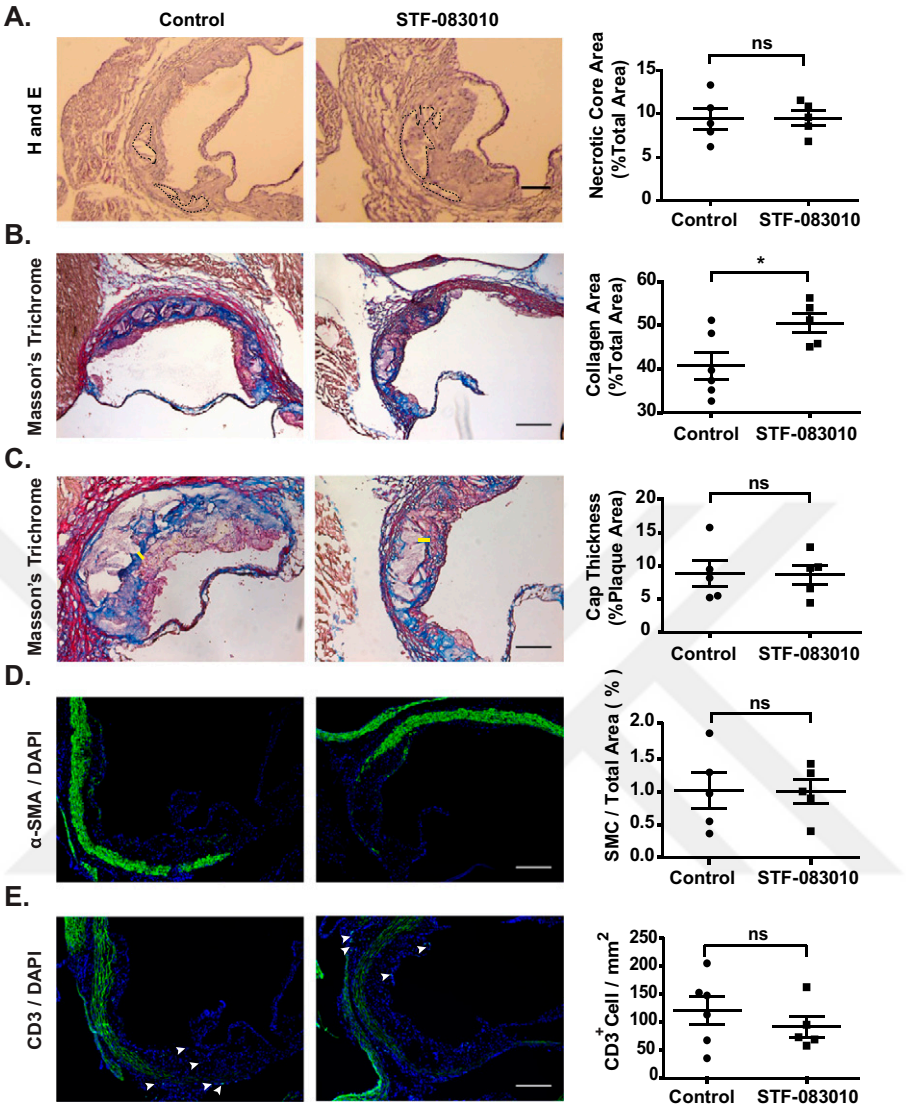

Fig. S8. IRE1 inhibitors alter plaque composition and inflammation. Immunohistochemical and immunofluorescence analyses of proximal aorta sections obtained from ApoE$^{-/-}$ mice treated with STF-083010 or controls. In each case, representative images are shown in *Left* and *Center*, and the quantification of the data appears in *Right*. (*A*) Necrotic area was calculated (from indicated area) in the H&E-stained plaque sections. (Scale bar: 150 μm.) (*B*) Masson's Trichrome collagen stain (collagen, blue; cytoplasm and muscle fibers, red; $n = 5$). (Scale bar: 200 μm.) (*C*) Fibrous cap thickness calculation from samples in *A*. (Scale bar: 100 μm.) (*D*) Anti–α-smooth muscle actin (VSMCs marker). (Scale bar: 200 μm.) (*E*) Anti-CD3 (T-cell marker). Arrowheads show CD3-positive cells ($n = 5$). Statistics are the same as in Fig. 1. (Scale bar: 200 μm.) ns, not significant. *$P \leq 0.05$.

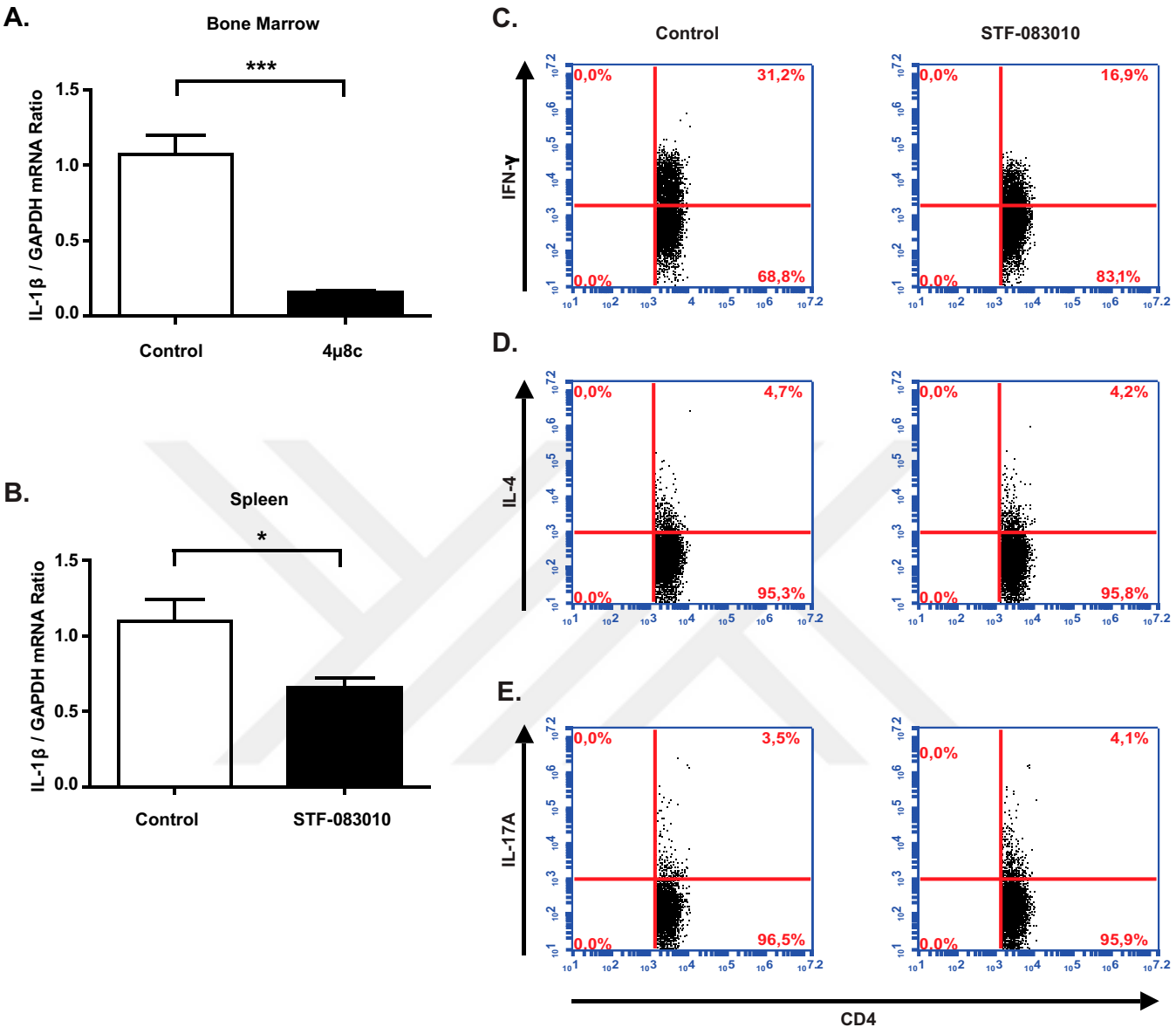

Fig. S9. IRE1 inhibitors reduce IL-1β levels in tissues and suppress Th1 immune responses. qRT-PCR analysis of *Il-1β* mRNA levels in (*A*) bone marrow or (*B*) spleen tissue of ApoE$^{-/-}$ mice that were fed a Western diet and treated with IRE1 inhibitors or vehicle (control). (*C*–*E*) Flow cytometry analysis of (*C*) IFN-γ, (*D*) IL-4, and (*E*) IL-17 levels in splenocytes activated with PMA/ionomycin ($n = 5$). Statistics are the same as in Fig. 1. *$P \leq 0.05$; ***$P \leq 0.001$.

Table S1. Top 25 up-regulated genes with STF-083010 treatment in mouse BMDM cells

Gene	Description	Fold change	*P* value
Gem	GTP binding protein (gene overexpressed in skeletal muscle)	5.28	0.0197
Aqp9	Aquaporin 9	4.26	5.00E-05
Slc7a11	Solute carrier family 7 (cationic amino acid transporter, y+ system), member 11	4.25	5.00E-05
Chac1	ChaC, cation transport regulator-like 1	4.20	5.00E-05
Trib3	Tribbles homolog 3	4.14	5.00E-05
Dclk1	Doublecortin-like kinase 1	4.10	0.0061
Slc1a4	Solute carrier family 1 (glutamate/neutral amino acid transporter), member 4	3.96	5.00E-05
Stx1a	Syntaxin 1A (brain)	3.96	0.03755
Soat2	Sterol *O*-acyltransferase 2	3.45	5.00E-05
Ifrd1	IFN-related developmental regulator 1	3.39	5.00E-05
Trim46	Tripartite motif-containing 46	3.37	0.00455
Dnmt3l	Similar to DNA cytosine-5 methyltransferase 3-like protein	3.33	0.00085
Zfp827	Zinc finger protein 827	3.32	0.0057
Bcar1	Breast cancer antiestrogen resistance 1	3.24	0.01765
Fzd4	Frizzled homolog 4 (*Drosophila*)	3.24	0.04035
Tmeff1	Transmembrane protein with EGF-like and two follistatin-like domains 1	3.22	5.00E-05
Slc7a5	Similar to solute carrier family 7	3.17	5.00E-05
Efcab5	EF-hand calcium binding domain 5	3.15	0.03165
Gm13889	Predicted gene 13889	3.10	0.02935
Matn2	Matrilin 2	3.06	5.00E-05
Aplp1	Amyloid beta (A4) precursor-like protein 1	2.98	0.0086
Asns	Asparagine synthetase	2.96	5.00E-05
Ddit3	DNA damage-inducible transcript 3	2.94	5.00E-05
Riiad1	Regulatory subunit of type II PKA R-subunit (RIIa) domain containing 1	2.93	0.04555
Map6	Microtubule-associated protein 6	2.86	0.0004

Table S2. Top 25 down-regulated genes with STF-083010 treatment in mouse BMDM cells

Gene	Description	Fold change	*P* value
Plxnb3	Plexin B3	−4.45	0.03955
Smpd3	Sphingomyelin phosphodiesterase 3, neutral	−3.94	0.006
S100a8	S100 calcium binding protein A8 (calgranulin A)	−3.83	5.00E-05
Fpr2	Formyl peptide receptor 2	−3.76	0.0461
S100a9	S100 calcium binding protein A9 (calgranulin B)	−3.72	5.00E-05
Cd177	CD177 antigen	−3.66	0.04935
Cx3cr1	Chemokine (C-X3-C) receptor 1	−3.48	5.00E-05
Chil3	Chitinase-like 3	−3.46	5.00E-05
Rhobtb1	Rho-related BTB domain containing 1	−3.45	0.00245
Hpgd	Hydroxyprostaglandin dehydrogenase 15 (NAD)	−3.28	5.00E-05
Syne1	Synaptic nuclear envelope 1	−3.09	0.03485
Gpr34	G protein-coupled receptor 34	−2.99	0.0171
Ccr2	Chemokine (C-C motif) receptor 2	−2.99	5.00E-05
Sult1a1	Sulfotransferase family 1A, phenol-preferring, member 1	−2.88	0.00875
Ltf	Lactotransferrin	−2.84	5.00E-05
Gm5086	Predicted gene 5086	−2.83	0.00595
Ccl2	Chemokine (C-C motif) ligand 2	−2.73	0.006
Cd69	CD69 antigen	−2.63	0.0091
Idi1	Isopentenyl-diphosphate delta isomerase	−2.61	0.02395
Ms4a6b	Membrane-spanning 4 domains, subfamily A, member 6B	−2.60	5.00E-05
Il1b	IL-1β	−2.59	0.0409
Ccnd1	Cyclin D1	−2.58	5.00E-05
Sesn1	Sestrin 1	−2.57	5.00E-05
Rab3il1	RAB3A interacting protein (rabin3)-like 1	−2.57	5.00E-05
Gm1966	GTPase, very large IFN-inducible 1	−2.57	0.0001

Table S3. Physical and biochemical characterization of ApoE$^{-/-}$ mice in STF-083010–treated and control groups

Variables and treatment	Control	STF-083010
n	6	6
Body weight (g)		
Before	30.3 ± 3.5	28.3 ± 2.2
After	33.3 ± 5.1	29.8 ± 2.5
Glucose (mg/dL)		
Before	120.5 ± 18.5	134 ± 13.3
After	79.0 ± 11.8	72.6 ± 15.1

Table S4. Physical and biochemical characterization of ApoE$^{-/-}$ mice in 4μ8c-treated and control groups

Variables and treatment	Control	4μ8c
n	7	9
Body weight (g)		
Before	28.8 ± 2.7	26.6 ± 1.9
After	31.1 ± 2.5	28.6 ± 1.2
Glucose (mg/dL)		
Before	93.9 ± 30.8	79.2 ± 19.6
After	91.3 ± 17.0	91.9 ± 20.0

Other Supporting Information Files

Dataset S1 (XLSB)